NANYANG TECHNOLOGICAL UNIVERSITY

GEOTECHNICAL PROPERTIES OF BIOCEMENT TREATED SAND AND CLAY

LI BING

SCHOOL OF CIVIL AND ENVIRONMENTAL ENGINEERING

2015

GEOTECHNICAL PROPERTIES OF BIOCEMENT TREATED SAND AND CLAY

LI BING

School of Civil and Environmental Engineering

A thesis submitted to the Nanyang Technological University
in partial fulfillment of the requirement for the degree of
Doctor of Philosophy

2015

Acknowledgements

This project would not have been possible and successful without the continuous guidance from my supervisor Prof Chu Jian. I would like to express the most sincere gratitude for his inspiration, patience and guidance. His endlessly support and invaluable experience came handy throughout all these years. His close monitoring and encouragement are especially appreciated.

I would also like to express my special thanks to Prof Andrew Whittle and Dr Volodymyr Ivanov as co-supervisors. I sincerely thank them for the wonderful opportunity to be part of this project, and their patience, guidance and invaluable knowledge sharing.

I wish to acknowledge the help provided by Mr. Heng Hiang Kim Vincent, Mr. Tan Hiap Guan Eugene, Ms Lim-Ding Susie and Mr. Koh Sun Weng Andy from the Geotechnical Laboratory, and Mr. Ong Chee Yung, Mr. Tan Han Khiang, Ms See Shen Yen, Pearlyn, Ms Maria Chong Ai Shing and the rest of the staff from the Environmental Laboratory for rendering the help on equipment, chemicals and laboratory testing.

The appreciation extends to Dr. Guo Wei, Dr. Maryam Naiemi, Mr Wu Shifan, Dr. He Jia and Mr Wang Yue for their invaluable friendships, helps and advices throughout this project.

Abstract

The application of microbial technologies to improve the mechanical properties of soils is a new and fast developing research area in geotechnical engineering. Microbially induced calcium carbonate precipitation (MICP) is the most commonly employed biocementation method. Application of MICP for sand has been studied by many researchers. However, few studies had been carried out for fine-grained soils such as clay or other types of low permeability materials.

In this research project, optimization of biocementation in sand and feasibility of using biocement to improve the mechanical properties of clayey soil were studied. Element tests using small cylindrical samples as well as model tests using soil of up to one cubic meter in volume were carried out. Different chemical compositions and types of bacteria were tested for both sand and clay.

The properties of the MICP treated soil were assessed by unconfined compression tests, triaxial tests, direct simple shear tests, and flexible wall permeability tests using a triaxial cell. The results show that biocementation using urease producing bacteria (UPB) with low activity is effective for both small samples and relatively large samples in the model tests. Results of consolidated drained (CD) triaxial tests on sand with different degrees of biocementation treatment indicate that the strength gained through bio-treatment is related mainly to the increase in cohesion provided by the biocementation effect. In addition to increasing the shear strength, the permeability of sand is also reduced by bioclogging. One method is to form a calcite crust of 2 to 3 mm thick on the top surface of sand. This method can reduce the coefficient of permeability of sand from 10^{-4} m/s to 10^{-8} m/s.

The possible applications of MICP to fine grained soils including kaolin, marine clay and bentonite were explored. The experiments show that a higher shear strength was observed for clayey soil mixed with UPB and cementation reagents compared to pure soil under the same water content. However, excess calcium cation used for the MICP process may impede the strength improvement. Another possible method is to make clay balls through premixing with bacteria and cementation reagents.

Table of Contents

Chapter 1
Introduction

1.1 Background

As a new approach, bio-mediated soil improvement methods have drawn considerable attention in recent years. Bio-mediated soil improvement broadly refers to "a chemical reaction network that is managed and controlled within soil through biological activity and whose byproducts alter the engineering properties of soil" (DeJong et al, 2010). Major processes involved in bio-mediated soil improvement methods include biocementation, bioclogging, biofilm formation, and biogas production. The main effects of the bio-mediated treatment include increasing the stiffness and shear strength of both sand and clay, reducing the permeability of sand, decreasing the compressibility of clayey soil, and increasing the liquefaction resistance of sand.

Geometric compatibility between the microbes and soil particles is essential to the effectiveness of the bio-mediated treatment. Microbes that are relatively small, usually 0.5 to 3 micrometers in length, are preferred, as they can travel through pores between soil particles (Madigan and Martinko, 2003). Most of the bio-mediated methods may be suitable for sand. However, as pore sizes of clay may be too small for the delivery of bacterial cells, the application of bio-mediated methods to clay is not an easy task. Few studies on MICP application in clay have been conducted.

Recent studies have shown that many types of microbes are capable of producing biocementation. These include urease producing bacteria (UPB), iron reducing bacteria (IRB), nitrifying bacteria, oligotrophic microaerophilic bacteria, sulphate

reducing bacteria (SRB), and dimorphic phytase-active yeast for the production of calcium-phosphate precipitation (Dejong et al., 2006; Ivanov and Chu, 2008; Chu et al., 2009; Roeselers & van Loosdrecht, 2010). The microbially induced calcium carbonate precipitation (MICP) process has been identified as the most effective approach for biocementation and bioclogging so far. Several groups of organisms can induce MICP through their metabolic processes. The most common one is UPB. It produces MICP through hydrolysis of urea. Heterotrophic organisms, like sulfate-reducing bacteria, can also induce MICP by reducing sulphate to H_2S and releasing HCO^{3-} if dissolved gypsum ($CaSO_4 \cdot 2H_2O$) presented in the environment. This hydrolysis process in the present of calcium results in the production of calcium carbonate and ammonium as well (Mobley & Hausinger, 1989; Stocks-Fischer et al., 1999; Fujita et al., 2000).

Many factors could influence the effectiveness of MICP. This includes urease activity, distribution and fixation of UPB, chemical concentration, retention time, properties of parent soil (including size, textures, interaction with water, etc.), etc. The effects of biocementation and bioclogging of soil are mainly assessed by measuring the unconfined compressive strength and coefficient of permeability of soil respectively. However, in-depth studies have not been made to evaluate the stress-strain and strength and dilatancy behavior of sand and how the shear strength or permeability varies with biocement content.

1.2 Objectives

The thesis aim to achieve the following objectives:

1) To investigate the factors affecting the optimization of biocementation in sand;

2) To study the mechanisms of biocementation and its effect on the effective shear strength of soil and to establish the relationship between shear strength and calcite content, and that between permeability and calcite content;

3) To carry out large scale model tests to upscale the size of MICP treatment and evaluate the three dimensional effect of MICP treatment for large samples.

4) To explore the feasibility of applying MICP to clayey soil.

The scope of work was mainly experimental studies including basic properties tests for both microbial and soil materials, the element tests to identify the factors affecting the MICP processes and both small and large scale model tests to evaluate the effectiveness of the established MICP process and the engineering properties of soil treated using the established biocementation and bioclogging methods. This project also included a study on possible microbial-treatment for fine-grained soil.

1.3 Outline of Thesis

This thesis is divided into nine chapters. Chapter 2 presents a literature review on previous theoretical and experimental studies, especially on the engineering properties of soil, instability of granular materials and yield of bonded soils. Bacteria cultivation method, sample preparation method and the experimental set-up for different type of soil properties tests are discussed in Chapter 3. The experimental methodology is also presented in this chapter. The factors to optimize MICP in sand are studied in Chapter 4 through investigating the variations of parameters (pH values, conductivities, calcium cations and urea in effluent) in solution as well as in small sand samples. The bulk biocementation and bioclogging by calcite crust on sand surface are discussed in Chapter 5, through establishing MICP in six sand boxes of 0.02 m^3 volume each. An upscale model test conducted with one cubic meter sand is presented in Chapter 6. The mechanism of MICP treatment in sand based on CD tests results conducted on sand samples with different calcite content levels are discussed in Chapter 7. The feasibility of introducing MICP in clayey soil is discussed in Chapter 8. Finally, the conclusions and recommendations for future study are made in Chapter 9.

Chapter 2

Literature Review

2.1 Introduction

Previous research work which is relevant to this study is reviewed in this chapter. Previous attempts of biological treatment of soil in geotechnical and geo-environmental engineering, including biocementation, bioclogging, bioremediation of soils, and microbially induced geo-disasters, are discussed in Section 2.2. Major factors influences microbially induced carbonate precipitation (MICP) formation studied by previous researchers, including urease activity, chemical concentration in cementation solution, bacteria fixation and flow rate of treatment are presented in Section 2.3. Introduction of engineering properties evaluation in soil including basic shear strength evaluation, critical state soil mechanics, dilatancy and strain localization in cemented granular materials, is presented in Section 2.4. Basic properties of clay are introduced in Section 2.5 as employing biocementation in clay is a new and important aspect in this study. Major observations would be summarized in Section 2.6.

2.2 Overview of Biological approaches in soil improvement

2.2.1 Effects of bacteria on soil shear stress in nature

Microbiology is the study of microorganisms, which are the largest biomass on earth. The major groups of organisms studied in microbiology are bacteria, unicellular algae, microscopic fungi, viruses, and protozoa (Favor, 2004). Many bacterial species exist simply as single cells, typically 0.5–5.0 micrometres (μm) in

length, in order to get large surface area to volume ratio and thus survive in nutrition-poor environment. However, despite their simplicity, bacteria contain a well-developed cell structure and have unique biological properties. Bacteria can display a wide diversity of shapes and sizes, called morphologies. The two largest groups of bacteria on earth are cocci (spherical shape) and bacilli (rod-shaped) (Cabeen & Jacobs-Wagner, 2005). The shapes of two main bacteria strains being involved in this study, *sarcina*, which belongs to the groups of cocci, and bacilli, are drawn in Fig. 2.1a and 2.1b respectively.

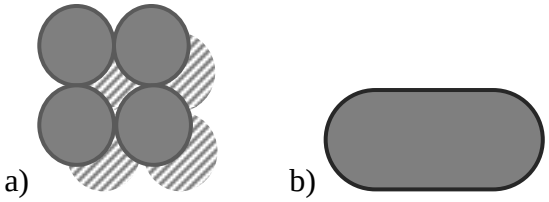

Figure 2.1 Morphologies and arrangements of bacteria strain referring in this study; a) *sarcina*, and b) *bacilli* (after Wikipedia, 2014)

Nearly all bacterial cell surfaces are negatively charged, because of the presence of proteins and other wall and cell membrane components which contain phosphate, carboxyl and other acidic groups. Electrical double layer forms around the bacteria cell; adding cations to bacteria suspension can thus shrink the electrical double layer and cause the cells to flocculate (Burke & Gibson, 1933).

Bacterial proliferation growth is the division of one bacterium into two daughter cells that are genetically identical to the original cell (binary fission). A population of bacteria introduced into a fresh, nutrient-rich medium usually display four major phases of growth: the lag phase, the log (logarithmic) phase, the stationary phase and the decline phase. Bacteria prepare themselves to adapt the growth conditions in lag phase; in exponential phase, new bacteria cell appear proportional to the present population by binary fission; the growth rate slows during stationary phase due to nutrient depletion and accumulation of toxic products, and then eventually dead in death phase (Zwietering, 1990).

Activity of bacteria could affect shear strength of soil in nature. For example, Kuo & Bolton (2008) reported a phenomenon, that West African deep sea clays at

shallow sediment depths have anomalously high undrained shear strengths, as shown in Fig. 2.2.

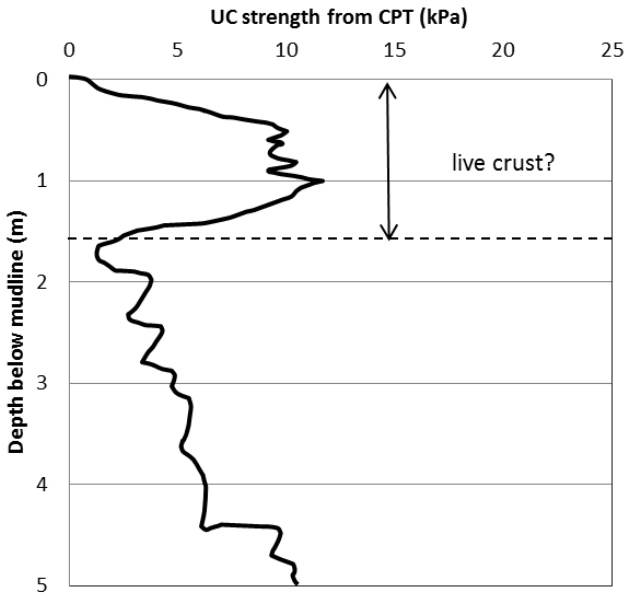

Figure 2.2 Undrained shear strength profile of marine clay sediment showing a crust on top (modified after Ehlers et al., 2005).

This phenomenon is not restricted to the West African deep sea clays, but rather worldwide (Ehlers et al., 2005). The origins of these crusts and why it is only constrained in the top few meters of marine clay sediment is currently unknown. One assumption of the origin of crust is that it is due to the overconsolidation at the top few meters. As the highest populations of bacteria also occur within the top meter of marine clay sediment, microbes are considered to be another explanation of such phenomenon (Parkes et al., 2000). Several hypothesizes were developed, that bacteria can build polymer bridges and thus aggregate the clay particles and enhance viscosity and shear strength of soil (Bennett et al., 1992; Turley et al. 1995; Deflaun and Mayer,1983; Dade et al. 1996).

2.2.2 Overview of bio-mediated soil improvement methods

As an environmentally friendly and recent method, bio-mediated soil improvement method has drawn more attention. Earliest attempt of bio-stabilization was using live plantings to add structural strength to a soil mass, which can be traced back to 12th century in China (Karol, 2003). In recent years, bio-mediated soil

improvement method broadly refers to "a chemical reaction network that is managed and controlled within soil through biological activity and whose byproducts alter the engineering properties of soil" (DeJong et al, 2010). An overview of these types of systems is presented schematically in Fig. 2.3. Major divisions of bio-mediated soil improvement system consist of biomineralization, which includes biocementation and bioclogging, biofilm formation, and biogas production. Main purposes of the treatment include decreasing permeability and compressibility, increasing stiffness and shear strength, and controlling the volumetric response of soil mass.

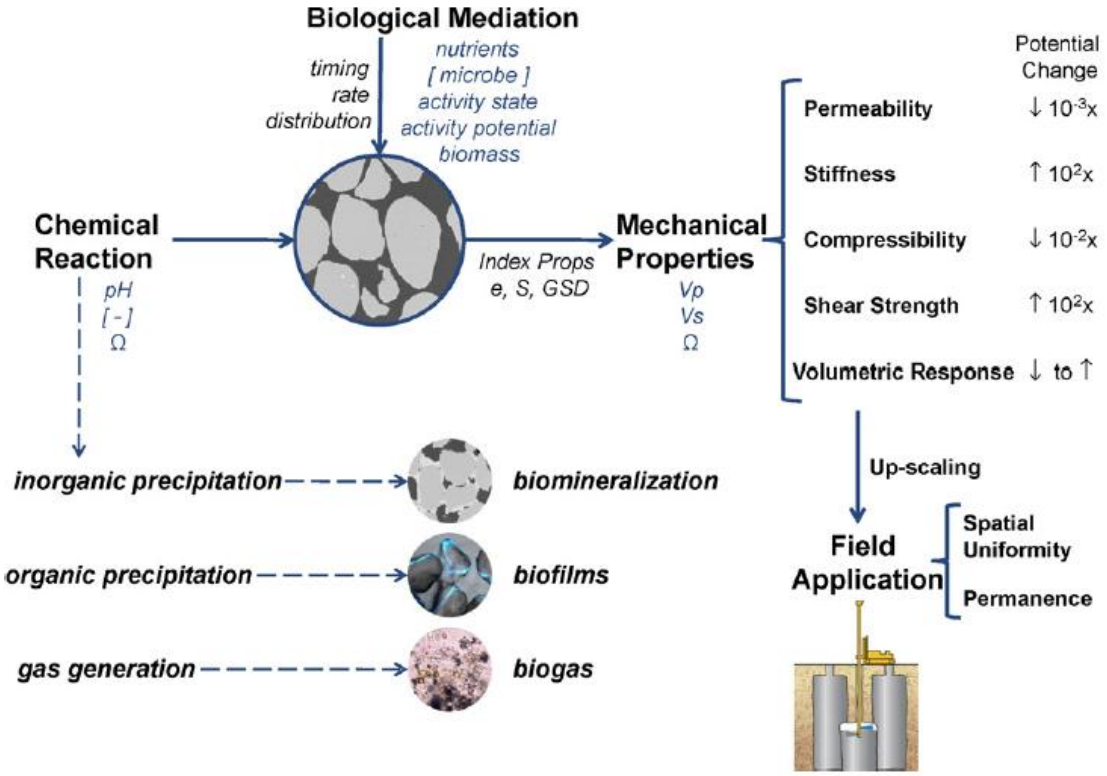

Figure 2.3 Overview of bio-mediated soil improvement system (DeJong et al., 2010)

Geometric compatibility between the microbes and soil particles is essential to the effectiveness of bio-mediated treatment. Microbes that are relatively small, usually 0.5 to 3 micrometers in length, are preferred, as they can travel through pores between soil particles (Madigan and Martinko, 2003). Comparisons between sizes of microbes and soil particles, as well as application range of bio-mediated soil improvement methods, are as shown in Fig. 2.4. Sand is suitable for generally all of the treatment, while biomineralization may cover the range of silt; biofilm can

be applied up to size of gravel. However, according to DeJong et al. (2010), the significant limitation of all the treatment methods is that the pore size of clay soil may be too small for the delivery of bacterial cells. The size of spherical shape prokaryotic cells is about 1 micrometre, which is significantly bigger than the pore size of clay. Therefore, biocementation of clay should be performed without migration of bacterial cells.

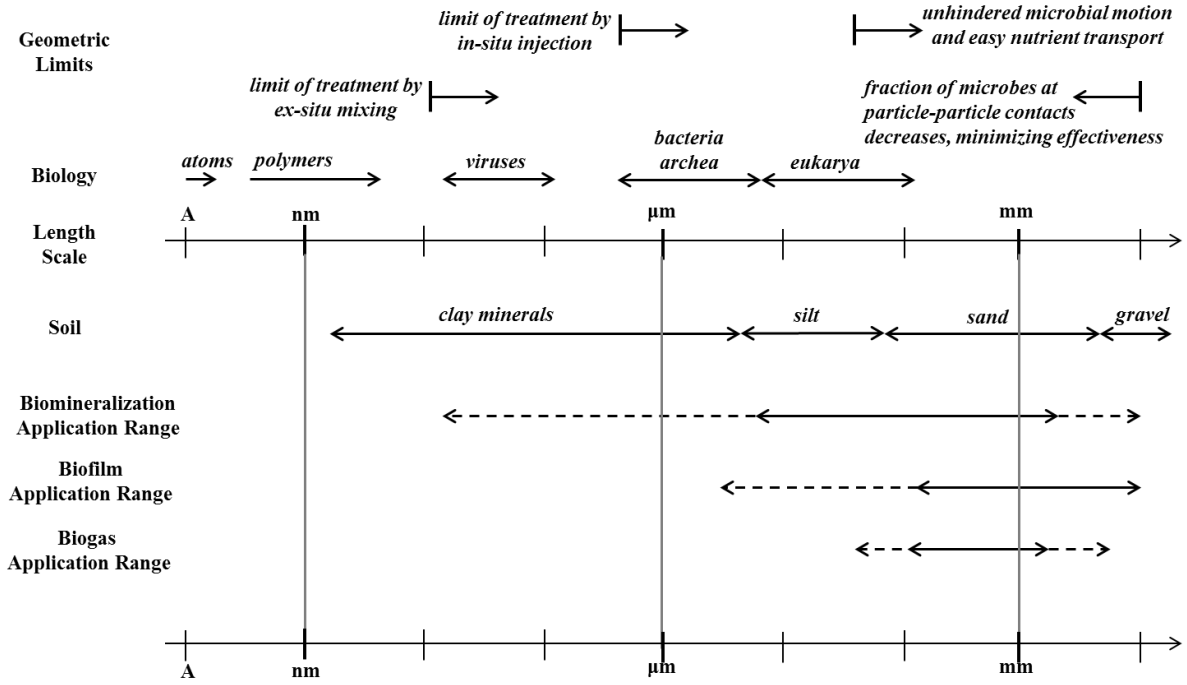

Figure 2.4 Comparisons between sizes of microbes and soil particles, as well as application range of bio-mediated soil improvement methods (modified after DeJong et al., 2010)

2.2.3 Biocementation

Interest on improvement of soil properties employing biocementation is growing promptly in recent years. Many types of microbes are capable of producing biocementation, for examples, urease producing bacteria (UPB), iron reducing bacteria (IRB), nitrifying bacteria, oligotrophic microaerophilic bacteria, sulphate reducing bacteria (SRB), and dimorphic phytase-active yeast (which could produce calcium-phosphate precipitation) etc. (Dejong et al., 2006; Ivanov and Chu, 2008; Chu et al., 2009; Roeselers & van Loosdrecht, 2010). The most well accepted and widely applied method so far is to produce microbial carbonate precipitation by urease producing bacteria.

1. Microbially induced carbonate precipitation *(MICP) using urease producing bacteria (UPB)*

Calcium carbonate ($CaCO_3$, known as calcite in mineralogy) is considered to be one of the most common minerals on Earth. It is naturally presented in general terrestrial environments, like fresh water and sedimentary rock masses, including marble, limestone, calcareous sandstone (Klein and Hurlbut, 1999; Hammes and Verstraete, 2002). The precipitation of $CaCO_3$ is governed by four parameters: the concentration of calcium, the concentration of carbonate, the pH of the environment, and the presence of the nucleation sites (Hammes and Verstraete, 2002).

Contribution of bacteria to the $CaCO_3$ precipitation, which is known as microbially induced carbonate precipitation (MICP), has caught much attention recently. Several groups of organisms can induce MICP through their metabolic processes. The most common one among these is photosynthetic organisms; it produces MICP by utilizing dissolved CO_2 in water and thus shifting the equilibrium of HCO_3^- and CO_3^{2-}, while increasing pH value (McConnaughey & Whelan, 1997; Ehrlich, 1998). Heterotrophic organisms, like sulfate-reducing bacteria, can also induce MICP by reducing sulphate to H_2S and releasing HCO_3^- if dissolved gypsum ($CaSO_4 \cdot 2H_2O$) presented in the environment. MICP can also be produced by organisms involved in the nitrogen circle. Hydrolysis of urea is the most easily controlled and widespread reaction that occurred in these organisms, which results in the production of carbonate ions and ammonium as well (Mobley & Hausinger, 1989; Stocks-Fischer et al., 1999; Fujita et al., 2000). MICP precipitation then occurs in the presence of calcium ions. Reactions involved in the three organisms are as shown in Table 2.1.

Hydrolysis of urea was promoted by bacteria through urease production, which is an enzyme that catalyses the hydrolysis of urea into carbon dioxide and ammonia. *Sporosarcina pasteurii*, which is one type of alkalophilic urease-producing bacteria, is usually adopted in current biocementation practice, for its high activity, non-repressed by NH_4^+, and its non-pathogenicity (Whiffin, 2004). As show in Table 2.1, *Sporosarcina pasteurii* uses urea as nitrogen and energy sources,

releasing ammonium and carbonate/bicarbonate as by-products, and creating an alkaline environment for preparation of MICP as well. Free calcium cation might be attracted to the negatively charged cell surfaces, and calcite would form using cells as the nucleation centre.

Table 2.1 Reactions involved in three major groups of organisms than can produce MICP (after McConnaughey & Whelan, 1997; Ehrlich, 1998; Mobley & Hausinger, 1989; Stocks-Fischer et al., 1999; Fujita et al., 2000)

MICP producing organisms	Reactions involved
1.Photosynthetic organisms	$CO_2 + H_2O \rightarrow (CH_2O) + O_2$ $2\ HCO_3^- \leftrightarrow CO_2 + CO_3^{2-} + H_2O$ $CO_3^{2-} + H_2O \rightarrow HCO_3^- + OH^-$ $Ca^{2+} + HCO_3^- + OH^- \rightarrow CaCO_3 + 2H_2O$
2.Heterotrophic organisms	$CaSO_4 \cdot 2H_2O \rightarrow Ca^{2+} + SO_4^{2-} + 2H_2O$ $2(CH_2O) + SO_4^{2-} \rightarrow HS^- + HCO_3^- + CO_2 + H_2O$ $Ca^{2+} + HCO_3^- + OH^- \rightarrow CaCO_3 + 2H_2O$
3.Organisms involved in the nitrogen cycle (hydrolysis of urea, this study)	$CO(NH_2)_2 + 2H_2O \rightarrow CO_3^{2-} + 2NH_4^+$ $CO_3^{2-} + H_2O \rightarrow HCO_3^- + OH^-$ $Ca^{2+} + HCO_3^- + OH^- \rightarrow CaCO_3 + 2H_2O$

As hydrolysis of urea can liberate ionic products (NH_4^+ and CO_3^{2-}) from non-ionic substrates (urea, $CO(NH_2)_2$), the overall conductivity of solution increases at a rate linearly proportional to active urease present (Hanss & Rey, 1971; Grunwald, 1984). Determination of urease activity can thus be transferred to measuring the increase of conductivity in the bacteria sample, in the presence of urea.

DeJong et al (2006, 2010) introduced *Sporosarcina pasteurii* to sand, producing MICP and tested the engineering properties before and after treatment. The monotonic undrained behaviours of untreated and bacteria-treated specimen are shown below in Fig. 2.5. Comparing the data of bacteria- treated specimen and pure sand at the same void ratio, it is can be observed that the initial peak strength is increased by four folds by the bacteria added, and the peak stress ratio was increased by more than 1.5 times.

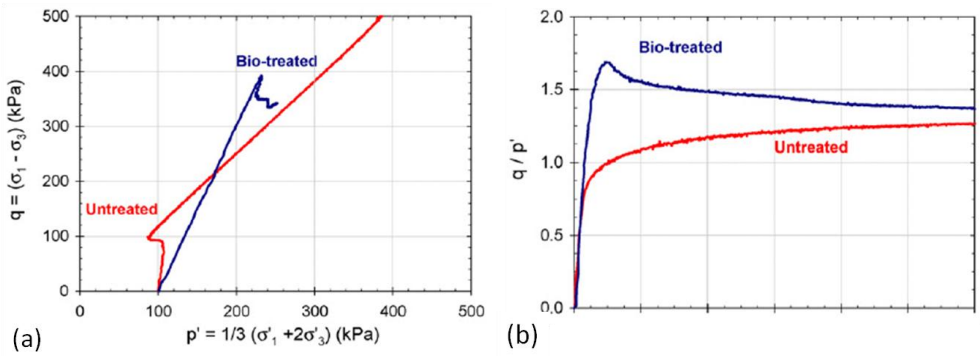

Figure 2.5 Undrained triaxial behavior of bio-treated and untreated sand (DeJong et al., 2010)

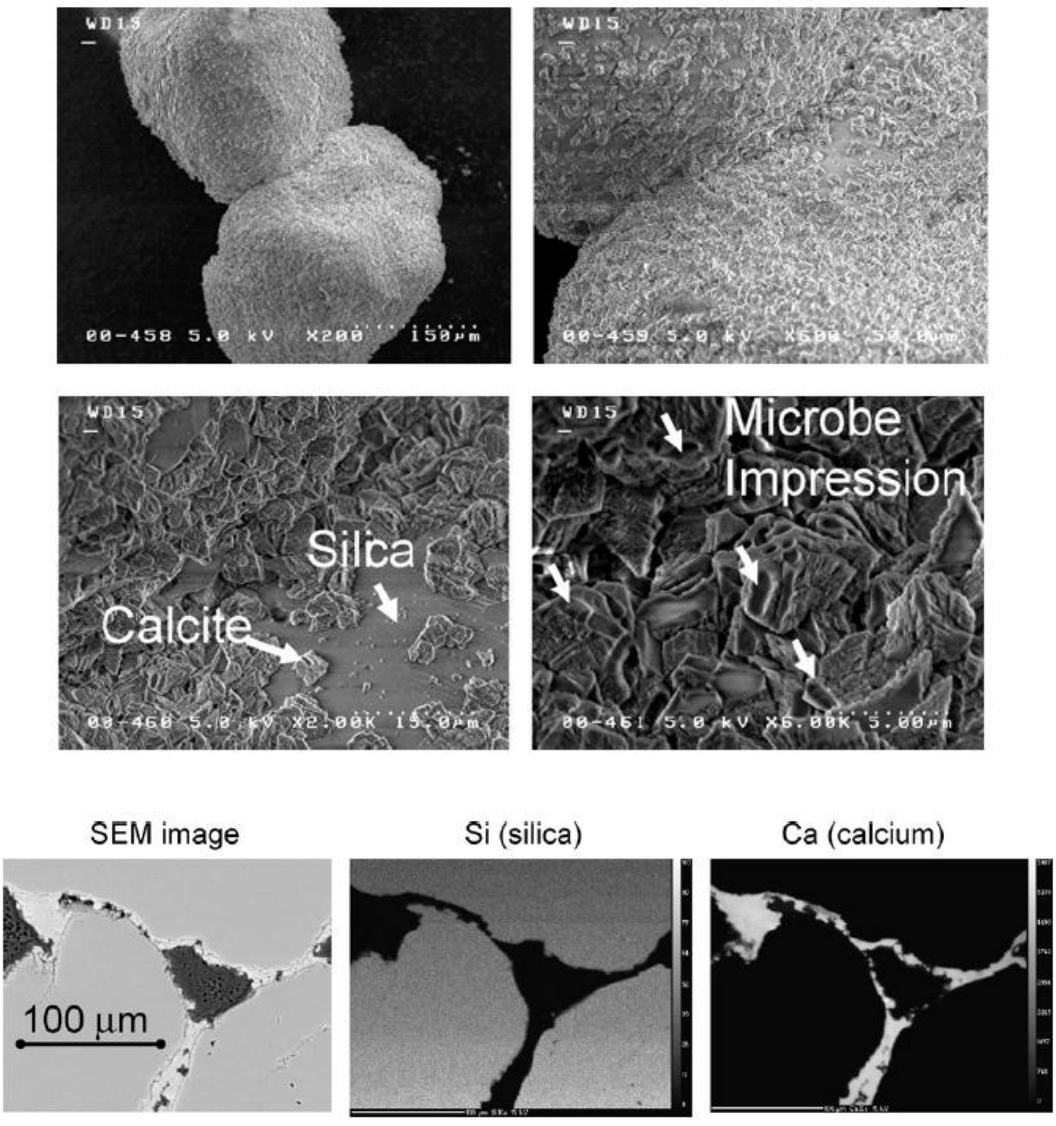

Figure 2.6 SEM picture of the silica sand particles (Si), precipitated MICP deposited at particle surface (Ca), microbial habitat, and the bonding formed by MICP between sand particles after bio-treatment (DeJong et al., 2010)

Under the scanning electron microscopy (SEM) (Fig. 2.6), the silica sand particles (Si), precipitated MICP deposited at particle surface (Ca), microbial habitat, and the bonding formed by MICP between sand particles, can all be observed clearly. It is reasonable to believe that it was these contact bonding that contribute to the increase of sand strength. Cementation by MICP in clay has not been tested before, for its lack of sufficient pore space. Besides *S. pasteurii, B. pasteurii* was also employed in some of the previous studies (Qian et al., 2009, 2010a, 2010b).

2. Cementation by iron hydroxides using iron-reducing bacteria (IRB)

Another example of sand cementation in nature is the formation of ferrihydrite in pores (Ross et al., 1989). Biological cementation of iron hydroxide can be found in the soil of all wetland plants where Fe^{2+}, produced by iron-reducing bacteria, react with oxygen released by the roots (Weiss, 2005). Plus, precipitation of iron hydroxide occurs naturally in areas with Fe^{2+}, high pH and redox potential, forming cemented concretions. Depending on its crystallization, iron hydroxide can also be a good cementing agent in soils (Dniker et al., 2003). $Fe(OH)_2$ is practically white in color with a greenish tinge when exposed to traces of oxygen. Prolonged presence of oxygen will reduce the iron to $Fe(OH)_3$ giving it the characteristic color of reddish brown.

Aggregation of iron hydroxides is affected by the following parameters: (1) pH, (2) size of crystals, (3) path of formation of the iron hydroxide, (4) ionic composition of the soil solution and (5) presence of certain organic molecules (Roden & Zachara, 1996). Iron hydroxides formed in nature are often poorly crystalline due low temperature and presence of contaminants. In comparison, crystals grown manually are often well-crystallized. These small crystals of iron hydroxides have a larger and more reactive surface which leads to increased aggregation (Mohapatra and Anand 2010).

Chu et al. (2009) thus proposed to use dissolved ferrous, producing from cheap crushed iron ore through the activity of iron reducing bacteria, for biocementation usage. Iron reducing process, which plays an important role in natural iron cycle, is made from the following reaction:

$$4Fe^{3+} + CH_2O + H_2O \rightarrow 4Fe^{2+} + CO_2 + 4H^+ \qquad \text{(Eqn. 2.1)}$$

Precipitation of iron hydroxide then occurred in high pH environment. Anaerobic sludge from water reclamation plant mixed with certain amount of glucose was used as the source of iron reducing bacteria (IRB). The oxidation-reduction potential (ORP) and ferrous concentration measured throughout the progress of the bacteria cultivation are shown in Fig. 2.7a and 2.7b respectively. Decreasing ORP indicated an increasing reduction potential, and ferric is continuously reduced to ferrous as shown in Fig. 2.7b. A cylindrical sand sample treated with iron-reducing bacteria is shown in Fig. 2.8. It can obviously sustain a relatively high weight, while pure sand cannot even sustain its self-weight in contrast. This method is hypothetically applicable in clay as well, as the IRB is anaerobic and can survive without oxygen.

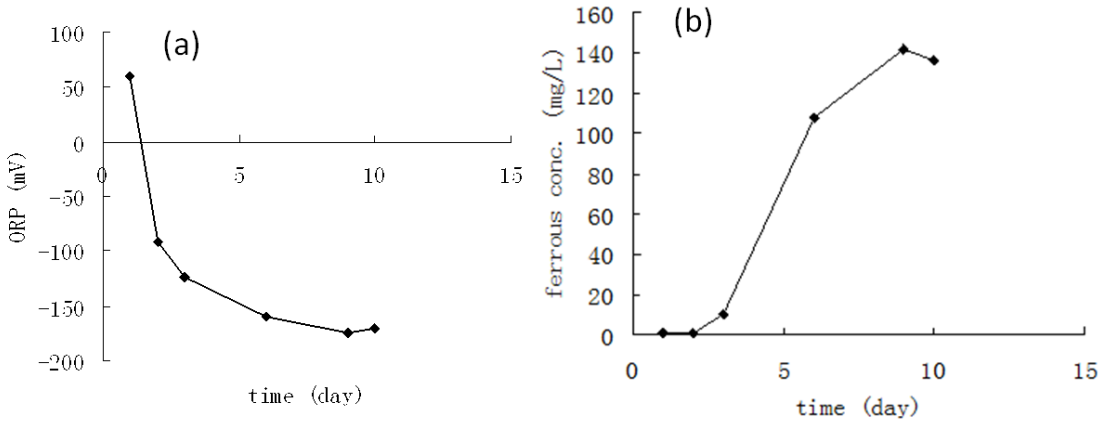

Figure 2.7 Plot of (a) ORP (b) ferrous concentration in the cultivation of iron-reducing bacteria (after Chu et al. 2009)

Figure 2.8 Iron-reducing bacteria treated sample subject to a weight (Chu et al. 2009)

3. Hypothetical cementation of ferrous sulfide using sulphate- reducing bacteria (SRB)

Another working hypothesis proposed by Ivanov (unpublished data) of biocementation in clay, is to create strong disulfide bridges within clay particles immersed with Fe^{3+} and S^{2-}. As it is assumed in Fig 2.9 that, ferric cation could serves as a bond opening for S-S bonds to form Fe-S-S-Fe bonds between clay particles, and complex of clay-Fe-S-S-Fe-clay bonds could be formed.

Depending on the shape and size of the colloid, the chain length of S-S bond may vary. Since disulfide bonds are typically quite strong (bond-dissociation energy of 250 kJ/mole), the S-S bonds may acts as crosslinkers and strongly affect the rheology of clay. This results in greater compression strength as compared to clay at the same moisture content (Stuttgart, 2008). Formation of disulfide bonds can be promoted by oxidants such as hydrogen peroxide, because of the intermediates of sulfenic acids (Kirihara et al., 2007).

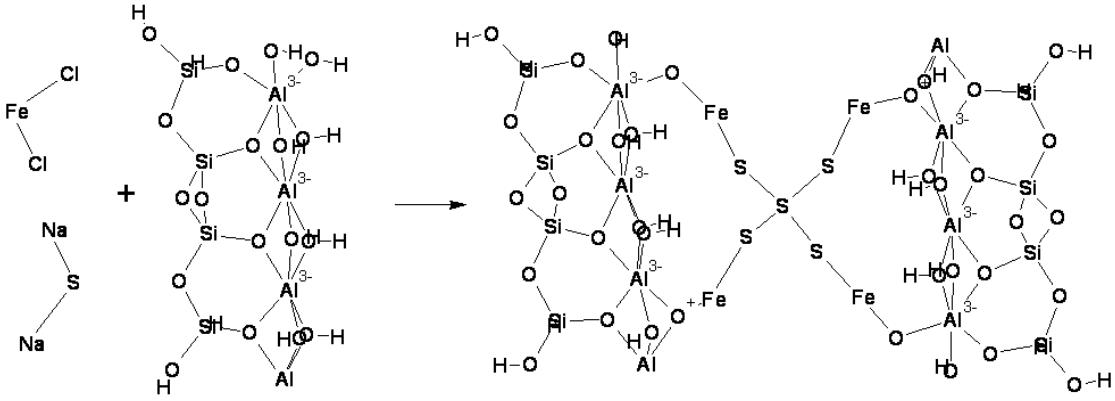

Figure 2.9 Hypothetical formation of Fe-S bonds between clay particles

Sulfate-reducing bacteria (SRB) can be used to produce S^{2-} ions to bond with Fe^{2+} ions to form strong Fe-S bonds. Sulfate content in Singapore marine clay typically ranges from 0.92 % to 1.7 % by weight (Tan et al., 2002). The reduction of sulfate to sulfide is an eight electron step process that proceeds via different intermediates (Rabus et al., 2006). Sulfate is firstly activated using ATP leading to the formation of adenosine phosphosulfate (APS). Subsequently APS is reduced to sulfite by APS reductase and finally the sulfite is reduced further to sulfide by dissimilatory sulfite reductase (DSR).

A very diverse and heterogeneous group of bacteria is capable of using sulfate as terminal electron acceptors. Research has shown tremendous morphological, ecological, nutritional and metabolic diversity among SRB. Morphologically SRB cells can take different forms including cocci, rods, curved types (vibroid), cell aggregates and multi-cellular filaments (Rabus et al., 2006). Most of the SRB are strict anaerobic; some species can survive exposure to oxygen for several hours. The ambient temperature and pH value in the environments inhabited by SRB can vary widely (Konhauser, 2007).

4. Other engineering practices using bio-mediated soil improvement methods

Besides the bacteria mediated soil improvement system as mentioned in the previous sections, there are some other chemical and bio-related products used in engineering practices, like enzymes, organic exopolymers like xanthan and guar, tree resins (mineral pitch), sulfonated oils, etc. (Scholen, 1992; Liu et al., 2010; Zhang et al., 2013). Many types of commercial products have also been developed, for example, Bio Cat®, EMC Squared®, Perma-Zyme®, and PSCS-320® as enzymes, Road Oyl® as tree resin. All of these products consist of high concentration protein and several types of organic compound; mechanisms behind them including ion-exchange with clay particles, breaking the diffused double layer of clay and absorb the water in between, or attach to the surface of clay to prevent further water absorption, etc. Their effectiveness is proven by their successful application *in situ*.

One example of these types of soil improvement products is organic polymer soil stabilizer STW, developed by Liu et al. (2011). Its main component is acetic-ethylene-ester polymer, which contains large amount of functional group $-OOCCH_3$ and has a milky appearance, as shown in Fig 2.10a. STW is water-soluble; it can form "an elastic and viscous membrane structure on soil surface at natural conditions" (Fig 2.10b) and enhance the cohesion of soil. Change of unconfined compression strength and cohesion of soil sample mixed with polymer are presented in Fig. 2.11a and 2.11b respectively; both of them are enhanced by four folds after 48hrs of treatment.

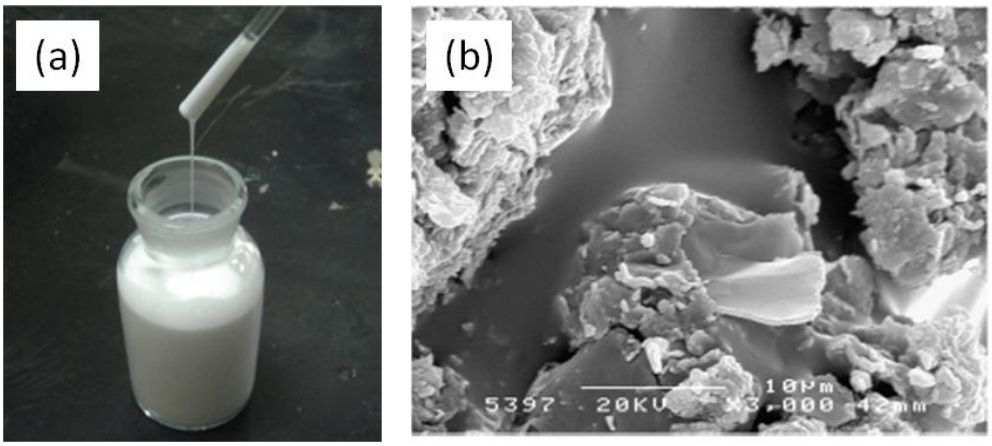

Figure 2.10 (a) The milky appearance of STW and (b) SEM picture of viscous membrane formed between soil particles (after Liu et al, 2011)

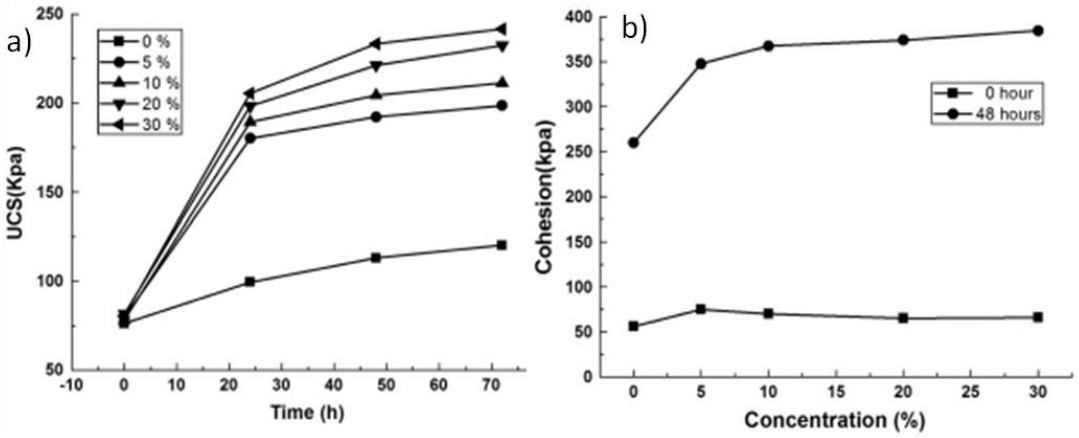

Figure 2.11 Improvement of (a) unconfined compression strength and (b) cohesion of soil sample mixed with polymer (after Liu et al., 2011)

2.2.4 Bioclogging

Clogging method in geotechnical engineering refers to filling the soil voids with grouts and thus controlling hydraulic conductivity of soil (Karol 2003). Chemical grouting was often used for this method. Suitable microorganisms may also be employed for the same purpose, through microbial growth and accumulation of cell bodies, production of slime in soil (also referred as biofilm), entrapment of gas, or production of undissolved inorganic sulphides/carbonate/ferrous matters (Baveye et al., 1998; Guo et al., 2013; Ivanov & Chu, 2008; Qian et al. 2009, 2010a, 2010b; Vandevivere and Baveye, 1992).

An overview of bioclogging method is shown in Table 2.2, including selection of microorganism group, mechanism of clogging, essential conditions for bioclogging,

and potential geotechnical applications (Ivanov & Chu, 2008). Bioclogging may be widely used for seepage control of the reservoir/drain channel, dike protection (by reducing piping effect), prevention of heavy metal/organic contaminant migration, etc., and repairing surface defects of cement-based materials.

The advantages and limitations described in biocementation also have effects in bioclogging. One additional problem is that the growth of clogging affects the transfer of nutrients and microbial metabolites; the growth of microorganism and the further formation of bioclogging may be inhibited (Ivanov and Chu 2008).

2.2.5 Bioremediation

Application of microorganisms in geoenvironmental engineering area has a much longer history and wider market than biocementation and bioclogging. Since the nature of microorganism metabolism process is to digest complex compounds and convert them to simpler compounds like water and carbon dioxide, microbes are used to remove unwanted pollutants from soil and water. This process is termed as bioremediation (Karol, 2003). Major inorganic contaminants that can be removed using microbial transformation include heavy metals, nitrogen and phosphorus, etc. The most well-known usage of bioremediation currently is the cleaning of oil spills (Mohamed and Antia, 1998).

In practice, bioremediation can be carried out *in situ* or *ex situ*. *In situ* treatment allows soils to be treated without excavation, but it needs longer time and prudent monitoring due to uncertain conditions in natural soil deposits. Examples of *in situ* treatment include enhanced microbial bioremediation, bioventing and phytoremediation. *Ex situ* treatment takes a shorter time and treating processes are easily controlled, but it leads to increased cost. Examples of *ex situ* treatment include landfarming, biopiling, composting and slurry bioreactors (Singh et al., 2009).

Table 2.2 Overview of bioclogging method (Ivanov & Chu, 2008)

Physiological group of microorganisms	Mechanism of bioclogging	Essential conditions for bioclogging	Potential geotechnical applications
Algae and cyanobacteria	Formation of impermeable layer of biomass	Light penetration and presence of nutrients	Reduce of water infiltration into slopes and control seepage
Aerobic and facultative anaerobic slime-producing bacteria	Production of slime in soil	Presence of oxygen and medium with ratio of C:N>20	Avoid cover for soil erosion control and slope protection
Oligotrophic microaerophilic bacteria	Production of slime in soil	Low concentration oxygen and medium with low concentration of carbon source	Reduce drain cannel erosion and control seepage
Nitrifying bacteria	Production of slime in soil	Presence of ammonium and oxygen in soil	Reduce drain channel erosion
Sulphate-reducing bacteria	Production of undissolved sulphides of metals	Anaerobic conditions: presence of sulphate and carbon source in soil	Form grout curtains to reduce the migration of heavy metals and organic pollutants
Ammonifying Bacteria	Formation of undissolved carbonates of metals in soil due to increase of pH and release of CO_2	Presence of urea and dissolved metal salt	Prevent piping of earth dams and dikes
Iron-reducing bacteria	Production of ferrous solution and precipitation of undissolved ferrous and ferric salts and hydroxides in soil	Anaerobic conditions: changed for aerobic conditions; presence of ferric minerals	Prevent piping of earth dams and dikes

2.2.6 Negative effects of microbial activities

Besides the beneficial application, microorganisms can also bring some negative effects in geotechnical construction. The most common microbial-mediated geotechnical problem so far is the foundation heave due to pyrite oxidation causing by sulfate reducing bacteria, which brought tremendous economic loss in Japan, England, etc. (Mitchell, 2005; Cripps et al., 1993). When the temperature in soil rises to be about 25°C or above, it facilitates the growth of sulfate reducing bacteria under an anaerobic condition and lead to the generation of H_2S. When the ground dries and permeable to air, H_2S is oxidized to H_2SO_4, leading to a decrease in pH. The reaction of H_2SO_4 with calcium carbonate forms gypsum, and with potassium and ferric ions forms jarosite. Both gypsum and jarosite causes foundation heave.

Furthermore, the environmental issues caused by bacterial treatment in soil including odour, the potential erosion of pipes because of the environmental pH changing, the reduction of flexibility and increase of brittleness in foundation, etc., are yet to be discovered and discussed.

2.3 Factors influencing MICP process mediated by UPB

MICP formation using UPB is focused in this section as it is the major methodology employing in this study. Many factors could influence the effectiveness of calcite formation, including productivity of UPB (which is represented by its urease activity), distribution and fixation of UPB, chemical concentration, retention time, original material properties (including size, textures, interaction with water, etc.), etc. The impacts are mainly presented by two factors, which are the variance of strength (for biocementation) and permeability (for bioclogging) in soil. The discussion is focused mainly on sandy material. Data published by Ng et al. (2014) on clayey soil will also be presented.

2.3.1 Urease activity of UPB

1. Optimization of UPB production

Many previous researchers found productivity of UPB, which is represented by its urease activity, is essential to MICP formation (Cheng, 2012; DeJong et al. 2006, DeJong et al., 2010; Whiffin et al., 2007). Many factors could affect the efficiency of UPB production, which will be presented below.

1.1 Overview of UPB strain and its production in previous researches

As presented in Section 2.2.3, *Sporosarcina pasteurii* is widely used in these studies, especially strain ATCC 11859, because of its halo-tolerant and alkali-philic characters (Bachmeier et al., 2002; Bang et al., 2001; DeJong et al., 2006; Ferris et al., 1996; Mitchell and Ferris, 2005; Mortensen and DeJong, 2011; Whiffin et al., 2007). Furthernore, it can produce high urease activity, not repressed by NH^{4+}, while being non-pathogenic (Whiffin, 2004). Urease activity of different strains of *S. pasteurii* used in these literatures varies from 5 to 20 mM urea/min (Harkes et al., 2010); 2.2 to 13.3 mM urea/min (Whiffin, 2004); average 11.3 mM urea/min (Cheng, 2012). Some other isolated Bacillus strains of UPB have urease activity varied from more than 3.3 mM urea/min (Al-Thawadi & Cord-Ruwisch, 2012); 8.3±0.1 mM urea/min for strain VS1, and 9.0±0.0 mM urea/min for stain VUK5 (Stabnikov et al., 2013).

The factors which could influence the production of UPB includes pH value, urea concentration, calcium concentration, temperature, etc (Ferris et al., 2003; Fujita et al., 2000; Stocks-Fischer et al., 1999; van Paassen, 2009; Whiffin, 2004). pH/urease activity vs. time in bacteria cultivation and long term urease activity in preserved UPB sample are shown in Fig. 2.12a and 2.12b respectively (Whiffin, 2004). As shown in Fig. 2.12a, pH value was observed to increase from 7 to 9 plus during the first 24 hrs of cultivation; urease activity and biomass of bacteria kept

increasing, yet the highest specific urease activity (urease activity/biomass) occurs at about 8 hrs. It has also been reported that increase in temperature up to 60°C results in increase in urease activity (van Paassen, 2009; Whiffin, 2004).

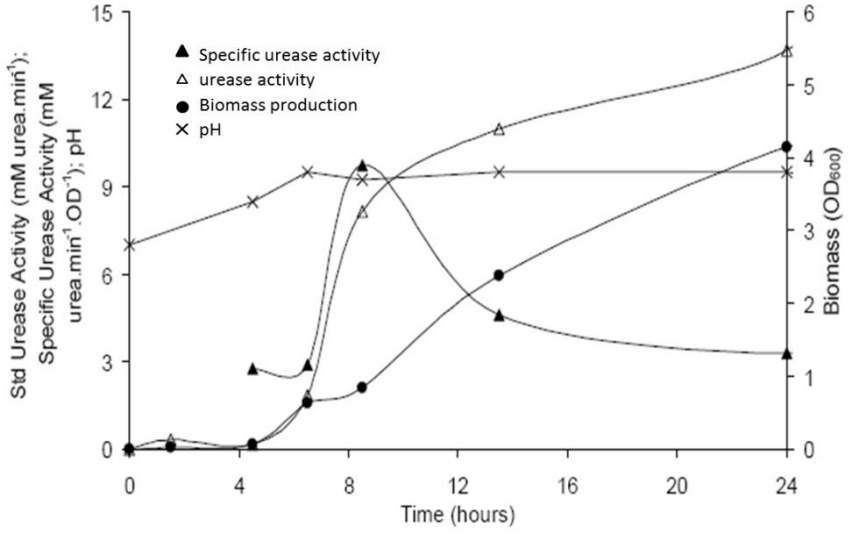

a)

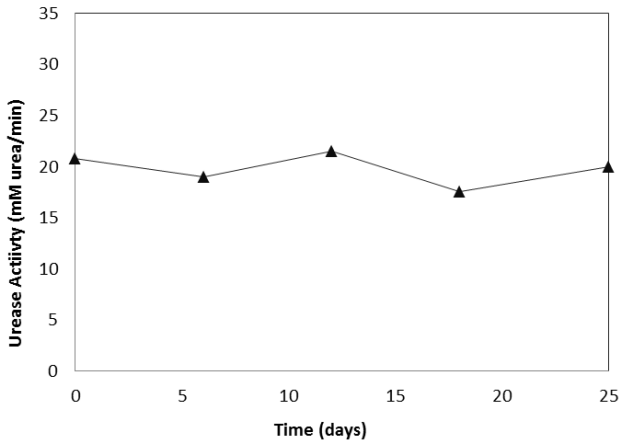

b)

Figure 2.12 Factors influencing urease activity of UPB strain *S. pasteurii*, a) pH value, b) time (after Whiffin, 2004)

1.2 Cultivation conditions of UPB strain VS1 (employed in this study)

The strain of urease producing bacteria used in this study is strain VS1. It is closest to the species *Bacillus*, and classified as spore-forming, gran-positive rods regarding to its morphology (Stabnikov et al., 2013). Cultivation parameters variation including biomass concentration, total urease activity and specific urease activity in one batch at 30˚C under aeration is shown below in Fig. 2.13. UPB

cultivation is optimized at around 48 hours according to biomass concentration and total urease activity; no obvious increase was found after that.

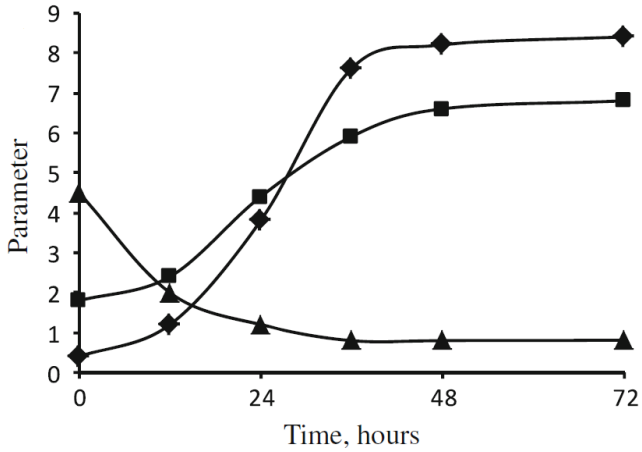

Figure 2.13 Parameter variation of UPB strain VS1 during 72 hours of cultivation: biomass concentration ((♦) g/L), total urease activity ((■) mM/min), and specific urease activity ((▲) mM/min/g biomass) (Stabnikov et al., 2013)

Cultivation method, i.e. pure cultivation or enrichment cultivation of bacteria also affects urease activity of UPB during large scale cultivation. As shown in Fig. 2.14 (after Stabnikov et al., 2013), it was found that urease activity of UPB strain VS1 produced by enrichment culture decreases up to 20 times after five times of transformation to fresh medium, which means the rate of elimination was about 5% per generation, as each cultivation batch included about four generation of UPB according to the bacterial growth curve. Such phenomenon might be explained by the changes of microbial diversity or genetic mutation within the enrichment culture.

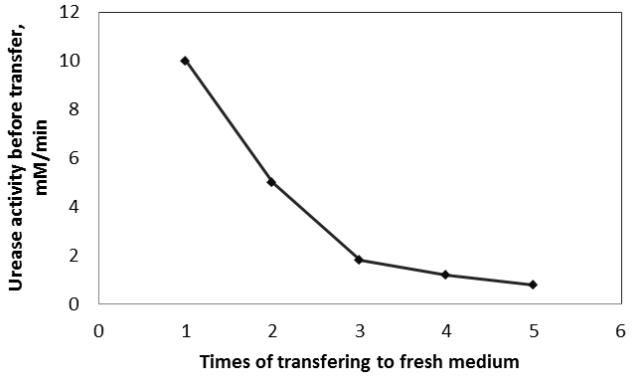

Figure 2.14 Decrease of urease activity after transfers to fresh medium of each batch for UPB strain VS1 (after Stabnikov et al., 2013)

2. Influence of chemical concentration on urease activity during cementation

Chemical concentration can also vary the UPB activity. Theoretically, the higher the amount of urea/calcium concentration, the more MICP would be formed. However, as the sensitivity of urease can be influenced by reactants (urea/calcium) and products (ammonium) of the biocementation process, a maximum urea/calcium concentration of 1.5M was found to produce the optimum amount of MICP by UPB strain *S. pasteurii* (Fig. 2.15, Whiffin, 2004). The value of pH variation (which is the main indicator of urease activity) in strain VS1 media containing different amount of $CaCl_2$ illustrates that activity of UPB strain VS 1 was inhibited in the presence of 2.5M calcium cation.

Moreover, the concentration of calcium cation itself could influence the both the bacteria activity and urease activity (Qian et al, 2009). As the surface of bacteria cells are usually negatively charged, rate of urease generation of UPB could be repressed by the present of calcium attaching to the bacteria cell, and rate of ureolysis by the enzyme urease could also decrease by the present of calcium in the solution. As shown in Fig. 2.16, higher Ca^{2+} concentration in the solution resulted in lower rate of urea decomposition by the UPB.

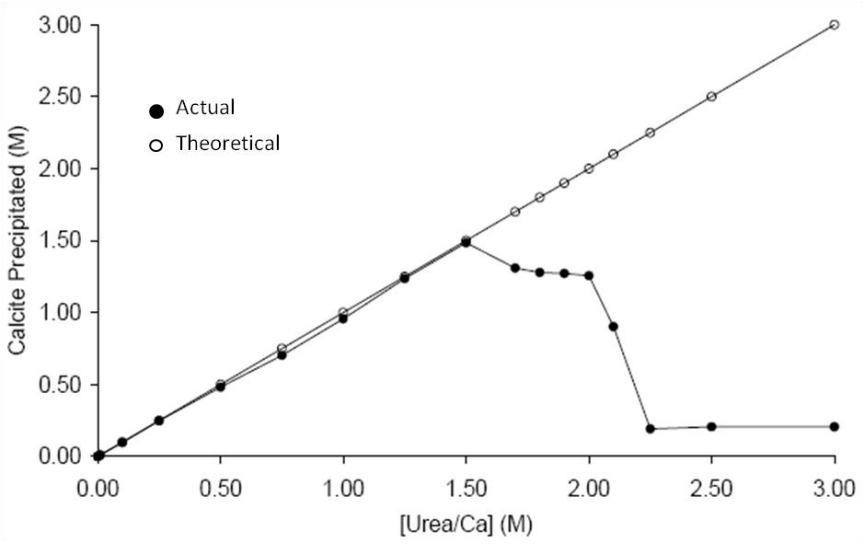

Figure 2.15 Actual and theoretical Urea/calcium concentration versus calcite precipitation employing UPB strain *S. pasteurii* (Whiffin, 2004)

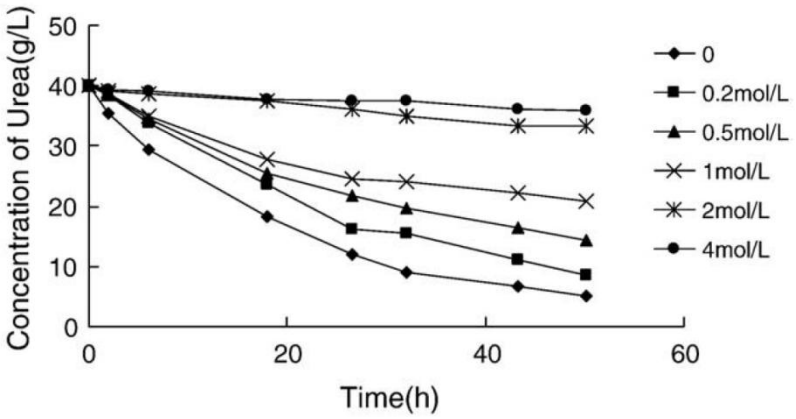

Figure 2.16 Rate of ureolysis by UPB with the presence of different concentrations of Ca^{2+} (after Qian et al., 2009)

3. Effect of urease activity on MICP process

Although urease activity is emphasized in UPB cultivation, it should be noted that the optimization of urease activity does not necessarily leading to the preeminent condition of MICP formation. Cheng & Cord-Ruwisch (2014) established a simple mathematical model to predict the amount of calcite precipitation presenting along the depth of a saturated sand column at different urea hydrolysis rate, i.e. different urease activity of bacteria, as shown in Fig 2.17.

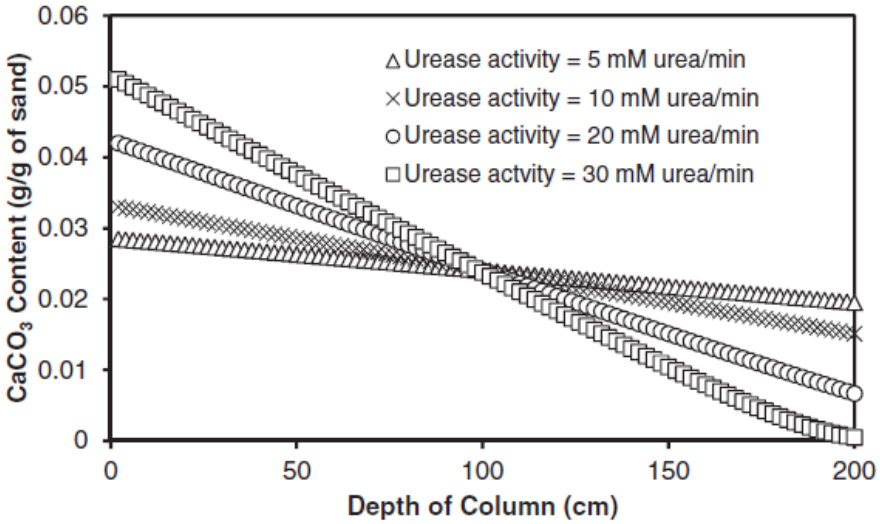

Figure 2.17 The amount of precipitated MICP as a function of depth under specified urease activities with constant infiltration rate as predicted using model described in Cheng & Cord-Ruwisch, 2014

For a fixed infiltration rate, the predicted homogeneity of the precipitated calcite distribution along the depth of a sample improves as the urease activity decreases. Therefore, using UPB with low activity could lead to a more uniform cementation within sand. Such observation, which is stronger MICP can be formed at lower urea hydrolysis rate was also made by Qian et al. (2009). Such assumption was also confirms by the results getting from other researchers (Fidaleo & Levecchia 2003; Martinez et al., 2013), in which the sets having lower urea-hydrolysis rate resulted in a more uniform MICP formation, providing other setting to be the same in control.

4. Effect of urease stored in cell and out of cell

Besides urease activity and chemical concentration, the location of urease also has impact on the MICP formation. According to Qian et al. (2010b), use of extracellular polymeric substances (EPS) isolated from bacteria cells inhibited MICP crystallization, as the organic molecules combined with calcium ions, which prevented calcium ion to participate in nucleation or react with carbonate ions to form MICP. On the other hand, bacterial cells could accelerate crystal nucleation, as their charged surface supply energy towards nucleation. Calcite crystal formed in EPS solution and solution of UPB cells are shown in Fig. 2.18a and 2.18b, which observed as global and cubic shape respectively. Such observation indicated that UPB cells acted as nucleation site during MICP formation.

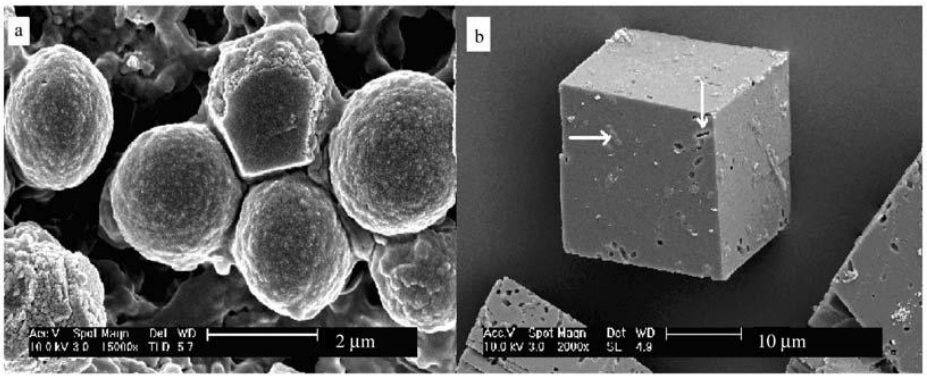

Figure 2.18 SEM images of calcite crystal forms in a) EPS solution and b) UPB cells

solution (Bacterial cells embedded are marked with white arrows in 2.18b) (Qian et al. 2010b)

5. Ureolysis under anaerobic condition

Most of the UPB strains are believed to be aerobic. Their growth and performance are assumed to be inhabited without the presence of oxygen. Parks (2009) performed experiments on ureolysis rate of *S. pasteuriin* under both aerobic and anaerobic condition. Remaining urea molecule and calcium concentration over time in anaerobic medium in one of her experiment is shown below in Fig. 2.19. The decreased concentration of both parameters proved its capability of ureolysis without the presence of oxygen. It was found that the rate of ureolysis in anaerobic was similar with that under aerobic condition when calcium is inclusive in the media yet no external electron acceptor offered. However, the growth of UPB in an anaerobic environment could not be confirmed.

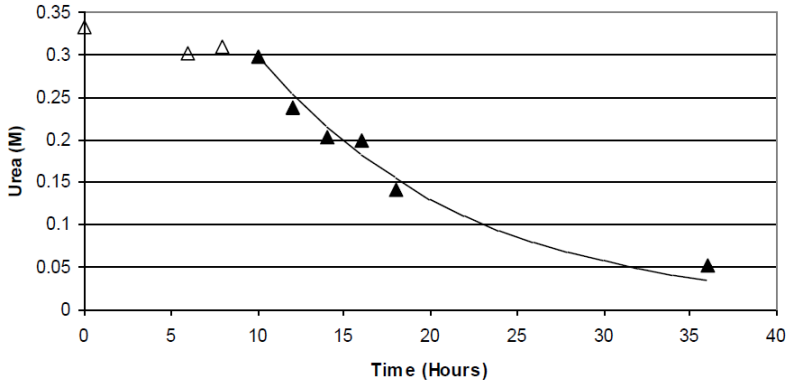

a)

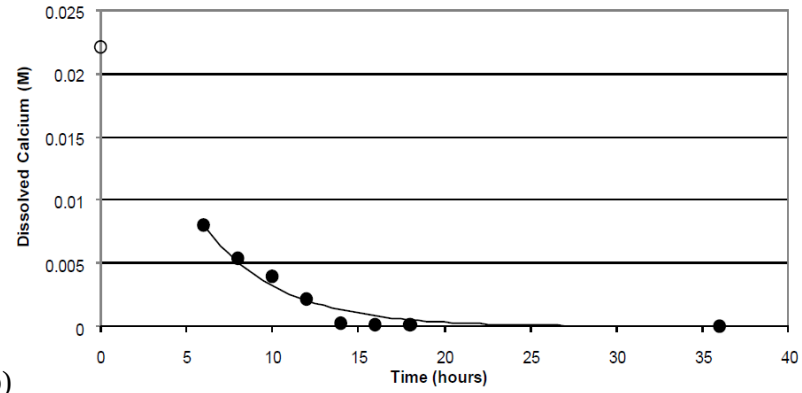

b)

Figure 2.19 One set of experiment data for *S. pasteurii* in anaerobic medium; a) urea, b) dissolved calcium concentration (Parks, 2009)

2.3.2 Effect of chemical concentration in cementation solutions

Chemical concentration of cementation solution, i.e. the amount of urea and calcium chloride added, may influence the formation of MICP through influencing the calcite crystal size and through varying UPB activity.

1. Influence of total chemical concentration on crystal formation

MICP formation depends partially on the chemical concentration of the cementation solution through pattern of crystal formation. Al Qabany & Soga (2013) indicated that low chemical concentration (as low as 0.1M $CaCl_2$/urea) resulted in a higher increase of treated sand strength. Unconfined compression strength versus calcite content of samples going through 0.1M/0.25M/0.5M/1M chemical concentration treatment respectively are drawn in Fig. 2.20; samples going through lower chemical concentration shows a certain level of advantage in UC strength enhancement under the same calcite content.

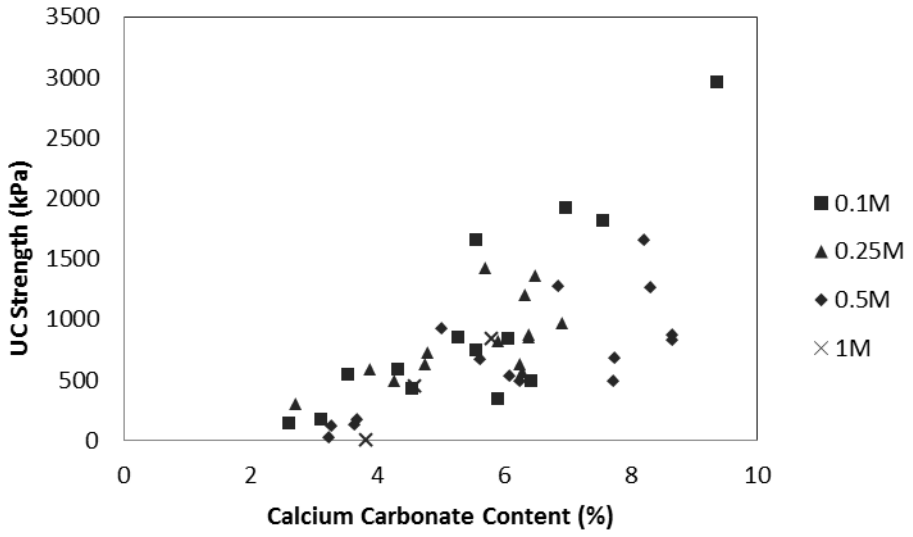

Figure 2.20 Unconfined compression strength versus calcite content for samples going through 0.1M/0.25 M/0.5M/1M chemical concentration treatment (after Al Qabany & Soga, 2013)

It is assumed by Al Qabany & Soga (2013) that a solution with a lower chemical concentration produces smaller crystal particles and ensures more uniform precipitation pattern. SEM images (Fig. 2.21) confirm that hypothesis, in which larger crystal particles were appeared in solution with 0.25M, 0.5M to 1M chemical concentration progressively. However, it should be noted that the operation cost would increase as higher volume of fluid is required to be injected into the field when applying lower chemical concentration solution.

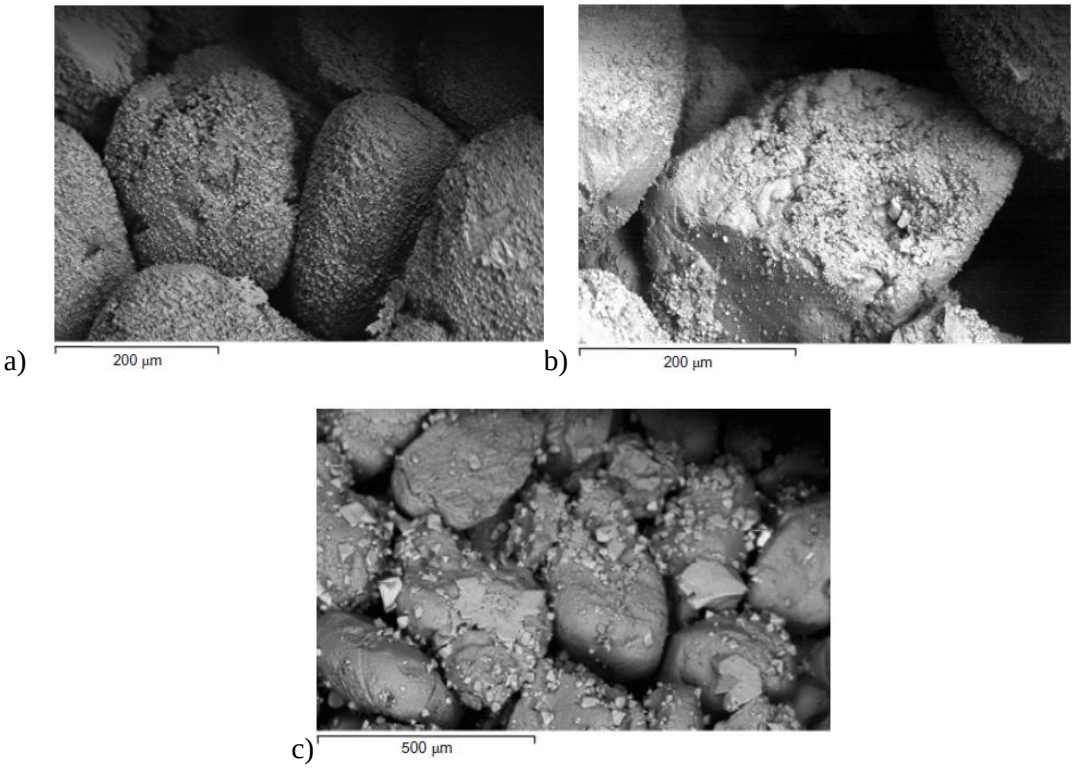

Figure 2.21 SEM images of samples going through: (a) 0.25 M; (b) 0.5 M; (c) 1 M $CaCl_2$/urea concentration (Al Qabany & Soga, 2013)

Similar conclusion was made by Muynck et al. (2010), in which an upper limit of calcium/urea dosage was observed for UPB treatment of lime stone regarding the consolidating effect; no improvement was found at higher dosage. However, such a conclusion could not be extended in permeability reduction, as higher calcium/urea dosage always resulted in lower water absorption (Al Qabany & Soga, 2013). It should be noted that calcium/urea ratio of 1:2.5 was adopted in this study rather than 1:1 as in Al Qabany & Soga (2013).

2. Urea to calcium ratio

Besides total concentration, the ratio of calcium to urea is another factor affecting the MICP process. Simulation of urease activity during biocementation with varying calcium/urea concentration is presented in Fig. 2.22 (Whiffin, 2004). It can be observed that increasing urea concentration while keeping calcium concentration constant resulted in a large increase of urease activity (Fig. 2.22a). On the other hand, doubling calcium content did not show effectiveness as high (Fig. 2.22b). Such a phenomenon might be attributed to higher diffusion of urea into UPB cell (as urea molecular is fairly small) and resulted in a higher concentration gradient. To conclude, the rate of urease activity is largely dependent on the calcium to urea ratio. Therefore, increasing urea concentration might be a solution at where the urease activity of UPB is too low to fulfill the required biocementation effect.

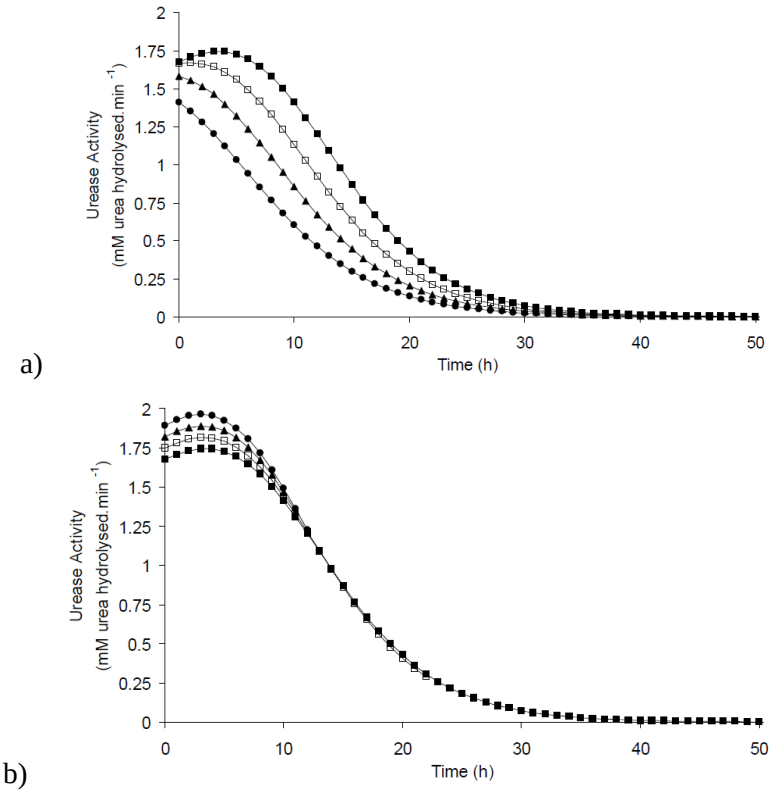

Figure 2.22 Simulated urease activity vs. time with a) 1.5M calcium and varies urea concentration (0.75(●), 1.0 (▲), 1.25 (□) and 1.5 (■)), and b) 1.5M urea and varies calcium concentration (0.75(●), 1.0 (▲), 1.25 (□) and 1.5 (■)) (Whiffin, 2004)

The result getting from Martinez et al. (2013) endorsed this assumption, that higher urea to calcium ratio is favorable in MICP precipitation. Variation of urea molecule, ammonium/calcium cations, and pH values monitored during two sets of biocementation, which engaged calcium to urea ratio of 1:3 and 1:1, are shown in Fig. 2.23a and 2.23b respectively.

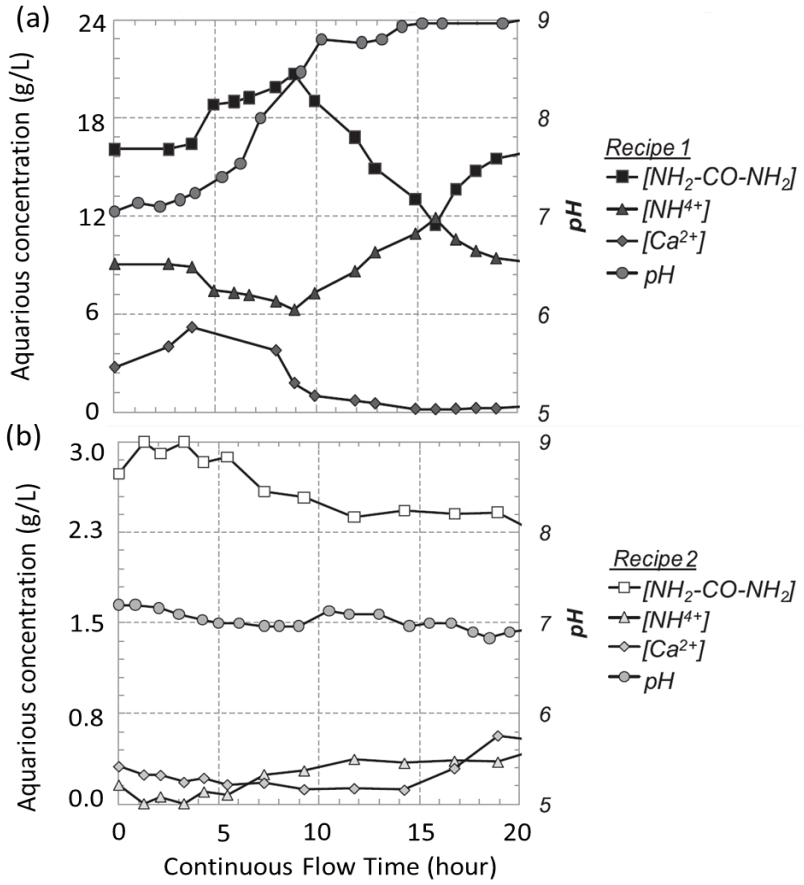

Figure 2.23 Variation of urea molecule, ammonium/calcium cations, and pH value monitored in biocementation solution containing calcium to urea ratio of a) 1:3, and b) 1:1 (after Martinez et al., 2013)

It could be observed that the consumption rate of calcium cations and urea were much higher in calcium to urea ratio of 1:3 set (Recipe 1, Fig. 2.23a) comparing to 1:1 set (Recipe 2, Fig. 2.23b). Furthermore, value of pH, which is considered to be indicator of microbial activity, kept increasing from 7 to 9 during the cementation process in the 1:3 set while maintained to be around 7 in the 1:1 set. Therefore, it is advised to use calcium to urea ratio lower than 1:1 in practice. Moreover, as urea is

relatively cheaper comparing to the calcium resources available, it is also more economical to increase the dosage of urea rather than calcium. However, lowering the proportion of urea can reduce the unfavorable by-products like ammonium on the other hand. Balance should be kept based on the two effects while making the decision on calcium to urea ratio.

2.3.3 UPB distribution and fixation

The crucial factor of accomplishing a uniform MICP formation is the even distribution of bacteria (Martinez et al., 2013). Transportation of UPB within sand is depended on many factors, such as properties of material-to-be-treated (surface texture, grain size distribution, mineralogy of sand); bacteria properties (cell wall charge and appendages); fluid properties (chemical composition, viscosity), et al. (Foppen & Schijven, 2005; Gilbert et al., 1991; Torkzaban et al., 2008). It is now well known that the use of fixation solution with high salinity after applying UPB can increase the absorption of bacteria by reducing electrostatic repulsion of bacteria and immobilizing it (Whiffin et al., 2007; Harkes et al., 2010).

Fig. 2.24a (Harkes et al., 2010) shows the activity of effluent treated with different composition of fixation solution, including 50mM $CaCl_2$, 9g/L NaCl, fresh surface water and deionized water. All fixation solution except deionized water were acceptable in practice, in which less than 30% activity being flushed out; in deionized water group, nearly all bacteria activity had been washed out.

Another observation made by them is that diluting of bacteria suspension may cause the urease enzyme to be released into solution from UPB cell, even though high salinity solution (which is 9g/L NaCl solution in this practice) is supposed to prevent the osmotic shock experiencing by the bacteria. Fig. 2.24b shows the normalized OD/activity of effluent flowing out from sand column after flushing with original UPB and UPB diluted 10 times with 9g/L NaCl respectively. Both sand columns were flushed by a following fixation solution (50mM $CaCl_2$). A

significant part of urease activity had been flushed out within effluent for diluted UPB. On the contrary, it can be assumed that high salinity and high bacteria concentration can increase the adsorption and filtration of bacteria, resulting in higher effectiveness of UPB activity in sand.

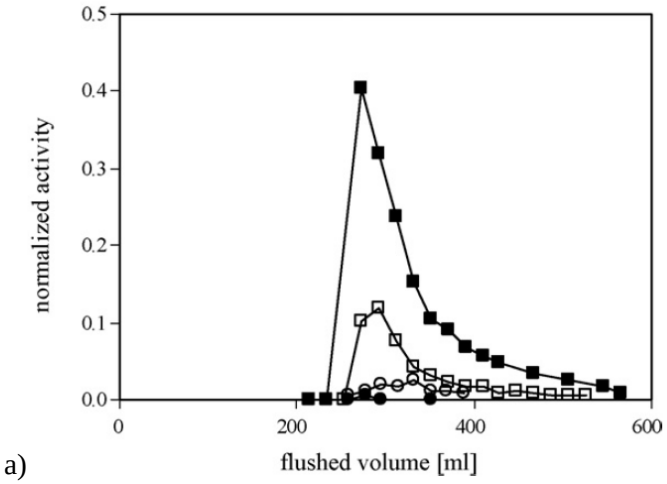

a)

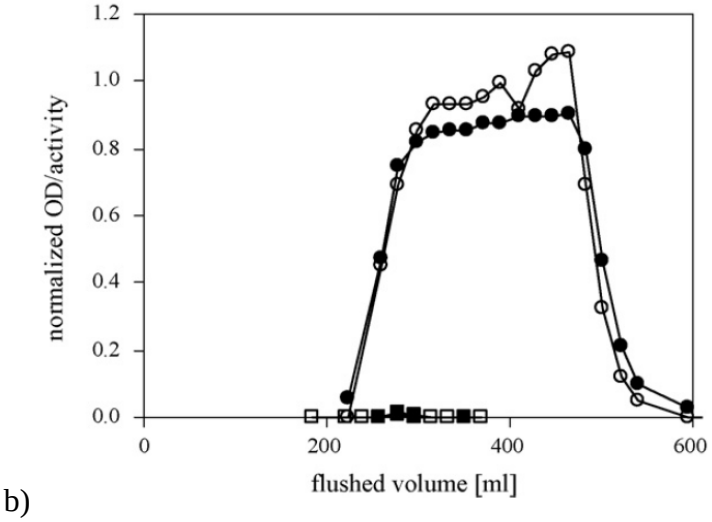

b)

Figure 2.24 Effluent measurements for a) column engaging fixation solution of 50mM $CaCl_2$ (●), deionized water (■), surface water (□), and 9 g/l NaCl (○), and b) two columns flushed with diluted bacterial suspension (OD (●), activity (○)) and undiluted suspension (OD (■), activity (□)) (Harkes et al., 2010)

Retention time is another factor related to bacteria fixation. Recirculation of bacteria resulted in a greater retention of bacteria. Conversely, long retention time (over 62 hours) of bacteria suspension would result in depletion of urea (its nutrition) and the resulting detachment of bacteria from sand surface (Martinez et al., 2013).

2.3.4 Flow rate and direction

Flow rate of bacteria suspension and cementation solution should be treated differently. Martinez et al. (2013) suggested a lower flow rate or stopped flow for bacteria suspension, as higher flow rate resulted in lower bacteria retention, i.e. more bacteria could be flush out with high flow rate of bacterial suspension. However, cementation efficiency may not be necessarily lowered along with low bacteria retention, as long as cementation time is long enough for chemicals to be reacted.

The preferred infiltration rate of cementation solution is controversial. The input rates of some experiments and their efficiency published in the literature are shown in Table 2.3 (after Al Qabany et al., 2012). According to Al Qabany (2012), doubling the input rate of cementation solution (from 0.042 to 0.084mol/L/h) leaded to nearly 50% reduction of cementation efficiency, regardless of its concentration. The results of DeJong et al. (2006), Rebata-Landa (2007) and Whiffin et al. (2007) show that cementation efficiency was similar when different flow rate up to 0.042 mol/L/h at diverse cementation solution concentration (from 0.1 to 1.1 M) were used. An upper limit of cementation flow rate (which is 0.042mol/L/h in this case) might then be concluded, under which the cementation efficiency could be guaranteed.

Table 2.3 Input rates of cementation solution in the literature (modified after Al Qabany et al., 2012)

	DeJong et al. (2006)	Rebata-Landa (2007)	Whiffin et al. (2007)	Al Qabany et al. (2012)	
Infiltration rate (mol/L/h)	0.0025	0.042	0.0088	0.042	0.084
Concentration (M)	0.1	0.25	1.1	0.1/0.25/0.5	
Efficiency (%)	92	95	88	>90	50

However, high infiltration rate of cementation solution might be preferred in large scale treatment. Cheng & Cord-Ruwisch (2014) proposed a model to predict the trend of cementation in depth cording to different filtration rate, as shown in Fig. 2.25. Higher infiltration rate of cementation solution resulted in a more homogeneous cementation while the lowest infiltration rate only allows partial cementation because of the clogging effect.

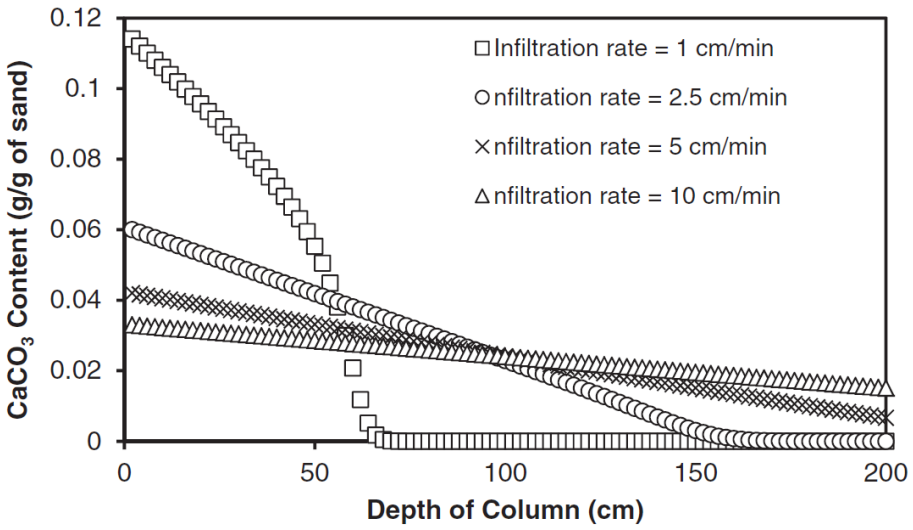

Figure 2.25 Calculated MICP content vs. depth at variance infiltration rates with constant urease activity of 20 mM urea/min (Cheng & Cord-Ruwisch, 2014)

Opposite flow direction of bacterial and cementation solution is preferred to achieve a more uniform cementation, as plugging effect near the injection source might be alleviated (Martinez et al., 2013). However, it might not be practical for the application *in situ*.

2.3.5 Large-scale biocementation experiment in sand

van Paassen et al. (2010) established a large scale sand biocementation experiment with 100 m^3 in volume. Poorly graded fine to medium sand was filled into a concrete container with dimensions of 8.0×5.6×2.5m. Three injection and three extraction wells each separated by 1 meter interval were installed along the longitudinal direction (x-direction) of the container. The wells were made of 300mm diameter PVC tubes, wrapped with geotextile. Top view of the

experimental setup with expected flow field is shown in Fig. 2.26. The expected distribution of reagents is presented in grey area.

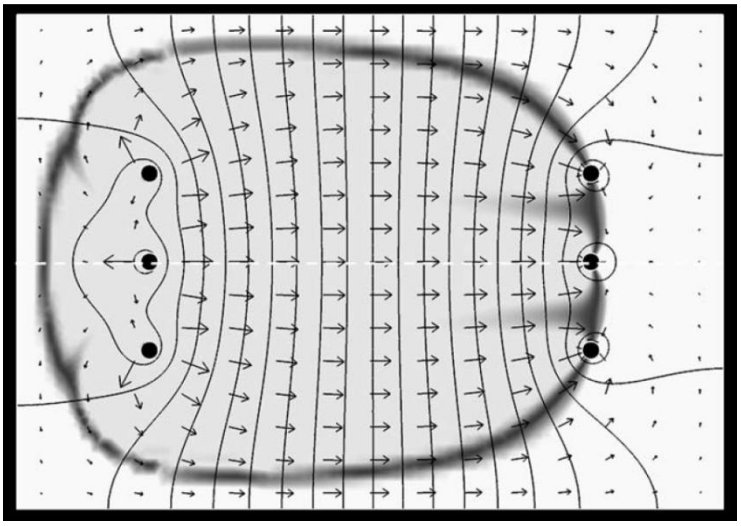

Figure 2.26 Top view with flow field of the setup for 100m^3 sand biocementation experiment (van Passen et al, 2010)

Sporosarcina pasteurii with urease activity of 1.1mol urea/L/hour was employed in the treatment. 5m^3 of bacterial solution followed by 5m^3 of fixation solution with 0.05M $CaCl_2$ were injected through the injection wells and pumped out from the extraction wells. 96m^3 of reagent solution containing 1M $CaCl_2$ and urea was then injected by ten batches. Tap water was used for rinsing the sample after treatment.

Figure 2.27 Remaining of the sand body (≈40m^3) after treatment (van Paassen et al, 2010)

The cemented sand body after treatment is shown in Fig. 2.27. Around 40m^3 out of 100 m^3 of sand volume retained a consolidated shape. It was observed that no cementation had taken place above the phreatic surface. Also, that there was cementation taken place around the corner indicated that the cementation was restricted by the flow field of reagent solution.

The $CaCO_3$ content of cross section along the longitudinal direction is shown below in Fig. 2.28, which varied from 0.8 to 24% by sand weight. The $CaCO_3$ content was lower around the injection point due to the high velocity of flow and thus the disturbance caused. Mean $CaCO_3$ content obtained was 6.8%, i.e. 110 kg/m^3, which made the cementation efficiency to be around 50% regarding to calcium supply. It might be seen that though the treatment was successful, there was still room for the cementation efficiency to be improved.

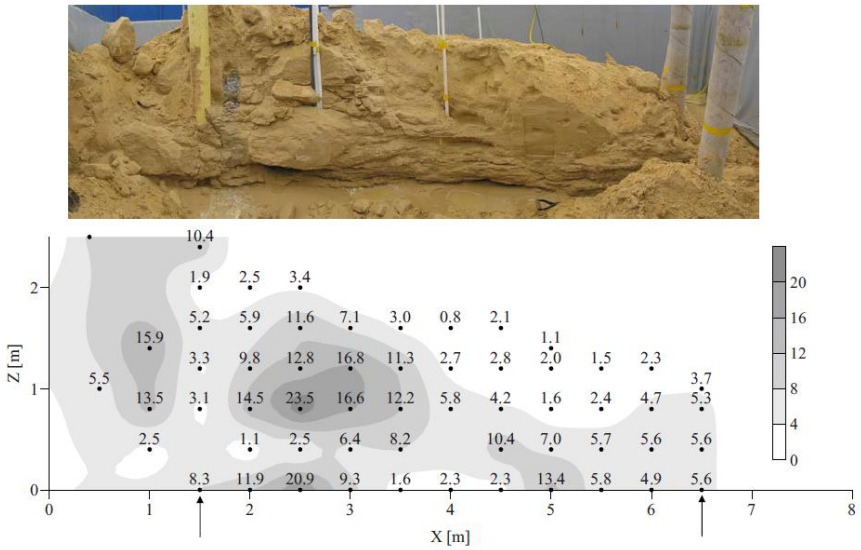

Figure 2.28 $CaCO_3$ content (w/w, %) of cross section along the longitudinal direction of the treated sand (van Paassen et al., 2010)

2.3.6 Summary of calcite content vs. UC strength relationship in sand

Strength of MICP formed by submersed treatment method

Most of the current research of MICP employed the treatment by submersed flow, i.e. biocementation was processed in a fully saturated condition during treatment

((Al Qabany,et al., 2012; Al Qabany & Soga, 2013; DeJong et al., 2006; Stabnikov et al., 2013; Whiffin et al., 2007; van Paassen, 2009; van Paassen et al., 2009, 2010). Calcite content vs. UC strength by MICP in some literatures is summarized in Fig. 2.29 below, along with some Portland cement mixed soil samples (Ismail et al., 2002; Muhunthan & Sariosseiri, 2008), and iron-based cemented soil samples (Ivanov et al., 2010). In Ismail et al. (2002), the Aberdeen soil refers to fine sand with D_{50} = 0.6mm, and Everett soil contains to clayey sized particles with D_{50} = 0.02mm. Number "0.1M" etc. in Al Qabany & Soga (2013) refers to the chemical concentration in cementation solution. Noted that the calcite content data reported by van Paassen (2009) and Whiffin et al. (2007) were in the form of kg/m^3 calcium carbonate; an average bulk density of sand 1800kg/m^3 was employed to convert the data in the former case; for data presented in van Paassen (2009), conversion were made based on the maximum calcite content indicated in the paper.

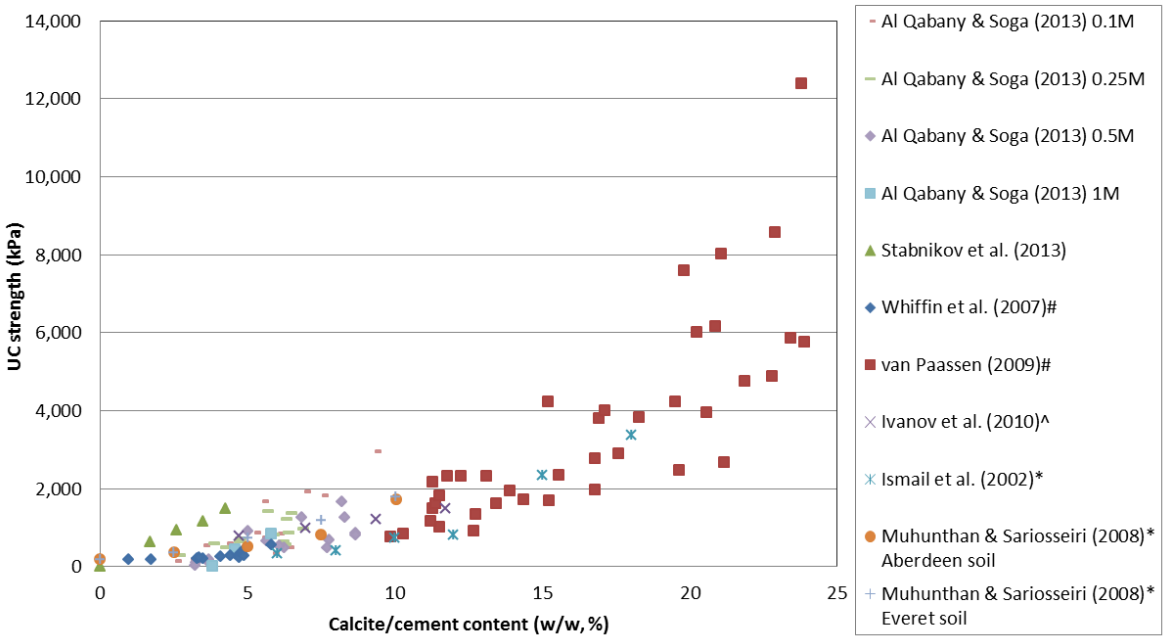

Figure 2.29 Calcite content vs. UC strength of soil cemented by MICP and other binders in literature (*by Portland cement; ^ by iron based grout; # converted from calcite content reported in kg/m^3)

Positive relationship between calcite content and UC strength was observed in all of these tests; data obtained by MICP formation also fall in the same range with

the ones acquired by iron based biocemented and cement mixed samples, which confirms that the calcite crystal acted as binder between soil particles to provide strength.

MICP by surface percolation method

Depending on the techniques applied, strength and calcium content may not be necessarily positively correlated. Besides of traditional submersed flow method as discussed in last section, a method namely surface percolation, which allows free drainage and unsaturated condition within sand samples during treatment was developed (Cheng, 2012; Cheng & Cord-Ruwisch, 2014).

Local strength obtained by Schmidt hammer and calcite content for percolation method and submersed treatment are shown in Fig. 2.30a and 2.30b respectively (Cheng, 2012). On the contrary of the submersed treatment, in which the local strength is positively correlated to the calcite content, and the highest calcite/local strength occurred at the top and bottom of the treated sand column (Fig. 2.30b), surface percolation treatment resulted in no correlation between those two parameters. Despite of its low calcite content, higher local strength was obtained in unsaturated zone at top part of the sand column; uniform local strength was also observed for surface percolation treated column (Fig. 2.30a). Converted calcite content vs. local strength of both methods are shown in Fig. 2.31. It could be observed that the local strength getting from surface percolation method generally maintained at the same level (and had higher value than in submersed method) regardless of its calcite content, rather than increased along with calcite content for submersed method as shown in Fig. 2.29.

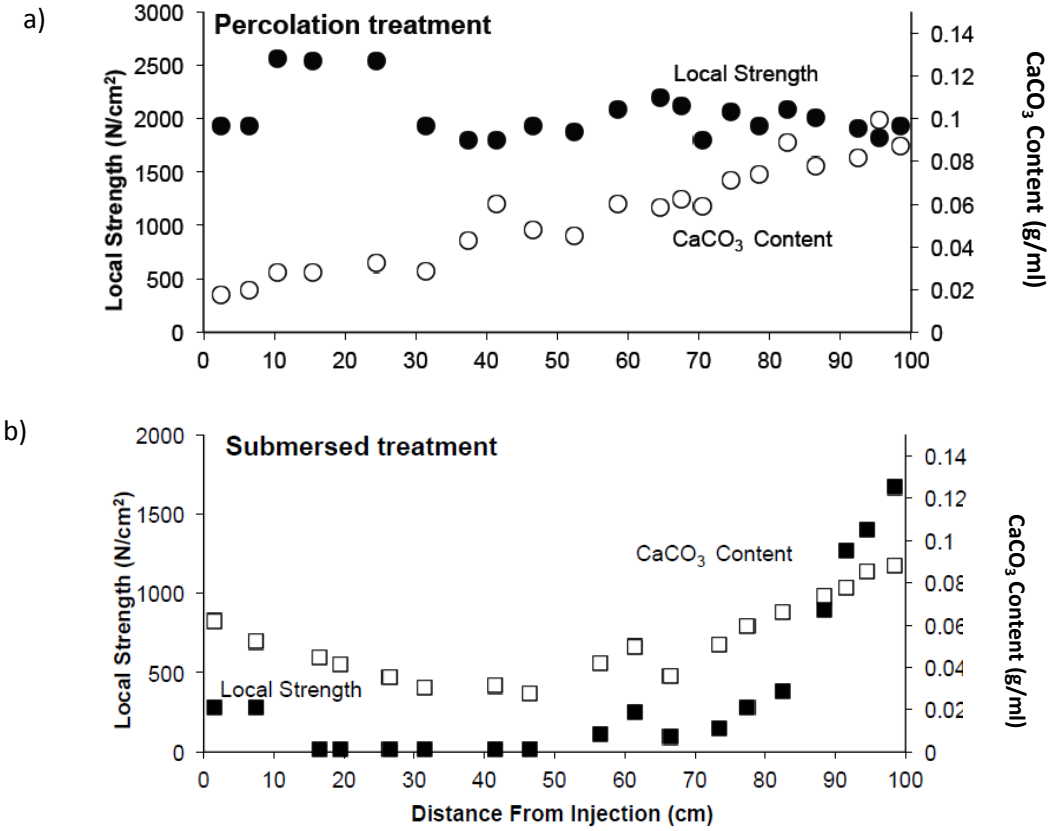

Figure 2.30 Profiles of calcite content and local strength and consolidated sand columns treated by the surface percolation (a) and submersed flow methods (b) (Cheng, 2012)

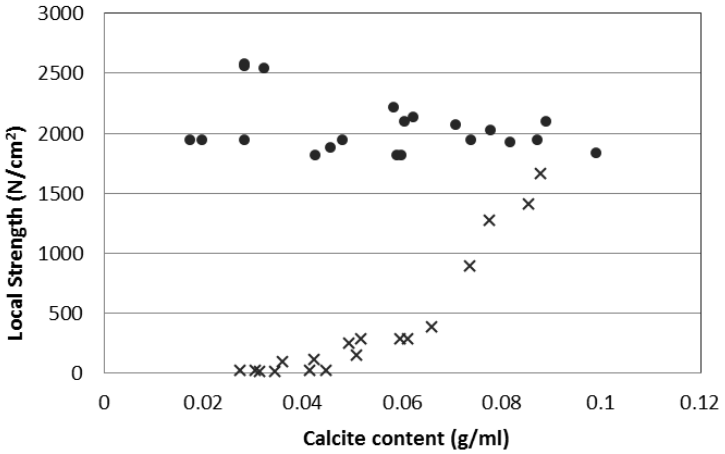

Figure 2.31 Calcite content vs. local strength from surface percolation method (●) and submersed method (×) as presented in Fig. 2.30 (after Cheng, 2012)

It was argued by Cheng (2012) that for the top of the percolated column, i.e. the unsaturated zone, MICP forms exactly between sand grains and performed as bridge, at where the menisci were saturated. On the contrary, at fully saturated bottom part, most calcite crystal precipitated on surface of the sand grain instead of

acting as binder, thus reduced the effectiveness of MICP. The SEM pictures show in Fig. 2.32 confirms this hypothesis, at where 80% of MICP forms as bridge crystals for top zone (Fig. 2.32A), while only 10% for bottom zone (Fig. 2.32B) within the column. Noted that this surface percolation method was proved to be working better in coarse sand compared to fine sand, as pore was blocked more easily at injection point for fine sand. However, it should also be noted that Schmidt hammer is usually employed in measuring strength of harder material like concrete or rock rather than soil; the "local strength" indicated in Fig. 2.30 and 2.31 may not be accurate.

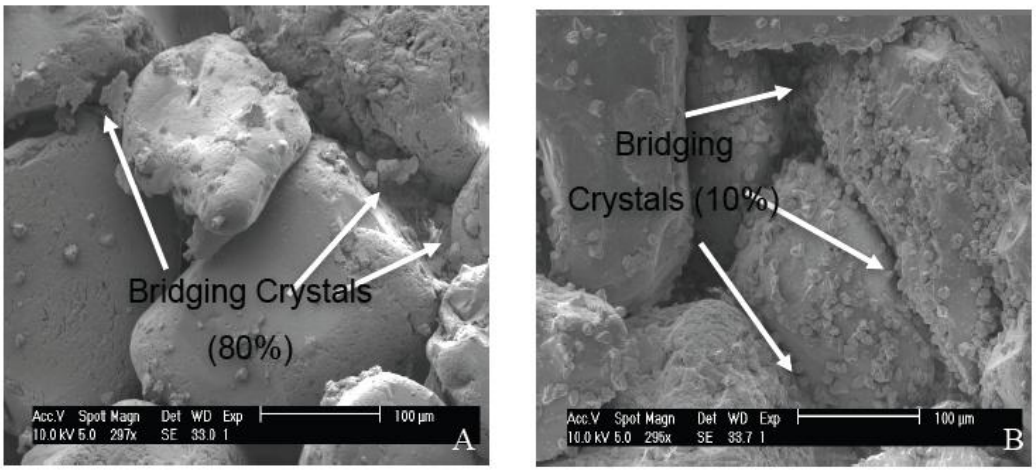

Figure 2.32 SEM images of cemented sand samples taken from top (A) and bottom (B) of the percolated column (Cheng, 2012)

2.3.7 Summary of calcium content vs. permeability in sand

For different project, soil with different permeability may be required. For example, lower permeability is preferred for sand dyke or pond construction. On the other hand, because plugging near injection point caused by low permeability could result in local cementation and preventing the further transfer of bacteria and cementation solution, higher permeability is usually preferred in MICP process for strength improvement, especially in large scale treatment. Cementation solution is also self-adjustable; when the voids were filled by calcite, flow rate would be higher, and force the solution to travel further (Martinez et al., 2013).

In general, permeability is lowered with higher calcite content as more voids are plugged. Summary of calcium content vs. permeability in literature is listed in Fig. 2.33. Number "0.1M" etc. in Al Qabany & Soga (2013) refers to the chemical concentration in cementation solution, while "RD" refers to relative density of sand sample before treatment. Noted that the calcite content data reported by Whiffin et al. (2007) were in the form of kg/m^3 calcium carbonate; an average bulk density of sand 1800kg/m^3 was employed to convert the data.

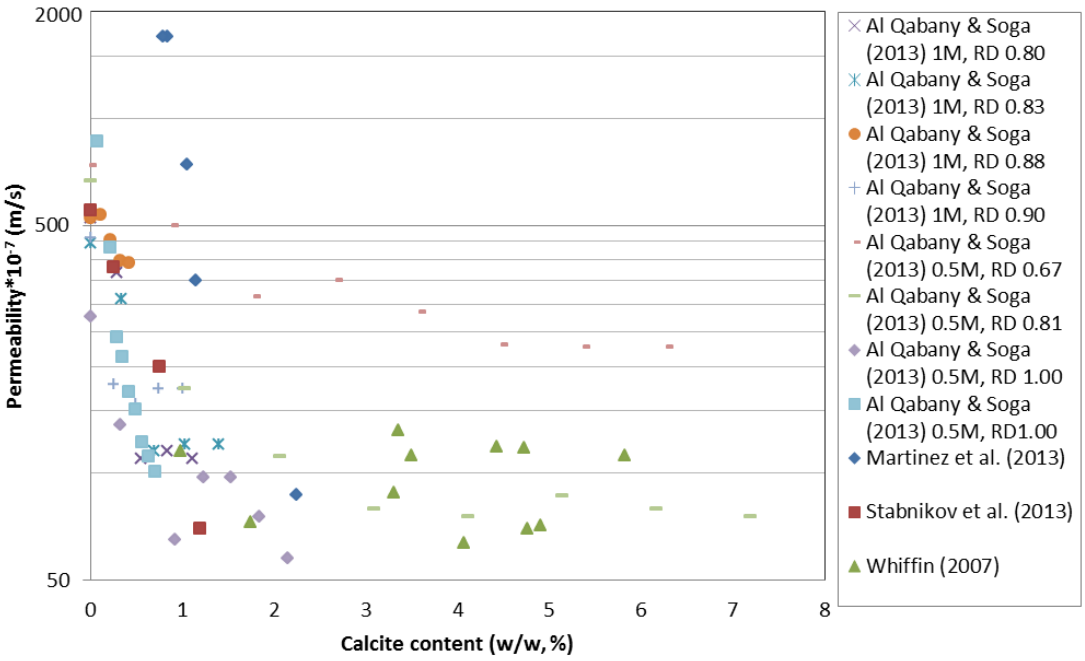

Figure 2.33 Calcite content vs. permeability of soil cemented by MICP in literature (*converted from calcite content reported in kg/m^3)

2.3.8 MICP application on residual soil

Ng et al. (2014) reports a series of experimental tests conducted to investigate the application of MICP on residual soil. Air dried soils were mixed with UPB and compacted into the mold. Cementation solutions containing different concentration of cementation chemicals $CaCl_2$ and urea were then introduced into soil sample by air compressor.

Calcite crystal and bonding between soil particles was observed. The SEM picture

is shown in Fig. 2.34. Resulted UC strength and conductivity versus calcite contents of residual soils after treatment are shown in Fig. 2.35. UC strength increased up to two times comparing to it of the untreated specimens, which was linearly proportional with calcite content of specimen. The reduction of hydraulic conductivity was also proportional to calcite content. The greatest improvement in reduction of hydraulic conductivity achieved was 90%.

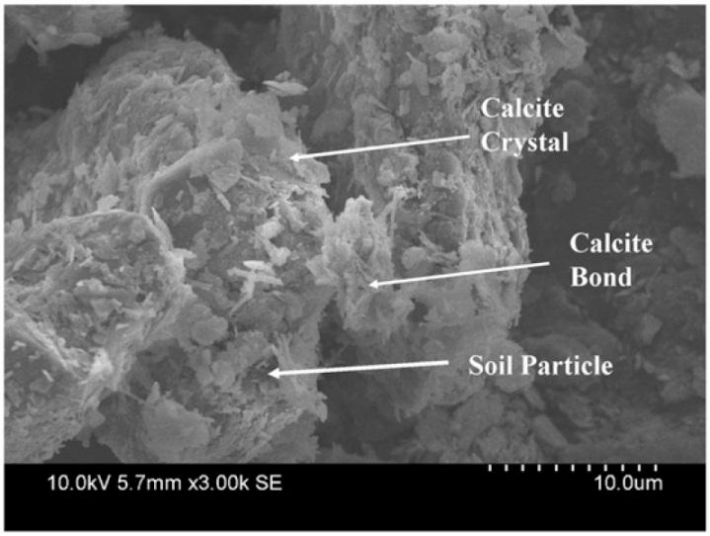

Figure 2.34 SEM images of the specimen treated with 0.5M cementation reagent (Ng et al., 2014)

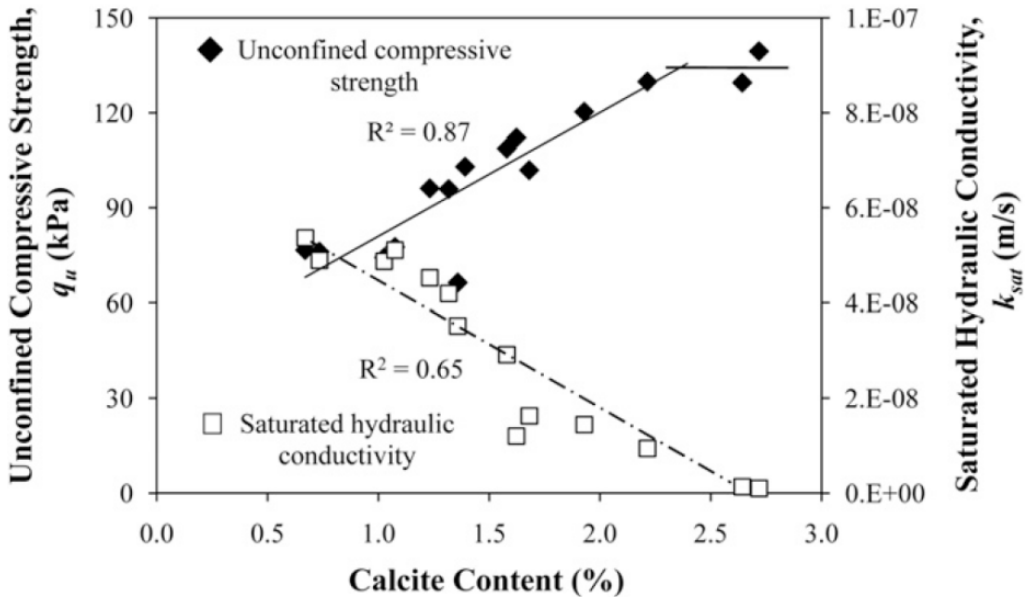

Figure 2.35 Correlations between the UC strength and saturated hydraulic conductivity versus calcite content in MICP treated residual soil (Ng et al., 2014)

2.4 Engineering properties of soil

2.4.1 Critical state soil mechanics

Unlike other civil engineering materials, the shear strength of a soil is not only a function of the material and the stress applied, but also a function of how was the stress applied; i.e. the stress-strain behavior of soil is path dependent. More advanced understanding of soil behavior undergoing shearing led to many other failure models developed. First attempt to relate volume change behavior, specimen density and confining pressuring during shearing was introduced by Casagrande in 1930's. Several constitutive models have been proposed afterwards. These include the Drucker-Prager model, Duncan-Chang or Hyperbolic model, and Cam Clay model. Each has its advantages and limitations (Brinkgreve, 2005).

Cam clay model was the first elasto-plastic model developed for saturated clay based on the critical state soil mechanics (CSSM) (Roscoe et al., 1958). As the stress-strain behavior of soil is path dependent, a path independent state is needed as a common reference state in constitutive modeling. Critical state is one of such a common reference state, referred to as the ultimate state where a soil element will continue to deform under a constant stress and volume condition. There is then a need to define new state parameters for critical state that is independent of arbitrary choice of orientation, as the traditional σ_{ij} and ε_{ij} are depended on the orientation of the reference axes as well as on the state of stress. Based on such criterion, mean effective stress p′, deviator stress q, volumetric strain ε_v and shear distortions ε_s are defined as stress and strain invariants. Under 2-Dimentional condition, i.e., axisymmetric condition, where $\sigma'_2 = \sigma'_3$, the stress and strain invariant can be expressed as:

$$p' = (\sigma'_1 + 2\sigma'_3)/3 \qquad \text{(Eqn. 2.2)}$$

$$q = \sigma'_1 - \sigma'_3 \qquad \text{(Eqn. 2.3)}$$

$$\varepsilon_v = \varepsilon_1 + 2\,\varepsilon_3 \qquad \text{(Eqn. 2.4)}$$

$$\varepsilon_s = 2(\varepsilon_1 - 2\,\varepsilon_3)/3 \qquad \text{(Eqn. 2.5)}$$

Thus, the work done in the deformation process can be calculated as $qd\varepsilon_s + p'd\varepsilon_v$. Mathematically, critical state can be defined as:

$$\frac{\partial p'}{\partial \varepsilon_s} = \frac{\partial q}{\partial \varepsilon_s} = \frac{\partial \varepsilon_v}{\partial \varepsilon_s} = 0 \qquad \text{(Eqn. 2.6)}$$

The final failure states of both drained and undrained tests fall on a critical state line (CSL). For a given soil, the CSL is unique; it is independent of the stress paths and initial state of soil, i.e. density and initial stress states (Atkinson & Bransby, 1982).

Typical effective stress paths on q-p′ space for consolidated undrained test on normally consolidated and overconsolidated clay are shown in Fig. 2.36. Soils reach to CSL eventually through different stress paths, by including negative or positive pore water pressure for overconsolidated clay/dense sand and normal consolidated clay/loose sand respectively.

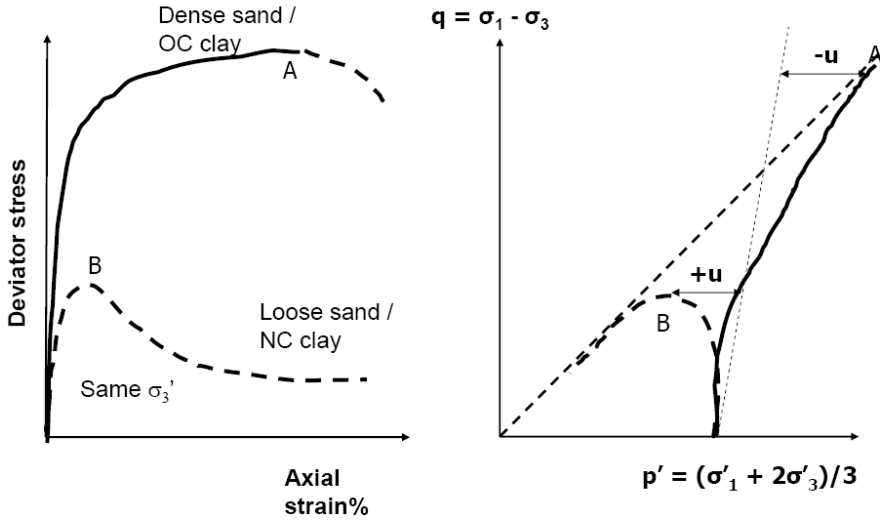

Figure 2.36 Effective stress path for CU test (after Chu, 2010)

Although curved on υ-p' plane, CSL could also be described by a straight line if plotted on the ln(p') scale. CSL, NCL and swelling line (κ-line) can be expressed by the following three equations respectively:

$$\upsilon = \Gamma - \lambda \ln(p') \quad \text{(CSL)} \qquad \text{(Eqn. 2.7)}$$

$$\upsilon = N - \lambda \ln(p') \quad \text{(NCL)} \qquad \text{(Eqn. 2.8)}$$

$$\upsilon = \upsilon_\kappa - \kappa \ln(p') \quad (\kappa\text{-line}) \qquad \text{(Eqn. 2.9)}$$

where Γ, λ, N, υ_κ and κ are soil constants; Γ and N are defined as the value of υ corresponding to p'=1.0 kN/mm^2 on the CSL and NCL correspondingly. At critical state, the specific volume υ occupied by unit volume of flowing particles decrease at the same rate with normally consolidated state as the logarithm of the mean effective stress increases.

The specific volume υ axis can also be exchanged to water content w for saturated clay, as these two parameters are correlated by this relationship:

$$(\upsilon - 1) \cdot S = w \cdot G_s \qquad \text{(Eqn. 2.10)}$$

where S is degree of saturation (S=1 for saturated soil), and G_s is the specific gravity of soil. Thus when soil is at its critical state there is also a unique relationship between shear stress and water content. Critical shear stress (critical state strength) increases with increasing effective normal stress and with decreasing water content. This fits the observation made by Hankle (1960), as shown in Fig. 2.34, unique relationship between water content and shear strength at failure.

2.4.2 Dilatancy and failure envelope in cemented granular materials

Dilatancy (increase in volume with increasing shear strain) is mainly observed in over consolidated clay/dense sand, as they are initially closely packed. Because of dilatancy, the measured failure envelope for a soil (τ, σ' values on stress-strain

plane) actually falls on a curve. Thus, by forcing a straight line to fit through all the measured τ and σ' values, the shear strength parameters c' and φ' determined by Mohr-Coulomb failure equations cannot be considered as fundamental soil properties. The assumption that c' and φ' are constant can lead to overestimation of shear strength (Terzaghi et al., 1996; Powrie, 2004; Schofield, 2006).

Nevertheless, dilatancy could be repressed by the presence of cohesion or bonding between the particles of cemented soil, which has been illustrated by several previous researchers (Coop and Atkinson 1993, Cuccovillo and Coop 1999, Ghatak et al., 2013; Kavvadas et al., 1993; Rabbi and Kuwano, 2012; Schnaid et al. 2001; Thian & Lee, 2013). Failure envelopes of cemented sand (naturally or artificially bonded) could be epitomized as straight envelopes defined by a unique friction angle φ, which is evidently not affected by cement content, and cohesion c, which is increased along with cement level.

a)

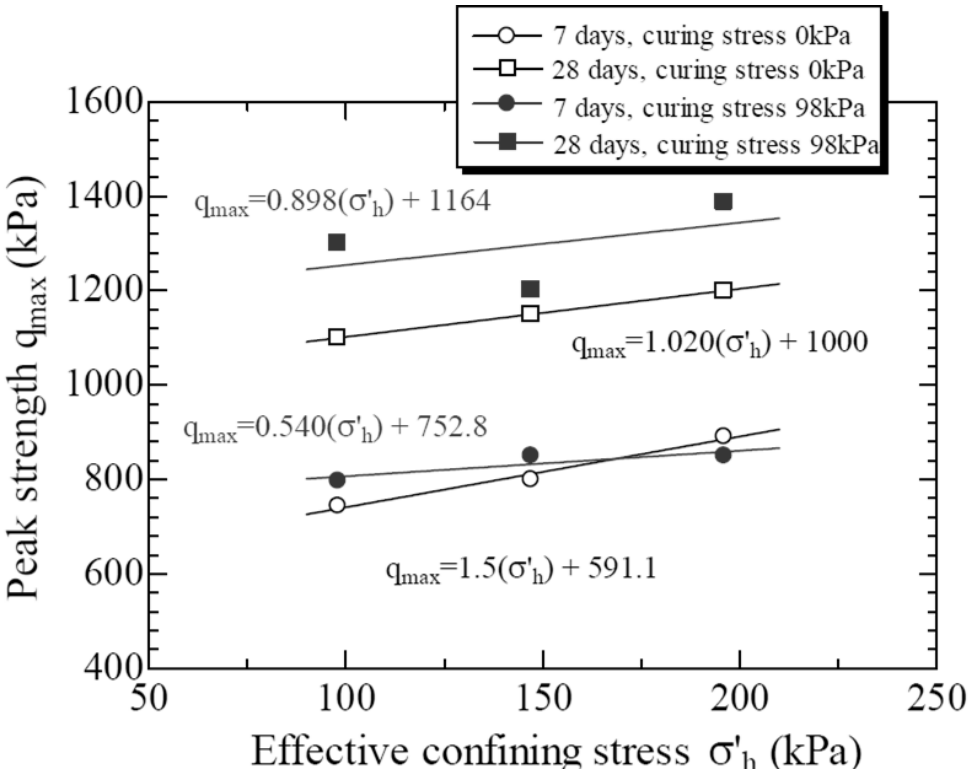

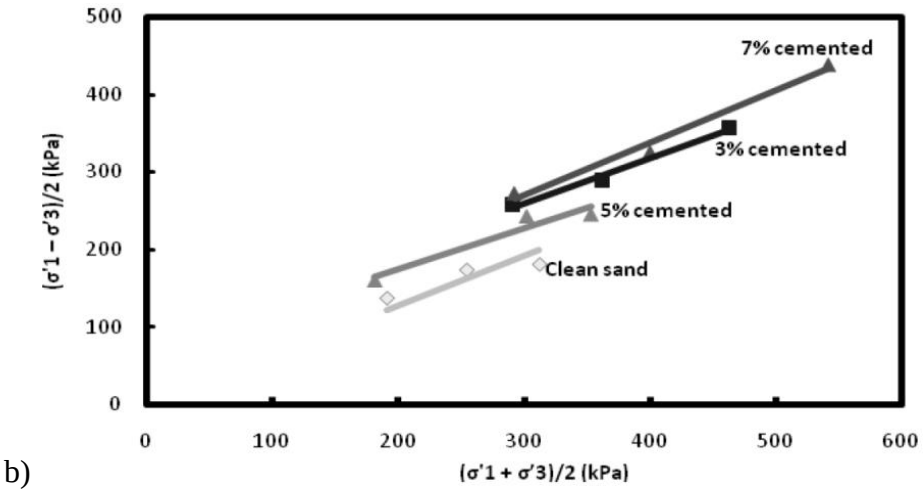

b)

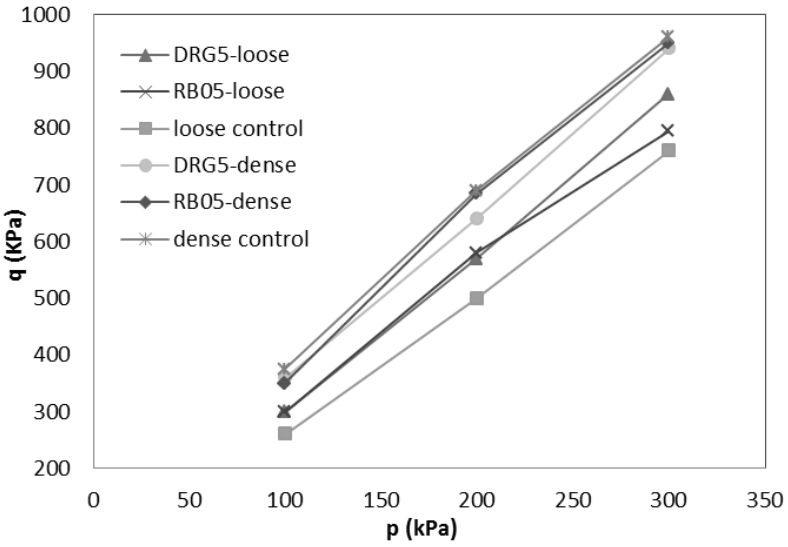

c)

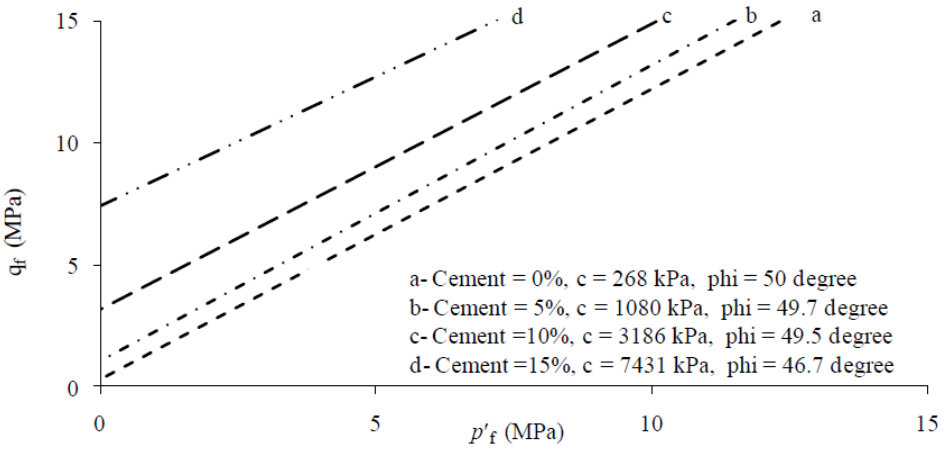

d)

Figure 2.37 Failure envelopes of artificially cemented sand at different level, a) Portland cement mixed sand (Rabbi and Kuwano, 2012) , b) Portland cement mixed mining sand (Thian & Lee, 2013), c) exo-cellular polymeric substances (EPS) treated sand at both dense and loose states; DRG5 and RB05 referred to bacteria strain (modified after Ghatak et al., 2013), and d) Portland cement mixed medium sand under higher confining pressure (Marri, 2010)

Some examples of failure envelopes of artificially cemented sand at different cementation level under consolidated drained tests are shown in Fig. 2.37, including Portland cement mixed sand (ρ = 1600 kg/m^3) under different curing time and curing pressure by Rabbi and Kuwano (2012) (Fig. 2.37a), Portland cement mixed mining sand (ρ = 1512 kg/m^3) by Thian & Lee, 2013 (Fig. 2.37b), exo-cellular polymeric substances (EPS) treated sand (at both dense and loose states, in which DRG5 and RB05 referred to bacteria strain) by Ghatak et al., 2013 (Fig. 2.37c), and Portland cement mixed well-graded, medium quartz sand (D_{50} = 0.393mm) under higher confining pressure (1MPa to 12MPa) (Fig. 2.37d) (Marri, 2010). Straight lines of failure envelopes generally parallel with each other governed by friction angle and cement level were found in each case.

2.5 Properties of Clay

2.5.1 Structure of clay minerals

The clay minerals in soils belong to the family called phyllosilicates. They all have crystalline structures in general and exhibit plasticity property in association with water. Thus, clay and non-clay minerals can be differentiated by Atterberg limit tests (Mitchell & Soga, 2005).

Two fundamental building blocks are involved in the formation of clay mineral structures, which are tetrahedral unit and octahedral unit. The combination of tetrahedral and octahedral sheets in different arrangements and conditions lead to the formation of different clay minerals (Murthy, 2003). The two types involved in this study include kaolinite, which is the component of kaolin, and montmorillonite, which forms bentonite primarily.

Kaolinite consists of a stacking of alternate layers of silica tetrahedrons and alumina di-octahedrons, having chemical composition of $Al_2Si_2O_5(OH)_4$; the tips of the tetrahedra share O^{2-} and OH^- with the octahedra. The thickness of one layer

is about 7 Å (one angstrom = 10^{-8} cm) thick. Unlike illite and montmorillonite, kaolinite has strong hydrogen bonds and is therefore stable. Water cannot enter between the sheets to expand the unit cells. The thickness of kaolinite particles range varies from 100 to 1000 Å, while the lateral dimension varies from1000 to 20,000 Å.

Montmorillonite is the dominant clay mineral in bentonite, weathered from volcanic ash. Its weak interlayer bonding is formed by van der Waals forces and cations balancing charge deficiencies; water enters easily between layers, hence its chemical composition is expressed as $Si_8Al_4O_{20}(OH)_4 \cdot nH_2O$. The basal spacing is from 9.6 Å to infinity after swelling, therefore it exhibits high swelling and shrinkage characteristics; such properties give rises to its industrial usage such as drilling mud or leakage prevention material (Bowles, 1984).

2.5.2 Surface chemistry of clay particles

1. Surface charge

The surface charge of kaolinite has been studied by many researchers (e.g. Schroth & Sposito, 1997; Wieland & Stumm, 1992; Zhou & Gunter, 1992; Ma & Eggleton, 1999). It is widely accepted that the surface charge carried on the surface of kaolinite is a result of both permanent and variable charges. Permanent charges refer to the isomorphic substitution of Al^{3+} for Si^{4+} in the tetrahedral layer, introducing a negative permanent charge. This is also known as the cation exchange capacity (CEC) of clay. The variable charge is pH-depended, and is related to the –AlOH and –SiOH groups at the particle edge and the $–Al_2OH$ groups at the octahedral layer (i.e. basal plane), as shown in the schematic structure and charges of kaolinite in Fig. 2.38 (Grim, 1962). The groups at the basal plane are less reactive than those at the edge. The protonation/deprotonation of basal plane groups are generally occurs only at a range of pH < 3 or pH > 9, and

thus are less considered (Huertas et al., 1998). Fig. 2.39 shows a possible breaking plane when edge groups forming; particle edge is negatively charged at high pH level and positively charged at low pH level. Actually positive charges in the protonation reaction of (Si–O)Al–OH sites formed only at pH below 6–6.5 (Tombácz & Szekeres, 2006). A higher pH value gives rise to more negative charges, which lead to a higher CEC value (Ma & Eggleton, 1999).

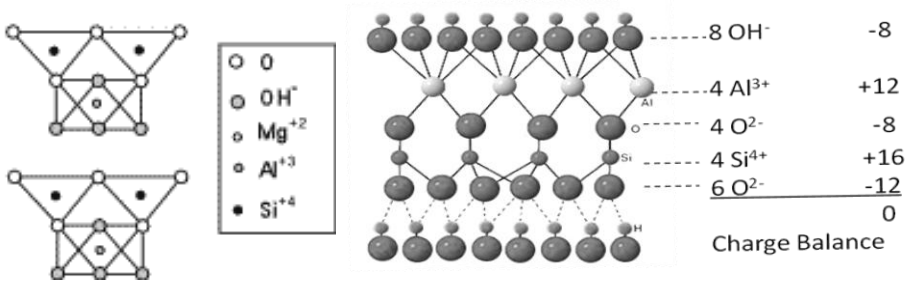

Figure 2.38 Schematic structure and charges of kaolinite (after Grim, 1962)

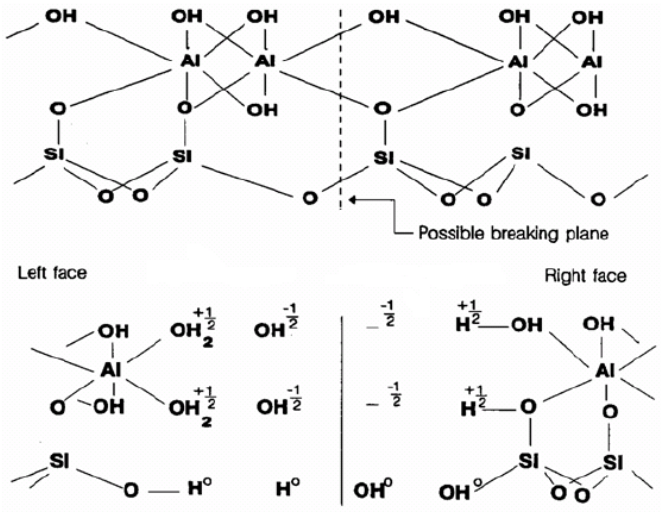

Figure 2.39 Kaolinite structure showing probable breaking plane and mechanism for edge charge (after Huertas et al., 1998)

2. Clay-water interactions and electrical exchange

Water molecules are strongly attracted to clay mineral surfaces due to their high surface activity. The negative charge on the surface of the clay particle, therefore, attracts the positive end of the water molecules (i.e. the hydrogen end). The clay-water interaction results in a tendency of the water molecular and other cations

present in water (e.g., Na^+, K^+, Mg^{2+}, Ca^{2+}) to diffuse away from the surface. This layer together with the charged surface of clay forms the "diffused double layer". The water located within the zone of influence is known as the adsorbed layer. Thick viscous absorbed layer helps clay to deform plastically without cracking, increasing cohesion between clay particles, and thus influencing strength and other properties of clay (Murthy, 2003).

Cations in the adsorbed layer and the pore fluid can exchange between each other. This kind of transfer is mainly driven by the difference of electrical potential between clay particle surface and the pore water. Gajo & Loret (2007) thus proposed to divide the adsorbed layer into two phases according to their electrical potential in order to account for the progressive electrical charge changes in the adsorbed layer. Adsorbed layer is considered together with clay particle surface as "solid phase", while pore water is presented as "fluid phase", which having electrical potential Φ_W. In contrast with traditional single adsorbed layer (SL) scheme as shown in Fig. 2.40a, where the electrical potential Φ is uniform in the whole absorbed water layer (Φ_S), the double layer scheme (DL) as shown in Fig. 2.40b assumes an intermediate electrical potential value (Φ_D) in the outer diffused layer, and attempted to represent actual nonlinear variation of the electrical potential in the absorbed water.

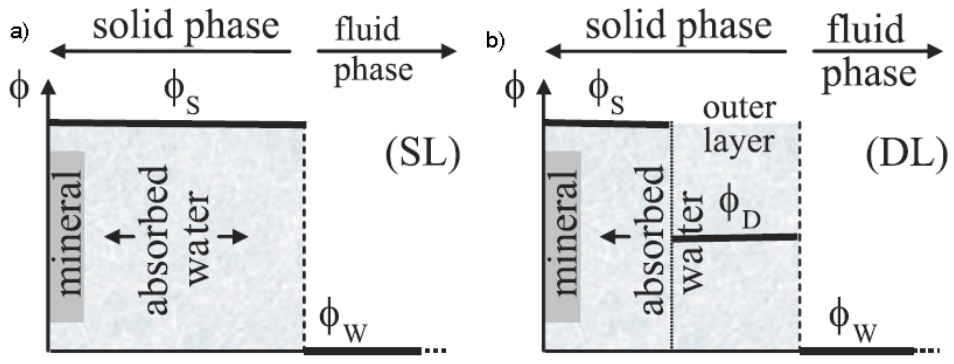

Figure 2.40 Ion distribution adjacent to clay particle surface for a) single layer scheme (SL) model and b) double layer scheme (DL) model respectively (after Gajo & Loret, 2007)

The four main exchange mechanisms between the solid and fluid phases are presented in Fig. 2.41. Exchange of water and ion exchange, as shown in Fig. 2.41(1) and Fig. 2.41(2) respectively, leave the electrical charge of the clay particle unchanged. However, as ions in pore water always tend to maintain electro-neutrality of the outer diffused layer, changes of the pH of the fluid phase do modify the electrical charge of clay mineral. As shown in Fig. 2.41(3), (4) and (4a), surface complexation occurs at the charged clay surface due to the acid–base equilibrium, known as acidification or alkalinization. "Competition" between hydroxyl and hydrogen ions results in dynamic equilibrium of SiO^-, SiOH and $SiOH_2^+$. Fig. 2.41(4) and (4a) present two possible forms of alkalinization; both of them are actually reversible. Base exchanges can strongly affect the mechanical properties of clay, which will be presented in the next section.

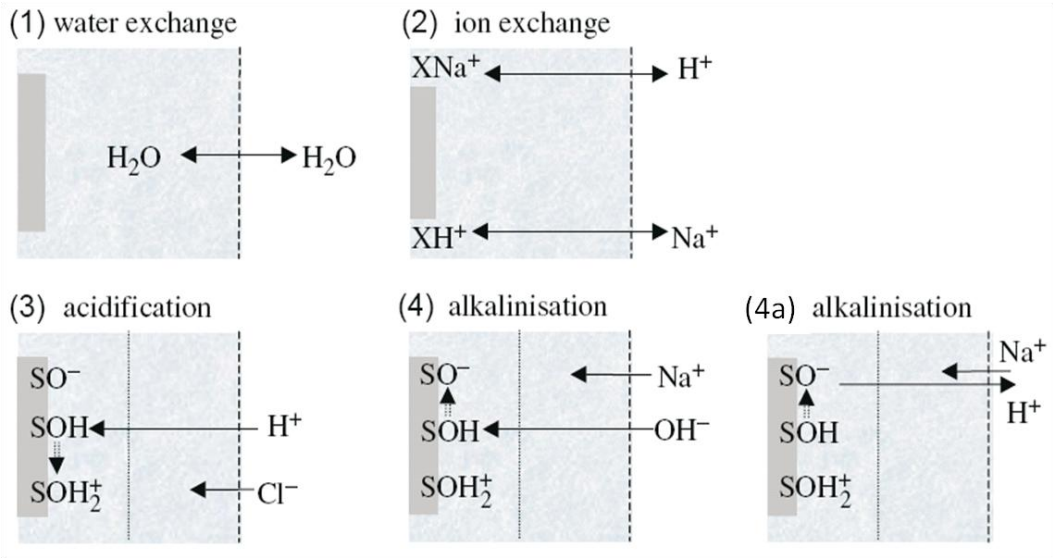

Figure 2.41 Four exchange mechanisms between solid and fluid phases (after Gajo & Loret, 2007)

3. Chemo-mechanical behaviour of clay

Soil clay particles can either be unattached to each (dispersed) or clumped together in aggregates (flocculated). As clay particles generally have negative charges, they tend to repel one another in nature. Cations, on the other hand, can make clay particles stick together by their positive charges. Common cations presented in soil

include sodium (Na^+), potassium (K^+), magnesium (Mg^{2+}), and calcium (Ca^{2+}); they attract water molecules and become hydrated due to their charge. These water-absorbed cations can form much thicker diffusion layer outside clay particles than H^+ and thus influences more on clay properties. Their ability of flocculation decreases as decreasing charges and increasing hydrated radii (Walworth, 2006). Table 2.4 shows charges, hydrated radius and therefore the flocculating power of the four cations in an increasing order.

Table 2.4 Charges, hydrated radius and flocculating power of sodium, potassium, magnesium and calcium (after Sumner and Naidu, 1998)

Cation	Charges per molecule	Hydrated radius (nm)	Relative flocculating power
Sodium (Na^+)	1	0.79	1.0
Potassium (K^+)	1	0.53	1.7
Magnesium (Mg^+)	2	1.08	27.0
Calcium (Ca^+)	2	0.96	43.0

According to Walworth (2006), flocculation tendency of soil depends on two categories: electrical conductivity (EC) and sodium adsorption ratio (SAR). SAR depends on the ratio of "bad" to "good" flocculators and is mathematically expressed by this equation:

$$SAR = \frac{[Na^+]}{\sqrt{[Ca^{2+}]+[Mg^{2+}]}} \qquad \text{(Eqn. 2.11)}$$

where concentrations are expressed in mM.

EC is measured in units of conductance over a known distance. Soil with a high EC is considered as salty. Thus, soil particles will flocculate if concentrations of (Ca^{2+} + Mg^{2+}) are increased relative to the concentration of Na^+, i.e. SAR is decreased, or if the amount of soluble salts in the soil is increased, i.e. EC is increased. Table 2.5 shows four types of soil classification according to flocculation condition of soil.

Table 2.5 Soil classification according to flocculation condition (after Walworth, 2006)

Soil Classification	EC	SAR	Condition
Normal	<4	<13	Flocculated
Saline	>4	<13	Flocculated
Sodic	<4	>13	Dispersed
Saline-Sodic	>4	>13	Flocculated

Chemo-mechanical interactions in kaolinite have been investigated by many researchers, e.g. Chattopadhyay (1972), Sridharan & Rao (1973, 1979), Rand & Melton (1977), Sridharan et al. (1988), Moore (1991), Di Maio & Fenelli (1994), Anson & Hawkins (1998), Wahid et al., (2011). However, published results on chemical influence on the mechanical properties of kaolinite are rather scattered and even partly contradictory (Wahid et al., 2010). For example, Chattopadhyay (1972) and Di Maio & Fenelli (1994) found that sodium chloride (NaCl) had negligible effects on the residual strength of kaolinite; however, Moore (1991) observed a significantly higher residual strength with increase in NaCl concentrations. Anson & Hawkins (1998) found a slight increase in the residual shear stress with higher calcium (Ca^{2+}) concentrations under high applied pressures, while Moore (1991) observed significantly residual strength increase at higher concentrations of calcium chloride ($CaCl_2$) solutions (from 0.2 to 1.0 g/l). Chen et al. (2000) concluded that van der Waals attractive forces dominated on compressibility of kaolinite below 300 kPa, and thus introduced the concept of "dielectric constant of pore fluid" to interpret compression and swelling indices of clay. Di Maio et al. (2004) further emphasized the importance of dielectric constant of pore fluid for active clays. It is also believed that the mechanical interactions become more important at higher vertical stresses, while pore fluid composition has basically no effect on compressibility at that range. Atterberg limits and one-dimensional properties of kaolinite mixed with 1M to 4M NaCl solutions has been studied by Sivapullaiah & Manju (2005, 2007), and confirmed the formation of sodium aluminum silicate hydroxide hydrate (NASH) by clay alkali reactions.

Wahid et al. (2010) conducted laboratory tests on kaolinite samples prepared with inorganic salt/acid/base solutions, including liquid limit, one-dimensional compressibility, permeability, residual shear strength, etc. The kaolinite samples were prepared by mixing (in proportions of) 70 g dry kaolinite with 1 litre of chemical solution and thus creating a clay suspension; after curing in a closed container for 3 months, the clay suspension was left to drain and desired final water content of paste was obtained by adsorbing the extra water with filter papers to avoid the effect of evaporation. The effect of the different solutions on the residual shear strength of kaolinite is presented in Fig. 2.42, where the residual friction ratio (tan φ_r' = τ/σ_v') against the effective vertical stress raised to the power of minus 1/3, in order to make the plots in the low pressure range to be linear (Chattopadhyay, 1972).

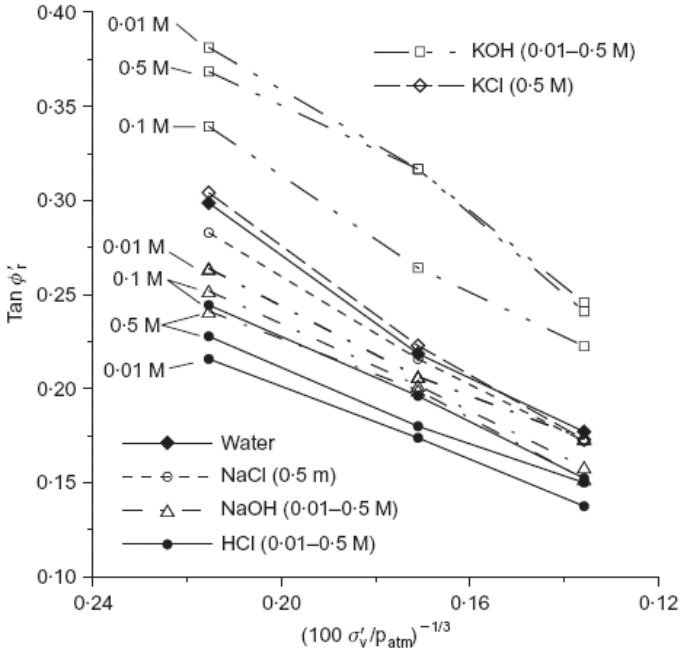

Figure 2.42 Influence of the solution's concentration on the residual strength of kaolinite (after Wahid et al., 2010)

As observed in Fig. 2.42, solutions of potassium hydroxide (KOH) result in a significant increase in residual friction angle, while sodium hydroxide (NaOH) solutions showed an opposite effect. This phenomenon may be attributed to chemical processes relating to the kaolinite dissolving in those alkaline

environments. Sodium chloride (NaCl) and potassium chloride (KCl) salt solutions show no practical effect on residual shear strength. In contrast to the result presented by Gajo & Maines (2007), that clay samples prepared with salt, acid and alkaline solutions induce increasing residual friction angle accordingly, Fig 2.39 shows the lowest residual friction angles of samples prepared by hydrochloric acid solution (HCl). In summary, pore fluid pH appears to play an important role in residue strength of kaolinite, while salt solutions has relatively insignificant influence (Wahid et al., 2010).

Chemical processes relating to the kaolinite dissolving in alkaline environments has been studied. For example, Fan (2006) proposed a possible mechanism of calcium-silicate-hydrate (CSH) gel formation by clay particle itself, under strong alkaline environment and in the present of calcium ion (Ca^{2+}), which may influence residual strength and other properties of clay. The -SiOH bond at edge of clay particles would dissolve in to SiO^- and H^+ in strong alkaline environment, known as alkalinization (Eqn. 2.12). In the meantime, $[Si_2O_5]^{2-}$ structure disintegrated gradually to $[SiO_4]^{4-}$ (Eqn. 2.13), and thus reacted with Ca^{2+} and formed CSH (Eqn. 2.14).

$$SiOH \rightarrow SiO^- + H^+ \quad \text{(Eqn. 2.12)}$$

$$[Si_2O_5]^{2-} + 6OH^- = 2[SiO_4]^{4-} + 3H_2O \quad \text{(Eqn. 2.13)}$$

$$[SiO_4]^{4-} + 2Ca^{2+} + mH_2O = xCaO{\cdot}SiO_2{\cdot}(m+x-2)H_2O + (2-x)Ca(OH)_2 \quad \text{(Eqn. 2.14)}$$

Similarly, $[Al_2O_6]^{6-}$ bond also disintegrated and reacted with Ca^{2+} to form hydrated calcium aluminates (Eqn. 2.15, 2.16 and 2.17). These reactions will continue until equilibrium is reached, and the formed CSH gel plays the role as aggregator, glue clay particles together.

$$AlOH + 2OH^- \rightarrow 2AlO_2^- + H_2O \quad \text{(Eqn. 2.15)}$$

$$[Al_2O_6]^{6-} + 12OH^- = 2[AlO_6]^{9-} + 6H_2O \quad \text{(Eqn. 2.16)}$$

$$2[AlO_6]^{9-} + 9Ca^{2+} + 12H_2O = 3CaO{\cdot}Al_2O_3{\cdot}6H_2O + 6Ca(OH)_2 \quad \text{(Eqn. 2.17)}$$

2.5.3 Influence of water content in shear strength of clay

Shear strength is one of the essential engineering properties of soil. Shear strength of clay mainly depends on interactions between soil particles, including friction and interlocking resistance. Shear failure occurs when the stresses between the particles are such that they slide or roll past each other (Lambe & Whitman, 1991). Many failure equations were proposed to describe shear strength of soil; the simple and most well accepted one should be the Mohr-Coulomb failure equation, in which the strength of soil was characterized by friction angle φ and cohesion τ.

The shear strength of soil varies with many factors, including the water content at failure, effective overburden stress, over consolidation ratio (OCR), consolidation path, stress states and stress anisotropy, etc. (Henkel, 1960; Ladd, 1986; Kulhawy & Mayne, 1990; Chu et al., 1999). For example, Henkel (1960) pointed out a unique relationship between water content at failure and strength of clayey soils, as shown in Fig. 2.43a and 2.43b, for Weald clay and London clay respectively. A linear relationship is observed between *w* and $\log(\sigma_1-\sigma_3)$ for normally consolidated clay, regardless of their drainage conditions. Similar relationship can be found for over consolidated clay, yet the curve lies slightly below that for the normally consolidated one.

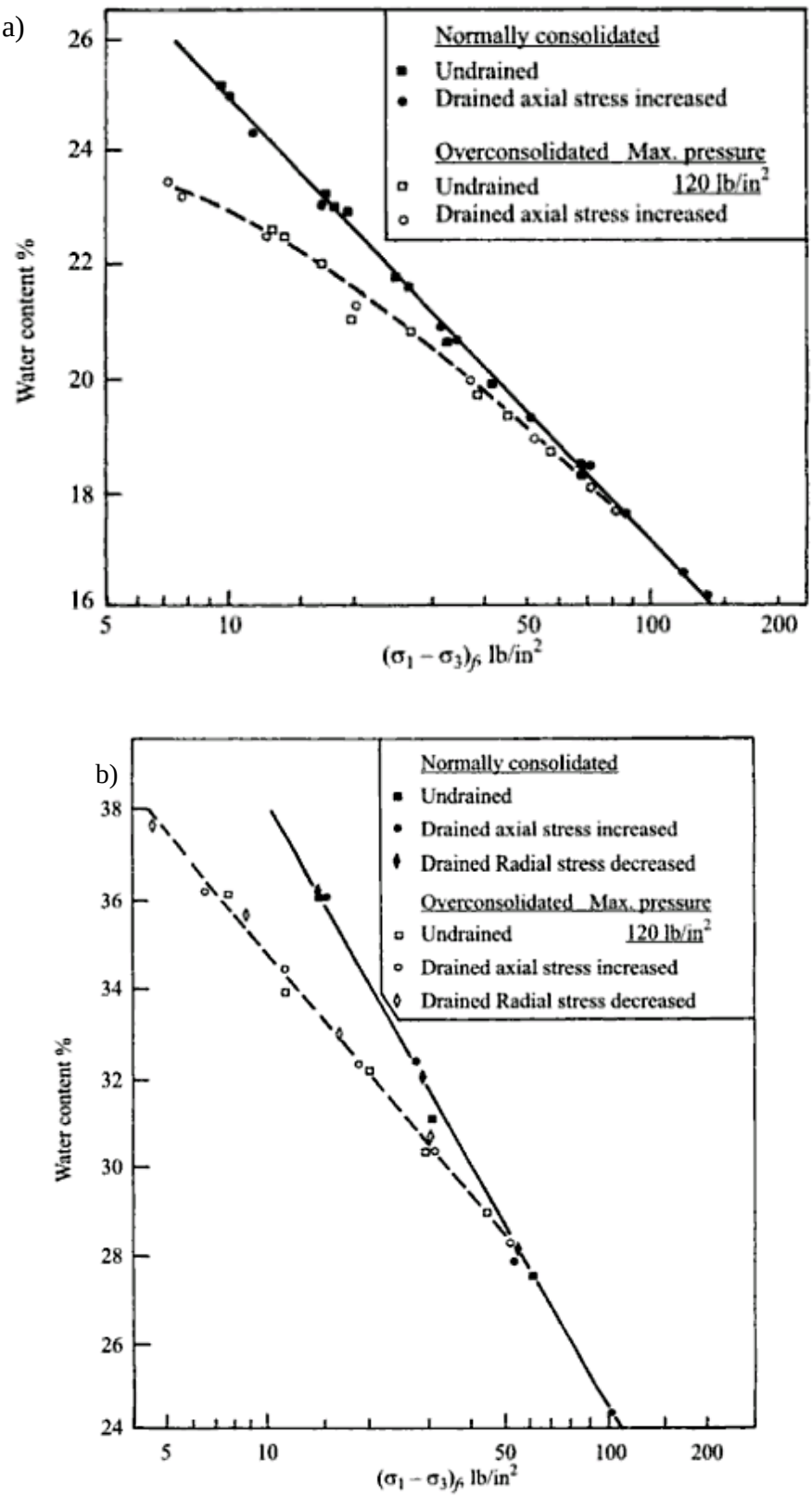

Figure 2.43 Water content vs. shear strength relation for: a) Weald clay, and b) London clay (after Henkel, 1960)

2.5.4 Atterberg limits represented engineering parameters

Clayey soil plasticity is represented by its Atterberg limits, namely liquid limit (LL) and plastic limit (PL). The difference of LL and PL is plasticity index PI. Atterberg limits described the soil consistency in terms of water content, and thus influences the strength of clayey soil: clay behaves as liquid and thus has no strength when having water content higher than LL, and becomes semi-solid with high shear strength with lowering water content while below PL; clay having high plasticity index are described as cohesive (Mitchell, 1993).

Engineering properties of clayey soil is correlated with Atterberg limits, and inherent in a specific soil. Mechanical parameters, the internal friction angle φ and cohesion c is partially dependent on texture and index of plasticity, as listed in Table 2.6 (after Baumgartl, 2006; translated from Kretschmer, 1997). A lower plasticity index usually represents higher internal friction angle yet lower cohesion for clayey soil according to the table.

Table 2.6 Typical correlations of mechanical parameters and Atterberg limits (after Baumgartl, 2006; translated from Kretschmer, 1997)

Texture	PI (%)	Internal friction angle φ' (˚)	Cohesion (kPa)
clay of high plasticity, LL>50%	50-75	17.5	0
	75-100	17.5	10
	100-130	17.5	25
clay and silt of medium plasticity, 35%<LL<50%	50-75	22.5	0
	75-100	22.5	5
	100-130	22.5	10
clay and silt of low plasticity, LL<35%	50-75	27.5	0
	75-100	27.5	2
	100-130	27.5	5

Adding of chemicals would influence the Atterberg limits of clay through ion exchange and influencing the thickness of double layer, which was reported by several researchers (Heeralal et al. 2012; Hugh, 1985; Maio & Fenelli, 1994; Siva Pullaiah & Savitha, 1997). Influence in Atterberg limits of bentonite by adding

different amount of $CaCl_2$ is shown in Fig. 2.44 (Heeralal et al., 2012). Liquid limit of bentonite is decreased dramatically from its original value of 280 to 100% by adding 1% CaCl2; plastic limit also reduced slightly.

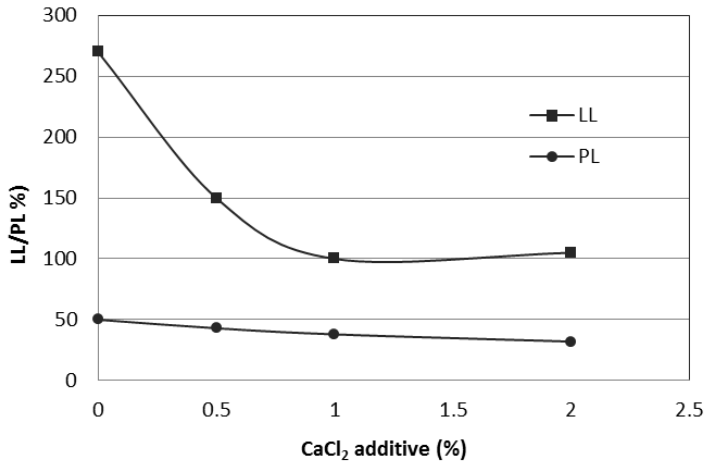

Figure 2.44 Influence of Atterberg limits of bentonite with different amount of $CaCl_2$ (Heeralal et al., 2012)

2.5.5 Clay cementation

Natural cementation

In-situ soft clay is most often encountered in their naturally cemented state. Cemented clay is defined as one "which contains particles held by strong bonds which are of a different nature to the equilibrium state which are due to inter-particle forces similar to those operative in non-cemented clays" (Bjerrum, 1967). The strength of the bonding depends upon the cementing material and the environment that the soil deposit is in. Calcium carbonate and amorphous silica are two of the common cementation binder in naturally occurred cemented clay.

Micro-fabric structure of naturally cemented clay has been studied firstly by Pusch (1970), as a meta-stable state of small aggregates connected by links of particles (Fig. 2.45a). Fig. 2.45b shows a more widely accepted model, made by Collins & McGown (1974), illustrating with possible assemblage of particles with several types of sub-structural pores within aggregation of particle groups. Nagaraj et al.

(1998) found no identifiable difference between intact and remoulded clay in terms of the pore size distribution and permeability, and thus concluded that the microfabric structure of the cemented clay should be of the same pattern with the uncemented one (Fig. 2.45c).

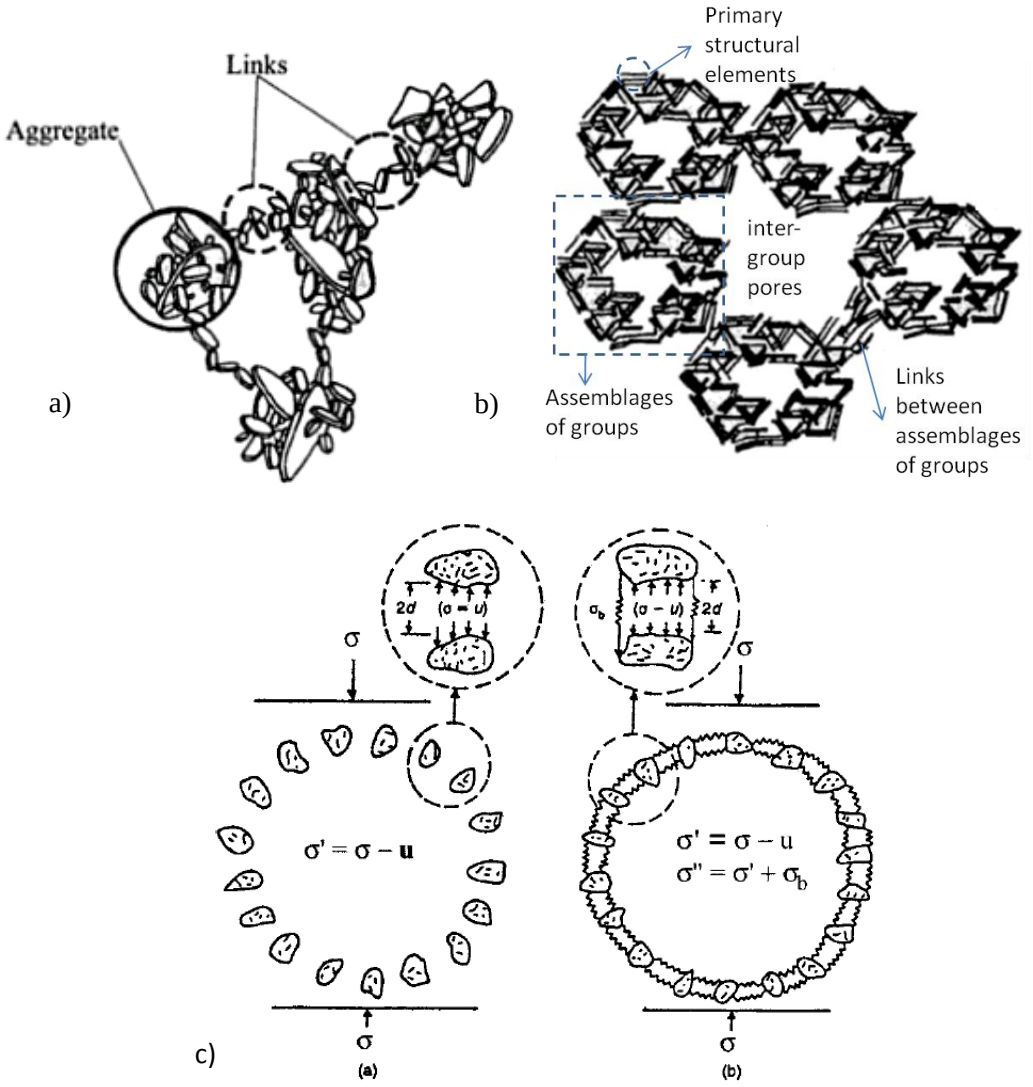

Figure 2.45 Cchematic presentation of a)micro-structure of naturally cemented clay proposed by Pusch, (1970), b) fabric element and pore types of assemblage of clay particles, by Collins & McGown, (1974); Griffiths & Joshi, (1990), and c) possible micro structures of (a) uncemented and (b) cemented soil by Nagaraj & Miura (1998)

Artificial cementation

Soft clay soils need to be treated before it can be applied for engineering usage, to increase their shear strength as well as control the deformation and permeability. One of the most commonly used soil treatment method is preloading. However, preloading is time consuming. Another commonly used method is to use lime and cement to induce cementation in soil. Other chemicals used for cementation of clay including sodium silicate, calcium chloride, acrylics, acrylamides, lignosulfites–lignosulfonates, phenoplasts, aminoplasts, polyurethanes, etc. (Karol 2003).

Portland cement is the most commonly used cement in cement-soil stabilization. The two major chemical reactions involved in cement stabilization are the primary hydration and the secondary pozzolanic reactions (Chin, 2006). The primary hydration occurs between cement and water, resulting in rapid strength gain and short-term hardening due to the formation of primary cementitious products, such as $Ca_3Si_2(OH)_X$ (calcium-silica hydrated gel) and $Ca(OH)_2$. The secondary pozzolanic reaction occurs when alkalinity of the pore water helps dissolving the silica and alumina of clays, which then react with the calcium ions, forming calcium silicate hydrate (CSH) and calcium aluminate hydrate (CAH), as described by Fan (2006).

Saitoh et al. (1985) proposed schematic diagrams to illustrate the change in structure of soil-cement mixtures during primary and secondary hardening reactions, as shown in Fig. 2.46a and 2.46b respectively. The initial condition immediately after mixing consists of clusters of clay particles, surrounded by cement slurry. The primary hydration reaction forms only the hardened clay clusters surrounded by cement shell. The secondary pozzolanic reaction involves the inner clay particles, leading to the formation of hardened soil bodies. The strength of the improved soil depends on the strength characteristics of both types of hardened bodies.

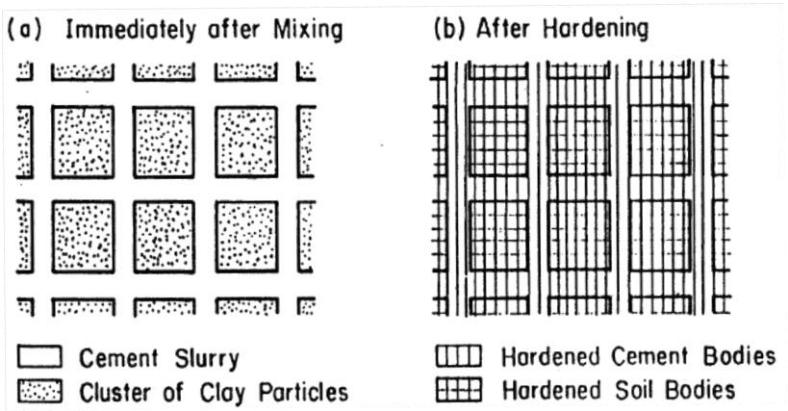

Figure 2.46 Change in structure of soil-cement mixtures during hardening (after Saitoh et al., 1985)

Characteristics of induced cemented clay have been changed in many aspects. Cohesion, yield stress, stiffness and the size of yield surface increase with the increase in degree of cementation, which is mainly controlled by water/cement ratio and curing time (Miura et al. 2001; Horpibulsuk et al., 2004a; 2005). However, with the inter/intra-particle voids in a meta-stable state, resistance to plastic deformation of induced cemented clay is reduced. This is reflected by the tests data that the greater the degree of cementation, the higher the compression index of the virgin compression line (Horpibulsuk et al., 2004b).

2.6 Summary

In this chapter, previous attempts of biological treatment of soil in geotechnical and geo-environmental engineering, including biocementation, bioclogging, bioremediation of soils, and microbial-induced geo-disasters, were discussed. Previous studies on basic properties of clay were presented. Engineering properties of soft clay deposit and problems encountered were considered. The main conclusions are summarized below:

1. Bio-mediated soil improvement methods have been developed in recent years. Major divisions of bio-mediated soil improvement system consist of bio-mineralization, which includes biocementation and bioclogging, biofilm

formation, and biogas production. Geometric compatibility between the microbes and soil particles is essential to the effectiveness of bio-mediated treatment. Sand is suitable for generally all the treatments. The significant limitation of all the treatment methods is that the pore size of clay soil may be too small for migration of bacterial cells there.

2. Many types of bacteria are capable of producing biocementation, for example, urease- producing bacteria (UPB), iron-reducing bacteria, nitrifying bacteria, oligotrophic microaerophilic bacteria, sulphate-reducing bacteria, etc. They have already exerted positive result in biocementation of sand in terms of shear strength development.

3. Microbially induced carbonate precipitation (MICP) formation employing UPB is the most common method adopted for biocementation so far. Many factors could influence the effectiveness of calcite formation. These including productivity of UPB (which is represented by its urease activity), distribution and fixation of UPB, chemical concentration, retention time, original material properties (including size, textures, interaction with water, etc.), etc.

   3.1 UPB strain *Sporosarcina pasteurii* is commonly used in previous studies because of its halo-tolerant and alkali-philic characters, as well as it can produce high urease activity and being non-pathogenic. Urease activity, which is the main indicator of its bacterial productivity mainly varied from 5 to 20 mM urea/min in these studies. Lower UPB activity could lead to more even cementation.

   3.2 Lower chemical concentration in cementation solution is favorable regarding the uniformity of calcium carbonate formation. Calcium to urea ratio less than unity is advised in practice to maintain UPB activity of longest time, and as urea is relatively cheaper comparing to the calcium resources available.

3.3 Use of fixation solution with high salinity after applying UPB (usually $CaCl_2$ solution) can increase the absorption of bacteria by reducing electrostatic repulsion of bacteria and immobilizing it, and getting more uniform cementation with sand. Dilution of UPB could result in urease activity being flushed out within effluent.

3.4 Positive relationship between calcite content and the UC strength is established for samples treated using the traditional submersed flow method, which confirms the calcite crystal acted as binder between soil particles and provided strength. Permeability is lowered with higher calcite content as more voids are plugged.

4. Failure envelopes of cemented sand at different cementation levels (naturally or artificially bonded) are believed to be represented as straight envelopes parallel to each other, defined by a unique friction angle φ, which is evidently not affected by cement content, and cohesion c, which is increased along with cement level.

5. The negative surface charge carried on the surface of kaolinite is a result of both permanent and variable charges. A higher pH value gives rise to more negative charges. Published results on chemical influence to mechanical properties of kaolinite are rather scattered and even partly contradictory. In summary, pore fluid pH appears to play an important role in residue strength of kaolinite, while salt solutions have relatively insignificant influence.

6. Engineering properties of clayey soil may be correlated with Atterberg limits. The internal friction angle φ and cohesion c is partially dependent on texture and index of plasticity. A lower plasticity index usually represents a higher internal friction angle and lower cohesion for clayey soil according to the table.

Chapter 3

Methods and Materials

3.1 Introduction

Material and methodology adopted in the experiment are introduced in this chapter. The cultivation of three sets of bacteria, namely Urease-Producing Bacteria (UPB), Sulfate-Reducing Bacteria (SRB) and Iron-Reducing Bacteria (IRB) that have been used in the experiment is explained in Section 3.2. Methods of element calcium and urea molecule monitoring, which are the key indicator of the effectiveness of biocementation, are described in Section 3.3. The mechanical properties of material engaged in this study, which are sand and clayey soil (kaolin, marine clay, and bentonite) are described in Section 3.4. Set-ups of strength test and other engineering properties measurement on soil, including unconfined compression (UC) test, triaxial tests, four-point bending test, flexible wall permeability test, oedometer test, clay ball slaking/split test, and SEM/FESEM for detecting the micro structure of biocemented soil, are presented in Section 3.5.

3.2 Cultivation of Bacteria

3.2.1 Cultivation of urease-producing bacteria (UPB)

Classification of obtained UPB

The strain of urease producing bacteria used in this study (namely strain VS1**)**, was obtained from beach sand in Singapore and soil polluted by urea. Selection criteria of this bacterial strain included its ability to synthesize urease enzyme, tolerance of high concentration of salt, tolerance of high pH, identification and check of biological safety.

VS1 was cultivated in liquid medium to obtain biomass pellets. The cells of isolated bacterial strain were Gram-positive, rod-shaped, spore-forming, and aerobic ones. The 16S rRNA sequence analysis method (Stackebrandt and Goebel, 1994) was adopted to identify the unknown bacterium to the genus or species level. The nearly full-length 16S rRNA gene was amplified by the Polymerase Chain Reaction (PCR) method. Purified PCR products were sequenced using the ABI PRISM 3730xl DNA sequencer and the ABI PRISM BigDye Terminator Cycle Sequencing ready-reaction kit. The sequences were finally assembled to produce the full-length sequence and the full-length sequence was compared with all other sequences available in the NCBI Genbank database. The probable identity of the bacterial strain was thus determined most likely to be *Bacillus* sp. (Stabnikov et al., 2011; Chu et al., 2012). SEM image of *Bacillus* sp. strain VS1 is shown in Fig. 3.1. This strain is close to the strain *Bacillus* sp. (CPB 2) isolated for MICP in Ghent University, Belgium (Hammes et al., 2003; Stabnikov et al., 2013).

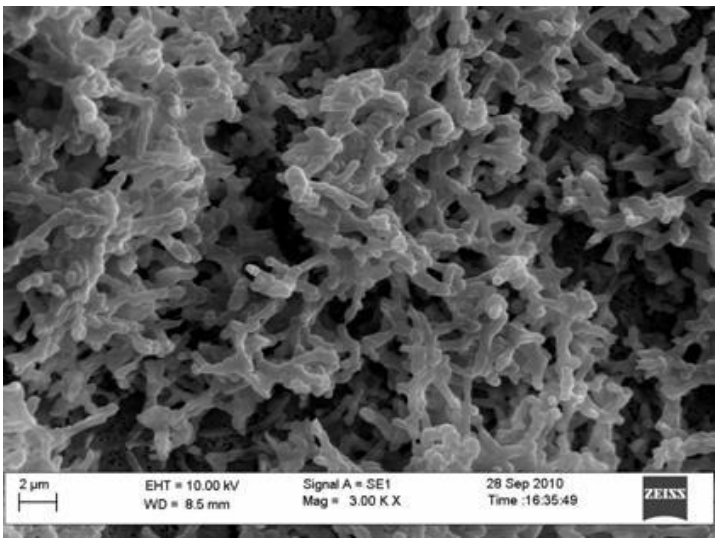

Figure 3.1 SEM image of *Bacillus* sp. strain VS1 of UPB used in this study.

Cultivation of UPB and urease activity determination

Medium for the cultivation of UPB was the same as it was used for isolation, which including following components:

- Tryptic Soy Broth DIFCO™, 30 g/L;

- Urea, 20 g/L;

- $MnSO_4 \cdot H_2O$, 12 mg/L;

- $NiCl_2 \cdot 6H_20$, 24 mg/L.

The liquid medium was autoclaved at 121°C for 15 min. Urea was put in after autoclaving to avoid its thermal degradation. Cell suspension of strain VS1 was then added to the liquid medium in 1:10 volume ratio, cultivated aerobically under non-sterile conditions for 2 days with constant air flow supply at rate 3L/min. 0.2% (v/v) of palm oil was used as antifoaming reagent. pH and urease activity have been monitored throughout the cultivation process.

Urease activity could be measured by change of pH, production of NH_4^+, production of carbon dioxide gas, or increasing of electric conductivity duel to

production of NH_4^+, in which the latest method was adopted. As described in Section 2.2.3, hydrolysis of urea can liberate ionic products (NH_4^+ and CO_3^{2-}) from non-ionic substrates (urea), the overall electric conductivity of solution increases at a rate linearly proportional to active urease present. Determination of urease activity in bacterial suspension can thus be transferred to the measure of the increase in conductivity in the bacterial sample, in the presence of urea. The procedure of conductivity measurement is as follows:

1. Mix together 90 mL of urea solution (1M) and 10 mL of UPB suspension.
2. Measure the electric conductivity at interval of 5 mins to 30 mins.
3. Plot results and read off results from calibration curve produced for different concentrations of ammonium. (This linear relationship between conductivity and urease activity is shown in Appendix A.)

3.2.2 Centrifuging and re-suspension of UPB

The process of centrifuging was engaged to separate the cell of UPB from its cultivation solution, in order to reduce odor, stabilize urease enzyme inside cell, and make releasing of urease enzyme slower and steadier to form more uniform biocementation. Each batch of fresh culture of UPB VS1 was centrifuged under 4°C at 10000 rpm for 10 min by refrigerated centrifuge model Kubota 5922™. Supernatant was dispensed (after testing its urease activity); remaining bacteria cell was re-suspended into 9g/L NaCl solution by BenchMixer™ vortex mixer at 3200 rpm for 10 min (high salinity solution was employed to prevent electric shock of cell and thus preventing urease enzyme being released from cell to its solvent). UPB culture after centrifuging (cell on wall with supernatant) and its re-suspended solution are shown in Fig. 3.2a and 3.2b respectively.

a) 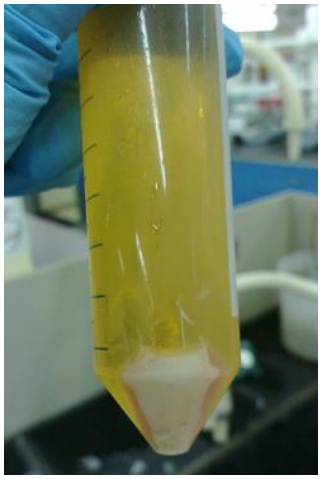 b) 

Figure 3.2 UPB culture a) after centrifuging (cell with supernatant) , and b) its re-suspended solution

3.3 Calcium/urea content monitoring

3.3.1 Calcium content determination

Calcium ion can be determined using the inductively coupled plasma atomic emission spectroscopy (ICP-OES) test. In conducting this test, an air-dried soil sample was oven dry overnight. About 2.00 g of this oven-dried soil sample was placed in a 50 ml volumetric flask. 50 ml of 2.5 % acetic acid was added to the flaks and shaken on shaker at 121 rpm for 3 hrs. Then the mixture was centrifuged and the supernatant liquor was collected in another 50 ml volumetric flask and tested for Ca^{2+} content by ICP (in ppm, mg/L). The results were converted to calcite content.

Noted that measuring the oven-dried weight difference of soil sample before and after washing by acid could also provide another set of calcite content data, assuming the weight loss in soil is all due to calcite crystal washed out by acid. This so-called “washing method” may not be as reliable as the ICP test. A comparison of the calcite content determined by ICP and that by the washing method is given in Fig. 3.3. It can be seen that the calcite determined by the washing method is higher than that by the ICP method. Even though a linear

relationship is observed and this relationship can be used for conversion between the two methods.

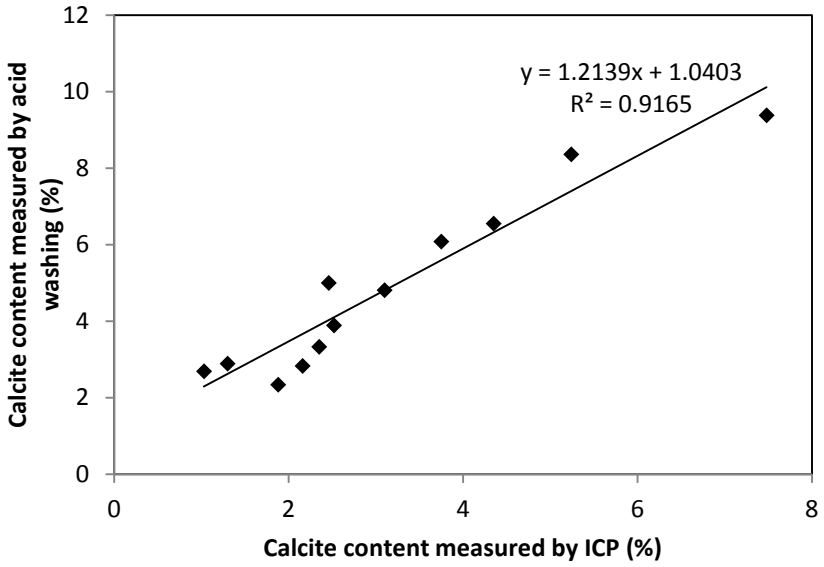

Figure 3.3 Linear relationship of calcite content getting from ICP vs. washing method

3.3.2 Urea content determination

The urea molecule remaining in effluent was measured by spectrophotometer (Shimadzu UVmini-1240^{TM}), following a method described by Knorst et al. (1997). 0.5ml of measuring solution, which containing absolute ethanol with 4% (weight to volume) of p-dimethylaminobenzaldehyde and 4% (volume to volume) sulphuric acid, was added into 2ml of diluted effluent (filtered through 0.45μm filter) and well mixing for 10min. Yellow compound forming by p-dimethylaminobenzaldehyde and urea molecule can be detected by the absorbance measuring at 422 nm against a reagent blank. Urea remaining in effluent then can be determined against the calibration curve (attach in Appendix B).

3.4 Properties of materials used

3.4.1 Properties of sand

Two types of sand were used in this study, standard Ottawa sand from the U.S. Silica Company (2010), and filtration sand imported from Riversand^{TM}, Australia (grade W9). Both were poorly graded fine sand, white in colour. A summary of the basic physical properties is shown in Table 3.1. The gradation curves are drawn in Fig. 3.4, using mechanical sieving method following ASTM D422-03 (1998). It can be seen that the two types of sand are similar to each other, regarding to the size distribution, chemical content, specific gravity, and other engineering properties.

Table 3.1 Engineering properties of the two types of sand employed in this study

Description	Grain Shape	Mean size (mm)	Chemical Content	Typical Specific Gravity	Hardness	Bulk Density
Ottawa sand	Round	0.30	99.5+% SiO_2	2.65	7 Mohs	1600 kg/m^3
River sand	Round	0.25	99.5+% SiO_2	2.63	-	1500kg/m^3

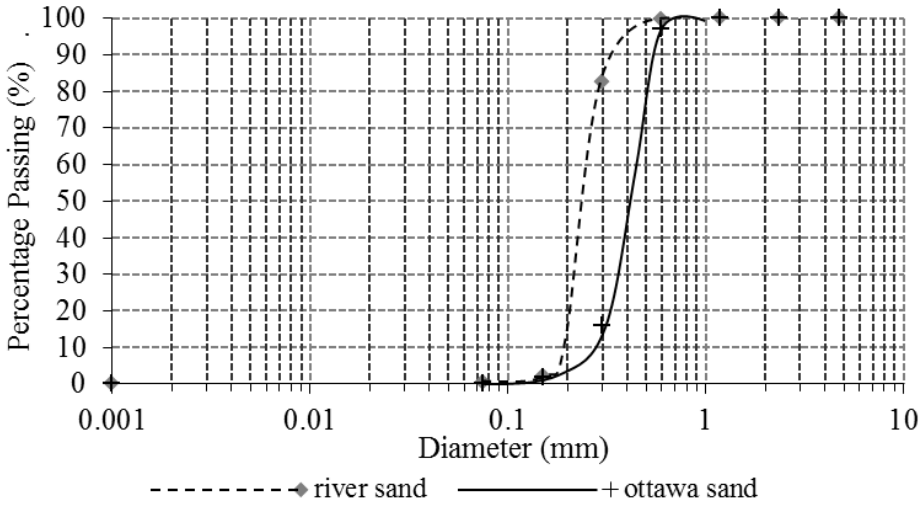

Figure 3.4 Gradation curves of river sand and Ottawa sand

3.4.2 Properties of clay

Three types of clayey materials were used in this study for testing the applicability of biocementation in clay: kaolin, marine clay, and bentonite.

Kaolin is a material commonly employed to study the engineering properties of clay, and is employed for the convenience of evaluation of soil property. For laboratory uses, it usually stored as white mineral powders with relatively low specific gravity. Kaolin usually occurs in small particle sizes and thus has considerable surface area per unit mass. These surface areas have a residual negative charge and when mixed with limited amounts of water, it behaves as swelling soil and exhibits a plastic behaviour. Kaolin employed in this study was imported from Kaolin (M) SDN BHD in Malaysia, FP grade. It is made by centrifuging the raw clay slurry and removing the impurities.

Marine clay (MC) used was taken from a construction site in Tuas, Singapore. This marine clay was greyish with high water content and was found to comprise mainly of clayey fines, silt, with small amount of sand and other impurities. Gradation curve of MC is shown below in Fig. 3.5.

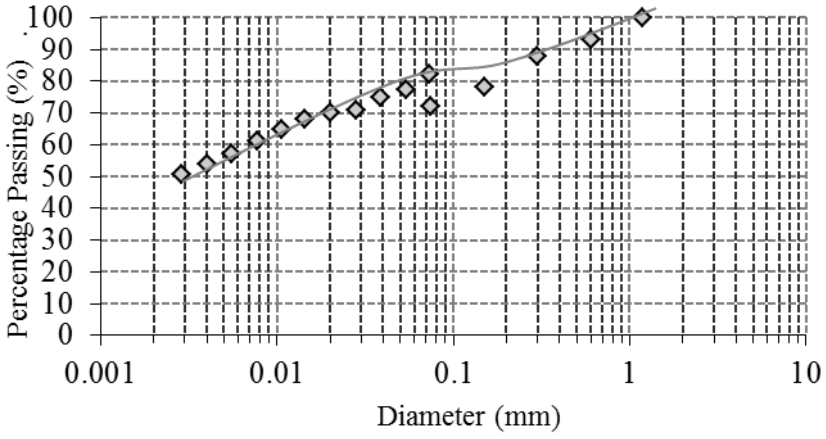

Figure 3.5 Gradation curve of marine clay employed in this study

Bentonite consists of montmorillonite with high absorbance of water, i.e. high plasticity. Bentonite used in this study is of drilling grade imported from

International Scientific Pte Ltd, Singapore. It was brown-yellowish colour. Production properties of this bentonite are listed in Table 3.2 below. It is contains most of the Ca- and Mg-montmorillonite based on the properties tested.

Table 3.2 Engineering properties of bentonite employed in this study

Suspension Properties Viscometer dial reading @ 600 rpm	Minimum 30
Yield point/plastic viscosity ratio	Maximum 6
Filtrate volume	16 cm^3 Max
Residue of diameter greater than 75 micron	2.5% Max
Moisture	10% Max

The basic properties of kaolin, marine clay (MC) and bentonite used in this study are summarised in Table 3.3. Water content (W/C) was determined according to the ASTM D2974-87. The specific gravities of each material were determined according to the density bottle method as specified in BS 1377 Part 2 (1990). The liquid limit (LL) was determined using a laboratory cone penetrometer in accordance to BS 1377 Part 2 (1990). The plastic limit (PL) test was conducted by manual kneading and rolling according to BS 1377 Part 2 (1990). The grain size distributions of the two marine clay samples were determined using wet and mechanical sieve analysis according to ASTM D422-03. Classification of soils were then determined accordingly to ASTM D2487-00.

Table 3.3 Basic properties of materials used in this study

Property	Kaolin	MC	Bentonite
Specific Gravity	2.54	2.54	2.39
Liquid Limit, LL (%)	91.0	43.6	432.0
Plastic Limit, PL (%)	48.2	21.9	60.1
Plasticity Index, PI (%)	42.8	21.7	371.9
Fine Content (%)	100	72.34	100
Soil Classification	MH*	CL*	CH*

*MH: silt with high liquid limit; CL: l clay; CH: clay with high liquid limit

3.5 Strength test and other mechanical properties tests

The following tests were conducted to determine the mechanical properties of either biocemented sand or clayey soil specimens.

3.5.1 Unconfined compression (UC) tests

Unconfined compression (UC) tests were conducted using cylindrical sample size either 50mm*100mm or 38*76mm, at a strain rate of 1.52 mm/min. Noted when specimen size was limited in some sand biocementation modelling, UC tests were conducted with small specimens of roughly 10mm*20mm in dimension at loading rate of 0.4 mm/min (2% as axial strain), to adopt the special sample size requirement. Details will be illustrated in later sections when applicable.

3.5.2 Triaxial tests

Several types of triaxial compression tests were conducted to measure strength properties of both sand and clayey soil specimens. These include unconsolidated undrained (UU) test, consolidated undrained (CU) test, and consolidated drained (CD) test. All triaxial samples were cylindrical with 50mm in diameter and 100mm in height. Apparatus adopted in this study is shown below in Fig. 3.6.

The triaxial compression tests were conducted by following the following three steps: saturation, consolidation, and shearing. The back pressure saturation method was adopted for saturation. B-value checked was conducted by calculating B as

$$B = \frac{\Delta U}{\Delta \sigma_3} \quad \text{(Eqn. 3.1)}$$

where $\Delta\sigma_3$ refers to the change of cell pressure, and ΔU refers to the corresponding change of pore water pressure. When B-value measured was greater than or equal to 0.95, the saturation was considered completed.

Figure 3.6 Overview of triaxial test apparatus.

K_0 consolidation was carried out for some of CU tests, using a method proposed by Lo & Chu (1991). During K_0 consolidation, the specimen was control to achieve $d\varepsilon_v/d\varepsilon_1 = 1$ using computer control. The vertical load was applied gradually on the specimen until the required σ_1' value was reached. The shearing stage was carried out using deformation control. A constant strain rate of 0.01mm/min was used for all the triaxial tests.

3.5.3 Four-point bending test

Four-point bending tests were conducted to get the maximum outer fibre stress of biocemented sand when other strength tests were not available due to limitation of sample size. Schematic picture and photo taken during tests are shown in Fig. 3.7. As indicated in ASTM D6272-10, support span-to depth ratio of 16:1 shall be use. Specimen width shall not exceed 1/4 of support span. Thus, samples were cut and rubbed by sand paper into roughly 100mm×20mm×5mm (support span 80mm) or 80mm × 15mm × 4mm (support span 60mm) specimen bars, depending on availability of samples. The round loading noses were made to have 6mm in

diameter (5 to 8mm as indicated in ASTM). A loading ring of unconfined compression apparatus was employed to measure P, the vertical load.

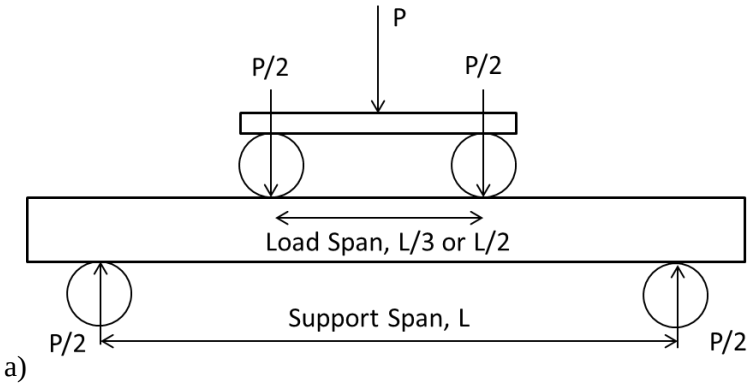

a)

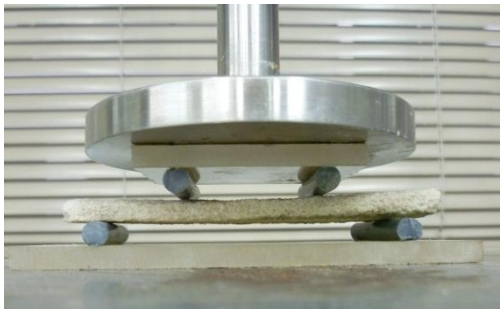

b)

Figure 3.7 Experiment setup for 4-point bending test, a) schematic, and b) *insitu*

According to ASTM standard D6272-10, loading rate was calculated as

$R = 0.185ZL^2/d$ (Eqn. 3.2) for a load span of one third of the support span, or

$R = 0.167ZL^2/d$ (Eqn. 3.3) for a load span of one half of the support span.

where:

R = rate of crosshead motion, mm/min,

L = support span, mm,

d = depth of beam, mm, and

Z = rate of straining of the outer fibers, mm/mm min. Z shall equal 0.01.

Maximum fibre stress S was calculated as

$S = PL/bd^2$ for a load span of one third of the support span, or

$S = 3PL/4bd^2$ for a load span of one half of the support span.

where:

S = stress in the outer fiber throughout the load span, MPa,

P = load at a given point on the load-deflection curve, N,

L = support span, mm,

b = width of beam, mm, and

d = depth of beam, mm.

3.5.4 Permeability test

Permeability tests were conducted using the flexible wall method in a triaxial cell, following ASTM D5084-10 & Carpenter & Richard (1986). The setup is shown schematically in Fig. 3.8. This test method is to establish a steady-state flow condition in a cylindrical specimen by maintaining a constant pressure difference at the two ends. Length to diameter ratios was set to be between 0.5 to 1 for all specimens, in order to get more accurate results (Carpenter & Richard, 1986). Pressures of 45 and 40 kPa were applied at the bottom and top of the specimen respectively using two GDS controllers. Thus the pressure difference was 5 kPa. A radial confining pressure of 50 kPa was applied using another GDS. The volume of effluent was measured directly by the GDS. Once a steady-state flow condition was obtained, the intrinsic permeability can be calculated (CRD-C 163-92, 1992). A typical specimen prepared for permeability measurement is shown in Fig. 3.9. The layer of modelling clay wrapping around the specimen was used to avoid the effect of permeant flow along the interface between the ring and sample.

Calculation of permeability was based upon Darcy's law, following Reeves (2006)

$$k_v = \frac{1.63qL}{A\{(p_1-p_2)-p_c\}} \times R_t \times 10^{-4} \qquad \text{(Eqn. 3.4)}$$

where k_v is permeability (m/s),

q is mean flow rate (ml/min),

L is specimen height (mm),

A is mean cross-sectional area (mm^2),

(p_1-p_2) is pressure difference (kPa),

p_c is static pressure corrector (kPa),

R_t is temperature correction factor.

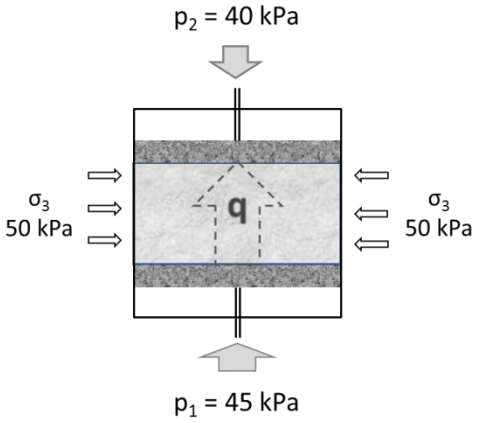

Figure 3.8 Schematic diagram of permeability test configuration

Figure 3.9 Image of a typical specimen prepared for flexible wall permeability test in triaxial apparatus

3.5.5 Direct simple shear (DSS) test

Direct simple shear (DSS) apparatus was also employed in this study to measure the undrained shear strength of clayey soil following ASTM D6528-07, as shown in Fig. 3.10. A stack of slip metal rings replaced the traditional reinforced membrane (Bjerrum & Landva, 1966) in this modified apparatus, which allows the soil specimen

to tilt rather than to slide along a predetermined failure surface, presenting condition closer to real case.

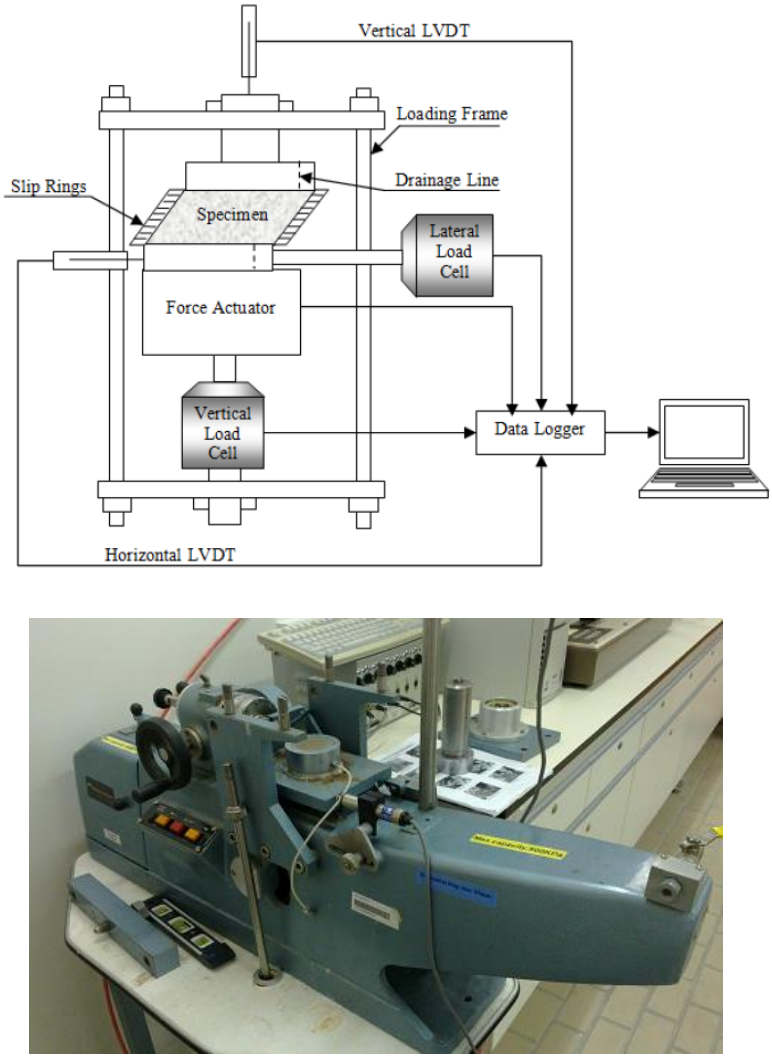

Figure 3.10 Schematic and image of direct simple shear apparatus setup (after Meng, 2010)

Specimens were cut to be in cylindrical disk form, with dimensions of 70mm*20mm, enclosed in a rubber membrane and confined in the stack of metal rings. After consolidating to a predetermined stress level, the specimen was sheared horizontally while maintaining vertical displacement to be constant, in order to keep the volume of specimen unchanged. Vertical/horizontally load and vertical/horizontal displacement were measured by load cells and LVDTs respectively and recorded by data logger.

3.5.6 Oedometer tests

Oedometer tests were conducted to test the effectiveness of biocementation. Two fixed ring oedometer apparatus on table-top set-up with lever arm ratio of 11 were utilized. The dimensions of the two specimen rings are 63.5 mm in diameter, 19 mm in height and 50 mm in diameter and 18mm in height respectively. The procedure follows ASTM D2435-03. A 24-hour multi-staged loading method was applied and the loading sequence was 1 kg, 2 kg, 4 kg, 8 kg, 16 kg, 32 kg, and then followed by the unloading procedures 16 kg, 8 kg, 4 kg and 2 kg. Taylor's Square Root of Time Fitting Method was employed to determine t_{90} for each loading increment.

3.5.7 Measurement of elastic modulus

Elastic modulus of samples was determined by PUNDITPLUS® ultrasonic non-destructive integrity tester, as shown in Fig. 3.11. It's working by measuring the time for P-wave traveling from one transducer to another; the elastic modulus of sample can then be calculated as

$$E=\rho V^2 \qquad \text{(Eqn. 3.5)}$$

in which ρ is density of sample and V is the velocity of P-wave traveling. Voltage was set to be 1200V, and pulse frequency was set to be 10/s in each test.

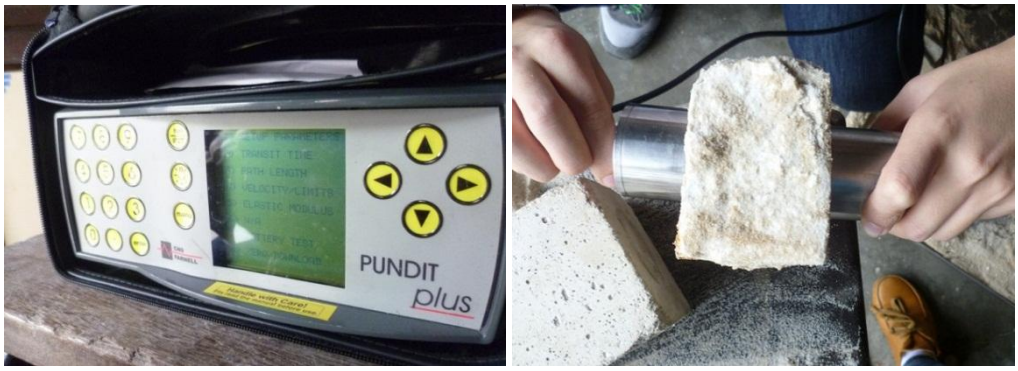

Figure 3.11 PUNDITPLUS® ultrasonic tester and measurement of elastic modulus

3.5.8 SEM, FESEM and EDS tests

SEM stands for scanning electron microscope, which uses electrons instead of light, and electromagnets rather than lenses to form images. Comparing to the traditional light microscopes, SEM has large depth of field and much higher resolution. As SEM utilizes vacuum conditions and uses electrons to form image, water must be removed from the samples since the water would vaporize in the vacuum (Goldstein et al., 1981). Procedure of forming SEM images is as follows:

1. Cut the soil sample into slices of 1cm×1cm square; place them into a 105°C oven for 24hrs to eliminate water.
2. Coat samples with a thin layer of titanium by sputter coater (for adding conductivity to the surface of soil sample).
3. Observe samples under SEM for any sign of inter-particle binder formation.

An updated version of SEM, the Field Emission Scanning Electron Microscope (FE-SEM), which can combine ultrahigh resolution imaging with optimized analytical functionality (through the accessorial EDS machine) was also employed in this study. Similar sample preparation procedure as SEM was adopted. EDS stands for Energy Dispersive X-ray Spectroscope. It can analyse the elemental or chemical characterization of a sample through the interaction of X-ray excitation and a sample based on the theory that each element has unique set of peaks on its X-ray spectrum because of their distinctive atom structure (Goldstein, 2003). Picture of FE-SEM with EDS machine employed in this study is shown in Fig. 3.12.

Figure 3.12 Image of field emission scanning electron microscope (FE-SEM) with energy dispersive X-ray spectroscopy (EDS) employed in this study

Chapter 4

Optimization of Microbially Induced Calcium Carbonate Precipitation (MICP) in Sand

4.1 Introduction

Many factors could influence the effectiveness of calcium carbonate formation by the MICP process. These include urease activity of urease producing bacteria (UPB), distribution and fixation of UPB, chemical concentration, retention time, original material properties, etc. In the previous studies, a commercially available UPB strain *sporosarcina pasteurii* with a urease activity ranging from 3.3 to 20 mM urea/min was commonly used (Al-Thawadi & Cord-Ruwisch, 2012; Cheng, 2012; Harkes et al., 2010; Stabnikov et al., 2013; Whiffin, 2004).

In this study, a UPB strain extracted locally from Singapore, VS1 (species *Bacillus*), was used. The UPB strain VS1 has a much low urease activity. Thus, the effectiveness of using this type of UPB for optimization study needed to be verified. Two sets of experiments, one in liquid solution and another in sand, were performed to access the potential application of MICP. Factors relating to optimization of the MICP process were assessed and discussed. These include pH value, urease activity variation over time, effectiveness of re-cultivated bacteria through consecutive batches, and the effect of centrifuging and re-suspension.

4.2 Urease activities of urease producing bacteria (UPB) VS1

4.2.1 Variation of bacterial properties during cultivation

During the cultivation of the UPB strain VS1, the dynamics of pH, biomass concentration, and urease activity was monitored over four days and the monitoring data are presented in Fig. 4.1a, 4.1b and 4.2 correspondingly. The biomass concentration was assessed via optical density of the sample at λ equals to 600nm (OD_{600}). The detailed OD_{600} information and corresponding biomass concentration information are listed in Appendix C.

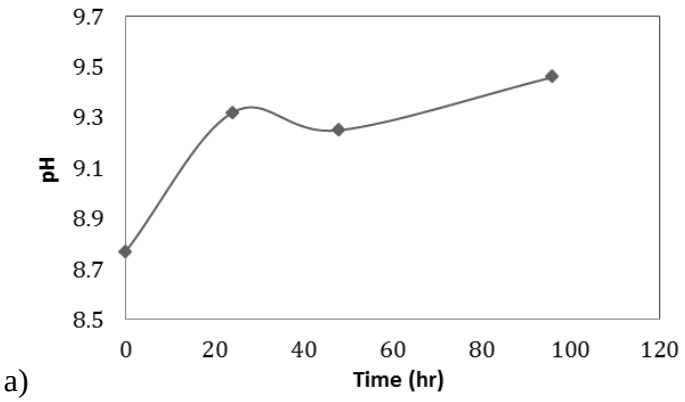

a)

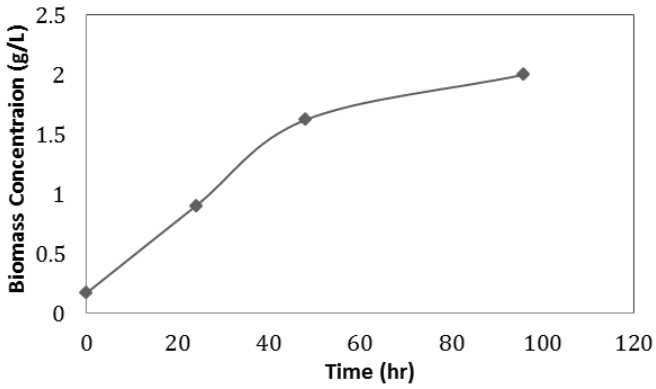

b)

Figure 4.1 Dynamics of a) pH value and b) biomass concentration during UPB cultivation

As shown in Fig. 4.1a, the pH value is observed to rise from 8.8 at beginning to 9.3 after one day due to the carbonate ions produced during the cultivation. This pH value remained relatively constant with little variations till the end of cultivation because of the ammonia ions generated. Biomass concentration as shown in Fig.

4.1b increased linearly during the first two days of cultivation and reached a relatively stationary phase after 96 hours.

The urease activity of UPB was measured by the conductivity variance during the hydrolysis of urea. This method was described in Section 3.2.1. As shown in Fig. 4.2, the total urease activity of UPB produced increased at a stable rate throughout the cultivation process. On the other hand, the highest specific urease activity (urease activity/biomass) occurs at the beginning and keeps dropping afterwards. This may be due to the repression effect caused by the continuously increasing NH_4^+ concentration. The relationship between biomass concentration and urease activity is almost linear as shown in Fig. 4.3. These results are consistent with those reported by Whiffin (2004) on cultivation of *Sporosarcina pasteurii*.

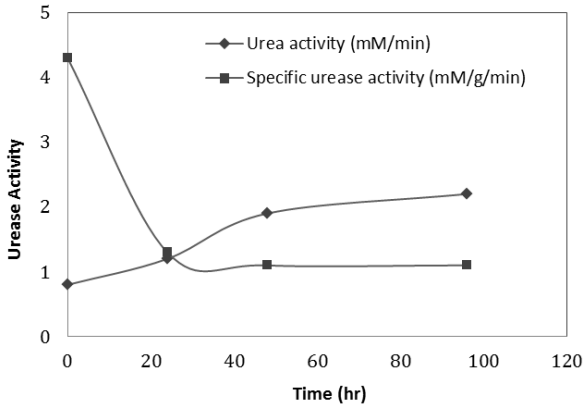

Figure 4.2 Dynamics of urease activity/specific urease activity during UPB cultivation

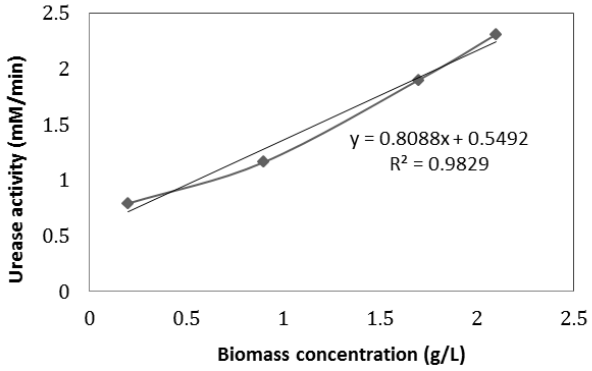

Figure 4.3 The linear relationship between biomass concentration and urease activity

As urease activity does not increase significantly after 48 hours, in this study, the cultivation time for the subsequent batches of UPB was shortened to two days. As shown in Fig. 4.4, the UPB strain VS1 stored in 4°C refrigerator was capable to

maintain its urease activity up to one month after cultivation. Similar results were observed by Whiffin (2004) and Stabnikov et al. (2013), as described in Section 2.3.1.

Some UPB strain VS1 was kept as feed for next batch and re-cultivate with new medium during the whole period of this study. The same cultivation condition as described in Section 3.2.1 was applied in every batch. Close final biomass concentrations were obtained, evidenced by similar final optical density OD_{600} after cultivation. The activities of three UPB batches are shown in Fig. 4.4, which were cultivated in year 2009, 2012 and 2013 respectively. It is noticed that the urease activity dropped to one fifth of its original value, from more than 2mM/min of batch 1 in year 2009, to less than 0.5mM/min in batch 3 in year 2013. This observation could be explained by the increased microbial diversity during cultivation or the mutation of bacteria gene across generations. Such phenomenon also occurs in nature and in industrial cultivation, which was observed by Stabnikov et al. (2013) on the same UPB strain VS1.

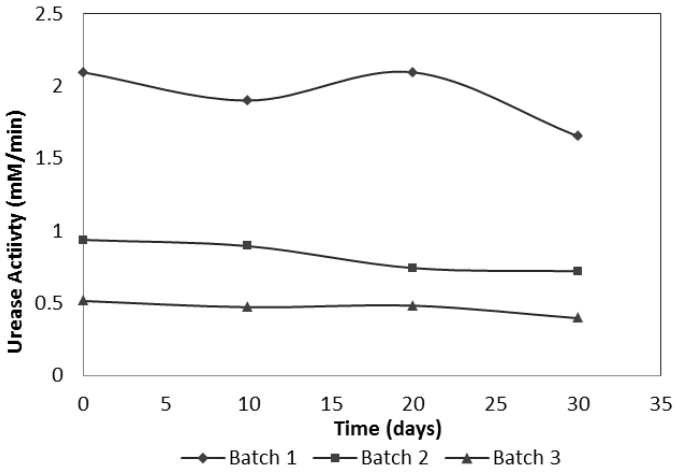

Figure 4.4 Urease activities obtained from different batches of UPB, strain VS1 in this study (batch 1 dated 2009; batch 2 dated 2012; batch 3 dated 2013)

It should be noted that even the highest urease activity obtained for the UPB strain VS1 in this study is not comparable to data represented in the literature, which fall in the range of 3.3 to 20 mM urea/min (Al-Thawadi & Cord-Ruwisch, 2012; Cheng, 2012; Harkes et al., 2010; Stabnikov et al., 2013; Whiffin, 2004), as mentioned in Section 2.3.1. However, low urease activity might not necessarily bring a negative impact in terms of uniformity of biocementation. The interplay

between urease activity and biocementation will be verified in the following sections.

4.2.2 Centrifuged and re-suspended UPB properties

The use of UPB cells after centrifuging has some advantages over the use of original bacterial suspension. First, in spite of the non-pathogenic character of UPB, cultivating and subsequently applying of UPB *in situ* could be malodorous, because of the ammonia generated during bacterial growth. This could impede the application in larger scale and incur some environmental issues. Separating of UPB cells from its culture could alleviate this odour problem.

Second, during the process of cultivation, some urease was released into the culture. The free urease in the culture would react quickly with chemicals presented, which consequently acted as a barrier and impeded the solution's permeation into the interior of the specimen. In contrast, the urease inside the cell, which was gradually released to its surrounding environment in a stable rate (Al Qabany et al., 2012; Cheng & Cord-Ruwisch, 2014; Cheng, 2012; DeJong et al., 2009, 2010; Harkes et al., 2010; Martinez et al., 2013; van Paassen, 2009), would react with the chemicals more steadily, which might lead to a more uniform cementation.

Most importantly, bicarbonate and carbonate anion appear in the culture during the cultivation stage, as urea was consumed by the UPB. Calcium ion added in cementation solution could react immediately with these anions, which may lead to quick calcite formation in solution rather than in between sand particles serving as binder, resulted in lower cementation efficiency. Moreover, centrifuging and re-suspension of UPB could lead to either condensation or dilution of UPB at any concentration, thus making the adjustment of urease activity of UPB controllable. Based on these reasons, centrifuged pure bacteria cell was tested in biocementation with control group conducted in original culture.

However, as suggested by Harkes et al. (2010), a large part of urease activity remains in the supernatant after centrifuging UPB, and dilution of bacterial suspension can cause the release of urease enzyme from the cells into solution,

even in salt solution (9g/L NaCl) which is supposed to prevent the osmotic shock experiencing by the cell and stop the release of enzyme (Section 2.3.1). To verify this assumption, urease activity of original UPB, centrifuged and re-suspended UPB at different concentrations, and also their supernatant were tested, with the results listed in Table 4.1 and plotted in Fig. 4.5. In addition to the re-suspension solvent of 9g/L NaCl, the re-suspension solvent of another concentration, 9g/L NaCl plus 50mM $CaCl_2$, was also tested, as 50mM $CaCl_2$ is a commonly used fixation solution (Whiffin et al., 2007; Harkes et al., 2010).

Table 4.1 Urease activities (mM urea/min) of original UPB suspension, supernatant after centrifuging, and re-suspended UPB at 1/2/4 times of concentration

Original UPB suspension	Supernatant after centrifuging	Centrifuged and re-suspended in			Solvent Type
		Equal volume (1time)	1/2 volume (2 times)	1/4 volume (4 times)	
0.962	0.501	0.468	0.832	1.7	NaCl
		0.332	0.85	1.89	NaCl + $CaCl_2$

It is observed in Fig. 4.5 that when the cells were re-suspended in 9g/L NaCl solution (equal volume as original UPB suspension), urease activity dropped to approximately half of its original value, from 0.962 to 0.468mM/min. The supernatant of original culture after centrifuging has urease activity of 0.501 mM/min. It might be concluded that the portion of urease inside the bacteria cells and that had been released to the cultivation solution in this UPB batch are approximately the same.

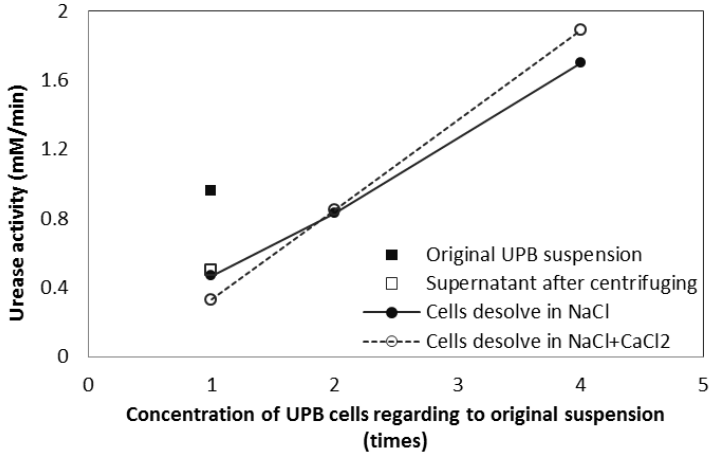

Figure 4.5 Urease activities of re-suspended UPB cells after centrifuging at different concentrations

As shown in Fig. 4.5, by concentrating the centrifuged UPB as re-suspending the cells in lower volume of solvent (half or one fourth volume as original UPB suspension before centrifuging), urease activity increased in proportion to the concentration factor. After concentration, the double-concentrated UPB cells are capable to attain a urease activity level 86% of original UPB suspension (0.962 vs. 0.830 mM/min). Similar observation was obtained in the case of using NaCl and $CaCl_2$ as solvent.

To find out the pattern of that how the enzyme was released to that solvent, the urease activities of both the re-suspended UPB (two-time concentrated suspension) and the solvent after re-suspended UPB being removed (filtered through 0.45μm filter) was measured, as shown in Fig. 4.6. Both UPB re-suspended in NaCl solution and NaCl plus $CaCl_2$ solution maintained their urease activities during the 3-day test. In contrast, little urease activity was observed in the solvent after the UPB being removed. Based on the results, in this study it was assumed that urease remains in UPB cell after centrifuging and re-suspension instead of being released to its solvent.

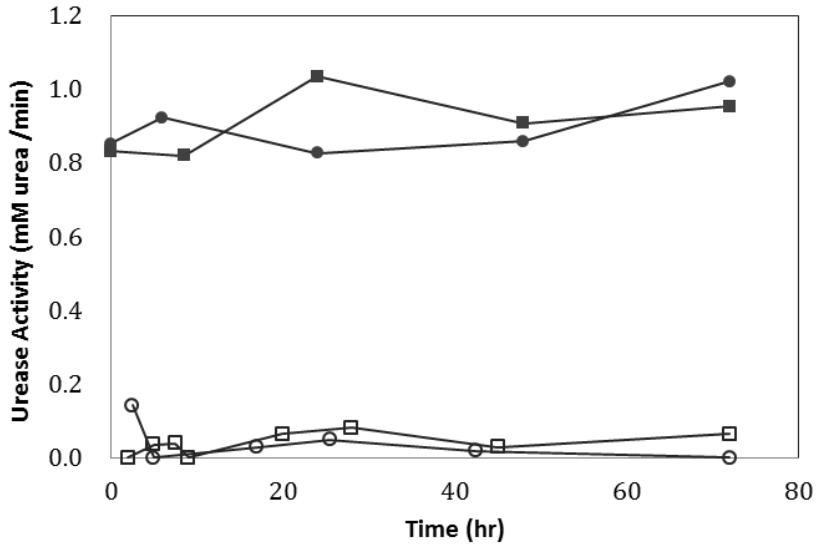

Figure 4.6 Urease activity vs. time of UPB suspended in 9g/L NaCl (■), its solvent (□), UPB suspended in 9g/L NaCl plus 50mM $CaCl_2$ (●) and its solvent (○)

4.3 MICP in liquid solution

4.3.1 Experiment setup

Six sets of samples were tested to measure the effectiveness in terms of UPB type, urease activity level, and reagent composition, as listed in Table 4.2. UPB was added directly into chemical solution in 250ml flask and then put onto shaker (121 rounds per min) for 12 days. The pH value, conductivity, and remaining calcium ion and urea molecule in solution (filtered through 0.45μm filter) were measured throughout the whole testing. The photographs taken during experiments and the calcite crystal attached at the bottom of the flask (Test 3 for illustration) are shown in Fig. 4.7.

As listed in Table 4.2, the cementation solutions of calcium to urea ratio 1:2 (Test 1, 2, 3) and 1:1 (Test 4, 5, 6) were both tested to verify the proportion of reagents for maximizing effectiveness of MICP formation. The "higher" activity UPB employed in Test 1 and Test 2 and the "lower" activity UPB employed in Test 4 and 5 referred to the original UPB suspension, which having urease activity of 0.962 and 0.424 mM/min respectively. The urease activities were dissimilar as they were taken from different batches of cultivation. In "centrifuged" Test 3 and 6, the 2-time concentrated UPB re-suspended in 9g/L NaCl solution, as described in Table. 4.1 (Section 4.2.2) was employed, which had an urease activity of 0.832 mM/min.

Table 4.2 Experiment setup for monitoring the effectiveness of MICP formation

Test No.	UPB Urease activity (mM urea/min)		UPB (ml)	Cementation Solution (ml)	Cementation Solution			Remarks (Bacteria type)
	Original suspension	Super-natant			$CaCl_2$ (M)	Urea (M)	Ratio	
1	0.962	0.501	50	200	0.75	1.5	1:2	higher activity
2	0.424	0.312	50	200	0.75	1.5	1:2	lower activity
3	0.832	-	50	200	0.75	1.5	1:2	centrifuged
4	0.962	0.501	50	200	0.75	0.75	1:1	higher activity
5	0.424	0.312	50	200	0.75	0.75	1:1	lower activity
6	0.832	-	50	200	0.75	0.75	1:1	centrifuged

a) 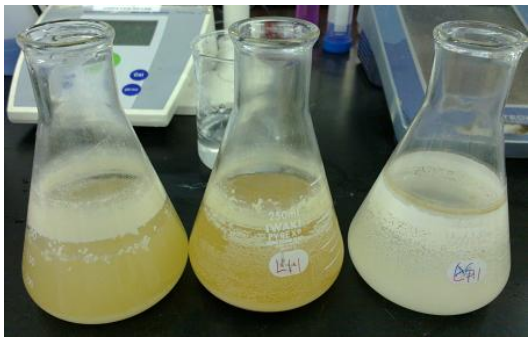 b) 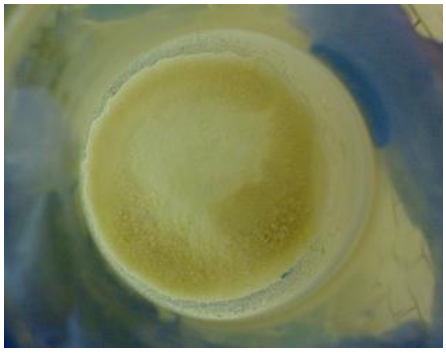

Figure 4.7 Images of a) Test 1, 2 and 3 during experiment, and b) apparent calcite crystal attached on wall and bottom of the flask

The urease activities were approximately the same for the "higher" (in Test 1 and 4) and "concentrated" (in Test 3 and 6) UPB suspensions. This value was roughly two times of that of "lower" activity UPB, despite that the biomass concentration for higher and lower activity UPB were similar as reflected by similar OD_{600} value of about 1.2 ABS, as shown in Table 4.2. The percentage of urease activity remained in supernatant for lower activity UPB batches (Test 1 and 4) after centrifuging (0.312/0.424 = 73.5%) was higher than that of the higher activity batches (Test 2 and 5, 0.50/0.962 = 52.1%), i.e. percentage of urease activity remained inside UPB cell was lower along with original activity after transferring into new medium and re-cultivation.

4.3.2 Parameter variations during the MICP process

Various parameters were monitored during the tests and the results are shown in Fig. 4.8. Regarding to the legends, "1to1" and "1to2", referred to the calcium to urea ratio and "high/low/centri (centrifuged)" referred to three UPB types employed.

The variance of pH values of the six sets, which were all adjusted to be 7 before testing, are displayed in Fig. 4.8a. As presented in Fig 4.8a, the pH values for both high (Test 1 & 4) and low activity (Test 2 & 5) groups in both cementation recipes continuously increased up to three days, and then maintained their levels for another two to three days before continuously decreased afterwards. Such phenomenon can be explained by the interplay between two reactions: urea-hydroloysis (Eqn. 4.1) and formation and precipitation of $CaCO_3$. During the first

three days of test, urea-hydrolysis was the dominant reaction, which produced CO_3^{2-}, pushed the reversible reaction (Eqn 4.2) to the right and raised pH up. After several days, with the depletion of urea, the formation and precipitation of $CaCO_3$ became the dominant reaction, which consumed the free CO_3^{2-} in the solution and pushed reversible reaction (Eqn 4.2) back to the left and lower pH down.

The pH values in solutions of 1:2 rose up higher than those of 1:1, as a higher ratio of urea to calcium strengthened the urea-hydrolysis. This observation was roughly consistent with Martinez et al. (2013), except that the pH value in 1:1 calcium/urea solution was constantly decreasing according to their results.

$$CO(NH_2)_2 + 2H_2O \rightarrow CO_3^{2-} + 2NH_4^{+} \quad (pH\uparrow) \qquad \text{(Eqn. 4.1)}$$

$$CO_3^{2-} + H_2O \leftrightarrow HCO_3^{-} + OH^{-} \qquad \text{(Eqn. 4.2)}$$

$$Ca^{2+} + HCO_3^{-} + OH^{-} \rightarrow CaCO_3 + 2H_2O \ (pH\downarrow) \qquad \text{(Eqn. 4.3)}$$

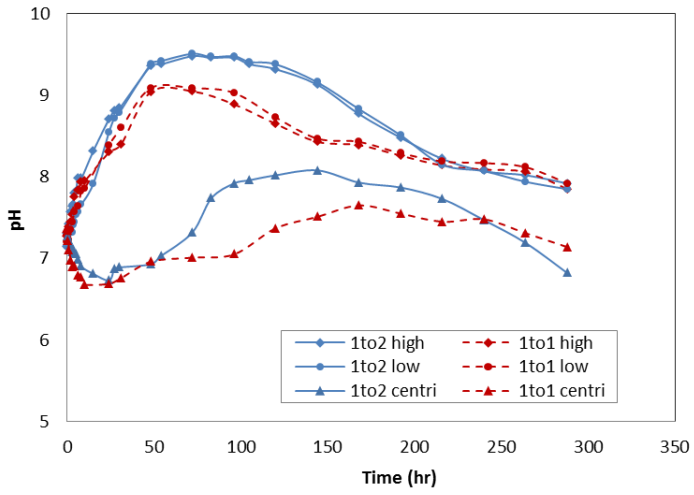

a)

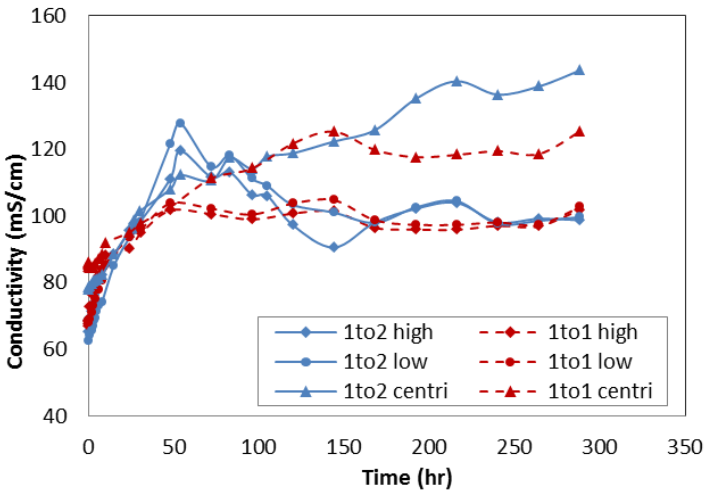

b)

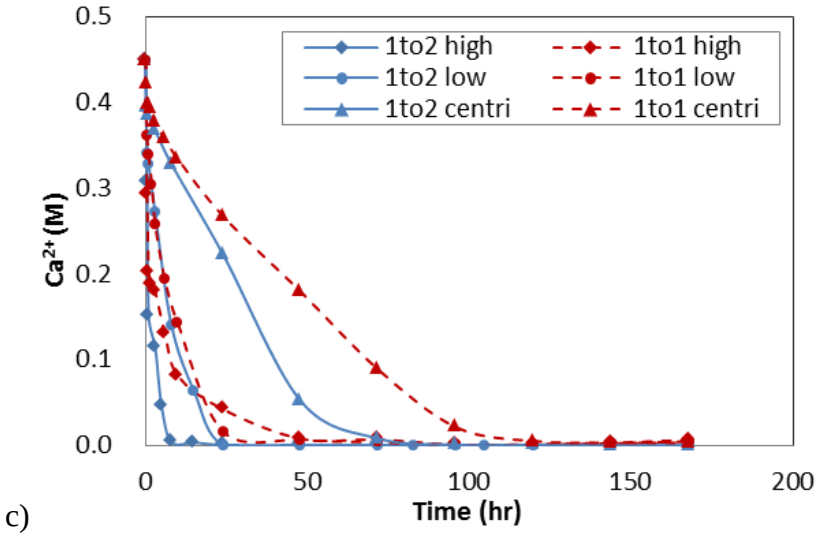

c)

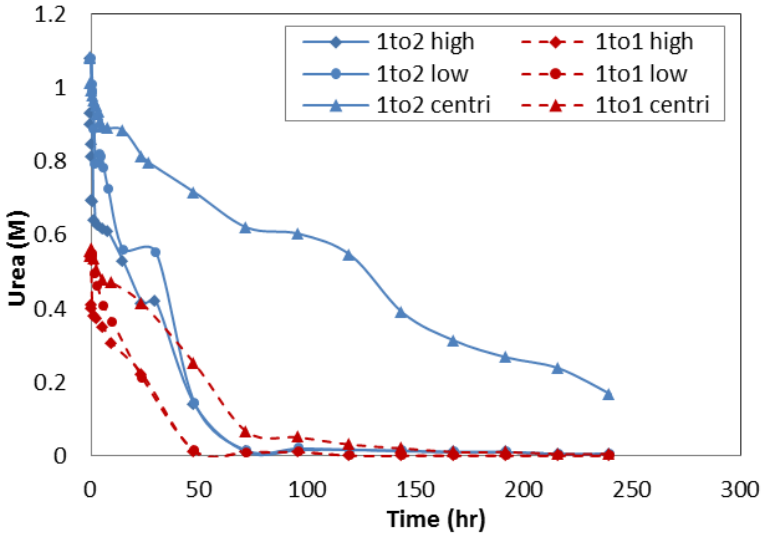

d)

Figure 4.8 Parameters monitored for all six sets in biocementation without soil; a) pH value, b) conductivity, c) calcium cation, and d) urea remaining in solution

Conductivity is another indicator of cementation process, as the release of free ion would result in the escalation of conductivity. As shown in Fig. 4.8b , consistent with pH value variances, the conductivity for Test 1, 2 and 4, 5 increased in the first three days before reduced (in Test 1 and 2) or remained roughly constant (in Test 4 and 5). Meanwhile, the variation of Ca^{2+} and urea in solution were also measured and shown in Fig. 4.8c and 4.8d respectively. The initial concentration of calcium cation was calculated as 0.45M, the product of the concentration of added calcium chloride 0.75M, a dilution factor 0.8 (200/250, as solution was diluted by 50ml of bacteria suspension), and a $CaCl_2$ masse ratio 0.755 (111/147, as $CaCl_2 \cdot 2H_2O$ was employed in this study). Similarly, initial concentration of urea was calculated as 1.08M, the product of the concentration of added calcium

chloride 1.5M, a dilution factor 0.8 and the purity of the industrial urea employed in this study 90%. It is shown that the urea and calcium cations were all consumed within 48 hours in the test using original UPB suspension (Test 1, 2, 4, and 5), at roughly the same reaction rates. In Test 3 and 6, the consumption rate of calcium and urea was lower, despite the fact that the urease activity for the centrifuged UPB was similar to that of the "higher activity" original UPB suspension, and significantly higher than that of the "lower activity" original UPB suspension. After 10 days test, there was still some urea molecules left in the solution in Test 6. The kinetic of ureolysis and MICP formation will be discussed more in Section 4.4.4.

All the parameters measured in Test 1, 3, and 6 are plotted together in Fig. 4.9a, 4.9b and 4.9c respectively. It can be observed in Fig. 4.9a that pH value/conductivity's peak value approximately concurred with the total consumption of Ca^{2+}/urea in the solution. Such phenomenon was also found in Test 2, 4, and 5. These figures could be found in Appendix D.

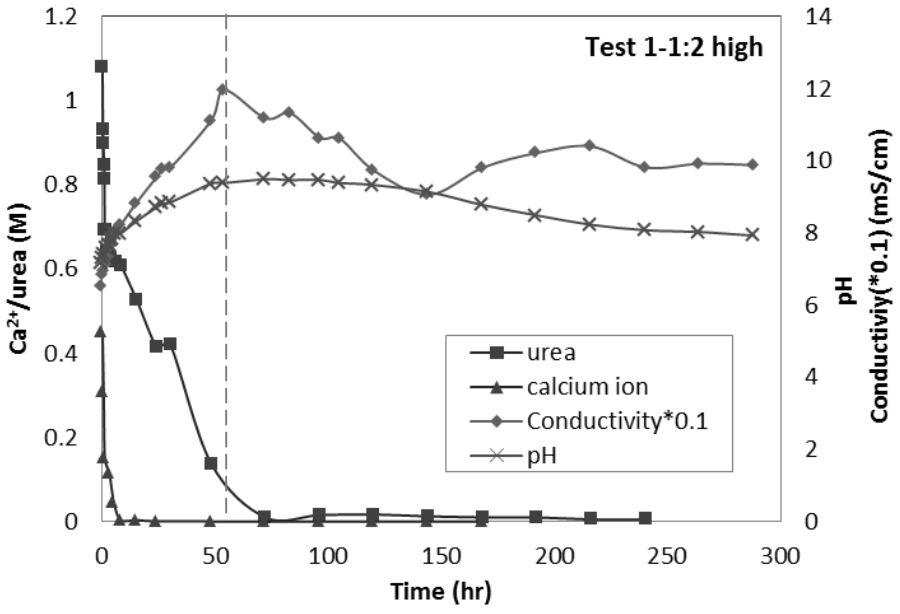

a)

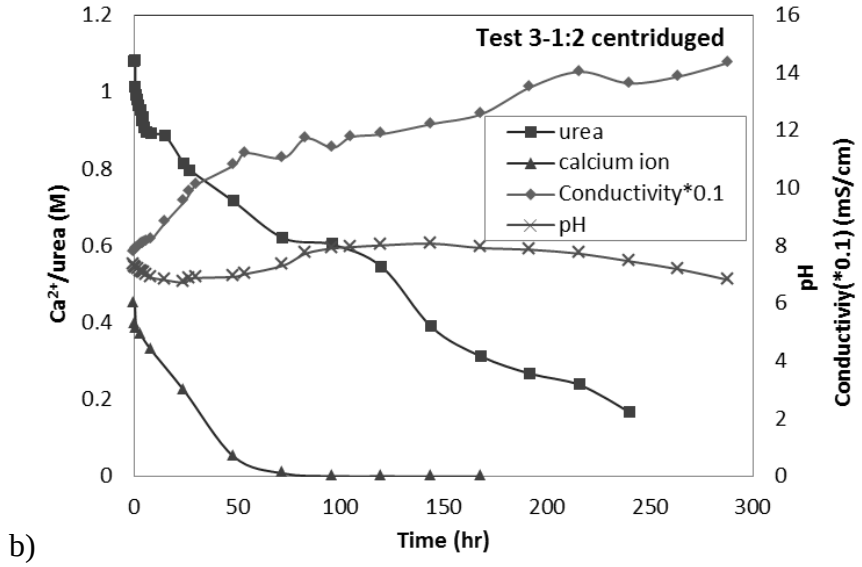

b)

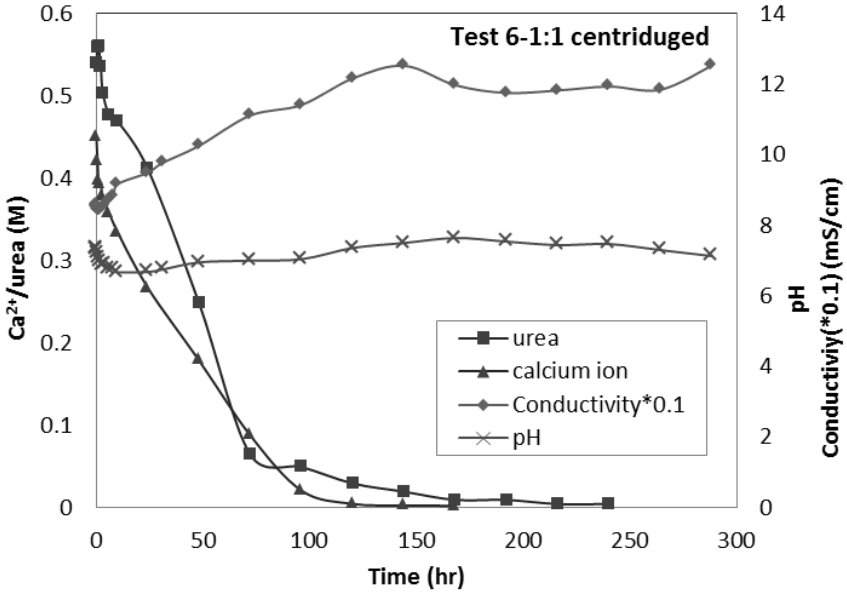

c)

Figure 4.9 All parameters including pH value, conductivity, calcium cation, and urea remaining in solution in a) test 1 (1:2 high), b) test 3 (1:2 centri), and c) test 6 (1:1 centri)

However, several different patterns for parameters variances were found in the test in which centrifuged UPB was used (Test 3 and 6). As shown in Fig. 4.9b and 4.9c, pH values in centrifuged UPB groups (Test 3 and 6) mostly fluctuated within a range between 7 and 8 throughout the whole test. It started with a decreasing trend during first 24 hours, and then kept increasing until 150hr, before it decreased again afterwards. On the other hand, conductivity kept increasing throughout the whole experiment. In conclusion, there was a "time lag" of reaction in the centrifuged bacteria employing group, which was reflected by the pH and

conductivity variance. This was assumed to be the time needed for urease to be released from the cell rather than reacted immediately with enzyme in solution.

4.4 MICP in sand

4.4.1 Experiment setup

Poorly graded fine sand Riversand^{TM} (as described in Section 3.4.1) was used for testing the MICP formation within sand. Dry sand samples were packed by funnel into the transparent plastic cylinder moulds of 50mm in diameter and 100mm in height. Initial void ratios were in the range of 0.52 to 0.62 ($D_r \approx 65$ - 85%). A layer of 1.5 cm-thick gravels having $D_{50} \approx 5$mm was placed on the top and the bottom of the sand, acting as filters. A photograph and a structural sketch of experimental setup are shown in Fig. 4.10.

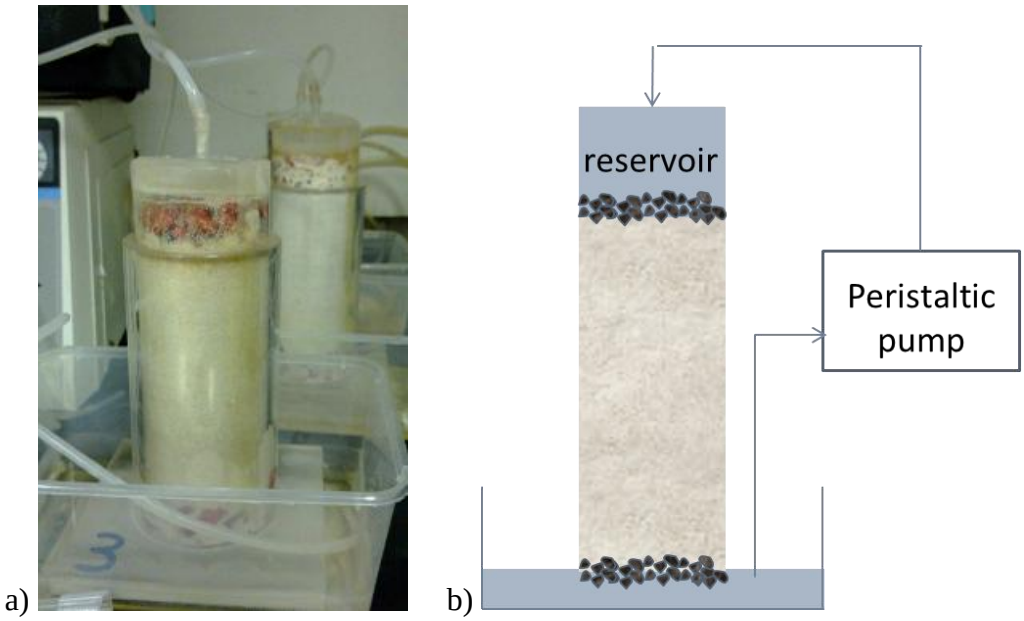

Figure 4.10 Setup for fundamental studies with sand; a) image of one specimen during treatment, and b) sketched structure

Detailed setups of each specimen are summarized in Table 4.3. The first six tests (Test 1 to 6 in Table 4.3a engaged similar parameters with the six tests without sand (as described in Table 4.2 in Section 4.3), regarding to both the UPB type and the reagents of cementation solution. UPB with higher activity, lower activity and centrifuged UPB (concentrated two times), and cementation solution engaging $CaCl_2$ to urea ratios of 1:1 and 1:2 were all tested. For comparing the efficiency of

reagent cementation solution and bacteria engaged in this study and those from the previous researchers, two more sets of sand samples were prepared, engaging cementation solution with a 3:3:1 recipe in Martinez et al. (2013) (Table 4.3b).

Initial permeability in each sample, as shown in Table 4.3, was measured by falling head method directly from the water head variance in the reservoir by Eqn. 4.4. Areas *a* and *A* were designed to be the same for the convenience of measurement, yet might not be very accurate.

$$Coefficent\ of\ permeability\ k_T = \frac{aL}{At} \ln\left(\frac{h_1}{h_2}\right) \qquad \text{(Eqn. 4.4)}$$

Table 4.3 Experiment setup for monitoring the effectiveness of MICP formation; a) set 1 to 6, employing 1:1 and 1:2 cementation recipe (engaged in this study) b) 3:3:1 recipe in Martinez et al. (2013)

a) Test No.	Bacteria type	Urease activity (mM/min)		Cementation Solution			Initial void ratio e of sand	Initial permeability ($*10^{-7}$ m/s)	Referred in later sections as
		Total	in supernatant	$CaCl_2$ (M)	Urea (M)	Ratio			
1	higher activity	0.962	0.501	0.75	1.5	1:2	0.53	676	1:2 high
2	lower activity	0.424	0.312	0.75	1.5	1:2	0.56	804	1:2 low
3	centrifuged	0.832	-	0.75	1.5	1:2	0.52	600	1:2 centri
4	higher activity	0.962	0.501	0.75	0.75	1:1	0.56	747	1:1 high
5	lower activity	0.424	0.312	0.75	0.75	1:1	0.62	715	1:1 low
6	centrifuged	0.832	-	0.75	0.75	1:1	0.56	661	1:1 centri

b) Test No.	Bacteria type	Cementation/UPB Solution				Initial void ratio e of sand	Initial permeability ($*10^{-7}$ m/s)
		Urea $CO(NH_2)_2$ (M)	Ammonium chloride NH_4Cl (M)	Sodium carbonate $NaCO_3$ (M)	Calcium chloride $CaCl_2$ (M)		
1a	higher activity	0.333	0.374	0.0252	0.1	0.57	698
2a	lower activity	0.333	0.374	0.0252	0.1	0.58	735

Four rounds of treatment were conducted in each test in series Test 1 to 6. Each treatment lasted for five days. For each treatment, 60 ml of UPB suspension (around one pore volume) was applied to the sample by surface percolation; 50mM $CaCl_2$ (performing as fixation solution) was added directly into the suspension once the filtration was finished, and then recirculated by peristaltic pump overnight (for 12 hours) at a flow rate of 1.5 ml/min. A sprinkler head was attached to the

end of peristaltic pump tube for evenly distributing the solutions. 240 ml of cementation solution with 0.75M $CaCl_2$ plus 1.5M urea (four times of pore volume) was added into the reservoir on top of the sand surface once the circulation of bacteria suspension was finished, and then recirculated at 20ml/min for five days. It shall be noted that the "reservoir" on top for storing the solutions was heightened by extra plastic sheets when necessary.

For tests 1a and 2a, the treatment process described in Martinez et al. (2013) (set 1B) was employed, using urea $CO(NH_2)_2$, ammonium chloride NH_4Cl, and calcium chloride $CaCl_2$ at a ratio of 3:3:1. In order to simulate the method which produced the best MICP in terms of cementation efficiency, according to Martinez et al. (2013), stopped flow for bacteria suspension and continuous flow for cementation solution at a reversed direction from bottom was involved. Original bacteria suspension of high and low activity was tested. Bacteria solution (60ml UPB with 3:3:1 chemicals solution) were injected, retained in sand overnight without recirculation. 480ml of 3:3:1 cementation solution was then injected from bottom with following recirculation for 5 days.

The clarity of effluent bacterial suspension after recirculation overnight (and OD_{600} value close to control, not shown) indicated almost full attachment of bacteria on sand particles.

After each treatment, the cementation solution was discarded and specimens were rinsed by distilled water. Subsequently, permeability was measured by recording the heading falling over time of distilled water in the reservoir, as described in Eqn. 4.1.

4.4.2 Monitoring data

Tests 1 to 6

The data monitored during process of Tests 1 (1:2 high), 3 (1:2 centri), and 6 (1:1 centri) are shown below in Fig. 4.11a, 4.11b and 4.11c respectively, of which calcium and urea maintained in the effluent are presented in a1, b1 and c1, while conductivity and pH variance are plotted in a2, b2 and c2 respectively.

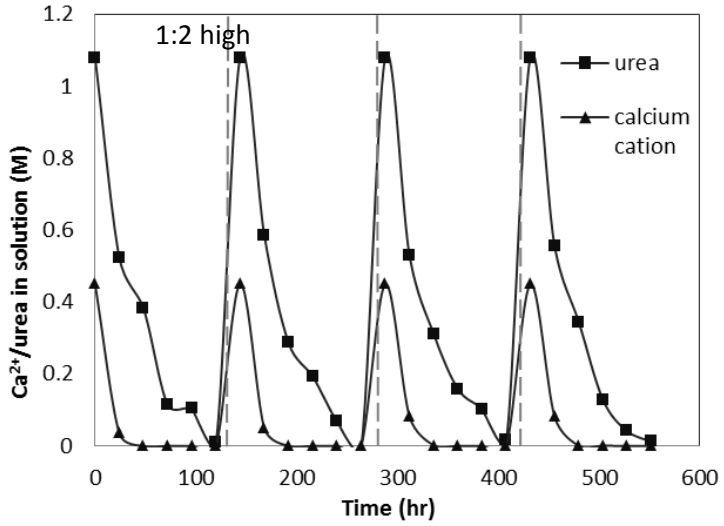
1:2 high
urea
calcium cation
Ca2+/urea in solution (M)
Time (hr)
0
0.2
0.4
0.6
0.8
1
1.2
0
100
200
300
400
500
600

a1)

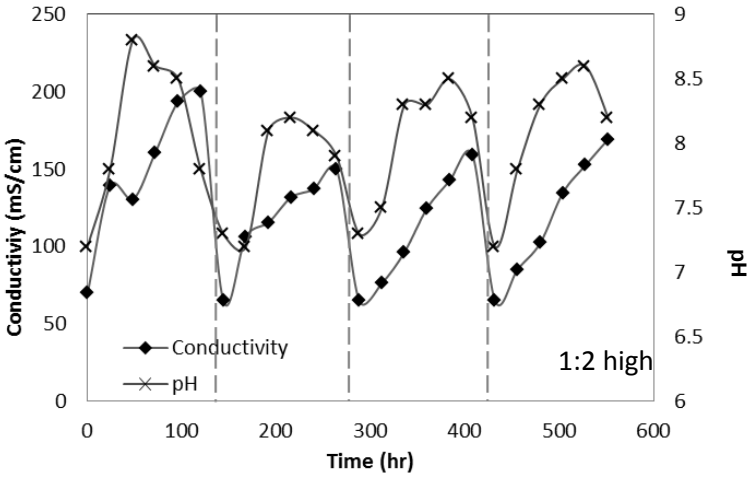
Conductivity
pH
1:2 high
Conductiviy (mS/cm)
pH
Time (hr)
0
50
100
150
200
250
6
6.5
7
7.5
8
8.5
9
0
100
200
300
400
500
600

a2)

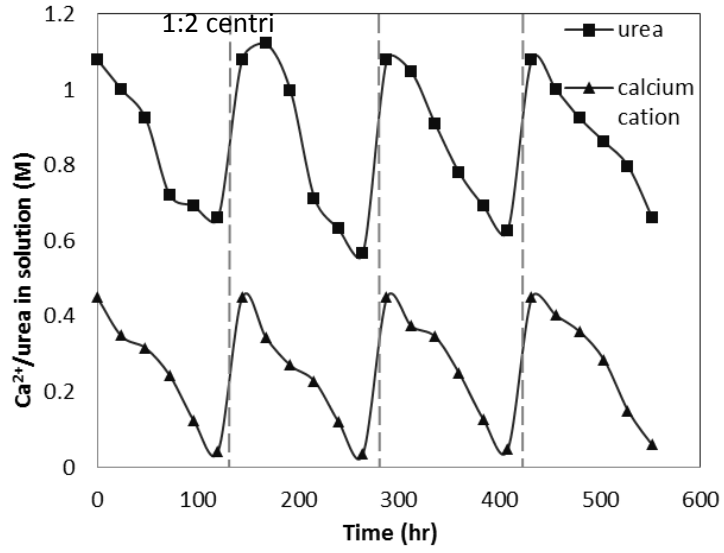
1:2 centri
urea
calcium cation
Ca2+/urea in solution (M)
Time (hr)
0
0.2
0.4
0.6
0.8
1
1.2
0
100
200
300
400
500
600

b1)

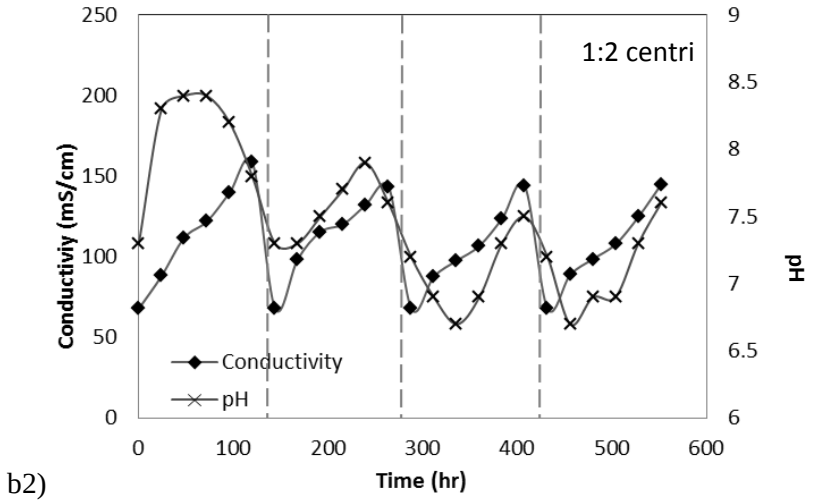

b2)

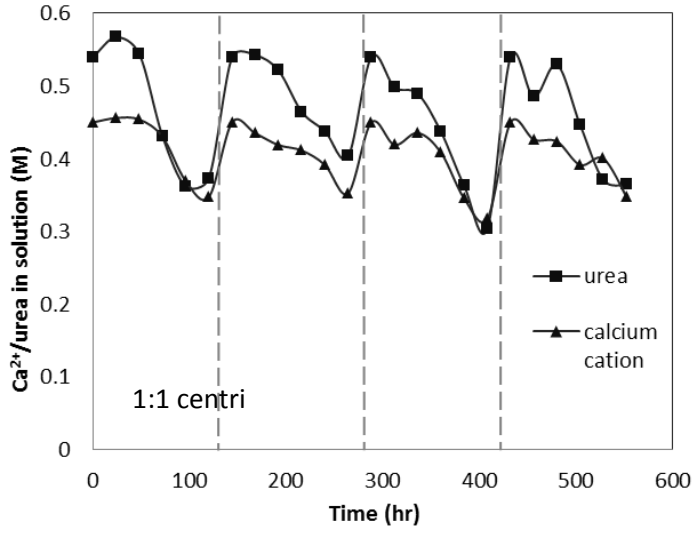

c1)

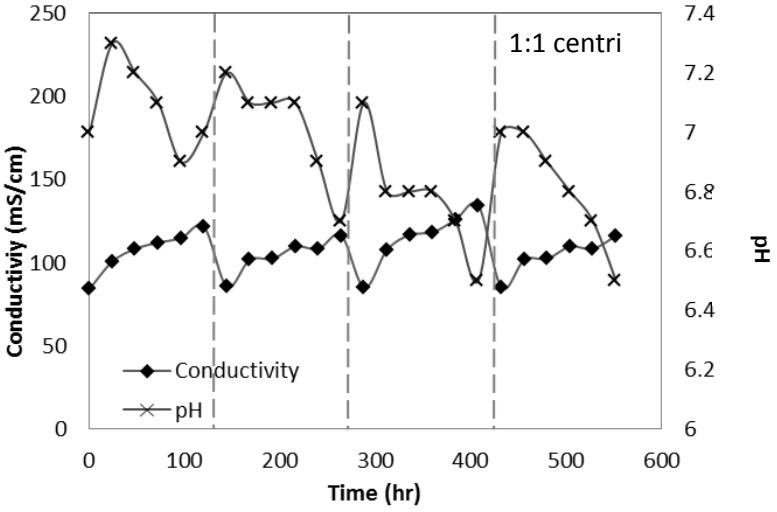

c2)

Figure 4.11 Parameters monitored including pH value, conductivity, calcium cation, and urea remaining in solution in sand during treatment for a) Test 1 (1:2 high), b) Test 3 (1:2 centri), and c) Test 6 (1:1 centri)

As shown in Fig. 4.11, similar repeated patterns of parameters in each round of treatment were observed in every test, which are divided by dash lines. This might be an indication that the MICP process was stable and the amount of calcite precipitated might be similar in each round of treatment.

The results of the parameters during cementation in each round from high activity original UPB suspension, using cementation solution with a ratio of 1:2 (Test 1, Fig. 4.11a1 and a2) were similar to the tests without sand as described in Fig. 4.8, Section 4.3.2. Calcium was consumed completely within the first day of treatment, while urea was used up gradually during the five days in one round. The conductivity and the pH value continued to increase in each round of treatment, instead of dropping after three days in solution without sand. This might be an indication of a slower chemical reaction rate comparing with that of pure solution without soil, because of the less contacting time between bacteria and cementation solution while recirculating. Other tests employing original bacteria suspension (Test 2, 4 and 5) demonstrated similar patterns, which could be found in Appendix E.

For centrifuged bacteria sets (Fig. 4.11b1, b2 and c1, c2), the lag of reaction is more obvious because urease was released from bacteria cell rather than in supernatant, which makes the cementation rate more stable and controllable. In Test 3 (cementation solution employing 1:2 recipe, shown in Fig. 4.11b1), calcium cation was almost consumed completely in each treatment, while there are still unused urea remaining in the solution after recirculating for five days. The pH value kept rising from around 7 to marginally above 8, but never attained a level in the original UPB suspension (Fig. 4.11b2). However, for cementation recipe 1:1 (Fig. 4.11c2), the pH value fluctuated around 7, indicating a low bacterial activity. The urea and calcium consumption rates were low, not all the calcium/urea was used after five days of recirculation. This observation fits the results getting by Martinez (2013); the pH reduction caused by calcite precipitation overcomes the pH rising by ureolysis, as the urea concentration is low in 1:1 recipe. Calcite precipitation might also be influence by this environment lack of alkalinity in consequences.

Tests 1a and 2a

The data obtained from Test 1a are shown in Fig. 4.12a and 4.12b. The data of set 2a shows a similar pattern which can be found in Appendix E. Both urea and calcium had practically been consumed completely within the first day of treatment. pH value fluctuated around 8 after the depletion of urea/nutrition in solution; continuous increase of conductivity was observed throughout each round of treatment, which might be the indicator of a constant activity of UPB.

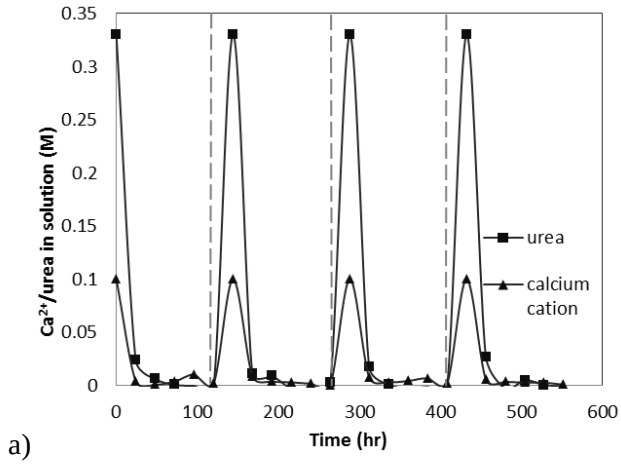

a)

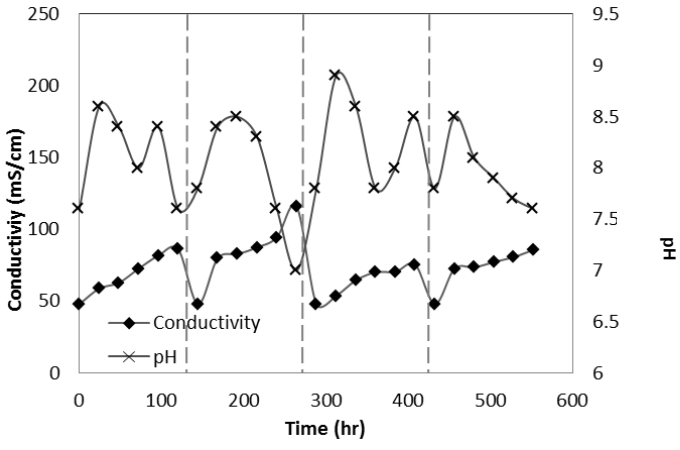

b)

Figure 4.12 Parameters monitored in Test 1a, including a) calcium cation and urea remaining in solution and b) pH value and conductivity

4.4.3 MICP formation in sand and resulted strength/permeability

Tests 1 to 6

Sand specimens were taken out of the moulds and used for unconsolidated undrained strength tests after four rounds of treatments, as shown in Fig. 4.13a and

4.13b. However, only samples from Test 1, 3 and 4 were maintained intact after taken out; specimens in other tests were broken at some point during trimming, as shown in Fig. 4.13c. Since all the specimens were handled and trimmed manually with equal care and delicacy, such phenomenon also revealed that probably some unevenness of MICP formation existed to some extent within these specimens.

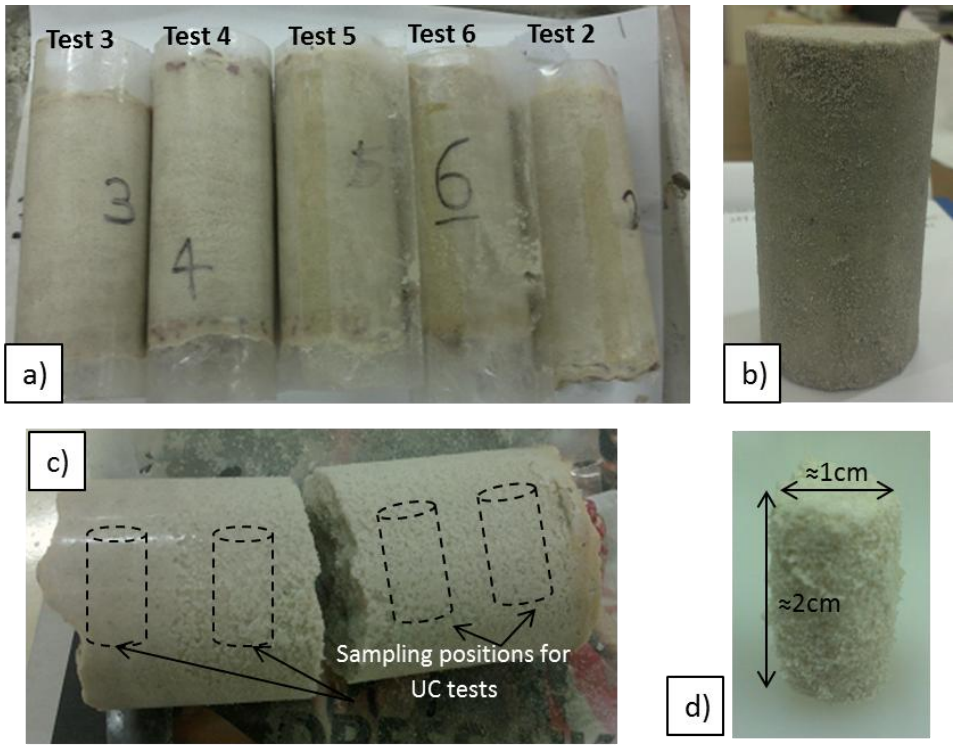

Figure 4.13 Images of a) specimens of Test 2 to 6 after taken out from moulds; b) specimen of Test 1 after trimming; c) breakage of specimen during handling (specimen of Test 5) d) one UC specimen from Test 5

To test the strength of the broken specimens, small cylindrical samples were carved out from different locations of specimens and trimmed into 1*2cm in dimension in Test 2, 5 and 6 for UC tests, as indicated in Fig. 4.13c. One UC specimen from Test 5 is shown in Fig. 4.13d. The small cylindrical specimens were also trimmed from the remaining of the specimens of Test 1, 3, and 4 after UU tests for comparison. Around 2g of sand samples were taken at different locations within the specimens during trimming for calcite contents measurement.

Results of UU tests

Unconsolidated undrained (UU) triaxial tests were conducted for the specimens from Test 1, 3 and 4, using samples of 50*100mm in dimension. The results are

shown in Fig. 4.14. The confining pressure σ_3 was set to be 50 kPa in all tests. Similar peak UU strength values were obtained in set 1, 3, and 4, ranging from 910 kPa (Test 1) to 1050 kPa (Test 3). In Test 3, the peak strength was maintained up to 8% of axial strain after the peak was reached at 2% axial strain. This might be due to the development of further cementation breakage within specimen after failure, as more uniform cementation was reached by the concentrated and re-suspended bacteria suspension. The residue strengths of the three tests were different from each other, within which Test 3 had the highest residue strength value. It might be partially attributed to the greater interlocking of the larger effective particles cemented together from smaller particles leaded by higher cement bonding effect (Lade & Overton, 1989; Marri, 2010).

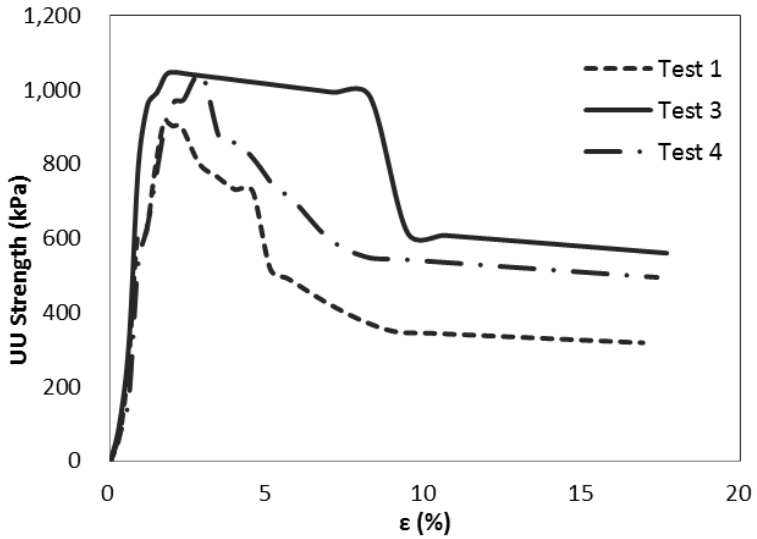

Figure 4.14 Stress-strain relationship of UU triaxial tests on set 1, 3, and 4

Calcite content and UC strength vs. depth

Calcium content and UC strength measured from the small cylindrical samples along depth within each specimen are shown in Fig. 4.15a to 4.15f respectively. Calcite content was measured by acid washing method, as describe in Section 3.3.1.

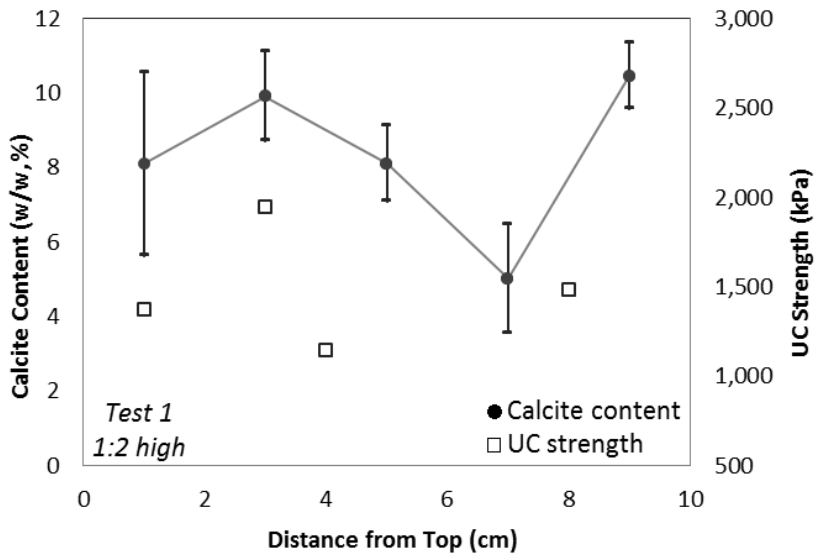
Calcite Content (w/w,%)
UC Strength (kPa)
Test 1
1:2 high
Calcite content
UC strength
Distance from Top (cm)

a)

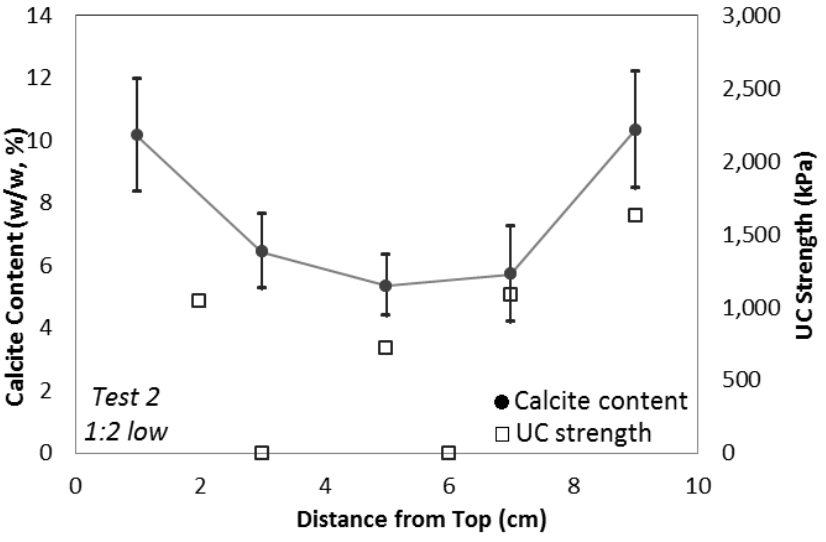
Calcite Content (w/w, %)
UC Strength (kPa)
Test 2
1:2 low
Calcite content
UC strength
Distance from Top (cm)

b)

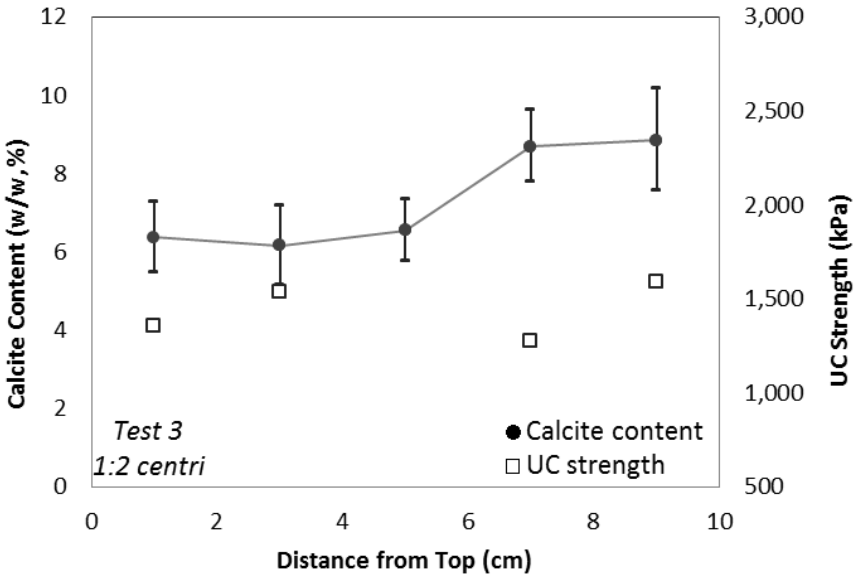
Calcite Content (w/w,%)
UC Strength (kPa)
Test 3
1:2 centri
Calcite content
UC strength
Distance from Top (cm)

c)

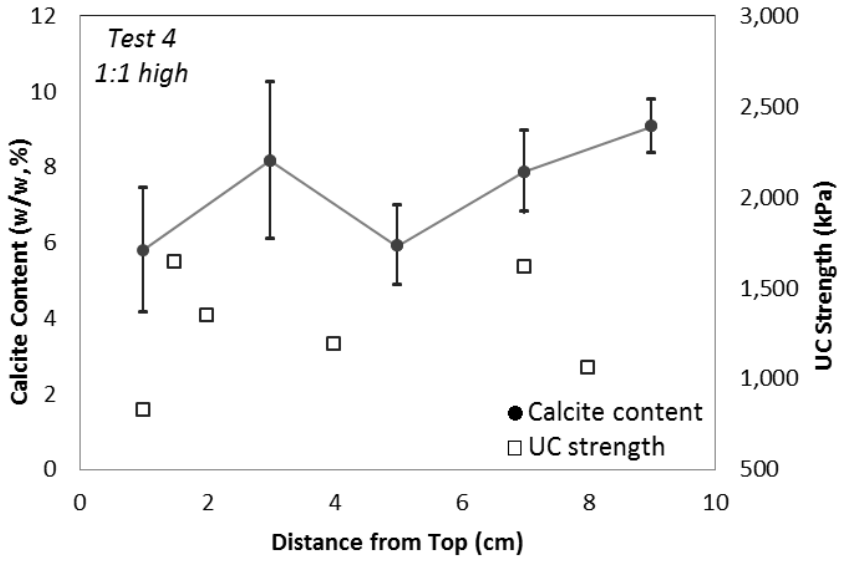

d)

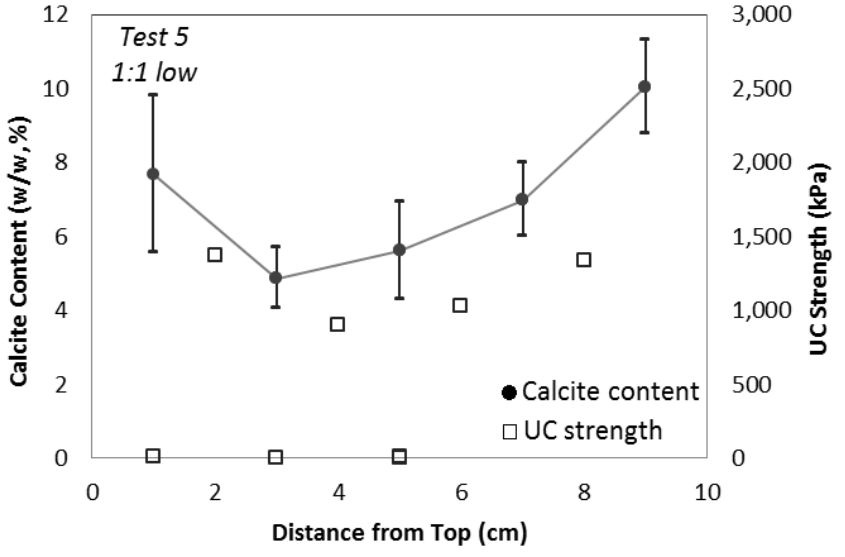

e)

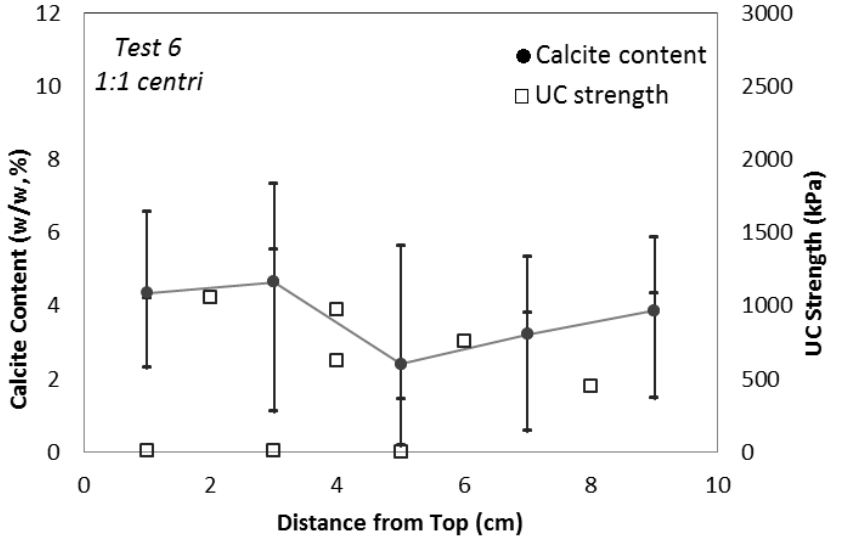

f)

Figure 4.15 UC strength (□) and calcite content (●) along depth in set 1 to 6 (a to f)

As it can be observed in Fig. 4.15, Test 3 (Fig. 4.15c) developed relatively the most uniform cementation regarding the UC strength. All the strength values were around 1500kPa, in spite of the different locations from which the samples were taken, and also the calcium contents along depth. This might be due to the fact that the centrifuged UPB stored urease inside bacteria cells and thus had slower and more stable reaction rate, which conformed with the prediction/results made by previous researchers (Cheng & Cord-Ruwisch 2014; Fidaleo & Levecchia 2003; Martinez et al., 2013; Qian et al., 2009).

However, such an advantage of centrifuged UPB could not be found in cementation solution using calcium to urea ratio of 1:1 (Test 6, Fig. 4.15f), within which the calcite precipitated were more scattered along depth and UC strengths were generally lower than 1000 kPa. Such an observation well tallied with the results of parameter variations during the treatments (Fig. 4.11c1 and c2), in which calcium and urea were not fully consumed and pH value did not rise above 7.5 throughout the whole test. Yet the effect of cementation recipe, i.e. the $CaCl_2$ to urea ratio, was not as obvious in the original bacteria suspension tests (Test 4 and 5, Fig. 4.15d and e, comparing to Test 1 and 2 in Fig 4.15a and b). Both the calcium contents and UC strengths were similar with each other between them. It also fits the parameter monitoring during treatment in these tests: trend of pH value variation, calcium consumption and ureolysis rate were analogous, with 1:1 recipe tests lagging slightly behind. Therefore, it might be concluded that stable urease activity in bacteria cell is an important factor in uniformity of MICP formation. Besides, pH value is also an essential influencing factor, as the effect of either the cementation solution recipe or the bacterial activity became insignificant as long as pH value is rising.

For the tests engaging non-centrifuged original UPB suspension, higher activity resulted in slightly better MICP formation, which is also evidenced by the phenomenon that the samples from both Test 1 and Test 4remained intact after taken out from the mould. Calcite content and UC strength in lower activity tests (Fig. 4.15b and e) exerted typical trends under submerged treatment method as described in Section 2.3.5, in which the highest calcite content/UC strength was always found to be at the top and bottom along treatment depth. Such phenomenon

might be due to the higher proportion of urease activity remaining in the supernatant rather than inside the bacterial cell for lower activity UPB comparing to the higher activity tests, as presented in Table 4.2 and Table 4.3a. Quick MICP precipitation formed immediately after the injection of cementation solution near the injection point, resulting in a blocking around the area nearby.

The UC strengths of the samples from the tests are plotted against their calcite contents, employing the average calcite content value at that specific layer, as shown in Fig. 4.16. Typical trend of UC strength increasing with calcite content was observed, regardless of the surface percolation treatment method employed at the beginning of treatment; the process of recirculation might redistribute the calcium/urea source provided.

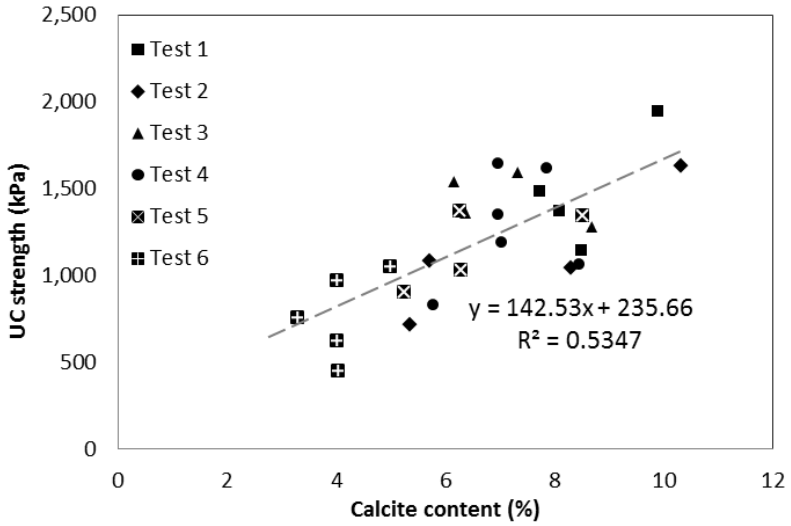

Figure 4.16 Summary of UC strength vs. calcite content in Tests 1 to 6

Variance of permeability after each treatment

The variations in coefficient of permeability *k* after each treatment in the six tests are plotted below in Fig. 4.17a. Test 3 and 6 resulted in more gentle reduction of permeability after each treatment, indicated the uniformity of centrifuged UPB produced MICP comparing to the original UPB suspension. Such property also ensured that further treatment is possible in future. Nevertheless, the very limited reduction of *k* in Test 6 also suggested the incapability of centrifuged UPB in cementation solution recipe 1:1. Difference between the tests employing original

UPB (Test 1, 2, 4 and 5) had not been revealed regarding the permeability variation. One explanation could be that the quick formation of MICP due to urease activity in supernatant for original UPB suspensions rapidly decreased the permeability of sand in the first treatment. Subsequent treatments did not vary the value of permeability much.

The calcite contents versus permeability after each treatment of the six tests are plotted in Fig. 4.17b, with the assumption that the same amount of calcite was produced in every round of treatment. As expected, permeability reduces with increasing calcite content, as more voids are filled with calcite precipitation. Difference between each test became smaller, comparing to Fig. 4.17a.

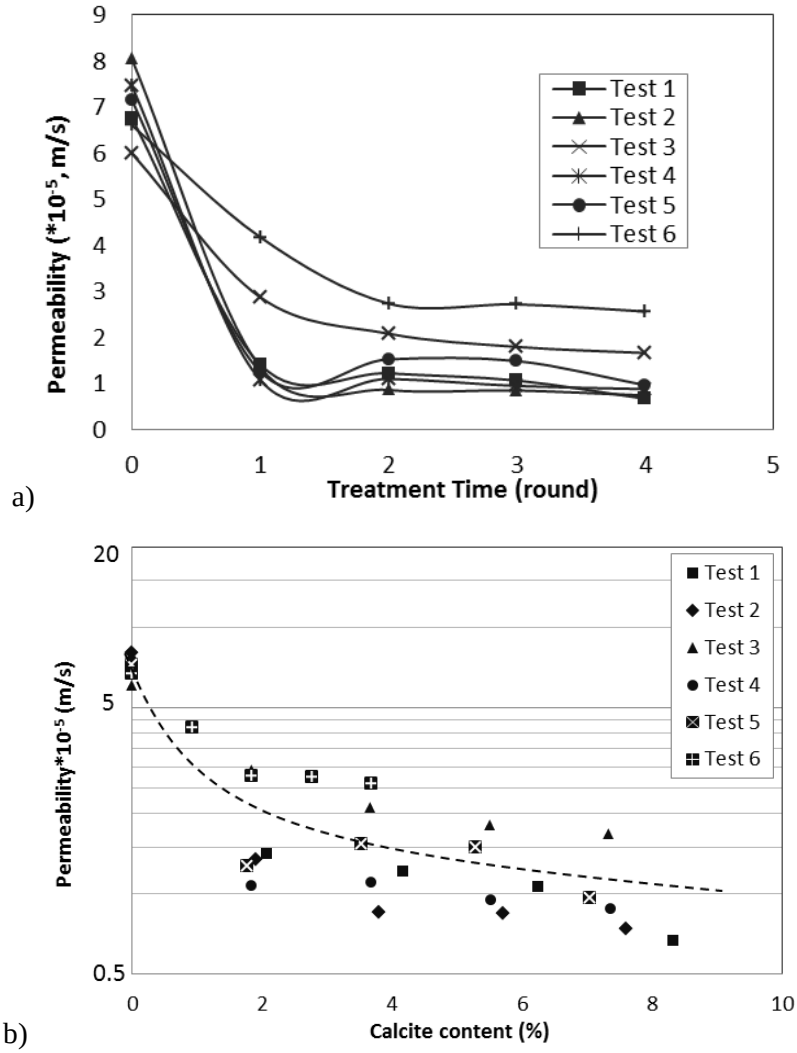

Figure 4.17 Coefficient of permeability variation in Test 1 to 6 a) after each treatment, and b) versus calcite content

Tests 1a and 2a

Calcium content and UC strength

A photograph of the specimens of set 1a and 2a after four treatments is shown in Fig. 4.18. The calcium contents and UC strength of the specimens along depth are shown in Fig. 4.19a and 4.19b respectively. As observed, the gain on strength and the calcite precipitation were very limited in both tests; their bottom parts all crumbled while taken out of the moulds, indicating weak cementation. As the time of mixing of bacteria and chemicals in 3:3:1 bacterial solution was not specified in the paper by Martinez et al. (2013), they were mixed at a different time before applying to the specimens. Calcium carbonate might have already formed in the bacterial solution at that time, resulted in pre-formed calcite crystals precipitating on surface of sand instead of forming in between sand particles and serving as bonding. Such presumption could be supplemented by the results that both calcite content and UC strength were maximized on the top part of specimens. However, it should also be noted that the calcium supply for Test 1a and 2a was about 50% lower than that of Test 1 to 6, as initial calcium concentration was only one fourth of 1:2 and 1:1 solution employed in this study, although volume of cementation solution was already more than doubled. The application of larger volume of cementation solution was not practical, which is also indicated by Al Qabany & Soga (2013).

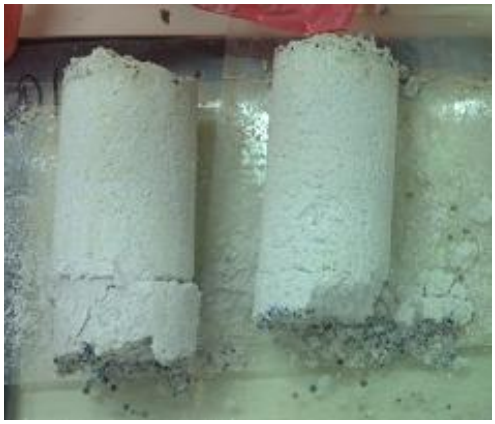

Figure 4.18 Image of specimens in set 1a (left) and 2a (right) after four treatments

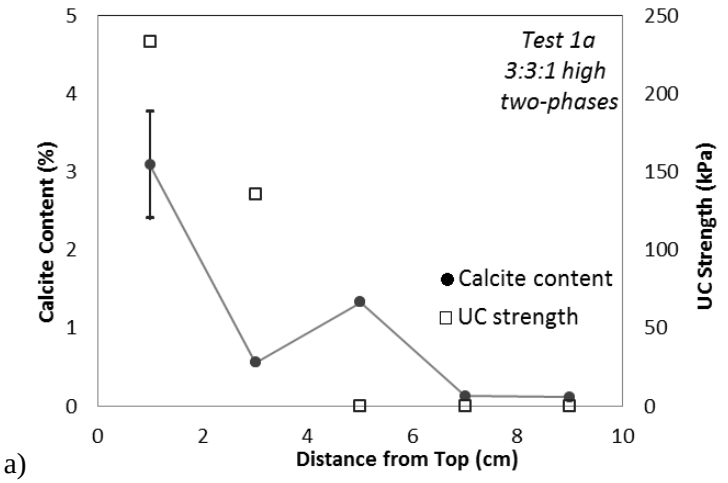

a)

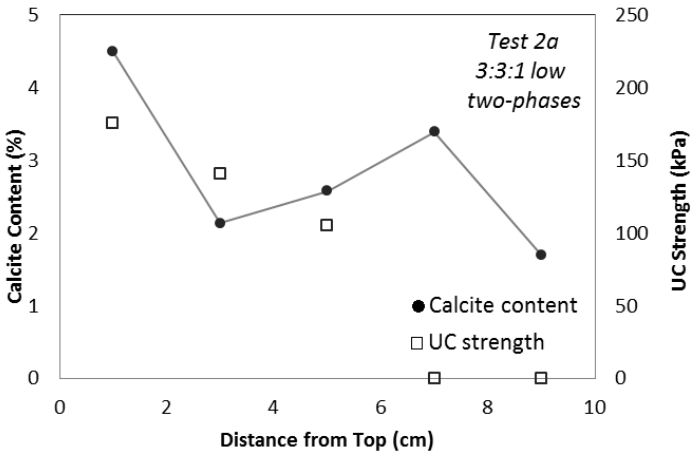

b)

Figure 4. 19 UC strength (□) and calcite content (●) along depth in a) Test 1a and b) Test 2a

The calcite contents against the UC strengths in Test 1a and 2a are plotted in Fig. 4.20, employing the average calcite content value in each layer. Calcite content and UC strength is also positively correlated, despite that the data points are more scattered.

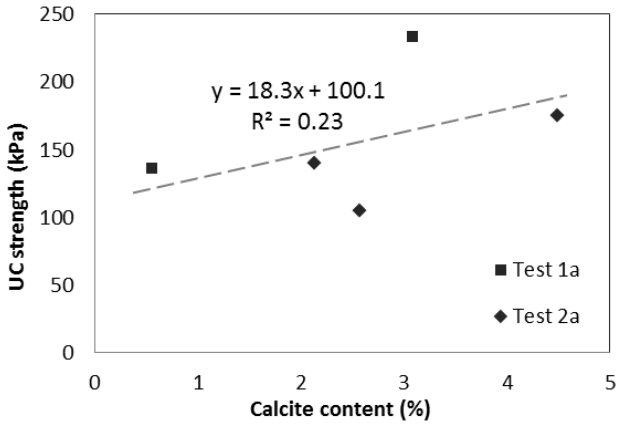

Figure 4.20 Summary of UC strength vs. calcite content in Test 1a and 2a

Variance of permeability after each treatment

The coefficients of permeability after each treatment of set 1a and 2a employing falling head method are shown below in Fig. 4.21. In spite of the weak cementation, large reduction of permeability was still observed from the first treatment, which might be another finding supplementing the presumption of calcite pre-forming on sand surface rather than in between of the sand particles. Fluctuation of *k* was observed after each treatment, as the calcite crystal formed in between the sand particles might be washed away during recirculation.

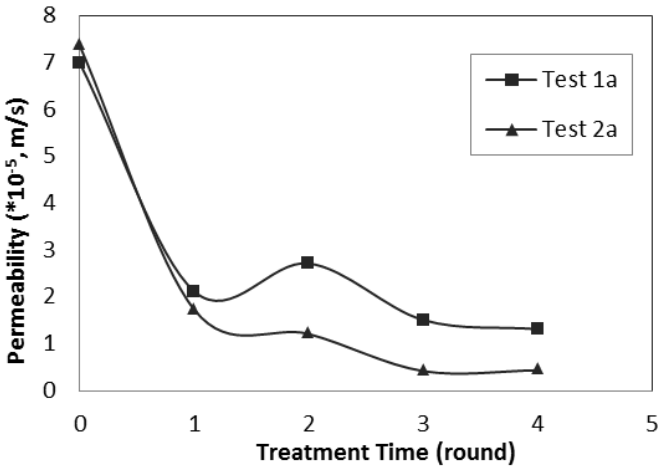

Figure 4.21 Coefficient of permeability variation after each treatment in Test 1a and 2a

4.4.4 Summary of treatment

The variations of material properties in the eight specimens before and after biotreatment are summaries in Table 4.4. Coefficient of ureolysis was determined by the first order integration of the differential equation

$$\frac{d[urea]}{dt} = -k_{urea}[urea] \cdot X \qquad \text{(Eqn. 4.5)}$$

$$\text{thus, } [Urea]_t = [Urea]_0 e^{-k_{urea}Xt} \qquad \text{(Eqn. 4.6)}$$

Similarly, Ca^{2+} precipitation rate could be determined by

$$\frac{d[Ca^{2+}]}{dt} = -k_{precipatation}[Ca^{2+}] \qquad \text{(Eqn. 4.7)}$$

$$\text{thus, } [Ca^{2+}]_t = [Ca^{2+}]_0 e^{-k_{precipatation}} \qquad \text{(Eqn. 4.8)}$$

where k_{urea} and $k_{precipitation}$ are ureolysis and calcium precipitation rate respectively, and X is the biomass concentration. Ureolysis rate k_{urea} in this study was calculated based on the assumption that the reaction is zero order with respect to biomass, i.e. X = 1. This method is adopted from Parks (2009). The values of reaction rate shown in Table 4.4 were taken after 0.5hrs from the beginning of reaction when stable reaction rate had been established, and before urea/calcium was depleted in solution.

Table 4.4 Summary of material properties in the eight specimens before and after biotreatment

Test No.	Calcite content at 100% efficiency (w/w, %)	Average calcite content in specimen (w/w, %)	Calcite precipitation efficiency (%)	Initial k ($*10^{-7}$, m/s)	Final k ($*10^{-7}$, m/s)	Urease activity of UPB (mM/min)	k_{urea} w/o soil (mM/min)	k_{urea} in sand (mM/min)	$k_{precipitation}$ w/o soil (mM/min)	$k_{precipitation}$ in sand (mM/min)
1	11.9	8.3	70	676	67	0.962	0.8-1.5	0.2-0.35	0.25-0.6	0.25
2	12.2	7.6	63	804	74	0.424	0.38-0.53	0.15-0.28	0.41-0.44	0.25
3	11.8	7.3	62	600	166	0.832	0.22-0.4	0.05-0.14	0.14-0.32	0.05-0.08
4	12.1	7.4	61	747	88	0.962	0.32-1.3	0.05-0.13	0.27-0.8	0.05-0.13
5	12.6	7	56	715	96	0.424	0.31-0.56	0.07-0.31	0.31-0.76	0.07-0.18
6	12.2	3.7	30	661	256	0.832	0.14-0.4	0.02-0.05	0.11-0.25	0.01-0.05
1a	6.7	1.4	21	698	131	0.962	-	0.4	-	>0.14
2a	6.8	2.9	42	735	44	0.424	-	0.4	-	>0.14

As it can be observed in Table 4.4, Test 1 to Test 5 resulted in similar treatment efficiency in terms of average calcite precipitation in sand. However, it should be noted that Test 3 established the most uniform precipitation along depth in terms of calcite content and UC strength gain regardless of the calcite content level, as low yet stable urease activity in bacteria cell (reflected from k_{urea} and $k_{precipitation}$) provided long-lasting steady cementation when urea supply is sufficient. The relatively low permeability reduction after the treatment in tests using centrifuged UPB (Test 3 and 6) reserved the possibility for further treatments. Nevertheless, pH value is essential, especially for centrifuged bacteria. Low pH value resulted from lack of urea in Test 6 leaded to the lowest calcite precipitation efficiency. Such phenomenon was not obvious in sets employing original UPB suspension.

The urease activity of original UPB suspensions (Test 1, 2, 4, 5) with the presence of calcium was similar to its original value. However, in centrifuged UPB engaged tests (Test 3 and 6), urease activities was much lower during reaction, as time is needed for urease to be released from cell. The reaction rates in sand specimens

were lower than those in the pure solutions. This is reasonable as the contacting time between bacteria and chemicals was less while recirculating in the sand specimens. Ureolysis rate and calcium precipitation rate were generally at the same level between each other in each test, as one mole of hydrolysed urea provided one mole of carbonate ion, reacted with same amount of calcium cation.

For test 1a and 2a, the reaction rate was similar, yet as calcite precipitated on surface of sand rather than in between sand particles, it could be washed out during treatment, which resulted in low calcite precipitation efficiency comparing to Test 1 and 6.

4.5 Conclusions

The effectiveness of a low urease activity bacteria strain VS1for MICP was studied. The results were discussed in this chapter. The performance of different UPB types for MICP in sand was compared. The UPB strains used had different urease activities. Some were centrifuged. The effectiveness of cementation solution with calcium to urea ratio of 1:2 and 1:1 were also tested. The main observations are as follows:

The use of centrifuged UPB resulted in a more gentle permeability reduction after each round of treatment as compared with the use of original UPB. This is the intended purpose of using centrifuged UPB. Compared with tests using the original UPB suspension, the ureolysis/calcium precipitation rate in tests using centrifuged UPB suspension is lower and the pH rising was also delayed. Little difference was observed between tests using original UPB suspensions with relatively higher urease activity and that with lower urease activity.

A sample treated using centrifuged UPB result in a more uniform calcite distribution in the sample and a higher UC strength than that using original UPB suspension. However, such an effect could only be observed when a cementation solution with calcium to urea ratio of 1:2 is used. The rising in pH is slower when a 1:1 cementation solution is used. The above differences can affect the calcium carbonate precipitation process in sand.

Chapter 5

Geotechnical Properties of Sand Treated by Crust or Bulk Cementation Methods

5.1 Introduction

The MICP process can be used to treat granular soils like sand to increase its shear strength through biocementation and reduce its permeability by bioclogging. As far as the reduction of permeability of sand is concerned, an economical method is to form an impervious layer of calcite crust on the top of sand layer. Model tests were carried out to study this so-called crust cementation method and the existing bulk cementation method in which biocementation is applied everywhere in sand. The testing results are presented in this chapter.

5.2 Experimental setup

Poorly graded Ottawa sand with D_{50} = 0.3mm, as described in Section 3.4.1, was used in this study. Six boxes with an inner dimension of 450 mm long by 300 mm wide by 160 mm deep were filled with Ottawa sand using the same dry deposition method. The sand in the boxes was then treated using different biocementation methods. As presented in Table 5.1, box No. S1, S2, & S3 were used for surface cementation, while box No. B1, B2, & B3 were for bulk cementation. The sand in the boxes was treated with different rounds of biocementation in order to investigate the effectiveness from various different treatment extents.

Initially, the sands were prepared to an initial medium to dense state with void ratios in the range of 0.58 to 0.61 ($D_r \approx 63$ - 75%). A photograph of the boxes undergoing biotreatment is shown in Fig. 5.1a. The coefficient of permeability of

the untreated sand is in the range3×10^{-5} to 5×10^{-5} m/s as measured using a constant head method.

The centrifuged UPB culture was used for all six boxes. The bacteria suspension was centrifuged at 4°C for 10 min to separate the bacteria cells from culture liquid, and then was re-suspended in 9g/L NaCl solution before used for the sand in the boxes. Following the same method presented in Chapter 4, a cementation solution of 0.75M $CaCl_2$ plus 1.5M urea was employed to provide the source of calcium cation and carbonate.

Table 5.1 Setup of the six surface/bulk cementation treatment boxes

Test No.	Weight of sand (kg)	Initial Void Ratio e	Treatment Method	Treatment Rounds	Centrifuged UPB supply in each round	Cementation solution in each round	Calcium supply (g, as $CaCO_3$)	Calcite at 100% efficiency (w/w, %)
S1	33.97	0.6	Surface Crust Formation	10	0.25L (4-time concentrat-ed)	5L (0.75M $CaCl_2$ + 1.5M urea)	2831.6	8.3
S2	34.03	0.59		20			5663.3	16.6
S3	34.01	0.59		30			8494.9	25
B1	34.36	0.58	Bulk Cementa-tion	10	2L (0.5-time diluted solution)		2831.6	8.2
B2	33.66	0.61		20			5663.3	16.8
B3	33.98	0.59		30			8494.9	25

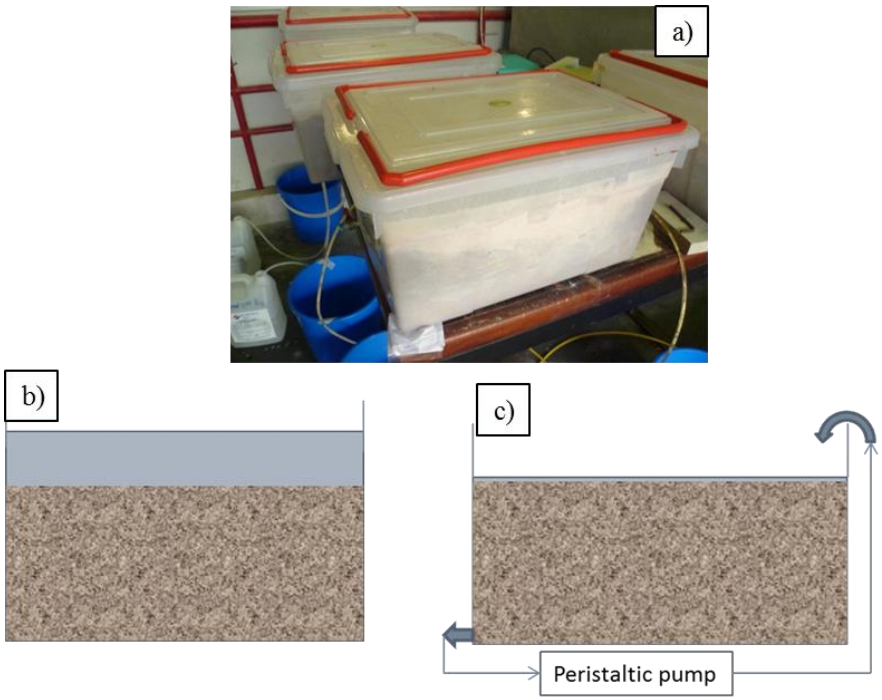

Figure 5.1 a) Image of sand boxes during treatment; graphic setup of treatment in b) crust formation sets, and c) in bulk cementation sets

In the first two rounds treatment using the surface cementation method, 0.25L of UPB cell suspension containing the centrifuged bacteria from 1L original UPB suspension (i.e. 4-time concentrated UPB) was sprinkled on the surface of each box in five times, 0.05L in each time. Solvent to dissolve UPB cells contained 9g/L NaCl plus 50mM $CaCl_2$. Same amount of cementation solution containing 0.75M $CaCl_2$ plus 1.5M urea was then sprinkled on the surface to form the initial layer of crust. This procedure was to prevent the bacteria from permeating into the sand specimen with the liquid, ensure the bacteria to disperse evenly, and accumulate gradually on the surface of sand. During this process, the sprinkling process was controlled manually to protect the initial hard crust without damaging the shape of sand surface.

In the subsequent rounds of surface cementation treatment, 0.25L of centrifuged UPB suspension was sprinkled on the surface and then left for 2 hours in order to evaporate the water in the suspension. 5L cementation solution was then added into each box to maintain a liquid level of 4-5cm above the sand surface for reaction for five to seven days as shown in Fig. 5.1b. Such an arrangement was made to make sure the new calcite precipitated attaching closely to the previous crust surface. pH value, conductivity and calcium content were monitored throughout the test. 1M Na_2CO_3 solution was employed to check for calcium cation's remaining presence by observing the precipitation formed during cementation. Such treatment method is similar to what had been described in Qian (2010b).

For the bulk cementation groups, first, 2L UPB suspension centrifuged from 1L of original cultivated UPB suspension (i.e., 0.5-time diluted UPB) was applied by surface percolation. Then, 50mM $CaCl_2$ fixation solution was added in the bacteria suspension and recirculated overnight at a rate of 200mL per hour. Subsequently, 5L of cementation solution was provided in a continuous motion after surface percolation and then recirculated for five to seven days at rate of 1L/hr. The combination of these procedures described above is counted as one treatment cycle (Fig. 5.1c). Parameters such as pH value, conductivity and calcium content were

also monitored during the treatments. All the sand samples were left for air drying before conducting the properties tests.

5.3 Properties of sand treated using the curst method

5.3.1 Overview

A photograph of a whole sample taken out from the box after the treatment is shown in Fig. 5.2a. The calcite crust formed in box S1, S2 and S3 are shown in Fig. 5.2b, 5.2c and 5.2d respectively. With additional treatments applied, the thickness of the crusts from S1, S2 and S3 also increase. The calcite contents measured in these crusts by ICP test were higher than 95%. Despite the purpose of the treatment was for crust formation, the sand in the box was still cemented to various extents. Nonetheless, the sand block could be taken out as one piece. The layer of sand just below the crust formed (about 2 to 3cm thick) was found to be weakly cemented. The joint section between the crust and the sand was very weak which made the crust to be separated easily from the block. This is especially the case in box S2 and S3, in which the crusts themselves are much stiffer than the sand layer below. Such phenomenon was caused by two possible ways of which the bacteria accumulates: either aggregate on top of the sand surface, or flow by gravity through the crevice between the crust and the four walls of box, then start to accumulate at the bottom of box.

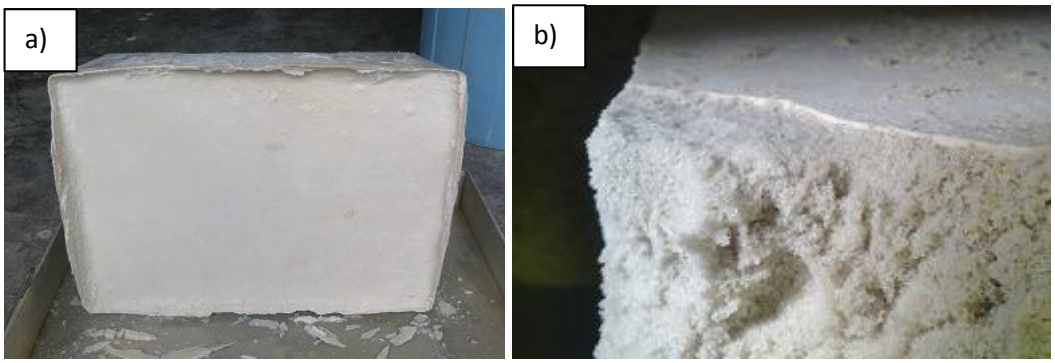

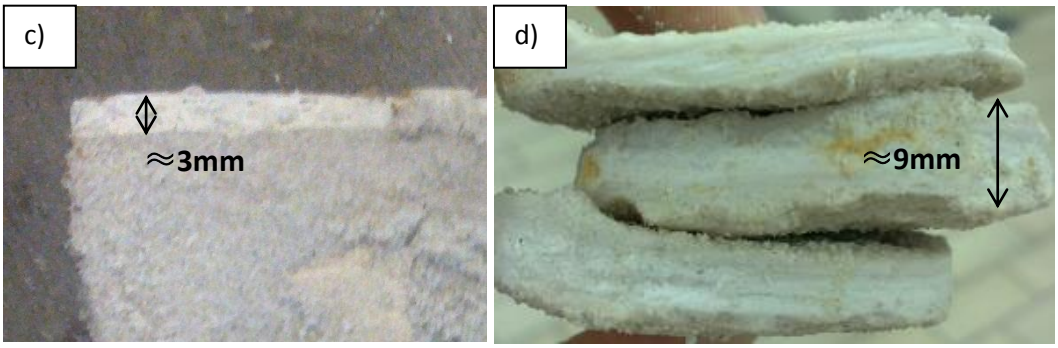

Figure 5.2 Images of a) whole sand block taken out after treatment (box S2); calcite crust formed in box b) S1, c) S2, and d) S3

Two FESEM photographs of the crust at different scales were taken and shown in Fig. 5.3a and 5.3b. The correspondent EDS spectrums which show three elements at the same site: calcium, carbon and oxygen, are presented in Fig. 5.3b respectively. From the picture, it is clear that these three elements are coincident with each other in spatial location, and also with the suspected calcite crystal screening in the FESEM image. This serves as a confirmation that the crust is made of pure and condensed $CaCO_3$.

a)

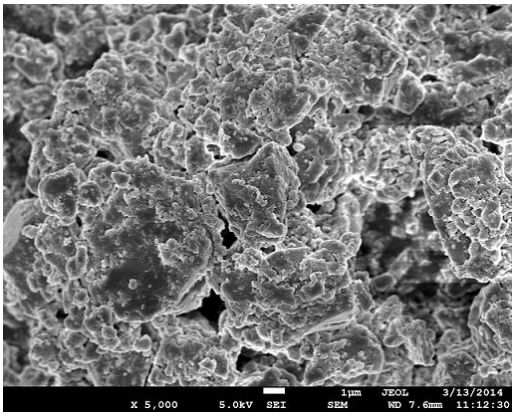

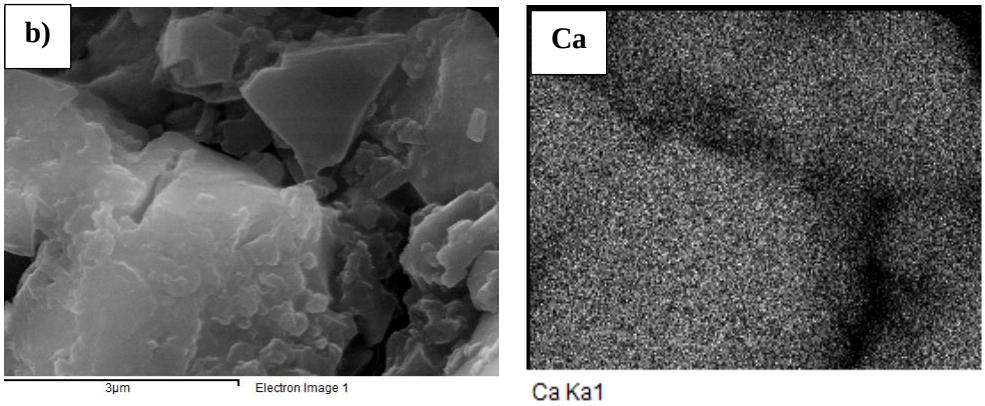

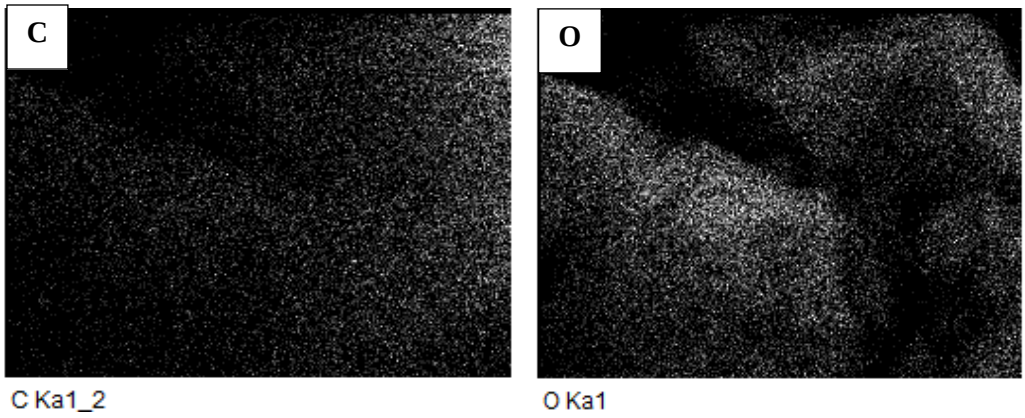

Figure 5.3 FESEM images of the crust at scale a) ×5000; and b) ×15000, as well as the correspondent EDS images showing elements calcium, carbon, and oxygen

Samples of the solution were collected from the treatment effluent. The parameters associated with these samples were recorded and the variances recorded from one typical round of treatment (the second round in box S2), including pH value, conductivity, and calcium cation left in effluent solution, are shown in Fig. 5.4. The continuous increase of conductivity, stable pH value maintaining to be 8, and reduction of calcium cation, which was fully consumed within three days, indicated the lasting reaction in the boxes.

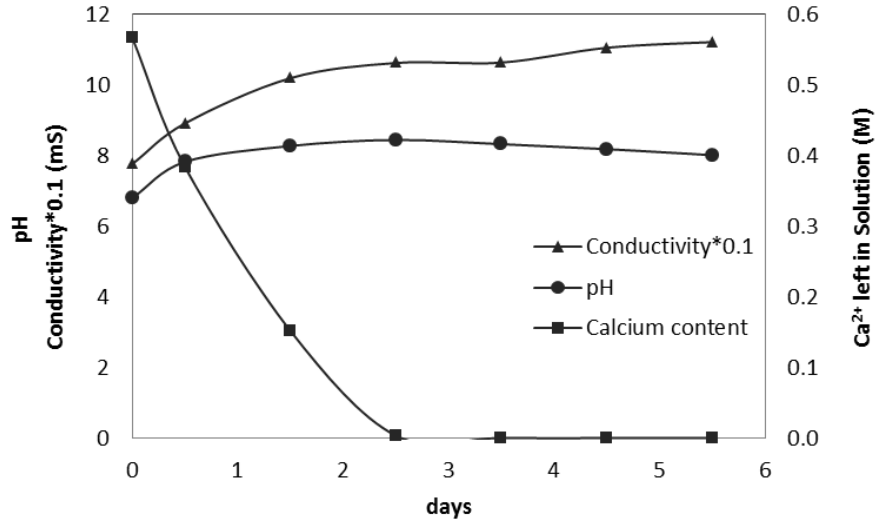

Figure 5.4 Typical parameter changes in one round of treatment of crust formation (the second round in box S2)

5.3.2 Stiffness and permeability of the crust layer

The curst formed in each set was separated from the sand below and tested for their properties. To test the strength of the crust formed in each box, the four-point

bending test, as described in Section 3.6.3, was employed to measure the maximum bending stress (outer fibre stress) of the crust. Three photographs of one specimen cut from the crust of box S2 before, during and after the four-point bending test (and its failure mode) are shown respectively in Fig. 5.5a, 5.5b and 5.5c.

a)
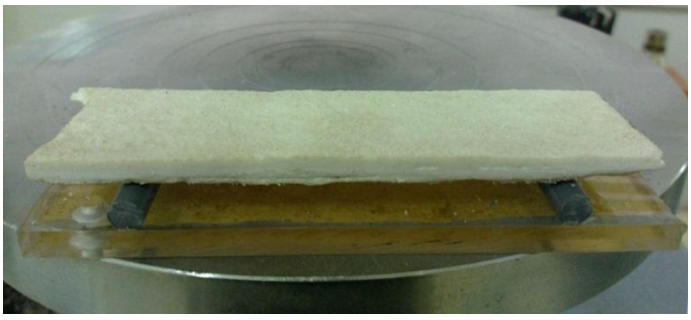

b)
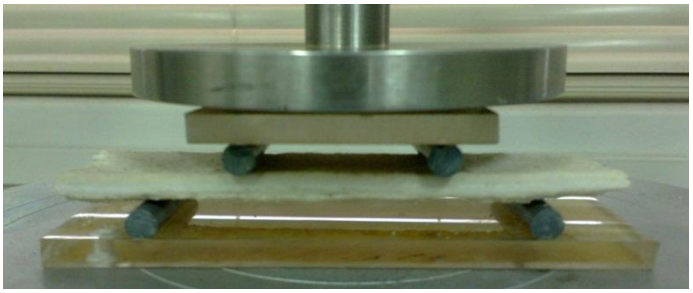

c)


Figure 5.5 Images of a calcite crust specimen cut from the crust of box S2 a) before, b) during, and c) after four-point bending test

The permeability of calcite crust was measured by triaxial apparatus employing flexible wall method, which is described in Section 3.6.4. The sand section with crust was sawed off from the block and trimmed into cylindrical specimens as shown in Fig. 5.6a and 5.6b for box S1. However, the attachment between the crusts and the sand layers below was too weak for the specimens from in box S2 and S3, therefore the crust specimens were tested by themselves as shown in Fig. 5.6c. Because the permeability reduction is mainly attributed to the crust, only the

thickness of crust is used to calculate the coefficient of permeability, regardless of whether sand layer was attached at below or not.

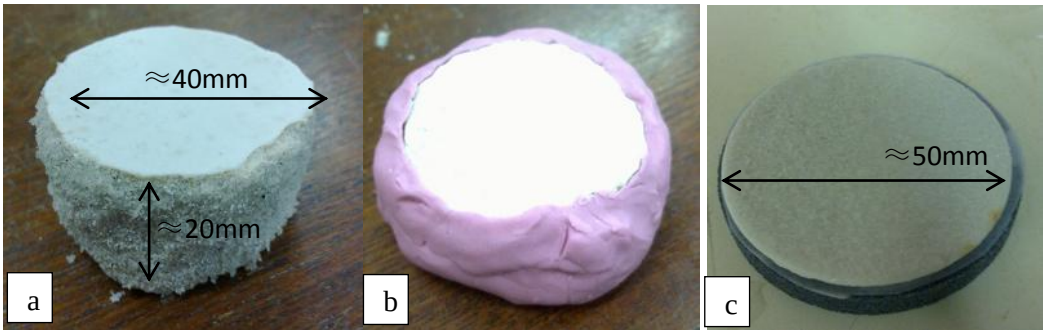

Figure 5.6 Specimens preparing for permeability test for calcite crust, a) with sand (in S1), b) before putting in triaxial apparatus, and c) crust only (in S2)

The maximum outer fibre stresses, S, and the coefficients of permeability, k, measured from the crust formed on top of sand block surface in the three boxes along with their thicknesses are summarized in Fig. 5.7. The crust thickness formed in S1, S2, and S3 varied from 0.2 to 0.6mm, 2 to 5mm, and 5 to 9mm respectively, which increased in proportion to the treatment rounds in S2 and S3, yet not in S1, as it took several rounds of treatment for the pure calcite crust to be built up initially. The maximum outer fibre stresses S varied from 0.6 to 2.5 MPa in the three boxes. The data showed a scattered pattern, yet did not have significant relevance with the variance of thickness, which indicated the uniformity of crust properties from different boxes. Such strength and stiffness of crust formed might help to maintain the shape of slope or forming wall of water pond in real applications *in situ*.

As shown in Fig. 5.7, the coefficients of permeability decreased in 100 times' scale from clean sand ($5*10^{-5}$ m/s) to S1($10*10^{-7}$ m/s) by the 0.2 to 0.6mm crust formed. Similar permeability reduction effect was also found from S1 to S2 ($0.1*10^{-7}$ m/s) with the 1.5mm increase of crust thickness. This effect was not as significant with following increase of thickness from S2 to S3, which having permeability at a scale of $0.01*10^{-7}$ m/s. However, it should be noted that the coefficients of permeability k of the surface crust from box S2 and S3, are around from 10^{-8} to 10^{-9} m/s, which have already fallen into the range of permeability of silty to of clayey

soil. Therefore, the crusts formed, considering its permeability alone are supposed to perform well in water sealing applications.

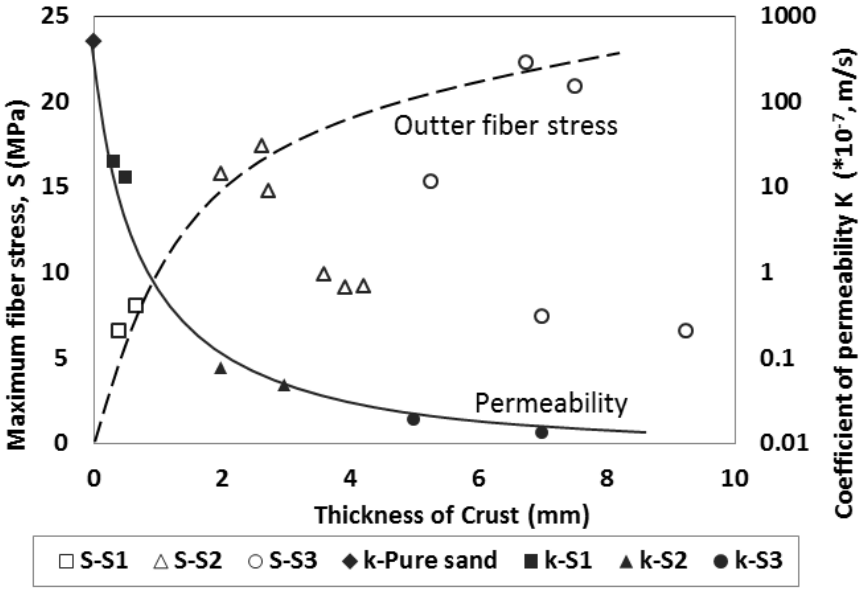

Figure 5.7 Summary of maximum outer fibre stresses S and coefficients of permeability k of the crust, versus their thicknesses in S1, S2 and S3

5.3.3 Strength and permeability of sand below the crust

The sand in the three boxes was drilled from different directions using 50mm diameter drilling bit to get specimens for sand properties tests. The photographs of drilling and the samples drilled for S3 are shown in Fig. 5.8a and 5.8b respectively. It should be noted that the specimens in other sizes and shapes were also employed in strength test, including cubical specimens (dimension 50*50*50mm, shown in Fig. 5.8c, or 30*30*30mm) for box S1, as drilling may not be applicable due to relatively weak cementation bonding. Small cylindrical specimens with 10*20mm dimension were also taken from each box, when standard cylindrical specimens (50*100mm) were not available. Typical failure modes of cylindrical (50*100mm) and cubical specimen (50*50*50mm) during UC test are shown in Fig .5.8d and 5.8e respectively.

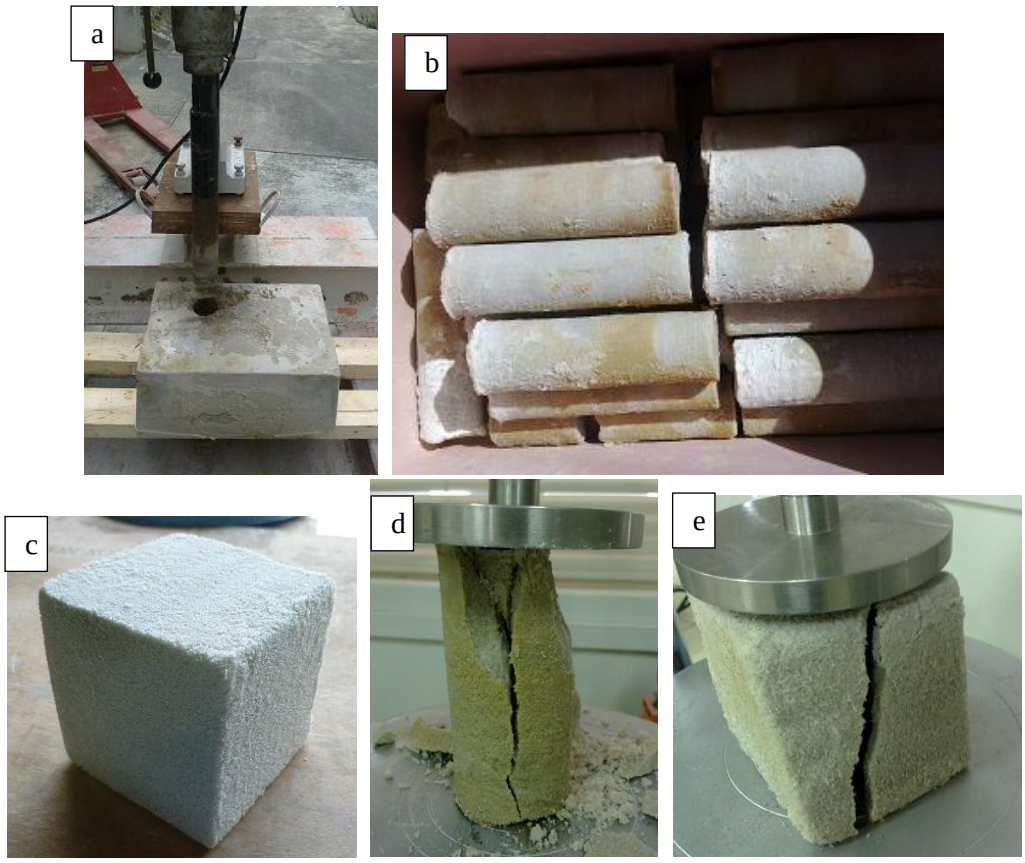

Figure 5.8 Images of a) sand block during drilling; b) cylindrical samples get from drilling in box S3; c) cubic specimens employed while cylindrical sample not available in box S1; and typical failure mode of cylindrical (d))/cubical (e)) specimen during UC test

The sand block below surface crust in each box was divided into four sections for the measurement of calcite content, UC strength, and permeability, which is (a) 0-3cm, (b) 3-6cm, (c) 6-11cm and (d) 11-16cm respectively, starting from the top sand surface. Specimens of various sizes and shapes were engaged in UC strength test, including the 50*100mm cylindrical specimens, 30*30*30mm or 50*50*50mm cubical specimens, and 10*20mm small cylindrical specimens, whichever was available. The stress-strain behaviour during UC compression with respect to on the calcite content, is shown in Fig. 5.9, taking one specimen from S1 with 2.5% of calcite content, and another specimen from S3 with 9.5% of calcite content respectively as example. Both behaviours were 50*100mm cylindrical specimens. The calcite content was determined by ICP test. As shown in Fig. 5.9, the former specimen exhibited relatively ductile failure mode, while the latter one showed brittle behaviour with a sudden failure at about 1% axial strain.

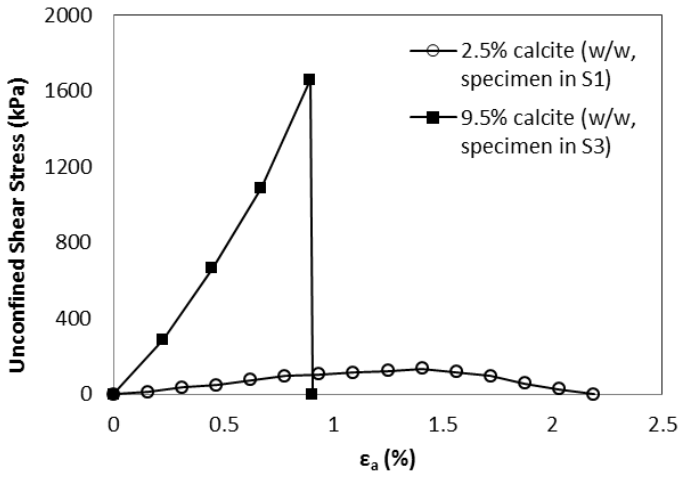

Figure 5.9 Typical stress-strain curves of specimens having higher and lower calcite content during UC test, taking two specimens having 2.5% and 9.5% calcite content (weight to weight of sand) in box S1 and S3 respectively as example

The UC strength and permeability versus calcite content resulted in these three boxes for the four sections are summarized in Fig. 5.10a and 5.10b. As shown in Fig. 5.10a, UC strengths varied in a range of 180 to 770 kPa, 220 to 1490 kPa, and 740 to 2780 kPa in sand blocks of box S1, S2, and S3 respectively. The calcite content reached as high as 13% in the sand block S3. Moreover, wide range of calcite content was discovered in each sand block, within which the highest and lowest value could differ as high as 10% at different locations in each box. Similar to previous test data and the data from literature, calcite content is positively related to UC strength, and standard deviation R^2 was found to be as high as 0.72 by fitting the data points exponentially.

As shown in Fig. 5.10b, the permeability varied from 25 to $150*10^{-7}$ m/s, decreasing with increased calcite content. R^2 value was 0.64 by fitting the data by logarithmic function. It could also be observed that the data became increasingly scattered when calcite content reached 4% and higher. This could be explained as that some calcite precipitated in between sand particles freely without performing as binders. These particles could be washed away by water flow during permeability test in triaxial apparatus, therefore rendered the coefficient of permeability higher.

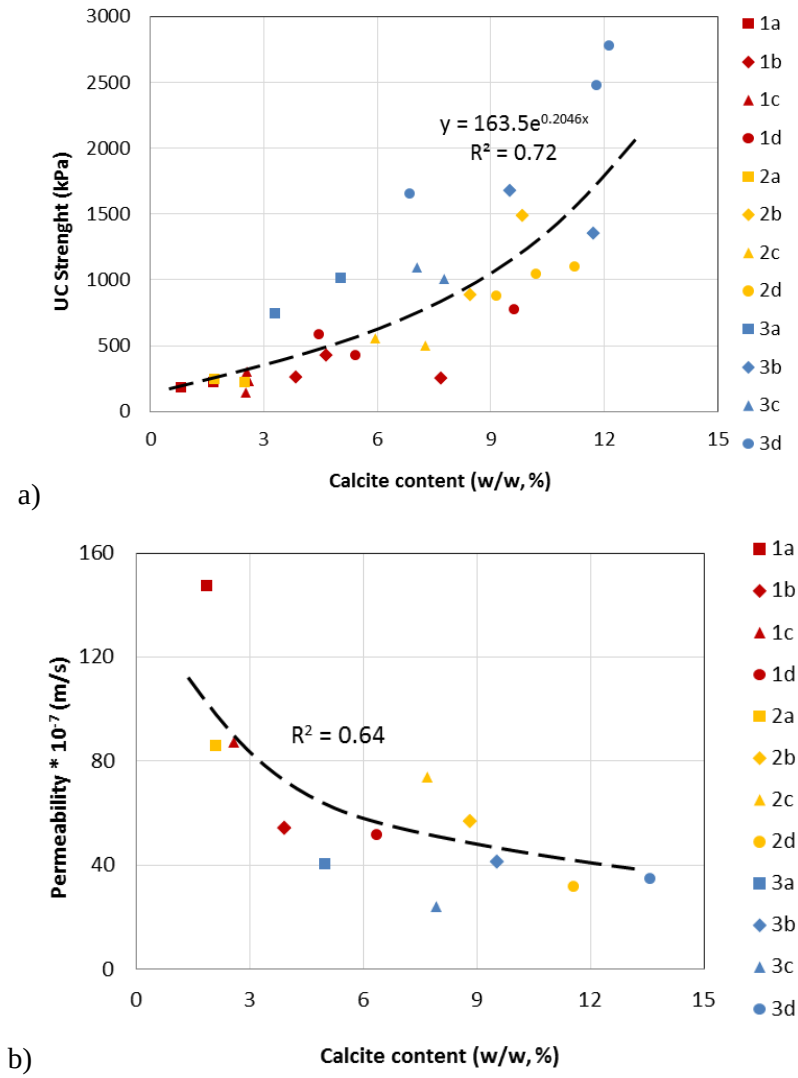

Figure 5.10 Summary of a) UC strength and b) permeability vs. calcite content in sand below the crust of test S1, S2 and S3 (a, b c, and d in legend refers to specimen getting from 0-3, 3-6, 6-11 and 11-16 cm below crust respectively)

5.3.4 Calcite distribution within the block

The distribution of calcite content/UC strength within box S3 by surface treatment is shown in Fig. 5.11. The calcite contents and UC strengths presented in the legends of Fig. 5.11 are roughly correlated by the relationship shown in Fig. 5.10a. The three sand boxes had similar distribution pattern. Note that the legend of the contour plot only represented a rough range. For the crust above, maximum bending stress S is presented instead of UC strength.

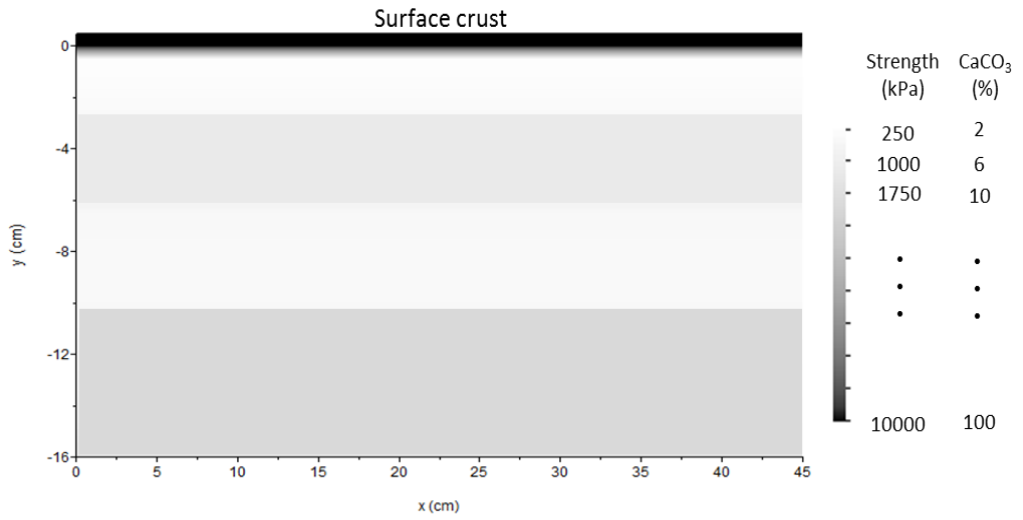

Figure 5.11 Summary of cross-sectional view of UC strength/calcite distribution in surface-treated boxes (taking box S3 as an example)

As presented in Fig. 5.11, a weak sand layer just below the surface crust (0-3 cm) could be observed, followed by a relatively stronger layer at 3-6 cm. Such a strength distribution was because the UPB suspension could infiltrate to that depth (3-6 cm) and accumulated there, most during the first several rounds of treatment when the crust had not been built up yet. The bottom part of the box is also stronger. Both bacterial suspension and cementation solution which infiltrated into the sand block intend to accumulate and together reacted at the bottom, as there is no outlet flow or inner circulation involved during treatment. Nonetheless, the calcite concentration and strength in the sand block below are much lower compared with the strength of the crust.

The calcite distributions in crust and sand block in terms of calcium supply for the three boxes are summarized in Table 5.2. The weight of crust was calculated by assuming the specific gravity of crust (calcium carbonate) to be 2.7. The proportion of calcium supply (calculated by $CaCl_2$ supplied) which contributed to the crust formation increased from S1 (6.4%), S2 (22.5%) to S3 (32.3%) with more rounds of treatment. It makes sense as the crust formed lowered the permeability, preventing further infiltration of bacteria and cementation solution into the sand block below in the following treatments. Yet higher percentage of calcium supply (all > 50%) had still travelled into the sand block to form bulk cementation compared to calcite crust in each box, which was not the desirable in this treatment. Noted that the efficiency of MICP formation in the sand below the crust was only

around 50% for all the three boxes regarding the calcite content, despite the fact that all calcium cation supply in cementation solution was consumed within three days after recirculation (Fig. 5.4). It might be an indication that some part of the calcium cation supplied could be maintained in the sand block in the form of CaO or $CaCl_2$ instead of $CaCO_3$, or simply precipitated in between sand particles, not performing as binder, which was washed away after treatment.

Table 5.2 Summary of cementation efficiency of crust and sand block in surface treatment

No.	Total mean calculated calcite content at 100% efficiency (w/w, %)	Mean Crust Thickness (mm)	Crust weight (g)	%Crust as in total $CaCO_3$ supply (%)	Calculated calcite content in sand block at 100% efficiency (%)	Resulted mean calcite content in block (%)	MICP Efficiency in sand block (%)
S1	8.3	0.5	182	6.4	7.8	4.2	53
S2	16.6	3.5	1276	22.5	12.9	7.4	57
S3	25	7.5	2734	32.2	16.9	8.4	49

5.4 Properties of sand treated using the bulk cementation method

5.4.1 Overview

The photographs of the sand block in box B2 and its cross section after cutting are shown in Fig. 5.12 a) and b) respectively. Compared with the surface crust formation sets, cementation in the bulk-cemented boxes were appeared to be more uniform. No obvious weak layer was observed during the cutting. A smooth pure calcite film was detected in each box, in the seam between plastic box and sand on the wall and bottom. High content calcite crystal in white colour could be observed near the outlet points of the box (left part in Fig. 5.12a).

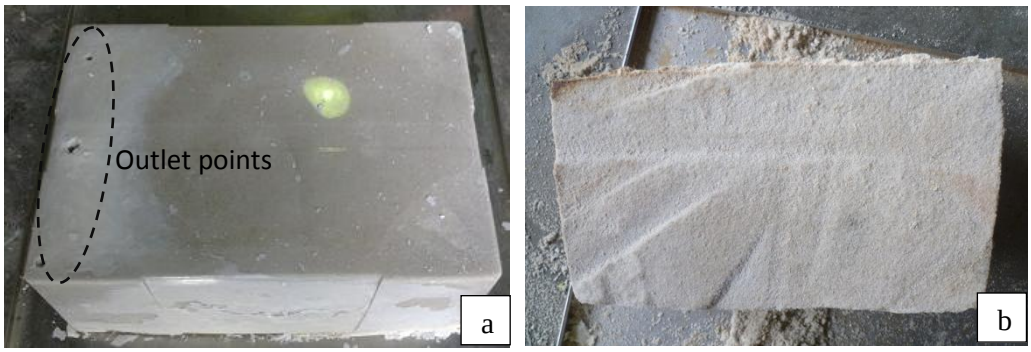

Figure 5.12 Image of a) aerial view, b) cross sectional view of sand block in box B2

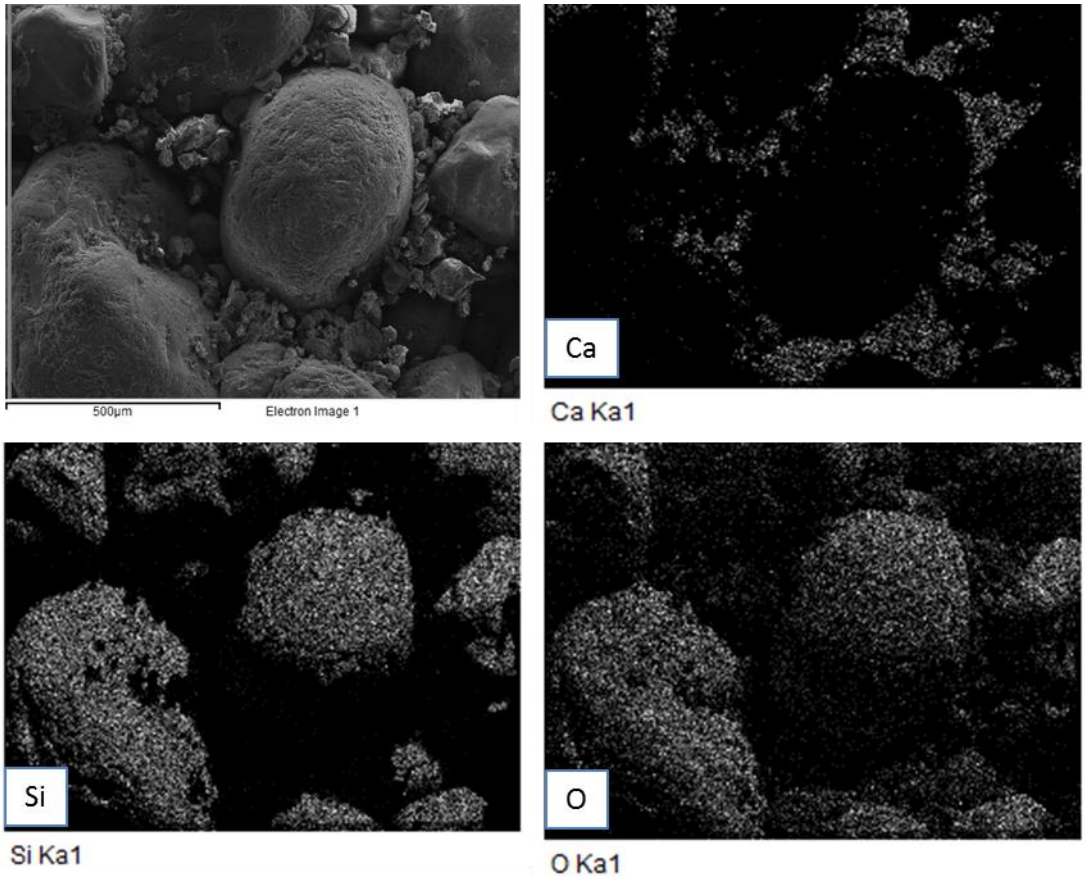

Figure 5.13 FESEM image and the correspondent EDS showing element calcium, silicon and oxygen of cemented sand in the bulk cemented sand box S2

Typical FESEM pictures and the corresponding EDS images for a sample taken from the bottom layer of Test S2 are shown in Fig. 5.13. It can be seen that the pores between sand grains are filled by precipitates. Fig. 5.13b indicates that the precipitates are mainly calcium based material or $CaCO_3$ which forms a chain around the sand grains. It is the presence of the calcium carbonate that leads to the increase in strength and decrease in permeability of the sand.

The third round in box B2 was select to demonstrate a series of typical parameters variances,, including pH value, conductivity, and calcium cation left in the solution are shown in Fig. 5.14. Continuous increase of the conductivity was observed. The pH value increased up to 9, even higher than in crust sets and data presented in section 4. The rate of calcium cation consumption was slower than surface crust groups, as the bacteria suspension employed was eight times diluted. Nevertheless, calcium cation was still fully consumed within four days.

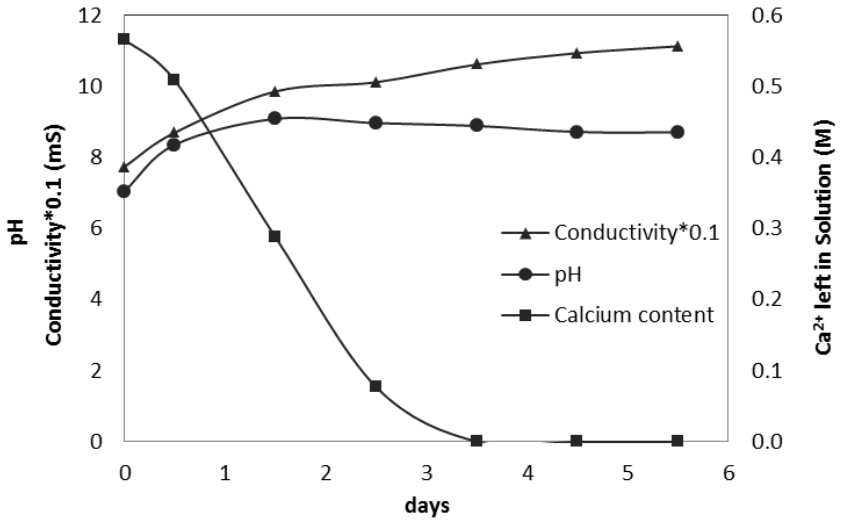

Figure 5.14 Typical parameter changes in one round of treatment in bulk cementation set (the third round in box B2)

5.4.2 Unconfined compressive strengths vs. calcite content

After biocementation, sand specimens were taken from five locations for engineering properties tests, as shown in Fig. 5.15. Similar sampling method as in Fig. 5.8 was employed in the bulk group. Area (a) refers to the inlet section and area (e) refers to the outlet part in the sand boxes.

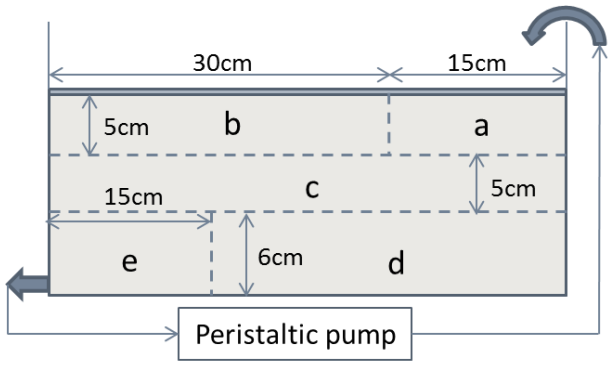

Figure 5.15 Indication of sampling section in bulk cemented sand boxes

Some typical stress-strain curves obtained from unconfined compression tests are shown in Fig. 5.16. Brittle failure mode was observed for almost all the specimens, especially for the specimens having higher calcite contents in box B2 and B3. UC strengths versus calcite contents in the three boxes are presented in Fig. 5.17. It varied in the range of 423 to 1239kPa, 1460 to 5382 kPa, and 2782 to 5977 kPa in box B1, B2 and B3 respectively. Calcite contents are positively related to UC strengths. Standard deviation R^2 reached 0.74 by fitting the data in a power

function. Besides the variation in calcite measurement and other possible experimental errors, the scatter of UC strength versus calcite content data might be caused by the non-uniformity in MICP precipitation.

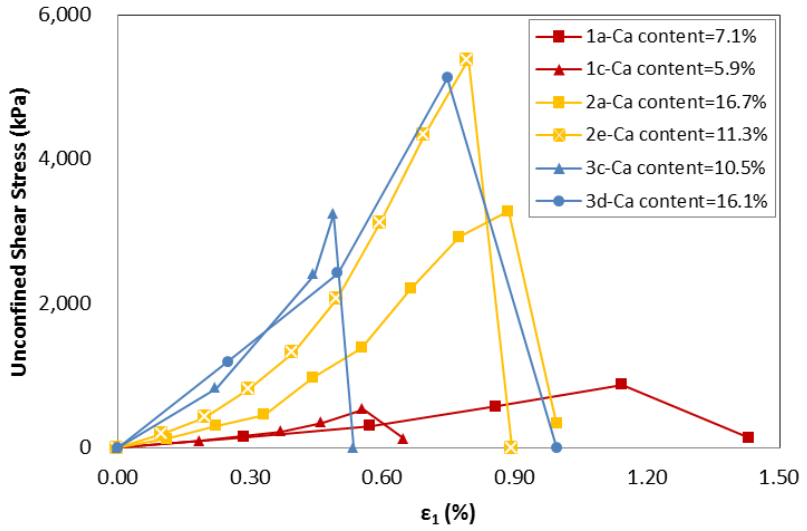

Figure 5.16 Typical stress-strain curves obtained from UC tests of bulk cemented sand boxes B1/B2/B3 (the alphabetic part in the legend refers to the location of specimen)

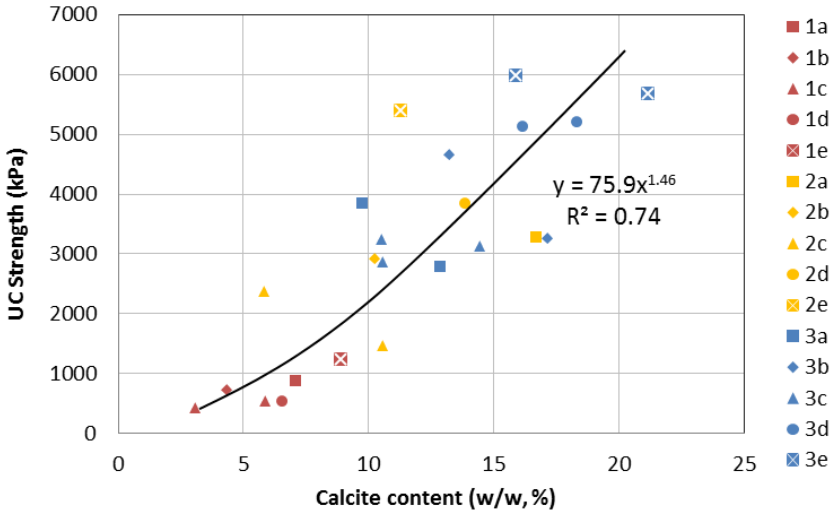

Figure 5.17 UC strength versus calcite content in bulk cemented boxes B1/B2/B3

Resulted average calcite content, UC strength, and the efficiency regarding to MICP formation in the three boxes are summarized in Table 5.3. The cementation efficiency η_{MICP} was calculated by the ratio of calcite content measured in the sand after treatment, divided by the total initial calcium supply converted from $CaCl_2$. As shown in Table 5.3, η_{MICP} appears to be decreasing with increasing treatment times, from 72% in box B1 to 58% in box B3. Such phenomenon could be

partially explained by the escalation of flow rate in the non-cemented area during additional rounds of treatment, thus hindering the further cementation.

Table 5.3 Summary of cementation efficiency in sand blocks under calcite crust

No.	Treatment rounds	Calcite content at 100% efficiency (w/w, %)	Resulted mean calcite content (%)	MICP Precipatation Efficiency (%)	Mean UC Strength (kPa)	COV-Absolute deviations/mean UC strength
B1	10	8.2	6	72	723	0.31
B2	20	16.8	11.4	68	3207	0.3
B3	30	25	14.6	58	4157	0.26

Significant increase in mean UC strength was observed for samples in box B2 (3207 kPa) as compared with those in box B1 (723 kPa). However, the increase of mean UC strength of samples in box B3 was less than 1000kPa (4157 kPa comparing to 3207 kPa in B2), even though same additional ten rounds of treatment had been conducted.

The uniformity of the treatment can be measured by the coefficient of variation (COV), i.e., the values of absolute deviations divided by its mean value. It should be note that the COV was lowered in tests on B3 (0.26) compared with it of B2 (0.30). The uniformity was increased by the additional 10 rounds of treatment in box B3. This observation is different from the data made by Bernardi et al. (2014), in which more rounds of treatments through percolation resulting in more scattered calcite percentage/UC strength in bio-treated bricks was reported. Besides the difference in treatment method, as recirculation after percolation was employed in this study, the evenness of cementation should also be attributed to the usage of centrifuged and re-suspended UPB, which resulted in a slower and steadier urease activity as compared with that of the original UPB suspension. Moreover, with the less viscosity of the bacterial solvent compared to cultivation solution for original UPB suspension, cells could travel further into the uncommented zone, instead of reacting fast and plugging near the inlet area. Such effect ensures the possibility of further treatment.

5.4.3 Influence of $CaCl_2$ and urea on strength of sand

Besides calcium carbonate, the unreacted calcium chloride and urea were also believed to have influence on the strength of cemented sand at zero water content. To understand to what extend does the UC strength of cemented sand obtained in previous chapters should be attributed to calcite, the effect of chemicals alone was studied.

Sand specimens packed in PVC tubes were submerged under solution with different amount of chemicals, including 0.375/0.75/1.5M $CaCl_2$ and 0.75/1.5/3M urea, plus one additional one with 0.75M $CaCl_2$ and 1.5M urea. The solution level was maintained just above the sand surface. They were then put into 105˚C oven for 48hrs before conducting the UC tests. Images of sand specimens adding 3M urea and 1.5 M $CaCl_2$ are shown in Fig. 5.18a and 5.18b respectively. It could be seen that the sand specimens stood by themselves by adding chemicals alone. Leaching of urea could be seen on the sand surface, as shown in Fig. 5.18a.

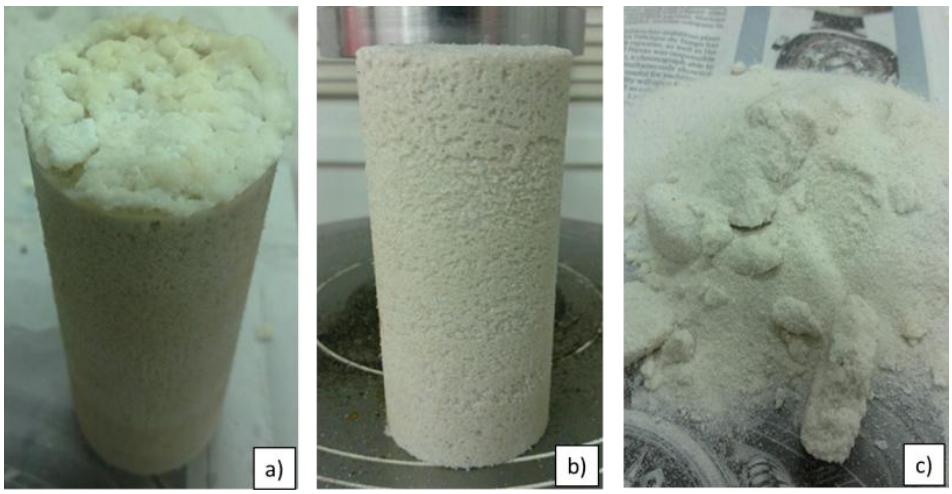

Figure 5.18 Image of specimen adding chemicals after 48hr oven drying; a) with 3M urea; b) with 1.5 M $CaCl_2$; c) with 1.5 M $CaCl_2$ after taking out for 30min, absorbed water in the air

Results of UC strength tests after oven drying are shown in Fig. 5.19. Resulted UC strength increases with increase of chemical concentration added. Nearly 500kPa and over 700 kPa of UC strength were obtained after two-days drying in oven, for sand specimens added 3M urea and 1.5M $CaCl_2$ respectively. Impact of urea in sand strength was not as much as $CaCl_2$. Over 1000 kPa of UC strength was

obtained in specimen containing 0.75M $CaCl_2$ plus 1.5M urea, which is the chemical dosage employed in the biocementation of this study.

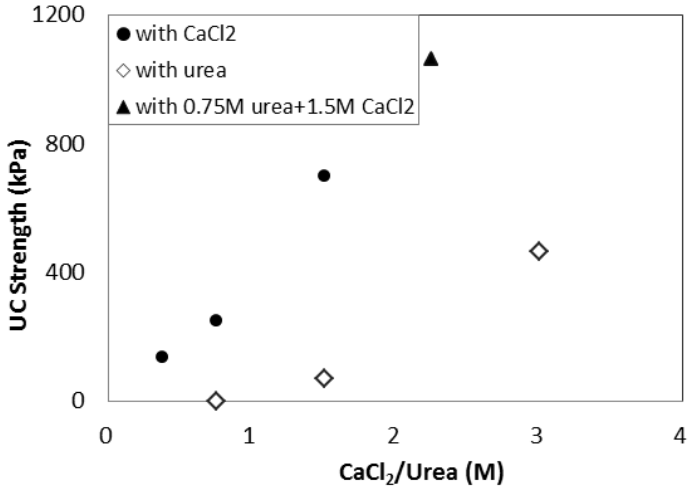

Figure 5.19 UC strengths of specimens treated by chemicals only after oven drying at 105˚C

Noted these UC tests were conducted within 20min after the specimen had been taken out of the oven. The effect of chemicals on sand strength disappeared after leaving in air for around more than 30min in air, and the sand columns disintegrated immediately (Fig. 5.18c). Such a phenomenon was more obvious on sand mixed with $CaCl_2$.

Therefore, to further investigate the contribution of calcite in strength of the biotreated sand, some biocemented sand specimens getting from the six boxes were oven dried at 105°C for 48 hours (degree of saturation S = 0%), or soaked under water overnight (degree of saturation S = 100%) before testing for their UC strengths. Image of UC specimens after oven-dried for 48hrs, its typical failure mode, sand specimens immediately after soaking under water, and after they had been soaked overnight, are shown in Fig. 5.20a, 5.20b, 5.20c and 5.20d respectively. Sudden failure occurred in each oven-dried specimen, in stress dropped to zero immediately at failure.

The resulted UC strengths of oven-dried, soaked, as well as air-dried specimens are summarized in Fig. 5.21. Noted the calcite contents for soaked sets were measured during the specimen trimming, before saturated under water, to cohere with the other two sets (air-dried and oven-dried).

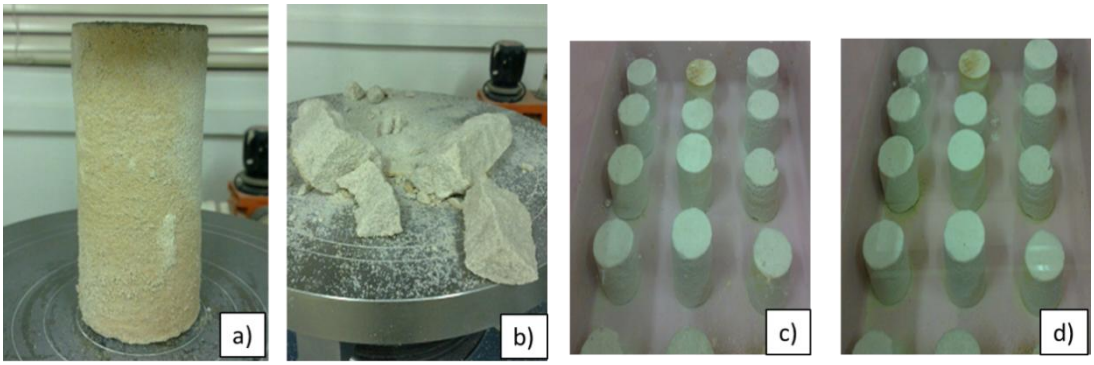

Figure 5.20 Image of UC specimens, a) oven-dried for 48hrs; b) typical failure mode of oven-dried specimen; c) immediately after soaking under water; and d) soaked overnight

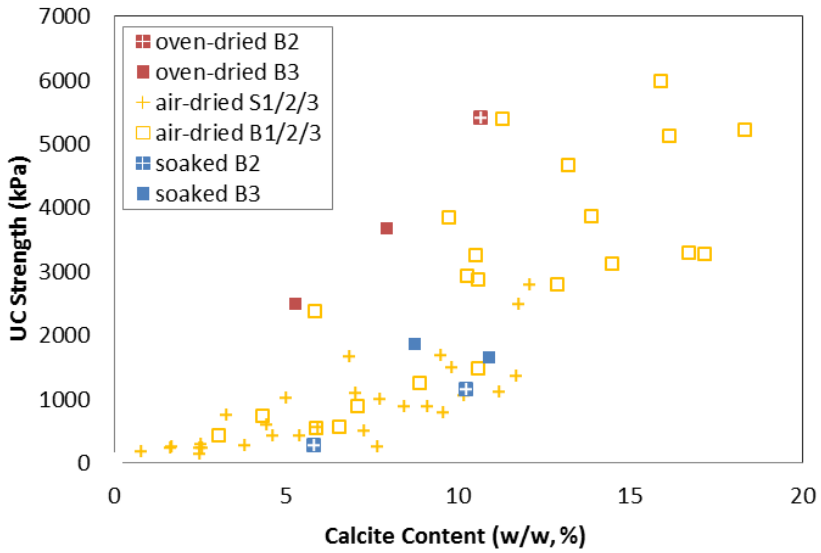

Figure 5.21 Comparison of UC strength vs. calcite content of oven-dried, air-dried, and soaked specimens getting from the six boxes

Resulted UC strength of soaked sets (dots in blue) basically coincides with those of the air-dried specimens (dots in yellow), which confirms the inactivity of pure calcium chloride/urea in the air-dried specimens. Furthermore, the effectiveness of calcite acting as binder remained stable even after soaking under water. The advantage of oven-dried specimens (dots in red) comparing to the other two sets could be viewed as the contribution of the unreacted $CaCl_2$ and urea.

5.4.4 Calcite distribution in bulk cemented sets

Distribution of calcite content/UC strength within test B2 is shown in Fig. 5.22. It can be seen that the UC strength/calcite content gradually decreased to the centre part of the box. Bottom portion of the sand box, especially where the bacterial and

cementation solution outflows from the box gains the highest calcite content and UC strength. Except the effect of gravity, bacterial cells also intended to accumulate around that region during recirculation, making the cementation favourable.

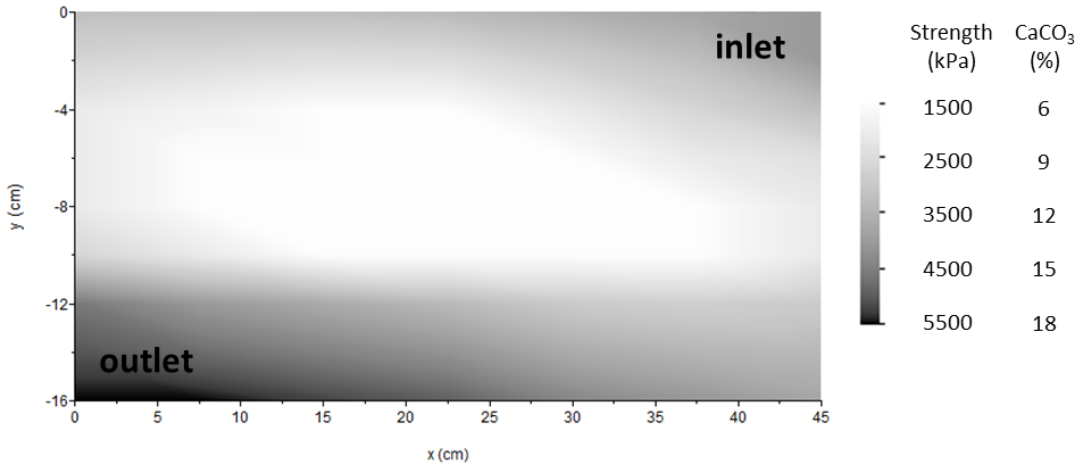

Figure 5.22 Summary of cross-sectional view of UC strength/calcite distribution in bulk-treatment test B2

Furthermore, similar to data presented in some previous researches (Al Qabany & Soga, 2013; Bernardi et al. 2014; DeJong et al., 2006; Stabnikov et al., 2013; Whiffin et al., 2007; van Paassen, 2009; van Paassen et al., 2009, 2010), sand near the inlet area gained greater calcite content and also higher UC strength correspondingly. This phenomenon could be due to thermodynamically favoured $CaCO_3$ precipitation at where the saturation states of calcium and carbonate ions greater than one and saturation indices greater than zero near the inlet part (Phillips, 2013; Zhang et al., 2010). The distribution of calcite in test B1 and B3 pattern was similar, except the variation becomes smaller from B1, B2 to B3, as explain in the previous section.

5.4.5 Permeability vs. calcite content

The permeability of samples taken from tests B1, B2 and B3 were also measured using the triaxial apparatus employing the flexible wall method. The data is shown in Fig. 5.23 by plotting permeability against calcite content.

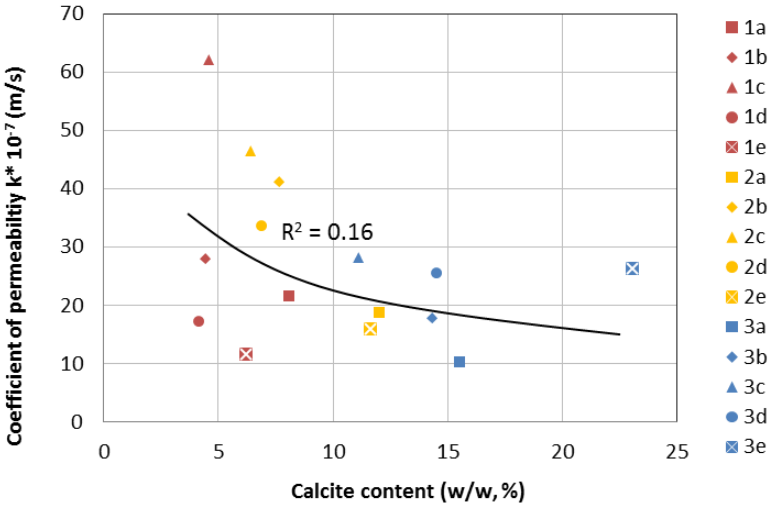

Figure 5.23 Coefficient of permeability vs. calcite content in bulk cemented sets

As shown in Fig. 5.23, the permeability values varied from 10 to 60*10^{-7} m/s in the three boxes. Standard deviation value R^2 only achieved 0.16. Discrepancy became smaller when calcite content reached 6% and higher, especially in box B3. Such phenomenon would be partially due to the trend of further cementation at previously cemented area during following treatments. As cementation solution could always find the optimum flow path in less cemented area, flow rate might be even higher in the non-cemented areas, thus making the cementation harder to form. This may also explain the unevenness of cementation in the box. Another reason could also be that some calcite simply precipitated in between sand particles instead of performing as binders. Those particles could be washed away by water flow during permeability test in triaxial apparatus, making the apparent coefficient of permeability to be higher, as stated in the previous section.

5.4.6 Elastic modulus

The elastic modulus of sand sample in box B1 and B2 were determined during cutting by PUNDITPLUS^{TM} Ultrasonic non-destructive integrity tester, as described in Section 3.5.7. In conducting this test, the voltage was set to be 1200V, and pulse frequency was set to be 10/s in each test. Resulted elastic moduli vs. calcite content are shown in Fig. 5.24. The calcite content presented was the average value in that layer. It can be seen that the elastic moduli increases linearly with calcite content, which varied from 2 to 34 GPa in the range of 4 to 13.5% of

average calcite content. Standard deviation was 0.95, fitting by an exponential curve.

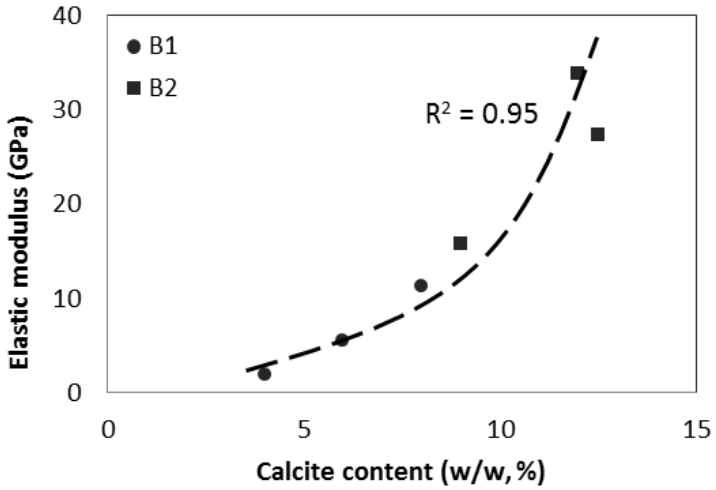

Figure 5.24 Elastic modulus vs. calcite content in box B1 and B2

5.5 Construction of a model pond and its engineering properties

5.5.1 Construction method

A water pond model was constructed by the combination of surface crust formation method and bulk cementation method. Some information had been reported in Chu et al. (2013). 28 kg of poorly-graded fine Ottawa sand with a mean grain size of 0.3mm was employed, which is the same material as in constructing the six boxes in previous section in this chapter.

Sand was compacted into its medium to dense state in a rectangular glass tank with dimensions of 48*38*20cm. Initial permeability was tested to be around $8*10^{-5}$ m/s. A rectangular hole of 34*26*7cm was excavated manually and supported by a plastic board before treatment, as shown in Fig. 5.25a. Similar to the initial stage in the construction of surface-treated boxes B1/2/3, spraying of UPB suspensions (1.35ml/cm^2 in terms of dry biomass) was followed by a spraying of cementation solution (2.3ml/cm^2 of 0.75M $CaCl_2$ + 1.5M urea solution) to form the shape of the water pond initially.

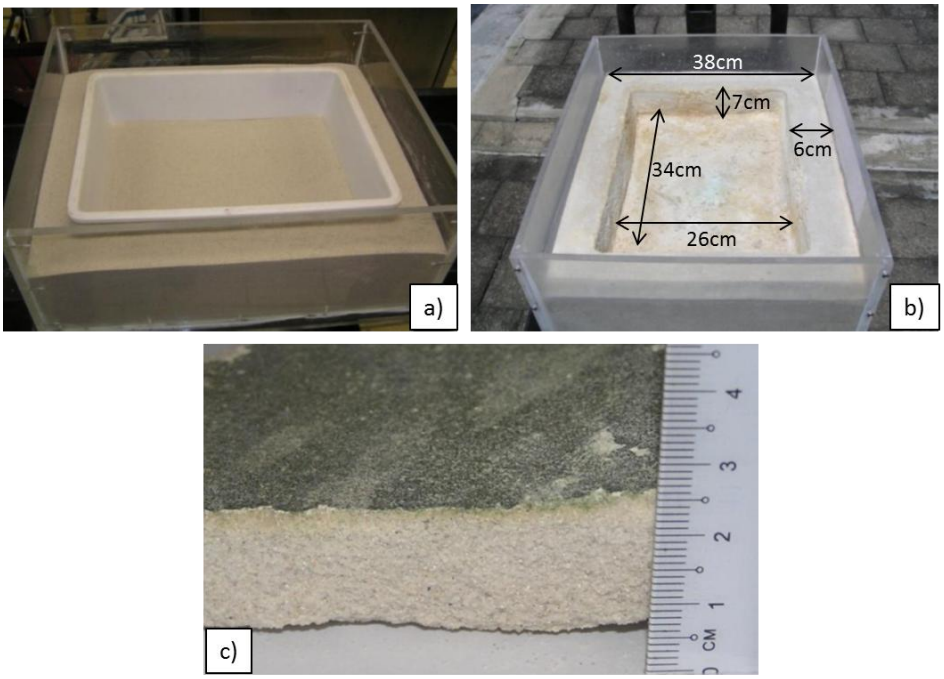

Figure 5.25 Images of a) the water pong before treatment; b) water pond after treatment; c) cross-sectional view of cemented part at pond wall

After spraying of bacterial solution (0.7ml/cm^2 in terms of dry biomass) for the second time, the tank was filled by cementation solution until the water level was 5mm above the sand surface and maintained for 2 days before draining from the bottom. Such treatment was repeated for four times. The sand pond was then left under the ultraviolet lamp for drying. Final product of the water pond after treatment is shown in Fig. 5.25b. A cross-section view of the base of the model pond is shown in Fig.5.25c. It can be observed that a cemented layer varied from 15 to 30mm was formed at the bottom and the four walls of the pond. A thin layer of algae (the green colour shown on top of sand in Fig. 5.25c) was also detected to be formed after another one month of drying in the shade.

EDS spectrum of the precipitated material between sand particles is shown in Fig. 5.26. The main elements were observed to be calcium (49%), carbon (19.9%), and oxygen (31.1%), which could be an indication of the calcite crystals formation performing as binder.

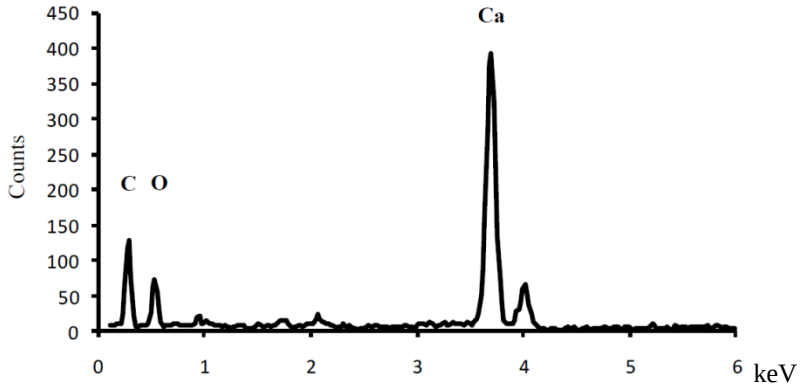

Figure 5.26 EDS spectra showing elements of filling material between sand grains

5.5.2 Permeability of water pond after treatment

The water pond was cut open for engineering properties testing after biocementation. Samples were taken at two different locations: (A) the walls, (B) the pond shore (bottom). Coefficient of permeability was determined using a triaxial apparatus employing flexible wall method. However, it should be noted that, as the biocementation in soil might not be uniformly distributed, cylindrical specimens might not usually been able to obtained. Some specimens may have irregular cross sections instead.

Special procedures were taken to solve this problem, as shown in Fig. 5.27. Impermeable modelling clay was employed to wrap the specimens and made uniform cylinders of 50mm in diameter. Mean cross sectional area of the sample can be calculated by taking the sample out and measuring the weight of water in the hole after test.

Resulted coefficients of permeability versus calcite content are summarized in Fig. 5.28. It can be seen that the permeability of both the walls and the bottom of the pond, at where the biocemented crust were formed had been reduced to around $3.5x10^{-7}$ m/s on average, while the permeability in the sand block below varied from 4.5 to $10.7*10^{-7}$ m/s. These coefficients of permeability were comparable to the value get from set S1, where a 0.2 to 0.5 mm pure crust was formed. However, the calcite content data was not available due to the lack of experience during the first stage of this study.

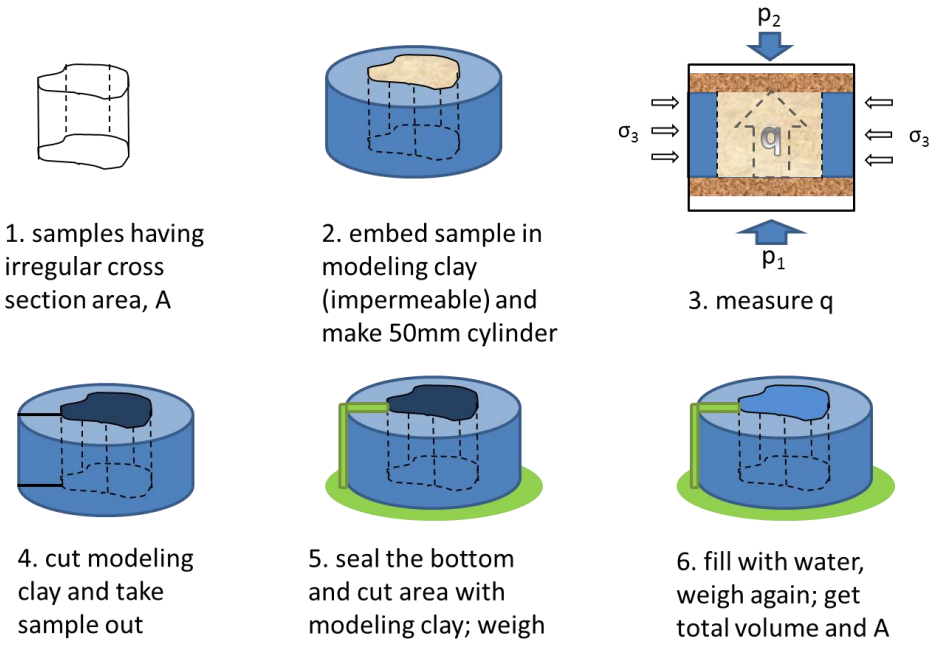

Figure 5.27 Procedures for permeability tests of specimens having irregular cross section

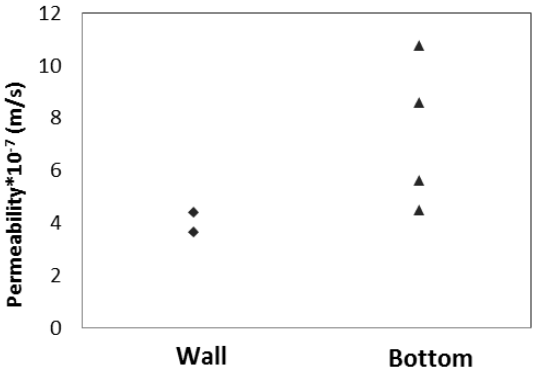

Figure 5.28 Summary of permeability getting from different locations in the water pond

5.5.3 Strength and stiffness of cemented sand

Four-point bending test, as described in Section 3.6.3 were conducted for the specimens taken from wall and the base of water pond. The results are summarized in Fig. 5.29. It can be seen that the maximum stresses in outer fibre measured for the wall and base are in the range of 90 to 256 kPa, which are 30 to 100 times smaller than the specimens getting from pure calcite crust under more treatment cycle, which varied from 6500 to 22000 kPa, as shown in Fig. 5.7, Section 5.3.2. However, the enhancement was still obvious comparing to pure sand having no cohesion or tensile strength at all. The wall to be constructed or the stability of the

slopes in the real application could be enhanced by this strength, and further construction cost could be reduced as well.

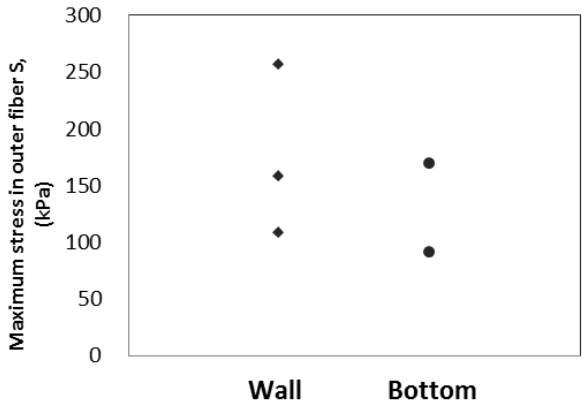

Figure 5.29 Summary of four-point bending tests of specimen taken from water pond

Small specimens of 10*20mm was trimmed and tested for their UC strength. Image of typical specimen indicating its failure mode is shown in Fig. 5.30. Failure modes were observed to be brittle failure in all the specimens.

Figure 5.30 Typical UC specimen and its failure mode trimming from the water pond

Large variation in the UC strength even for samples taken from the same zone was observed, as shown in Fig. 5.31, due to the non-uniformity in the treatment of the soil and also the disturbance to the samples during sample preparation. Similar to the bending strength obtained from the 4 point tests, the strength of the sample at the bottom of the pond is slightly lower than that of the sample at the wall, which might be due to some of the cementation solution/bacterial suspension infiltrates into the base below crust. Therefore, UC strength was detected in the base part C, although the value was much smaller.

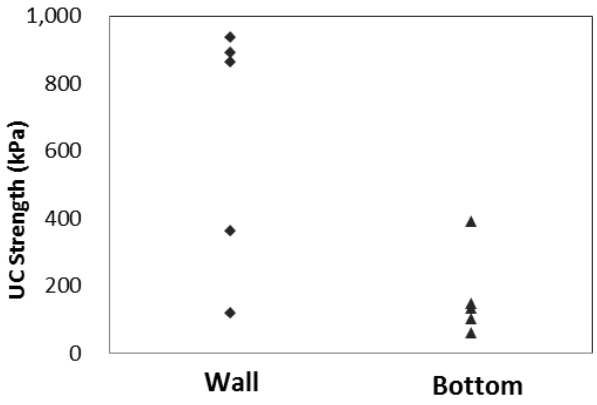

Figure 5.31 Summary of UC test in the specimens getting from water pond

5.6 Conclusions

Two biocementation methods were adopted in this study: crust and bulk cementation. Use the first method, a layer of calcite crust was formed on the top surface and the surrounding surfaces of the sand in the box. The thickness of this layer was around 3 to 4 mm for a few rounds of treatments. The thickness of the crust increases with the number of treatments. After 30 rounds of treatment, the thickness of the layer can increase to 7 ± 2 mm. The outer fibre stress of the curst as measured using a 4-point bending test was as high as 20 MPa. The coefficient of permeability of the crust layer was reduced from 10^{-4} m/s before treatment to 10^{-9} m/s. Thus the crust method is capable of forming an imperious layer on the surface of sand for bioclogging purpose.

Using the bulk cementation method, the UC strength of the treated sand can be as high as 5977 kPa. The UC strength increases with increasing calcite content. The uniformity of biocementation within the sand block was increased with the increased rounds of treatment. The FESEM pictures and the corresponding EDS images for biocemented sample confirmed that it is the presence of the calcium carbonate which leads to the increase in strength and decrease in permeability of the sand.

Chapter 6

Up-Scaled Model Test of Biocementation in Sand

6.1 Introduction

Traditional ground reinforcement methods are conducted by injection of cement or chemical grouts. To simulate the progress of bio-grouting by MICP *in situ*, an up-scaled model test of 1 m^3 was performed under a controlled environment using conditions and injection techniques anticipated in practice. The method used for the treatment of the 1 m^3 of sand was the bulk cementation method established in Chapter 4. Experimental setup, treatment method, monitored data and the resulting engineering properties of the treated sand are presented in this chapter.

6.2 Experimental setup and treatment methods

1440kg of dry fine sand was packed at a loose state into a plastic box with dimensions of 112cm in length, 96cm in width and 95cm in depth, as shown in Fig. 6.1a. Volume sand in box was 1.02 m^3. The sand used was import from Riversand^{TM} in Australia. Sand property is described in Section 3.4.1. After flushing with tape water, the sand surface settled by 5 cm, which reduced the volume of sand to be 0.97m^3, making the initial void ratio $e_0 \approx 0.78$ and $D_R \approx 6\%$. This setup will be referred as cubic meter block in the later sections.

Two plastic cylindrical drains ($\varphi \approx 50$ mm) were used for the model test. One was for injection and another for the extraction purpose, as shown in Fig. 6.1b. The asymmetric spiral cylindrical drains are capable of resisting bending and pleating.

It was perforated with small holes (φ ≈ 2 mm; three holes in every 2cm interval) permitting talent flow. A layer of geotextile was wrapped outside the drain.

After the sand surface was flattened and smoothed, tap water was directly sprayed on the sand until the sand surface was fully submerged under the water. A reservoir of water above the sand surface is formed with a depth of around 5cm. Afterwards, the box was left still for 24 hours for sand settlement and fine content removal. This procedure was repeated for three times until no further settlement of the sand structure could be observed visually.

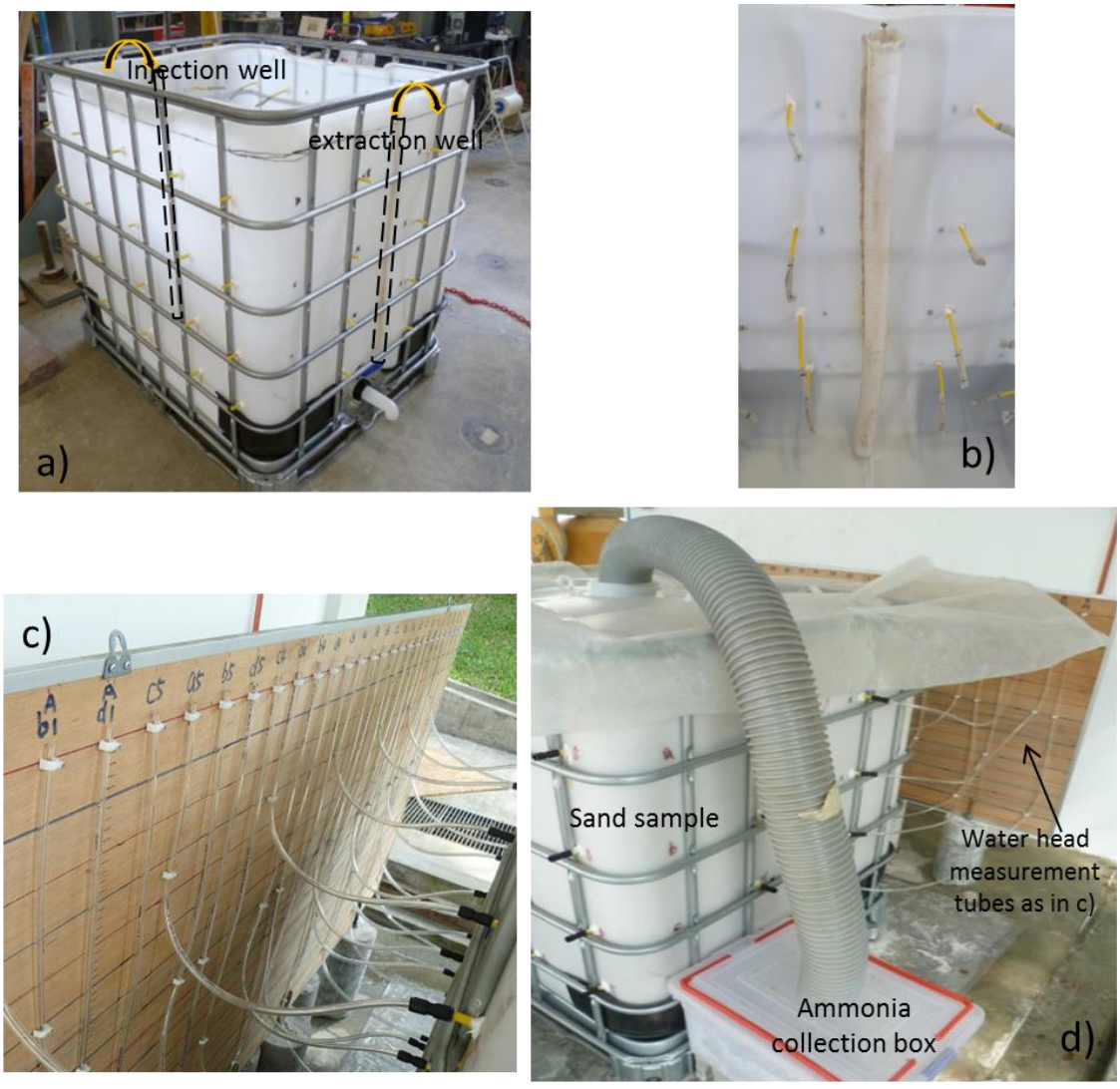

Figure 6.1 Images of experiment setup of the cubic meter sand block; a) the sand box; b) plastic tube working as injection/extraction well; c) (attempted) hydraulic gradient measurement setup; d) (attempted) ammonia collection setup

Holes were drilled at the four walls for water head measurements inside the sand block at a grid of 2×4 on inlet/outlet wall and 5×4 on the two side-walls, as shown in Fig. 6.1a and 6.1c. However, this arrangement only worked for one time while washing the sand with tap water. Hydraulic gradient was observed through the tubes to be 0.6 m/m between the inlet and outlet wells at a total flow rate of around 1500L/hr. In contrast, during most of the treatments, the water head difference was too low to measure. The holes were completely plugged by calcite after two rounds of treatment and the tubes were removed afterwards for draining after the geotextile wrapping the extraction well became almost completely impermeable. The arrangement shown in Fig. 6.1d was designed to collect and treat ammonia generated during the biocementation process. The acidity of the water in the box was adjusted using sulphuric acid to pH = 3; it was connected to the sand surface by a plastic hose as shown.

Original urease producing bacteria (UPB) VS1 suspension without centrifuging was employed for the treatment of the sand block. The urease activity of UPB used varied from 0.8 to 0.4 mM urea/min after several batches of re-cultivating with similar biomass concentration in the solution, as explained in Section 4.2.1. This value was considered to be extremely low, comparing to the numbers quoted in the literature, which were in the range of 3.3 to 20 mM urea/min (Bachmeier et al., 2002; Bang et al., 2001; DeJong et al., 2006; Ferris et al., 1996; Mitchell and Ferris, 2005; Mortensen and DeJong, 2011; Whiffin et al., 2007). However, the data shown in Chapter 4 have indicated that the UBP with low activity is still effective.

The biotreatment process for this $1m^3$ sand block was divided into two major steps: preliminary and secondary treatments, each involved five batches of treatment. During the preliminary treatment, 20 litres of bacteria suspension was poured into the box through the inlet tube with flow rate at 20L/hr, followed by 50mM $CaCl_2$, recirculating for two hours, and left overnight for maximizing the attachment to the sand surface. Sequentially 50L cementation solution (containing 0.75M $CaCl_2$ plus 1.5M urea) was injected through the injection well, transporting along the length of sand box (110 cm) towards the extraction well, and then recirculating for one week. This process was considered as one round of preliminary treatment.

To enhance the efficiency of reaction, the hydraulic retention time should be long enough to assure the time of bacteria/chemical contact and reaction. Therefore, the flow rate of cementation solution was also maintained to be 20L/hr, which made the hydraulic retention time in the box to be around 21.3 hours. The hydraulic gradient was nearly not detectable as the flow rate to too low. Description of the preliminary treatment is as drawn in Fig.6.2a. Aerial view during the circulation process is show in Fig. 6.2b. Symmetric flow from the injection to extraction well was expected theoretically.

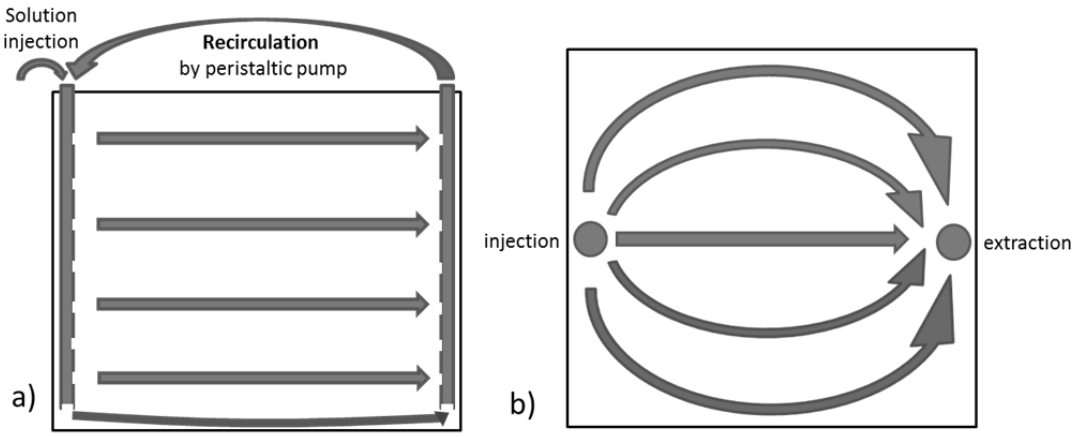

Figure 6.2 Illustration of a) side view; and b) aerial view of the cubic meter sand box during preliminary treatment

Target of the preliminary treatment was to construct the structure of sand block initially, obtaining uniform calcite distribution in the sand block without local clogging, by recirculating at a relatively low rate and maximizing the hydraulic retention time. Preliminary formed calcite crystal could also help the formation of calcite at later stage, as the rate of crystal growth is directly related to the available crystalline surface. More calcite may intend to precipitate at where calcite crystal had already existed (van Paassen, 2009). This initially stable structure of sand block also helped to balance the inner pressure, preventing the possible destruction of structure by high flow rate of cementation solution in latter stage.

After building up of the preliminary structure, 200L of cementation solution was injected at higher flow rate in each batch to accelerate the treatment process. One option to inject such large volume of fluid is to increase the injection pressure, as used by van Paassen (2009). Nevertheless, the possibility of inner fracture was also increased along with the increasing injection pressure. Several sudden pressure

drops were reported during the treatment described in van Paassen (2009). Transporting well was even exposed after three events of inner failure, and the problem of leakage was severe.

Therefore, surface percolation was employed combined with injection/extraction well to deal with the large quantity of cementation solution, as well as maintaining the injection pressure at 1atm in the meantime. The process is roughly sketched in Fig. 6.3. The small holes on the injection/extraction well had all been clogged by that time, making the main transporting paths being the surface infiltration and the opening of well at bottom.

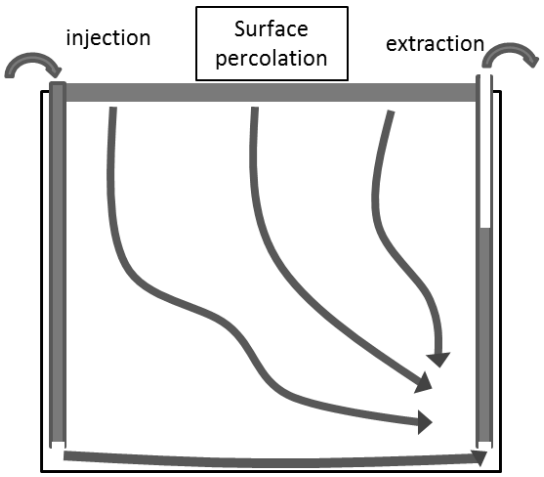

Figure 6.3 Illustration of secondary treatment method of cubic meter sand box

Similar to the preliminary treatment, during the secondary treatment, 20 litres of bacteria suspension was poured into the box through the injection well with flow rate at 20L/hr, recirculating for one hour, and left overnight for maximizing the attachment to the sand surface. 50mM of $CaCl_2$ was added in during recirculation of UPB. 200L of cementation solution was then added at rate of 30L/hr through the injection well, until a reservoir about 5cm in height was formed on top of sand surface. The fluid was then removed from the extraction well at roughly the same rate as injection. Noted minor adjustment of flow rate was made during injection/extraction, to prevent the reservoir from overflowing and avoid the mixing of fluid for injection/extraction.

One round of the cementation process lasted for about 7 ~ 8 hours. New batch of bacteria was then added in the evening, and another round of cementation process

began in the following morning. Five rounds of this second step of treatment lasted for five days, one day per treatment, which was considered to be fast and might be practical for industrial usage. Total cementation solution supply was 1250 litres in the two steps of biocementation. The ultimate mean calcite content (g/g sand) that could be achieved in the cubic meter box after biotreatment was calculated to be 4.92%, by assuming 100% cementation efficiency.

Parameters during treatment were monitored through the effluent. To get precise measurement of the solution, a plastic pipe was put into the middle of the tank, which was 45cm in length, with 40cm buried into the sand. It was 1.5cm in diameter, wrapped with geotextile at the end. Another plastic hose was inserted into the pipe to siphon the solution out. pH value maintained above 8 at all times during both the two steps of treatment. Calcium cation left in the effluent was checked by 1M $NaCO_3$ solution along the treatment, one time per day during the first step and three times per day during the second step. Consumption of calcium was considered to be completed as no sediment was found in the effluent in both treatment steps.

6.3 Engineering properties of sand after biotreatment

After the five rounds of preliminary treatment and five rounds of secondary treatment, the plastic box was sawed open, and the treated sand block is as shown in Fig. 6.4. Some traces of hydraulic flow lines could be visible near the bottom of the block. Comparing to the 60% of uncemented part indicated in van Paassen et al. (2009), in which only about $40m^3$ of cemented body out of the $100m^3$ was clearly visible after extraction, and was limited by the induced hydrological flow field of cementation solution after biotreatment, the sand block in this treatment was perfectly stood by itself as a whole, indicating firm and uniform cementation.

Figure 6.4 Image of the $1m^3$-sand block after treatment

The sand block was then cut into 27 pieces for testing of its engineering properties, approximately $0.036m^3$ each piece. The block was divided into three layers by height (A, B and C, counting from the sand surface) and 9 pieces per layer, as shown in Fig.6.5. Legend of sampling position referring in later sections would be based on this figure. For example, block A2 is referring to the area just around the top of inlet well, while block C8 is referring to where nearby the tip of the extraction well.

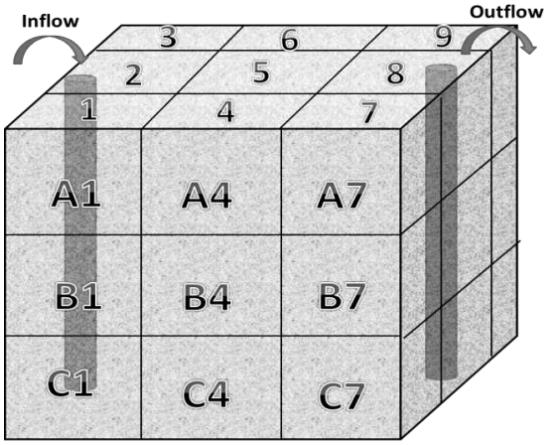

Figure 6.5 Indication of sampling positions in the cubic meter sand box

Similar to handling the six small sand boxes as described in Section 5.3.3, each piece was moulded by 50 mm drilling bit into several cylindrical specimens for its

engineering properties tests. Image of a) cutting of the first layer A, the second and third layer B and C, and part of the specimens drilled for strength and permeability test are shown in Fig. 6.6a, 6.6b, and 6.6c respectively.

Figure 6.6 Images of the cubic meter biotreated sand box during: a) cutting of the first layer A; b) cutting of second and third layer B and C; c) part of the specimens drilled for strength and permeability test

6.3.1 UC Strength and its variation in the sample

UC strength versus calcite content is summarized in Fig. 6.7. Calcite contents in sand samples were determined by ICP test as described in Section 3.3.1. Overall mean calcite content in the sand box was 4.55%, which was 5.5, 3.3 and 4.8% in layer A, B and C respectively. Cementation efficiency is calculated to be 93% in terms of calcite precipitation, which is comparable with data reported in the literature, varying from 50% to 92% (Al Qabany et al., 2012; DeJong et al., 2006; Rebata-Landa, 2007; Whiffin et al., 2007).

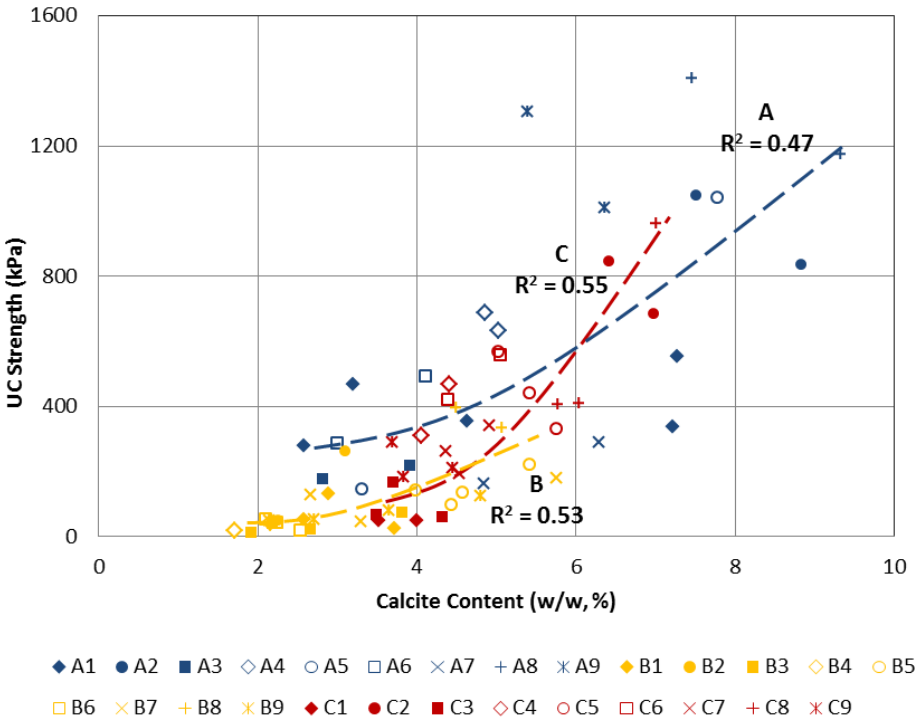

Figure 6.7 Summary of UC strength versus calcite content in cubic meter box

As shown in Fig. 6.7, unconfined compressive strength varied in the range of 10 to 1400 kPa while having 2 to 9% calcite by weight in the whole block. Calcite content related positively to the UC strength. The distributions of calcite content/UC strength along the two cross sections in the centre of box are shown in Fig. 6.8a and 6.8b respectively, which are the surface from the inlet to outlet tube (plane 2-5-8), and the surface perpendicular to it (plane 4-5-6).

As illustrated in Fig. 6.7 and 6.8, specimens in top layer A generally intends to have relatively higher calcite content and UC strength, followed by bottom layer C. The middle layer B gained the lowest calcite content as well as UC strength. This observation is similar with the data perceived from the small boxes presented in Chapter 5 and in some previous researches (Al Qabany & Soga, 2013; Bernardi et al. 2014; DeJong et al., 2006; Stabnikov et al., 2013; Whiffin et al., 2007; van Paassen, 2009; van Paassen et al., 2009, 2010).

Sand near the inlet area gained greater calcite content and also correspondingly higher UC strength as expected, as $CaCO_3$ precipitation was thermodynamically favoured near the inlet part (Phillips, 2013; Zhang et al., 2010). In addition, as the rate of crystal growth is directly related to the available crystalline surface, more

calcite may intend to precipitate at where calcite crystal had already existed. However, as local clogging may appear near surface in layer A, preferential flow paths could develop due to the faster local flow velocity around the clog. Upper limit may apply regarding to the MICP precipitation and UC strength gain. Bottom portion of the sand box also gained high calcite content and UC strength. The out flow part resulted in better cementation as bacterial cells intended to accumulate around that region, making the cementation favourable.

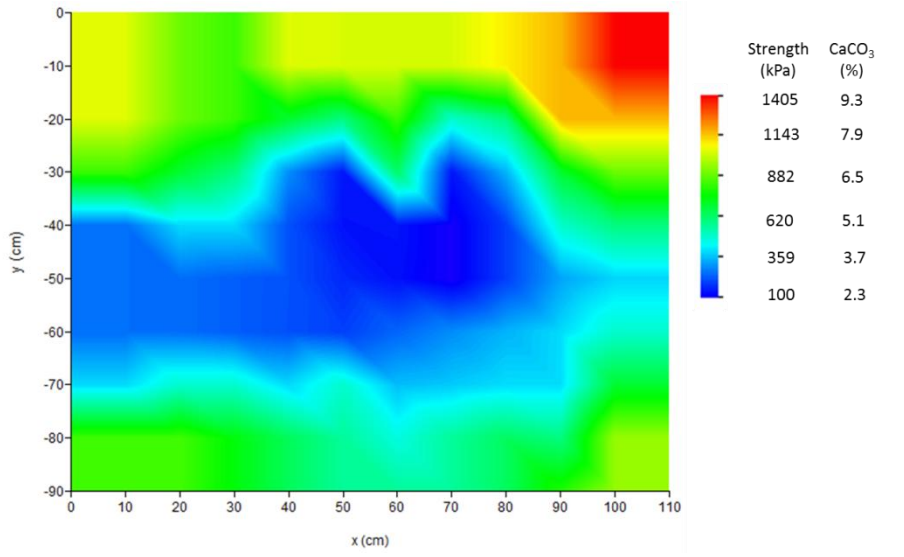

a)

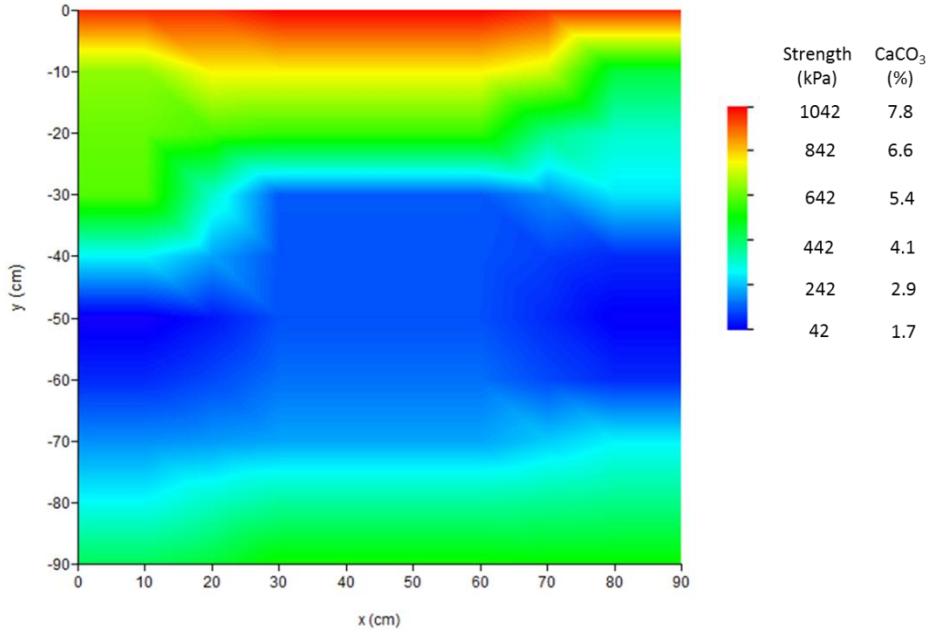

b)

Figure 6.8 UC strength/calcite content distribution of a) cross sectional view of the inlet/outlet tube surface (plane 2-5-8) b) perpendicular cross-sectional view (plane 4-5-6) *noted the scale/max/min value in a) and b) are different

In Fig. 6.8b showing perpendicular cross-sectional surface (plane 4-5-6), it could be seen that the $CaCO_3$/UC strength distribution is generally symmetric. Nearly no advantage has been shown in the principle flow axes horizontally from well to well, indicated balanced inner pressure distribution in the sand box.

6.3.2 Influence of $CaCl_2$ and urea on the UC strength of biotreated sand

Similar to what has been described in Section 5.4.3, to further investigate the contribution of calcite in strength of the biotreated sand, some specimens in the cubic meter box were also oven dried at 105°C for 48 hours (degree of saturation S = 0%), or soaked under water overnight (degree of saturation S = 100%) and tested for their remaining UC strengths.

The resulted UC strengths of oven-dried, soaked, as well as air-dried specimens are summarized in Fig. 6.9. The calcite contents for soaked sets were measured during the specimen trimming, before saturated under water, to be consistent with the other two sets, air-dried and oven-dried samples. The letters A/B/C in the legend refers to the location of specimens.

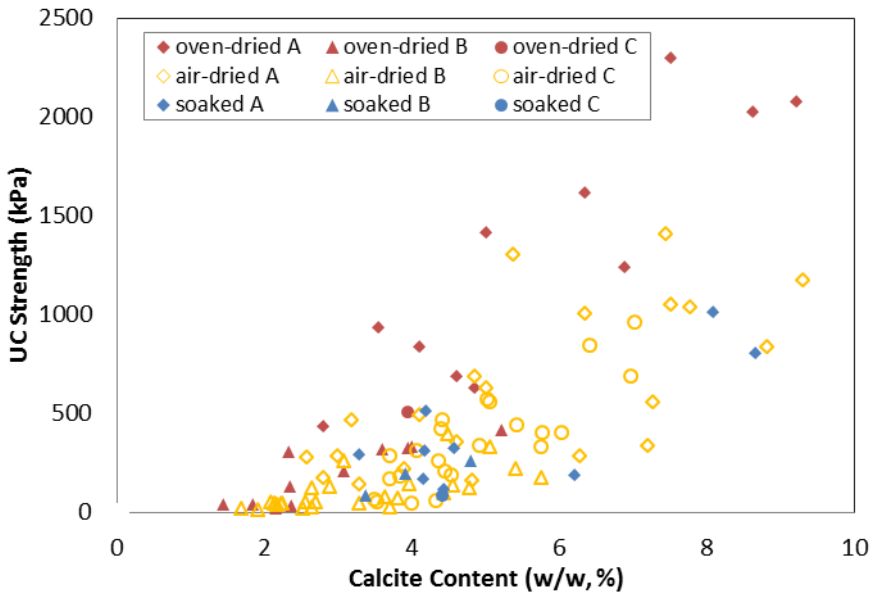

Figure 6.9 Comparison of UC strength vs. calcite content of oven-dried, air-dried, and soaked specimens getting from the cubic meter box

Resulted UC strength of soaked sets (dots in blue) basically coincides with those of the air-dried specimens (dots in yellow), which confirms the inactivity of pure

calcium chloride/urea in the air-dried specimens. The effectiveness of calcite acting as binder was proved to be stable after soaking under water. The advantage of oven-dried specimens (dots in red) comparing to the other two sets could be viewed as the contribution of the unreacted $CaCl_2$ and urea.

To further understand effect of $CaCl_2$ and urea in the strength of oven dried sand specimens, a simple calculation was engaged by comparing the two calcite determination methods employed in this study. As described in Section 3.3.1, discrepancy was found between calcite content measured by inductively coupled plasma atomic emission spectroscopy (ICP) test, which involved in the determination of calcium cation quantity after washing sand sample in water, and the calcite content calculated by mass differences before and after washing by acid. The portion of unreacted calcium chloride/urea could be roughly calculated by the variance between different calcite determination methods. As indicated in section 3.3.1, their relationship measured experimentally was expressed as

$$y = 1.21x + 1.04 \quad \text{(Eqn. 6.1)}$$

in which x is the calcite percentage determined by ICP test, and y is which measured by the mass differences.

Such disparity could come from two channels. The first portion, *a*, could be the mass of bacteria and some fine contents washing out along with acid during calcite content measurement. This part was not supposed to be varied with the value of x. The second part could come from the unreacted $CaCl_2$ and urea (molecular weight = 111+60*2 = 231, as calcium chloride to urea ratio applied was 1:2), which was also attributed as $CaCO_3$ (molecular weight = 100) in ICP test. Assume the mean reaction efficiency of calcium cation was *b*, i.e. (1-*b*) % of calcium carbonate measured in ICP test was remained as calcium chloride and urea. The calcium carbonate content measured by washing method could therefore be expressed as

$$y = 0.4x \times \frac{100}{40} \times b + 0.4x \times \frac{231}{40} \times (1 - b) + a = (2.31 - 1.31b)x + a \quad \text{(Eqn. 6.2)}$$

By matching of the two equations, the values of *a* and *b* were calculated as 1.04 and 84% respectively. In other words, roughly 84% of material supply was

converted to calcium carbonate and acting as binder, and the bacteria mass/fine content and other impurities in the sand was approximately 1.04%. The portions of additional UC strength in oven-dried specimens are supposed to come from the 16% of calcium chloride and urea remaining in the sand sample.

6.3.3 Permeability and its variation in the sample

Coefficient of permeability versus calcite content is summarized in Fig. 6.10. Similar to data presented in previous chapters, the trend of permeability coefficient k was generally lower at higher calcite content level, despite of their large variation. However, it could be observed that the fitting line of layer A lies above it of layer B and C, which means specimens in layer A resulted in higher coefficient of permeability at the same calcite level comparing to layer B and C.

As explained before, such phenomenon could be due to the combination of the following two effects. Firstly, as surface percolation method was employed in the major treatment stage (as described in Section 6.2, which provided 80% of calcium supply in this cubic meter box treatment), the saturation states of calcium and carbonate ion should be the greatest near the surface, thus created an area where calcite precipitation was thermodynamically favoured. And as the rate of crystal growth is directly related to the available crystalline surface, more calcite may intend to precipitate at where calcite crystal had already existed.

However, such primary advantage might also cause local clogging near surface in layer A. Preferential flow paths could develop due to the faster local flow velocity around the clog. The image showing typical inner structure of sand specimen in layer A confirms such assumption as shown in Fig. 6.11. The preferential flow paths in centimetre scale caused porous structure can be observed. Such effect might hinder further MICP formation in these areas, as more rapid flow velocity lowered the reaction rate of bacteria and chemicals, by reducing their contacting time between each other. The re-convergence of flow could also be hindered by such preferential flow paths.

The combined effect of these factors interacted with each other, resulted in higher calcite content, greater UC strength, yet also larger coefficient of permeability near surface layer A.

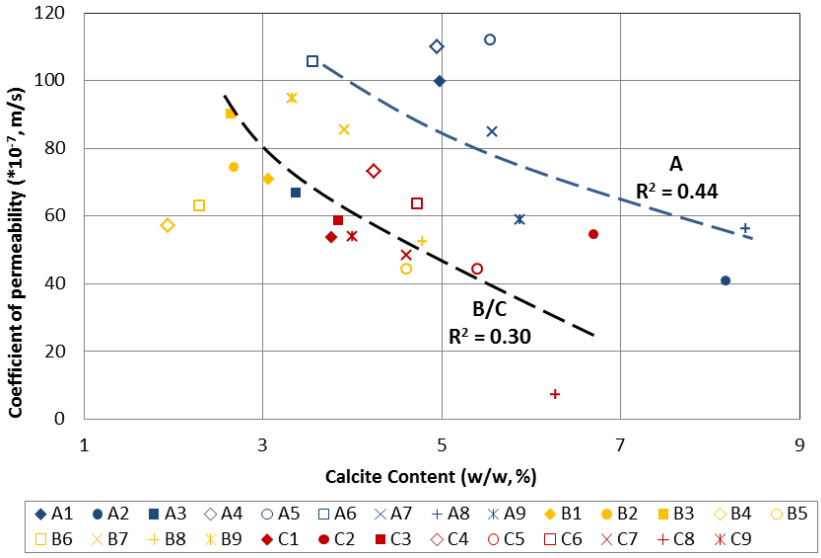

Figure 6.10 Summary of permeability versus calcite content in cubic meter box

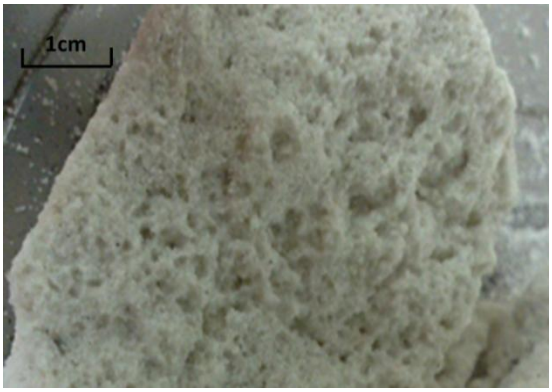

Figure 6.11 The porous structure in the sand block (top layer A)

6.4 Conclusions

To simulate the bio-grouting method in situ, an up-scaled experiment with one cubic meter in volume was performed under the conditions and using the injection techniques to simulate those anticipated in practice. The following observations have been made from the model tests:

Cementation efficiency is a measure of the mean calcite content achieved in sand divided by the initial total calcium supply calculated using the chemical formulae.

For the one cubic meter box model test, the cementation efficiency was calculated to be 93%. This value is considerably higher compared with that in the small cylindrical samples and the values reported in the literatures which range from 50 to 92% (Al Qabany et al., 2012; DeJong et al., 2006; Rebata-Landa, 2007; Whiffin et al., 2007). These test data confirmed that the effectiveness of the low activity UPB strain VS1 and the treatment method used in the study.

With the use of one injection point for the model test, the properties of the biocemented sand is highly nonhomogeneous within the one cubic meter sample. Specimens at the top layer gained the highest calcite content and the highest UC strength. The highest UC strength achieved was 1400 kPa after 5 rounds of treatment. The corresponding calcium carbonate precipitated was 9% by weight. This is followed by the bottom layer with UC strength up to 1000 kPa. Specimens in the middle layer had the lowest calcite content as well as the lowest UC strength. In spite of its higher calcite content and greater UC strength, sand samples in the top layer showed a higher coefficient of permeability compared with that for the sample having the same calcite content in the middle or at the bottom layer. This could be caused by the preferential flow paths developed due to a faster seepage velocity around the clogs.

Chapter 7

Stress-strain-strength Behaviour of Biocemented Sand

7.1 Introduction

The effect of cementation on the strength, stress-strain and permeability behavior of naturally and artificially cemented sands, including soil treated using Portland cement, have been investigated by a number of researchers (Coop and Atkinson 1993, Cuccovillo and Coop 1999, Ghatak et al., 2013; Kavvadas et al., 1993; Rabbi and Kuwano, 2012; Schnaid et al. 2001; Thian & Lee, 2013). However, studies on the failure mechanisms and stress-strain behaviour of soil treated using the MICP method are rare. Results on several sets of consolidated drained (CD) triaxial tests are presented and discussed in this chapter. The engineering properties of biocemented sand presented in Chapters 4, 5, and 6, along with some other published data are also analysed in this chapter.

7.2 CD tests on MICP cemented sand

7.2.1 Test setup

Triaxial consolidated drained (CD) tests were conducted to evaluate the influence of biocementation on sand. A comparison of these tests with CD tests on uncemented sand at similar initial state was also made. As summarized in Table 7.1, five sets of CD tests were conducted on cemented sand with different levels of calcite content (set C, D, E), as well as non-cemented pure sand (set A and B).

River sand (as described in Section 3.4.1) was used in this study. Sand samples with two different initial relative densities were prepared. The initial void ratio for

specimens in series A was controlled to be around 0.78. This value was selected to be consistent with the sand samples in the cubic meter box test before biotreatment. Samples in series B were in medium to dense state with initial void ratio of 0.57, which matched the void ratio of the specimens from the six small boxes before treatment.

Sand samples in series A were prepared using the moist tamping method. Sand was oven dried and mixed with distilled water to achieve a water content of 5%. The wet sand was then divided into four portions and tamped layer by layer within a 3-part split mould. 10 times of tamping was used for each layer. Cell pressure and back pressure of 510 and 500kPa respectively were applied gradually by two GDS controller for saturation. B-value above 0.95 was measured. Shearing was applied at a rate of 0.05mm/min after the specimen had been consolidated.

Samples in series B were prepared using the water sedimentation method. Distilled water of 2cm in depth was poured into the mould first. Sand was then deposited into the water with a funnel until the sand level almost reached top of the water. This step was repeated until the pre-set sample height was reached. Care was taken that sand should be poured continuously to make sure no segregation occurred in the sample. The saturation, consolidation and shearing processes were conducted subsequently, following the same procedure as in series A.

The specimens used for series C, D, and E were taken from block samples. A coring machine was employed to drill specimens from the cubic meter sand box (Chapter 6) and the three bulk-treated small boxes (Chapter 5) respectively (as shown in Fig. 5.8, Section 5.3.3). The specimens used for CD test were all about 50mm in diameter and 100mm in height. Specimens used for these three series of test had different calcite content. The specimens in series C, D, and E had an average calcite content of 5.0±0.5%, 7.8±0.6%, and 12.9±1.3% respectively.

Consolidation stresses σ_3' of 50, 100, 200 and 400 kPa were applied in each set of specimens. One additional test under σ_3'=300 kPa was conducted on specimen A3 in series A. Other information of each specimen is given in Table 7.1.

Table 7.1 Detailed information of CD test specimens, and void ratio calculation for each biotreated specimens in set C, D and E

Remarks	No.	Specimens' origin	Confining stress σ_3' (kPa)	Peak deviator stress q (kPa)	Peak σ_1' (kPa)	τ (kPa)	Peak p' = ($\sigma_1'+2\sigma_3'$) /3 (kPa)	Initial e_0 before treatment	Void ratio upon test	Dry density ρ_d	Specimen Volume V_T (mm^3)	Sand Volume V_s (mm^3)	Void Volume V_v (mm^3)	Calcite Content (w/w, %)	Calcite Volume V_c (mm^3)	Sand Volume after treatment Vs' = Vs+Vc (mm^3)	Void Volume after treatment Vv' = Vv - Vc (mm^3)	e' = Vv'/Vs'
Reconstituted sand specimen of φ50mm	A1	loose to medium-packed clean sand	50	117.5	167.5	58.7	89.2	0.78		1.52	-							
	A2		100	231.7	331.7	115.8	177.2	0.77		1.53								
	A3		200	443.1	643.1	221.6	347.7	0.77		1.53								
	A4		300	681.7	981.7	340.9	527.2	0.78		1.52								
	A5		400	871.8	1271.8	435.9	690.6	0.77		1.52								
	B1	medium-packed clean sand	50	229.6	279.6	114.8	126.5	0.57		1.69								
	B2		100	415.4	515.4	207.7	238.5	0.57		1.69								
	B3		200	883.4	1083.4	441.7	494.5	0.56		1.70								
	B4		400	1841.0	2241.0	920.5	1013.7	0.57		1.69								
Taken from $1m^3$ model (Chap 6)	C1	cubic box-layer A	50	667.9	717.9	333.9	272.6	0.78	0.70	1.59	152928	85915	67014	5.41	4652	90567	62361	0.69
	C2		100	1243.4	1343.4	621.7	514.5		0.71	1.58	170834	95974	74860	4.91	4713	100687	70147	0.70
	C3		200	1587.2	1787.2	793.6	729.1		0.68	1.61	178060	100034	78026	4.48	4483	104516	73544	0.70
	C4		400	2658.0	3058.0	1329.0	1286.0		0.69	1.60	183489	103084	80405	4.58	4725	107809	75680	0.70
Taken from the six small boxes (Chap 5)	D1	bulk 3	50	1668.6	1718.6	834.3	606.2	0.59	0.50	1.80	177531	111655	65876	7.56	8442	120097	57434	0.48
	D2	bulk 1	100	1796.5	1896.5	898.3	698.8	0.58	0.51	1.79	192313	121717	70596	8.37	10192	131909	60404	0.46
	D3	bulk 1	200	2175.4	2375.4	1087.7	925.1	0.58	0.48	1.82	185355	117313	68042	7.22	8466	125779	59575	0.47
	D4	bulk 1	200	2672.1	2872.1	1336.0	1090.7	0.58	0.48	1.83	186798	118226	68571	7.91	9353	127579	59218	0.46
	D5	bulk 2	400	3730.3	4130.3	1865.1	1643.4	0.61	0.51	1.79	142050	88230	53820	7.93	6998	95228	46822	0.49
	D6	bulk 1	400	3790.5	4190.5	1895.2	1663.5	0.58	0.46	1.85	159094	100693	58402	8.18	8240	108933	50162	0.46
	E1	bulk 2	50	2851.2	2901.2	1425.6	1000.4	0.61	0.41	1.91	184708	114725	69982	11.67	13384	128109	56599	0.44
	E2	bulk 2	100	3292.6	3392.6	1646.3	1197.5	0.61	0.41	1.91	191886	119184	72702	12.05	14361	133545	58341	0.44
	E3	bulk 3	100	2883.7	2983.7	1441.8	1061.2	0.59	0.43	1.89	208012	130825	77187	12.09	15819	146644	61368	0.42
	E4	bulk 2	200	3210.1	3410.1	1605.0	1270.0	0.61	0.41	1.92	183486	113966	69519	11.64	13264	127230	56256	0.44
	E5	bulk 3	200	3539.6	3739.6	1769.8	1379.9	0.59	0.47	1.83	174426	109702	64724	14.25	15629	125331	49095	0.39
	E6	bulk 3	400	4549.6	4949.6	2274.8	1916.5	0.59	0.44	1.88	188321	118441	69880	13.07	15476	133917	54404	0.41

Both the void ratios of specimens before and after treatment are given in Table 7.1. The initial e was measured before bio-treatment, and the void ratio after treatment was measured after treatment before CD test. The differences between the void ratios of specimens before and after treatment were supposed to be caused by the calcite introduced in the void between sand particles. As the volume of calcite formed was assumed to reduce the volume of voids while increase the volume of solid by the same amount, void ratio could also be calculated by the calcite content of one specimen. The calculation of void ratio by calcite content using set C, D and E are also shown in Table 7.1. It was assumed that the specific gravity of both calcite and sand particles to be 2.7. The calculated void ratio and the measured ones before CD tests (the two emphasized columns in Table 7.1) are plotted against each other in Fig. 7.1 for comparison. It can be seen that the two values generally coincident with each other. This also confirms the reliability of the calcite content measurement.

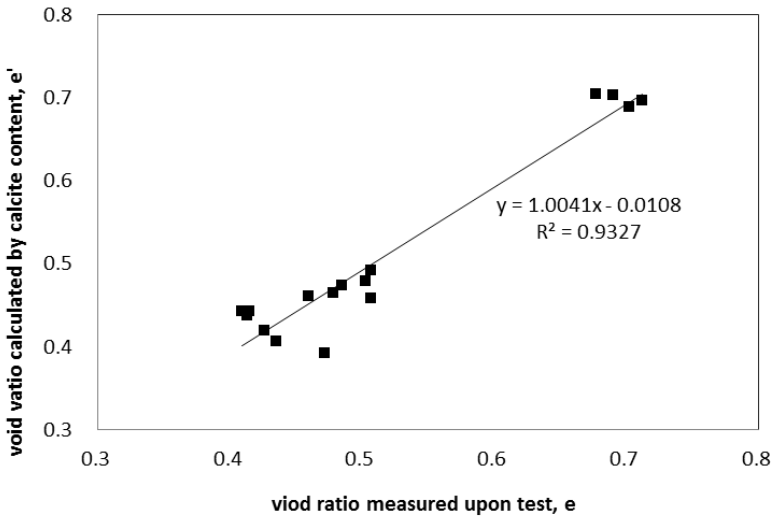

Figure 7.1 Void ratio e measured by weight and volume of specimens in CD test, versus the void ratio e' calculated by calcite content by assuming specific gravity G_s of calcite to be 2.7

7.2.2 Analysis of CD tests results

The specimens of Test A2 and Test E2 after failure are shown in Fig. 7.2a and 7.2b respectively. As can be observed, the non-cemented specimen A2 only shows bulging type of failure; the biotreatment specimen E2 shows shear band type of failure.

a)  b) 

Figure 7.2 Images of typical sand specimens in a) non-cemented set (A2) and b) cemented set (E2) after failure in CD test

The stress-axial strain curves resulting from the CD tests for series A to E, under consolidation pressure of 50 kPa and 400 kPa are shown in Fig. 7.3a and 7.3c respectively. As shown, the peak strength q and the stiffness are much higher in the bio-treated sand. All bio-treated specimens experienced an initially stiff stage, in which stress alomost increased linearly up to the yield point at about 0.5% to 1.5% strain. This could be observed in the enlarged part of initial stage up to 2% axial strain, shown in Fig. 7.3b and 7.3e for consolidation pressure 50 kPa and 400 kPa respectively. Sudden failure occurred beyond that, and substantial strain softening behaviour was observed. On the other hand, no obvious strain softening behavior was shown in non-cemented sand sets.

a)

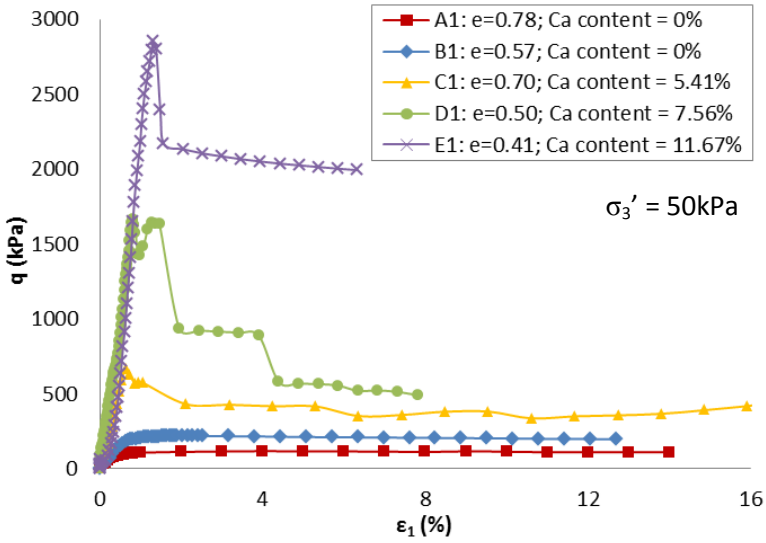

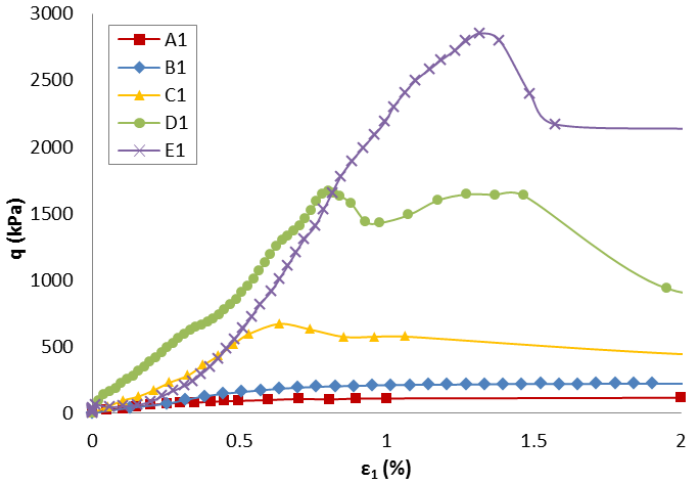
A1
B1
C1
D1
E1
q (kPa)
ε1 (%)

b)

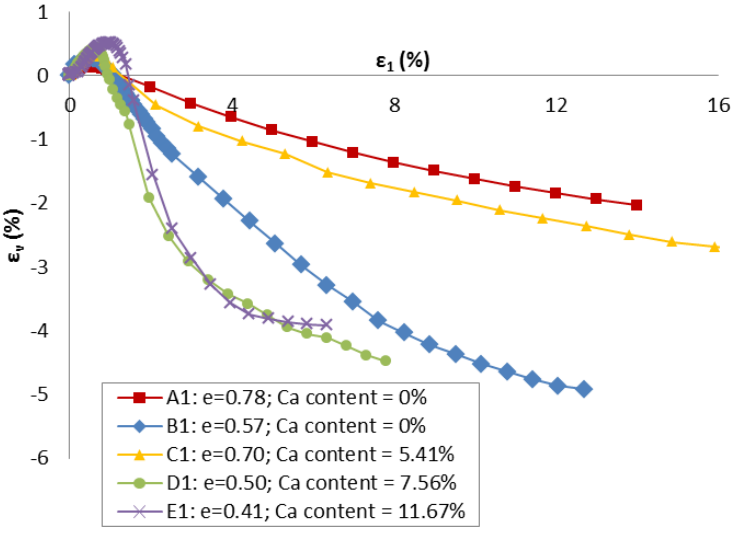
εv (%)
ε1 (%)
A1: e=0.78; Ca content = 0%
B1: e=0.57; Ca content = 0%
C1: e=0.70; Ca content = 5.41%
D1: e=0.50; Ca content = 7.56%
E1: e=0.41; Ca content = 11.67%

c)

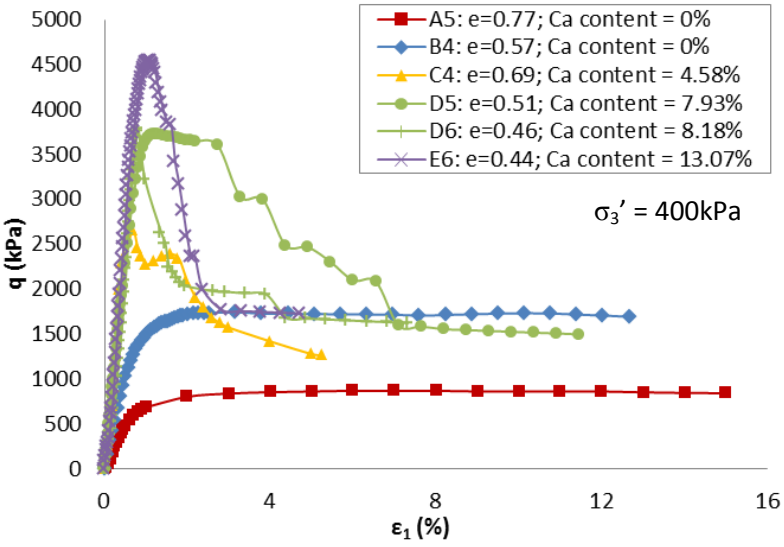
A5: e=0.77; Ca content = 0%
B4: e=0.57; Ca content = 0%
C4: e=0.69; Ca content = 4.58%
D5: e=0.51; Ca content = 7.93%
D6: e=0.46; Ca content = 8.18%
E6: e=0.44; Ca content = 13.07%
σ3' = 400kPa
q (kPa)
ε1 (%)

d)

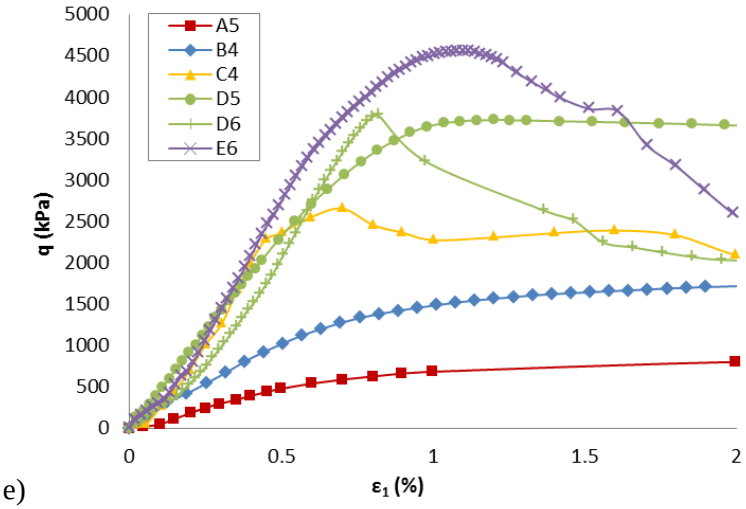

e)

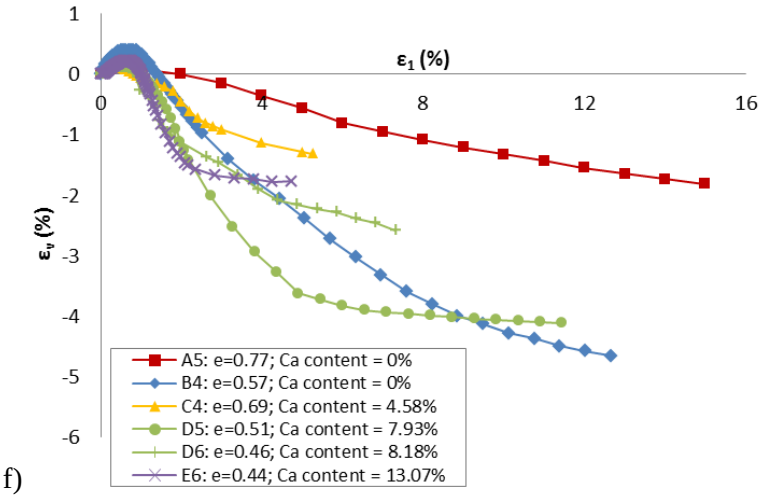

f)

Figure 7.3 CD test for non-cemented and biocemented sand at different calcite content level; a) stress-axial strain curves under consolidation pressure of 50 kPa; b) initial part of 7.3a, 0 to 2% of ε_1; c) ε_1 vs. ε_v curves under 50 kPa; d) stress-axial strain curves under 400 kPa; e) initial part of 7.3d, 0 to 2% of ε_1; and f) ε_1 vs. ε_v curves under 400 kPa

The volumetric vs. axial strain curves during CD test for sets A to E, under consolidation pressure of 50 kPa and 400 kPa are shown in Fig. 7.3c and 7.3f respectively. All sets of specimens exhibited dilative behaviour. It is observed in Fig. 7.3a and d that the maximum dilatancy ratio $d\varepsilon_v/d\varepsilon_1$ generally occurred at the same strain with peak strength, and lowered again under further shear strain; this will be illustrated in detail later. The dilation of the cemented sand specimens might be explained by the increasingly larger void ratio within the shear bands of cemented sand specimens as axial strain increases beyond the peak deviator stress (Jiang et al., 2011).

The peak strength q vs. p' as well as their stress paths and the fitted failure

envelopes are shown in Fig. 7.4. Bio-treated sets showed improvement regarding the failure profile (peak q reached) comparing to the non-cemented set. Straight lines of failure envelopes which are generally parallel with each other governed by friction angle and cement level are found in each case. The formation of the biocementation bonds improved the resistance of specimen's to shearing in terms of (apparent) cohesion rather than friction. Such observation is in agreement with data presented by many previous researchers for artificially cemented sand samples, especially Portland cement mixed sand samples (Coop and Atkinson 1993, Cuccovillo & Coop, 1999; Ghatak et al., 2013; Jiang et al., 2011; Kavvadas et al., 1993; Marri, 2010; Rabbi & Kuwano, 2012; Schnaid et al. 2001; Thian & Lee, 2013). Some of the examples are presented in Fig. 2.30 of Section 2.4.2. However, it should also be noted that there was lack of data under low confining pressure; the parts of failure envelopes shown in Fig. 7.4 represented by the dash lines might have different trends, and the c' obtained might not be true cohesion.

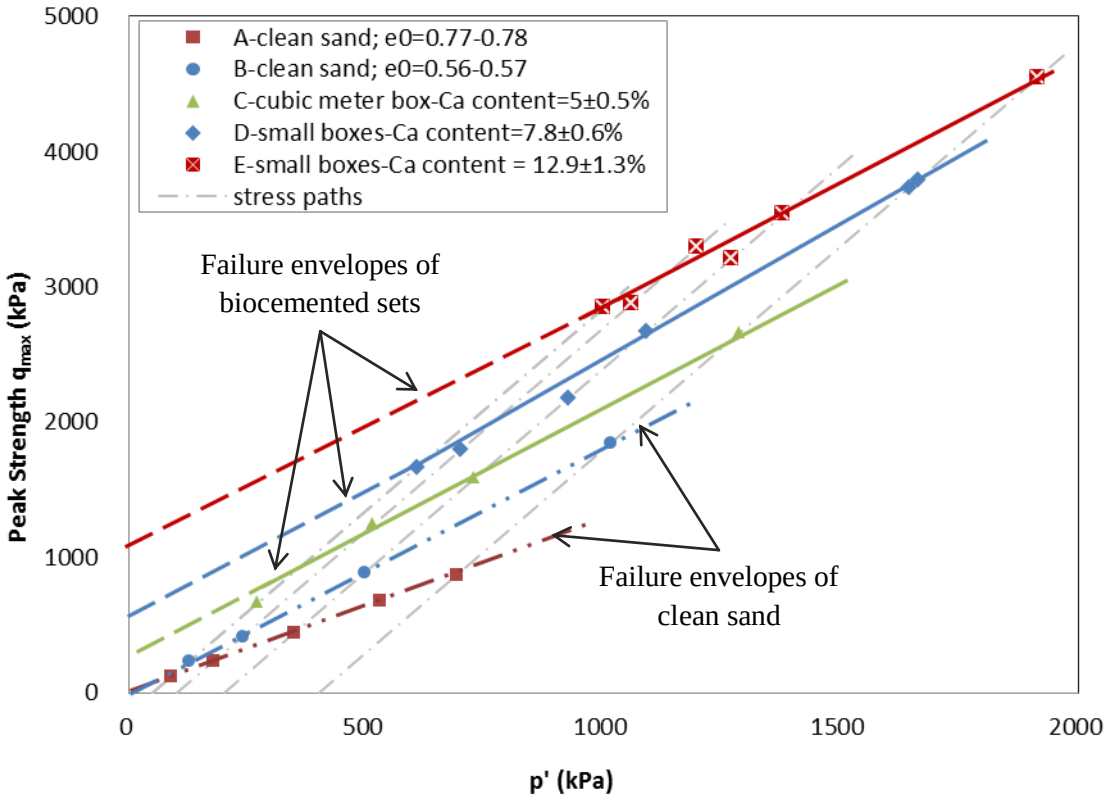

Figure 7.4 Summary of peak strength vs. p', stress paths and fitted failure envelopes of clean sand and cemented sand with different levels of calcite content in consolidated drained tests

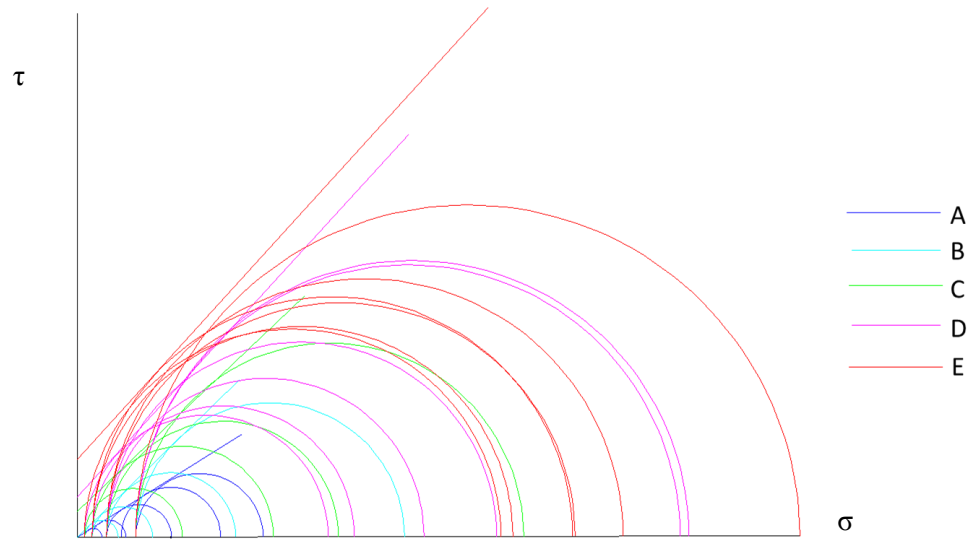

Figure 7.5 Mohr circles drawn for the five sets and friction angle/cohesion calculated by best fitted envelopes

Mohr circles drawn of all sets are presented in Fig. 7.5; the friction angles φ*'* and cohesion intercept *c'* calculated by the best fitting lines of these circles are presented in Table 7.2. Large improvement of cohesion c' was obtained because of the biocement added, from zero in clean sand sets A and B, to 175.5, 273.5, and 532.6kPa for set C, D and E respectively.

Table 7.2 The friction angles φ*'* and cohesion intercept *c'* calculated by the best fitting lines of the Mohr circles in Fig. 7.5

Series	Calcite Content (%)	Friction angle φ' (°)	Cohesion c' (kPa)	Remarks
A	0	32	0	loose clean sand
B	0	44	0	medium clean sand
C	5.0±0.5	44	175.5	$1m^3$ box
D	7.8±0.6	48	273.5	bulk-cemented small boxes
E	12.9±1.3	48	532.6	

The friction angle φ' increased from 44 to 48 degree from set B to set D and E; noted they had similar initial void ratio before biotreatment, if applied. This behaviour is consistent with the results reported by previous researchers (Consoli at al., 1998; Jiang et al., 2011; Schnaid et al., 2001; Thian & Lee, 2013), in which cement content appears to have little effect on the friction angle of sand specimens. However, φ' was increased considerably from 32 to 44 degree from set A to set C, which might partially be due to the greater interlocking of the larger effective particles cemented together from smaller particles (Lade & Overton, 1989).

Besides, the cement agent that fills up the voids in the cemented sand specimens resulted in a more closed and dense structure, comparing to the relatively open and porous matrix of uncemented sand specimens; this might also lead to a higher friction angle (Schnaid et al., 2001). Furthermore, such effect might also be due to the shearing of the specimens in larger pieces that could hold several particles together by the cement bonding, rather than the individual grains (Marri, 2010).

Dilatancy ratio $(-d\varepsilon_v/d\varepsilon_1)_{max}$ vs. axial strain curves for several tests are plotted in Fig. 7.6. It is observed that the dilatancy ratio was the maximum right before the peak strength (which is indicated in Fig. 7.6 by the small arrow) was reached. The peak dilatancy ratio increases with increasing cement level, then decreased towards a critical state, or zero $d\varepsilon_v/d\varepsilon_1$. The dilatancy ratio is suppressed under higher confining pressure as expected, as seen from the comparison between the data under 400kpa confining pressure (represented by dash lines) with that under 50kPa confining pressure (represented by continuous lines).

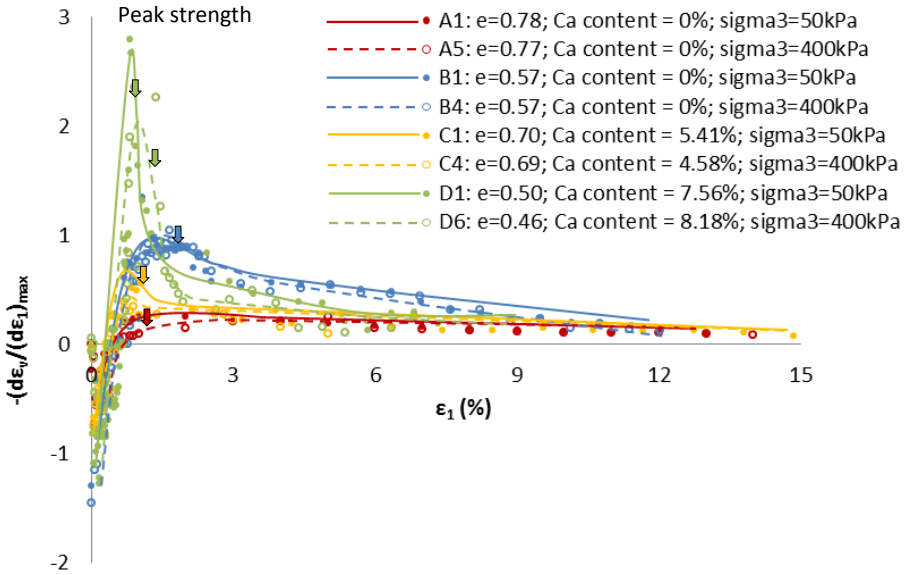

Figure 7.6 Dilatancy ratio $(-d\varepsilon_v/d\varepsilon_1)_{max}$ vs. axial strain curves in specimens A1/A5, B1/B4, C1/C4 and D1/D6

The curves of maximum dilatancy ratio versus void ratio, maximum stress ratio $(q/p')_{max}$ versus void ratio, and maximum dilatancy ratio versus maximum stress ratio obtained from tests in all the five series are shown in Fig. 7.7a, 7.7b, and 7.7c respectively. One unique relationship between the maximum dilatancy ratio versus void ratio is observed for both cemented and non-cemented sand specimens. In terms of the maximum stress ratios, two relationships are observed in Fig. 7.7b,

one for the cemented sand (series of tests C, D and E), another for the non-cemented sand (series of tests A and B). These relationships indicate that the strength gained in the bio-treated sand is not due to dilatancy only. These biocementation increases the failure stress ratio. This could be due to an increase in cohesion as observed in Fig. 7.4. This can be seen further by the maximum dilatancy versus maximum stress ratio curve shown in Fig. 7.7c. Two relationships are observed in Fig. 7.7, one for the cemented sand and another for the non-cemented sand. The curve for the cemented sand (series C, D and E) lies above the curve for the non-cemented sand, i.e. the effect of cement content is to move the plot of q/p' versus $(-d\varepsilon_v/d\varepsilon_1)$ upward.

Note that the behaviour of dilatancy would be disappeared at loose state at the critical void ratio, marked as e_{cs} in Fig. 7.7a. Similarly, it should also be noticed in Fig. 7.7b and 7.7c that a $(q/p')_{cs}$ could be predicted at the critical void ratio e_{cs}, at where no dilatancy would occur $(-d\varepsilon_v/d\varepsilon_1=0)$. The two relationships obtained in non-cemented and cemented set might join together eventually; more sets of cemented specimens at higher void ratio should be conducted to confirm this assumption.

Rowe's theory on stress-dilatancy relation (Rowe, 1962) is expressed as below,

$$\frac{\sigma_1'}{\sigma_3'} = \left(1 - \frac{d\varepsilon_v}{d\varepsilon_1}\right) tan^2(45 + \frac{\varphi_u}{2}) \qquad \text{(Eqn. 7.1)}$$

Maximum stress ratio expressed as σ_1'/σ_3' versus $(1-d\varepsilon_v/d\varepsilon_1)$ of all tested series are plotted Fig. 7.7d. According to Rowe's theory, the best fitting line for the data points is expected to pass through the origin, which is the case in clean sand. However, this is not the case for biocemented sand series. Therefore, it may be conclude that the particles breakage due to biocementation had apparently changed the shear strength envelop of sand. The observation regarding the stress-strain and dilatancy behavior of biocemented sand agrees with published data on cement treated sand (Consoli at al., 1998; Jiang et al., 2011; Schnaid et al., 2001; Thian & Lee, 2013). The peak stress ratios increase with increasing biocement content, as biocement introduced the component of cohesion into the stress-dilatancy relationship by increasing bonding between sand particles.

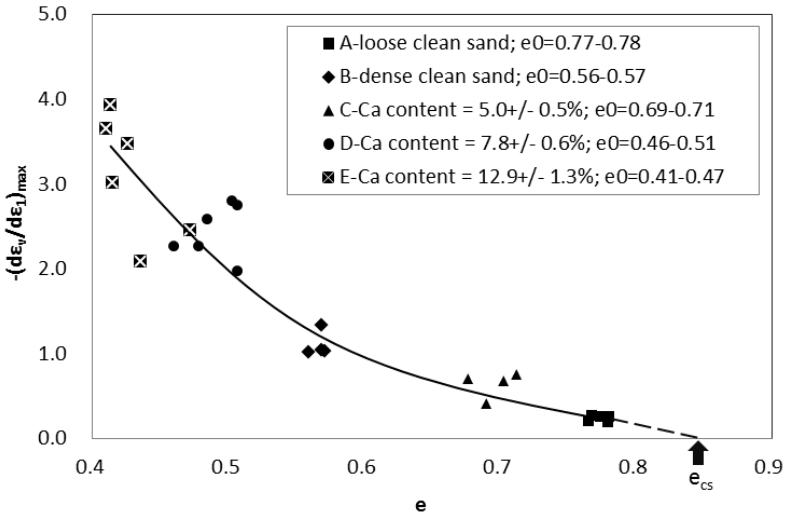
A-loose clean sand; e0=0.77-0.78
B-dense clean sand; e0=0.56-0.57
C-Ca content = 5.0+/- 0.5%; e0=0.69-0.71
D-Ca content = 7.8+/- 0.6%; e0=0.46-0.51
E-Ca content = 12.9+/- 1.3%; e0=0.41-0.47
$-(d\varepsilon_{1p}/d\varepsilon_1)_{max}$
e
e_{cs}

a)

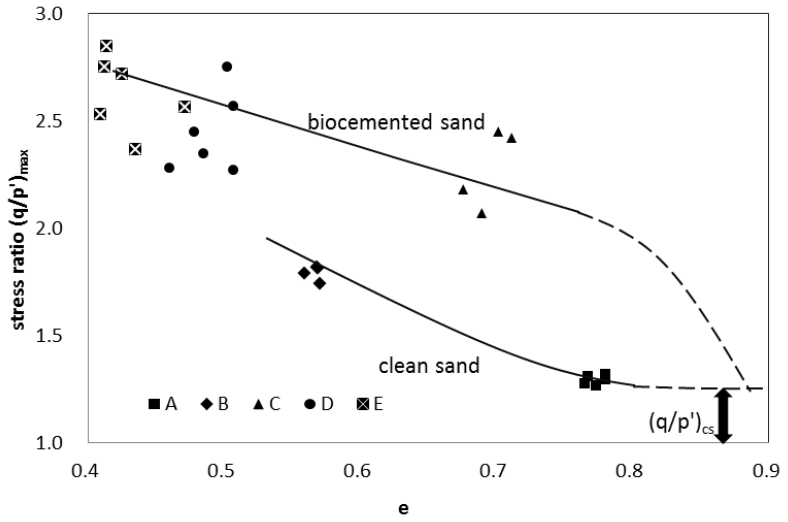
biocemented sand
clean sand
A B C D E
stress ratio $(q/p')_{max}$
e
$(q/p')_{cs}$

b)

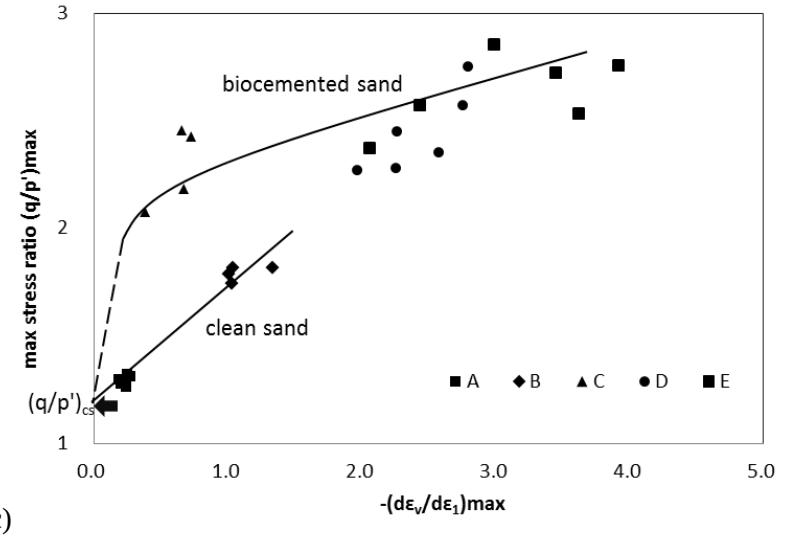
biocemented sand
clean sand
A B C D E
max stress ratio (q/p')max
$-(d\varepsilon_v/d\varepsilon_1)max$
$(q/p')_{cs}$

c)

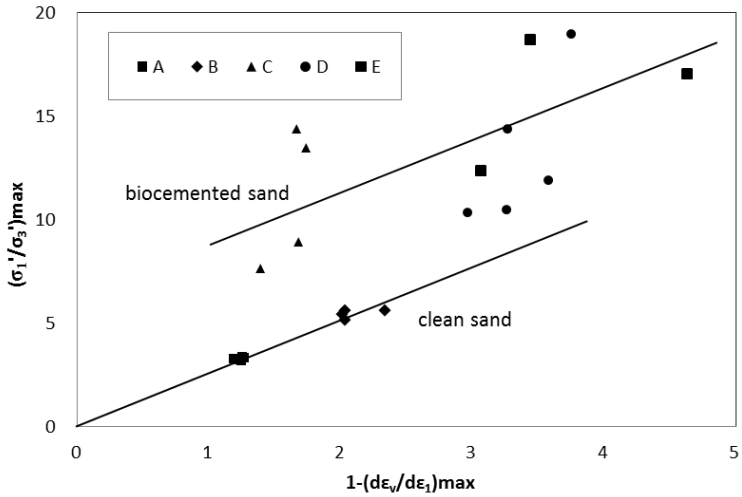

d)

Figure 7.7 a) Maximum dilatancy ($-d\varepsilon_v/d\varepsilon_1$) vs. void ratio e (upon test), b) maximum stress ratio $(q/p')_{max}$ vs. void ratio, c) maximum dilatancy vs. maximum stress ratio in the five CD test sets, and d) maximum stress ratio σ_1'/σ_3' versus ($1-d\varepsilon_v/d\varepsilon_1$) curves

7.3 Effect of calcium carbonate on UC strength and permeability of MICP treated sand

7.3.1 UC strength

A plot of unconfined compression (UC) strength versus calcite content obtained for all the tests presents in Chapters 4, 5, and 6 is shown in Fig. 7.8a. These include the test on the six cylindrical specimens presented in Chapter 4, the test on bulk-treated sand in the boxes discussed in Chapter 5, and the test on the samples from one cubic meter box in Chapter 6.

It can be seen from Fig. 7.8a that there is a positive relationship between calcite content and UC strength. The data from the small boxes had a larger scatter than the data from the column test (Chap. 4). This is indicative that the UC strength is controlled not by calcite content alone. Another reason could be due to the uniformity of the samples as the UC strength is much affected by the uniformity of the biotreatment in the UC specimen.

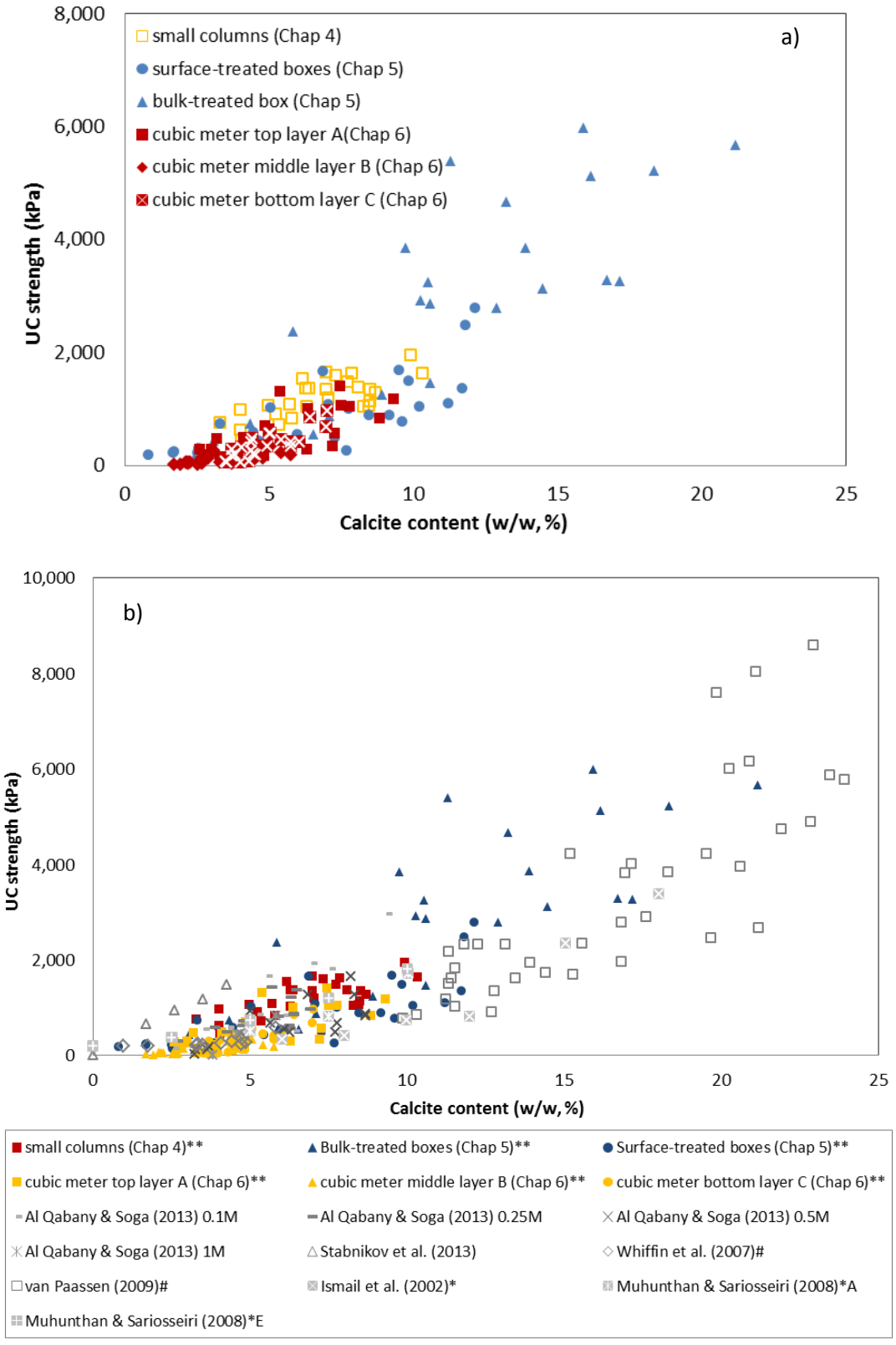

Figure 7.8 Summary of UC strength vs. calcite content: a) data getting from this study; b) data in this study vs. some data on biotreated sand by MICP and other binders in literature (**data obtained in this study; *by Portland cement; #converted from calcite content reported in kg/m^3; *A - Aberdeen soil; *E - Everett soil)

A comparison of data getting from this study with other published data obtained by other researchers (Al Qabany, et al., 2012; Al Qabany & Soga, 2013; DeJong et al., 2006; Stabnikov et al., 2013; Whiffin et al., 2007; van Paassen, 2009; van Paassen et al., 2009, 2010) are also plotted in Fig. 7.8b. There are several differences in these data: firstly, the sands tested are different. Secondly, the bio-materials used are different. For example, the UPB used in this study had lower urease activity compared with the UPB used by other researchers (0.4 to 1 mM urea/min versus 5 to 20mM urea/min in other studies). In Fig. 7.8b, one set of data on cement treated sand is also plotted for comparison. In Ismail et al. (2002), sand with D_{50} = 0.6mm (Aberdeen soil) and D_{50} = 0.02mm (Everett soil) were used. And thirdly, the chemical concentration was different. In the presented study, the concentration in Al Qabany & Soga (2013) 's test, a series chemical concentration of 0.1M, 0.25M, 0.5M and 1M were used. The calcite content data reported by Whiffin et al. (2007) and van Paassen (2009) were in the form of kg/m^3 calcium carbonate. A conversion was made to calcite content using an average bulk density of sand $1800kg/m^3$. For data presented in van Paassen (2009), conversion was made based on the maximum calcite content indicated in the paper. All the data indicate that the UC strength is controlled by the calcite content in bio-treated sand. However, the large scatter also suggests that the UC strength is also affected by other factors, for example, the uniformity of the samples. Data obtained in this study generally gained the same or higher UC strength at the same calcite content level, which confirms the efficiency of low activity UPB, applied in potential applications from small to large scale experiments.

7.3.2 Permeability

A plot of calcium content vs. permeability is shown in Fig. 7.9a, using data obtained in this study. A comparison with published data is also shown in Fig. 7.9b. In Fig. 7.9b, number "0.1M" etc. in Al Qabany & Soga (2013) refers to the chemical concentration in the cementation solution, while "RD" refers to relative density of sand sample before treatment. The calcite content data for Whiffin et al. (2007) was converted from kg/m^3 to w/w% as explained before, using an average bulk density of sand $1800kg/m^3$.

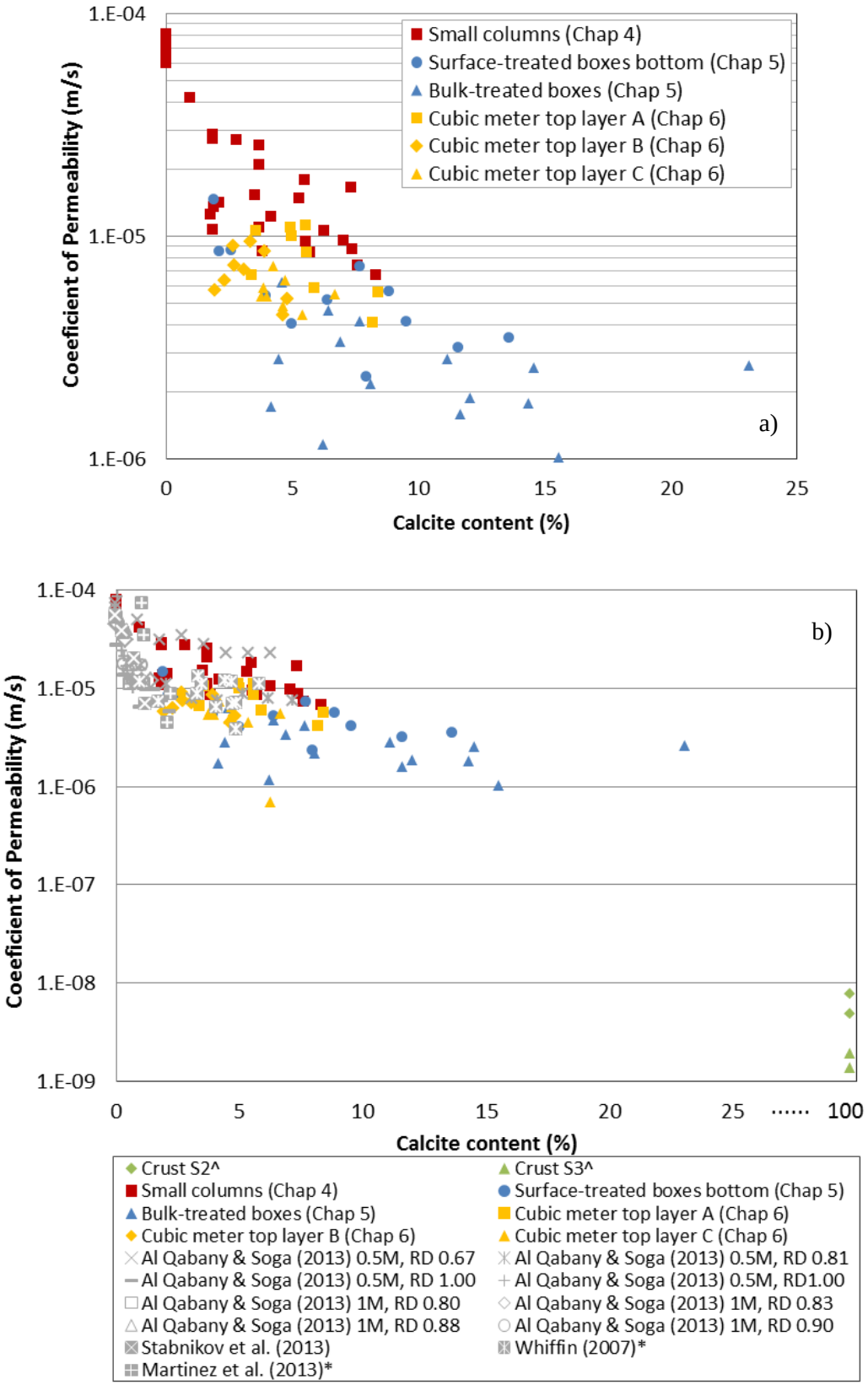

Figure 7.9 Summary of calcite content vs. permeability of a) data (getting from bulk-cemented specimens) in this study; c) data obtained in this study and sand cemented by MICP in literature (^data on crust having 100% calcite content; *converted from calcite content reported in kg/m^3)

In general, permeability reduces with increasing calcite content as more voids are filled with calcite precipitation, as shown in SEM photo presented in Fig. 5.13, Section 5.4.1. Data from this study show a consistent trend with the published data. Higher permeability is usually preferred for the MICP process for strength improvement, because clogging the near injection points will cause the permeability around this area to reduce and make the distribution of bacteria and cementation solution into other area difficult.

Biocemented sand with lower permeability could also be achieved by bioclogging through surface cementation method, as described in Section 5.3. Coefficient of permeability of surface crust in sand box S2 and S3, as described in Section 5.3.2, are also dawn in Fig. 7.9b. Thicknesses of these crusts formed are 2-3mm and 5-7mm respectively. It can be observed that a 2 to 3mm calcite crust is sufficient to reduce the coefficient of permeability from 10^{-4} to 10^{-8}m/s.

7.4 Conclusions

The effects of biocementation on the shear strength, stress-strain and permeability behavior of MICP treated sands were studied. The main conclusions are summarized as follows:

Triaxial CD tests were carried out on pure sand samples and sand treated using the MICP method. CD tests on biotreated samples show a higher effective stress failure envelope than that obtained from the CD tests on pure sand. Different failure envelopes are resulted on samples with different $CaCO_3$ contents. Within the tested stress range, these failure lines appear to be straight and parallel with each other. The higher the $CaCO_3$ content, the higher the friction angle. In other words, the failure envelopes moved upward with increased calcite content. These observations reveal that the effect of biocementation contributes mainly to the increase of cohesion. Similar observation has been reported for sand treated using cement grout.

The relationship between the maximum dilatancy versus void ratio obtained from CD tests on both cemented and pure sand specimens are more or less the same. However, the maximum stress ratio versus dilatancy relationship for cement sand

is different from that for non-cemented sand. The maximum stress ratios of the cemented sand are higher than that for pure sand. As the amount of dilatancy for both cemented and pure sand is about the same, the increase in the mobilized stress ratio is a result of biocementation.

.

Chapter 8

Biocementation of Fine-Grained Soil

8.1 Introduction

Several studies have been conducted on MICP application to sand and patents on soil biocementation have been obtained in Australia, European Union, and USA. So far, the applications have been constrained to granular soil only (DeJong et al., 2009; 2013; van Paassen et al., 2009; den Harmer et al. 2009). However, there are few studies made on fine-grained soil such as clay or other low permeability type of soil. This could be because the particle and pore sizes of fine-grained soil are small so the microorganisms are relatively difficult to penetrate and survive.

The feasibility of using biocementation to improve the mechanical properties of fine-grained soils is explored in this chapter. The materials tested include kaolin, bentonite and marine clay. Effectiveness of biocementation on fine-grained soil through the MICP process and the possible related chemical effect are evaluated. A new methodology namely bio-encapsulation conducted by clay is also assessed.

8.2 Biocementation of kaolin

Kaolin is a material commonly used to study the engineering properties of clay as described in Section 3.4.2. It was employed in this study as its mechanical behaviour has been well understood. Experiments including unconfined compression (UC) test, isotropic consolidated drained (CID) tests, direct simple

shear (DSS) tests, oedometer tests and consolidated undrained (CU) tests were conducted on microbially treated kaolin samples as well as the control samples.

8.2.1 Urease activity in kaolin suspension

In order to find out whether the MICP approach will be effective for clayey soil, set of experiments was conducted using UPB mediated MICP for kaolin suspension. The bio-reagents were selected in such a way that 7.4g of $CaCO_3$ could be produced through the MICP process theoretically per 10g of soil. The water content of the samples was set to be 1000% (10g kaolin in 100g water) for ease of operation. Two $CaCl_2$ to urea ratios 1:1 and 1:2 were tested, as shown in Table 8.1. The resulted urease activity of UPB and the pH value variation with time in the suspension is shown in Fig. 8.1a and 8.1b respectively.

Table 8.1 Setup of UPB activity and pH changes in clay particle suspension

Test	kaolin	DI water	UPB	$CaCl_2$	Urea	ratio
1	10g	85ml	15ml	8.2g	9g	1:2
2	10g	85ml	15ml	8.2g	4.5g	1:1

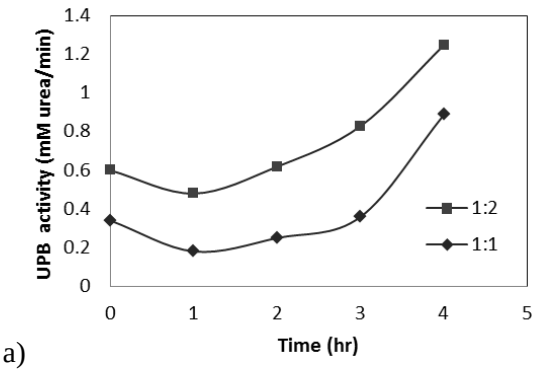

a)

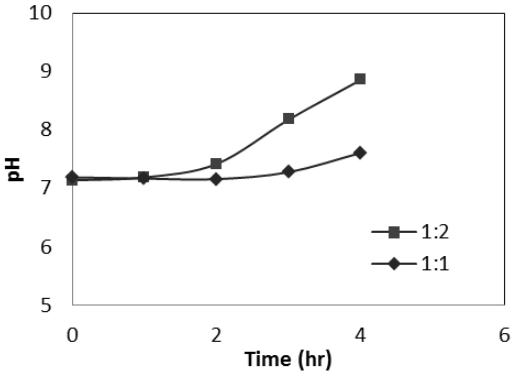

b)

Figure 8.1 Dynamics of a) urease activity of UPB; b) pH value in kaolin suspension

Fig. 8.1 shows that the urease activity increases with time in both sets. The pH value also increases. Ca^{2+} to urea ratio of 1:2 (set 1) is better for MICP in terms of urease activity of bacteria and pH values.

8.2.2 Sample preparation procedure and water content measurement

A major problem with the use of biotreatment for clay is that the pore spaces of clay particles are too small for bacteria (Mitchell & Santamarina, 2005). Thus, the method adopted to prepare the sample can affect the behaviour of the soil samples prepared. For sand, the percolation method has been adopted to deliver bacteria and other chemical reagents. However, this method was not applicable to clay for its low conductivity.

The sample preparation method by kneading adopted in this study for fine-grained soil is as follows. As shown in Fig. 8.2, this method involves layer by layer hand mixing. A small portion of kaolin with 50% water content was taped into a thin layer by a small faced hammer. Powdered chemicals $CaCl_2$ and urea was then sprinkled on top of the kaolin surface, followed by 3-4ml of UPB suspension. Another portion of kaolin was then put on top and tapped into a thin layer again. This step was repeated until the soil and the predetermined amount of chemical/UPB had been used up. This "lasagne" shaped sample was cut in the middle; half of the sample was put on top of the other and tapped into thinner layer. The last step was repeated for 4 to 5 times. The main purpose of this mixing method is to expose as much contact surface between clay particles, bacteria and chemical powders as possible to form possible bridges between clay particles.

After mixing, the mixed soil was put in to cylindrical moulds of 50 mm diameter and 100 mm height, with plastic sheets wrapped on the inside wall of the mould for formation of UC and triaxial tests samples. The samples after preparation were stored in a moisture controlled room under 25°C temperature for one to two days for curing.

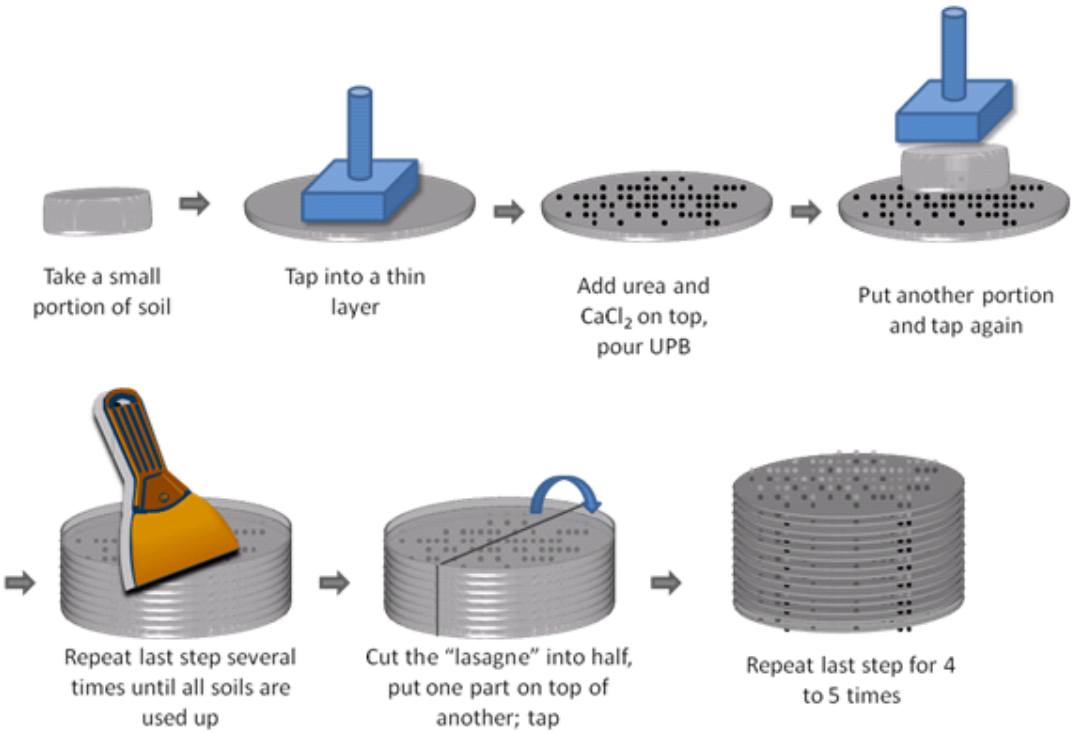

Figure 8.2 Mixing steps of clay with low water content and biocementation solutions/suspension

Values of water content determined for the soil samples mixed with chemicals were modified by the weight of chemicals added. During the measuring of soil properties as strengths or Atterberg limits, the chemicals were dissolved into the solution in liquid form. However, after the evaporation of the water during water content measurement, the chemicals were deposited into solid form and mixed with soil. Therefore, the weight measured after evaporation consists of two parts: the original weight of the soil and the added weight of chemical deposits. Consequently, the water content shall be adjusted based on the original weight of the soil.

The rationale behind this analysis can be demonstrated with a simple illustration. For example, when testing the UC strength of a soil specimen containing 100g of dry soil, 20g of chemicals and 60g of water, the actual water content should be 60g/100g × 100% = 60%, while the chemicals are presented in liquid form. However, while measuring the water content by drying sample in 105°C oven, the chemicals are deposited into solid form and become inseparable with the soil. In this case, the water content determined based on the weight directly measured would be 60g/(100g+20g) = 50%, which is mistaken since the chemicals' weight

should not be taken into account. Therefore, in this chapter the water contents of the chemical-mixed soil samples are modified with their chemical contents.

Theoretically the weight of the bacteria added into some samples also leads to such issue. However, since the amount of dry bacteria added is insignificant (usually less than 0.5g per 100g soil), the influence brought by it is deemed as negligible and thus omitted.

8.2.3 UC strength curves for kaolin treated with and without UPB

UC strength tests were carried out initially to study the effect of MICP in clayey soil. A comparison of two UC tests, one on kaolin sample treated with UPB and bio reagent, and another on control sample containing $CaCl_2$ and urea only, is made in Fig. 8.3. The specimens were prepared by the kneading method as described in Section 8.2.2. More information on the two specimens is listed in Table 8.2. The quantities of chemicals added were determined to achieve 0.75mol/L $CaCl_2$ and 1.5mol/L urea. The two tests were conducted under the same condition, except that UPB was used for Test 2, but not for Test 1. The effect of UPB can be seen clearly by the comparison between the two stress strain curves in Fig. 8.3. The shear strength was increased by more than two folds (from 30 kPa to 70 kPa plus) for the specimens with UPB added. The stiffness also increased. This observation is consistent with the result reported by Ng et al. (2014), in which UC strength increased up to two times after MICP treatment compared to the untreated specimen.

Table 8.2 Detailed information of the specimens prepared for UC tests

Test	Kaolin (g)	$CaCl_2$ (g)	Urea (g)	Original UPB suspension (ml)	w/c prepared (%)	w/c upon test (%)	Void Ratio	S_u (kPa)
1	200	7.5	8.1	-	45	44.84	1.09	28.9
2	200	7.5	8.1	15	45	44.68	1.05	73.7

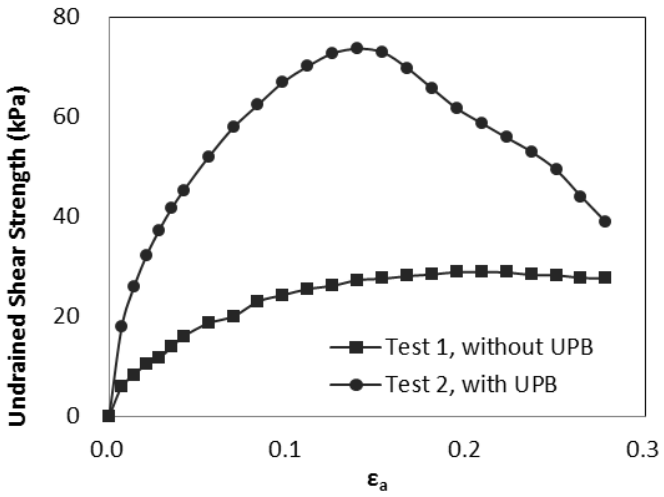

Figure 8.3 Result of UC strength tests for trial batch on biocement-treated kaolin

8.2.4 Isotropic consolidated drained (CID) triaxial tests on kaolin

To study the effect of microbial-treatment on drained shear strength of soil, several sets of triaxial CID tests were conducted on biotreated kaolin samples under effective consolidation stress of 50, 100, 200 and 300 kPa respectively. A control group of tests were also carried out on specimens mixed with 0.75M $CaCl_2$ plus 1.5M urea only. Detailed information of the two groups is summarized in Table 8.3.

Table 8.3 Summary of clay specimens' properties conducting CID tests

Test	Condolidation pressure σ_3' (kPa)	Peak q (kPa)	Kaolin (g)	$CaCl_2$ (g)	Urea (g)	UPB suspension (ml/100g soil)	Intial void ratio	Water content upon test (%)
1a	50	49.1	200	8.3	9	-	1.34	45.98
1b	100	163.6	200	8.3	9	-	1.49	51.87
1c	200	301.1	200	8.3	9	-	1.43	49.22
1d	300	392.4	200	8.3	9	-	1.43	49.13
2a	50	97.4	200	8.3	9	20	1.52	55.36
2b	100	202.1	200	8.3	9	20	1.25	46.80
2c	200	330.2	200	8.3	9	20	1.51	54.30
2d	300	479.1	200	8.3	9	20	1.46	53.52

Soil samples were also prepared employing the kneading method described in Section 8.2.2. Similarly, samples were taken out of the 50 mm diameter moulds and trimmed into triaxial cylindrical specimens of 38 mm in diameter and 76 mm

in height. The reason for using a smaller diameter samples was to remove large voids that might form on the surface the sample due to trips of air bubbles between the soil and the moulds. Strips of filter paper were used for drainage as shown in Fig. 8.4. All the tests were conducted until 20% axial strain.

Figure 8.4 Images of specimen 2a: a) before conducting CID test, and b) after failure

The q vs. ε_1 curves obtained from CID tests on both the UPB added group and control group are plotted in Fig. 8.5a. A higher shear strength is observed in the tests on speicmen treated with bacteria under the same consolication pressure as compared with the tests on the control specimens which were mixed with chemicals only. The ε_v vs. ε_1 curves for both groups of tests are in Fig. 8.5b. The samples from both groups are in compression indicating a normally consolidated behaviour. The effective stress paths and failure envelopes obtained from both groups are shown in Fig. 8.5c. It can be seen that bacteria treated sets resulted in a higher failure envelope. As the volumetric behavior is similar (Fig. 8.5b), the higher shear strength is likely a result of the microbial-mediation effect.

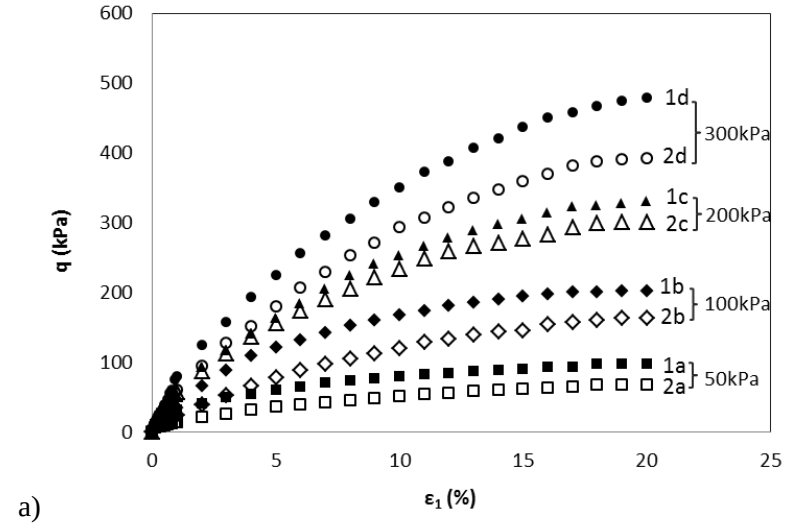

a)

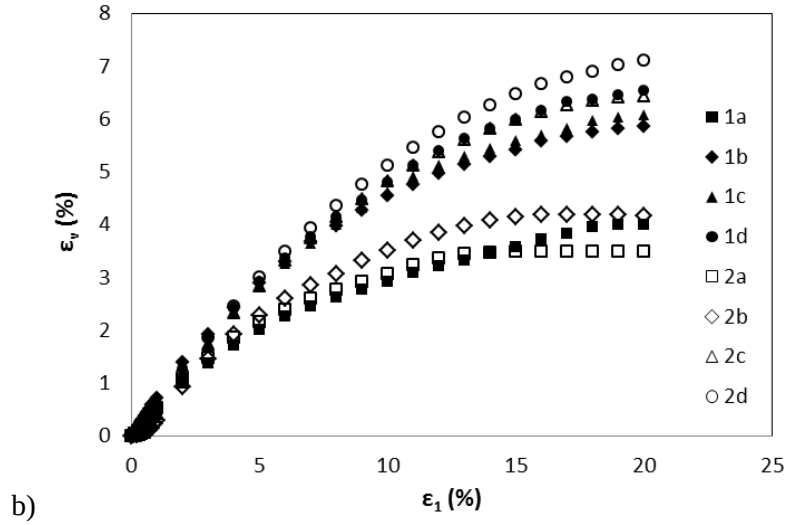

b)

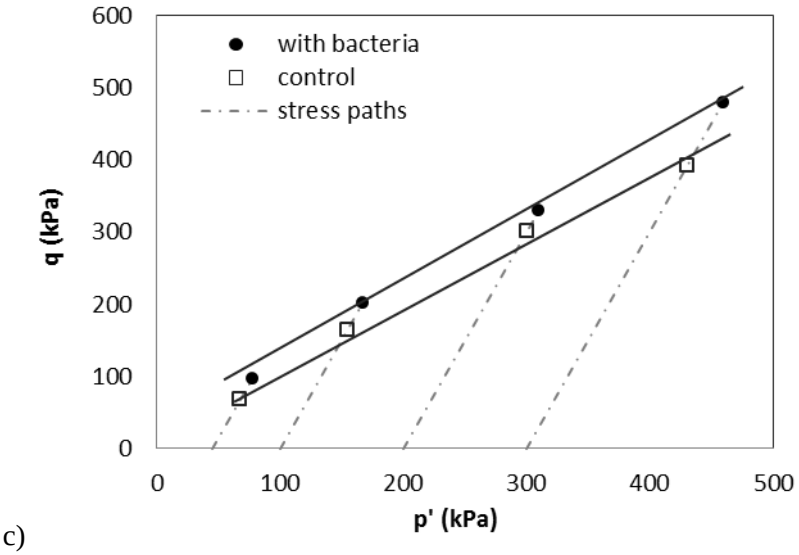

c)

Figure 8.5 The results of isotropic consolidated drained tests on biocemented clay, a) q vs. ε_1; b)ε_1 vs. ε_v; and c) q vs. p

8.2.5 Direct simple shear (DSS) tests on kaolin

Direct simple shear (DSS) tests on kaolin samples treated with UPB and bio reagent, and samples in the control group containing $CaCl_2$ and urea only were conducted under consolidation stresses of 100, 200 and 300 kPa respectively. The DSS samples were prepared using the method described in Section 8.2.2, except that sample for the DSS tests were prepared in bulk, wrapped with plastic sheets for curing overnight, then cut into cylindrical disks with 70 mm in diameter and 20 mm in height using a cutter. The testing procedure adopted was described in Section 3.5.5. The specimen properties are shown in Table 8.4. Shear stress (τ) vs. strain curves, normal stress (σ) vs. strain curves, and σ vs. τ curves are shown in Fig. 8.6a, 8.6b, and 8.6c respectively.

Table 8.4 Summary of clay specimens' properties conducting DSS tests

Test	Consolidation pressure (kPa)	Maximum τ (kPa)	$CaCl_2$ (M)	Urea (M)	UPB suspension (ml/100g soil)	Intial void ratio	w/c pre-test (%)
1a	100	27.5	0.75	1.5	-	1.37	54.42
1b	200	44.4	0.75	1.5	-	1.39	53.46
1c	300	60.4	0.75	1.5	-	1.36	53.36
2a	100	34.1	0.75	1.5	20	1.32	51.18
2b	200	55.9	0.75	1.5	20	1.34	50.45
2c	300	68.7	0.75	1.5	20	1.27	47.44

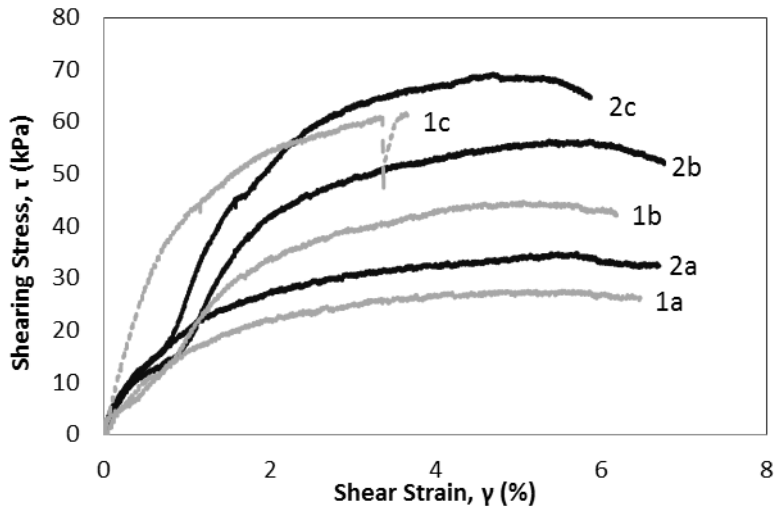

a)

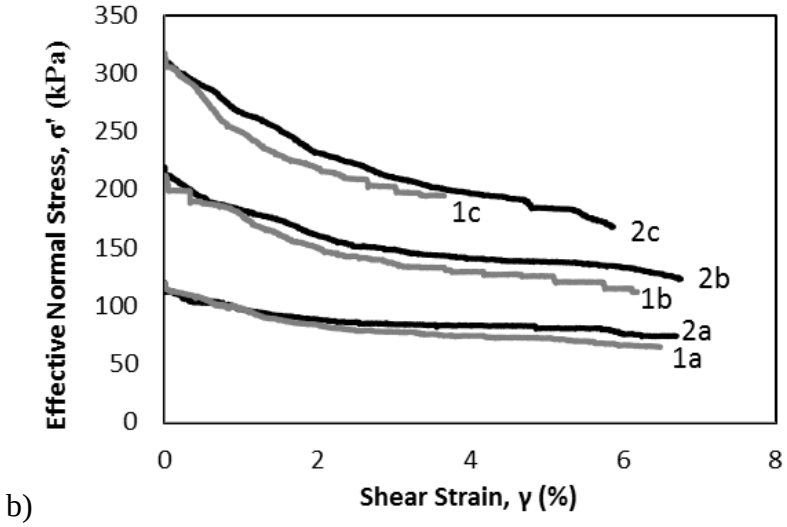

b)

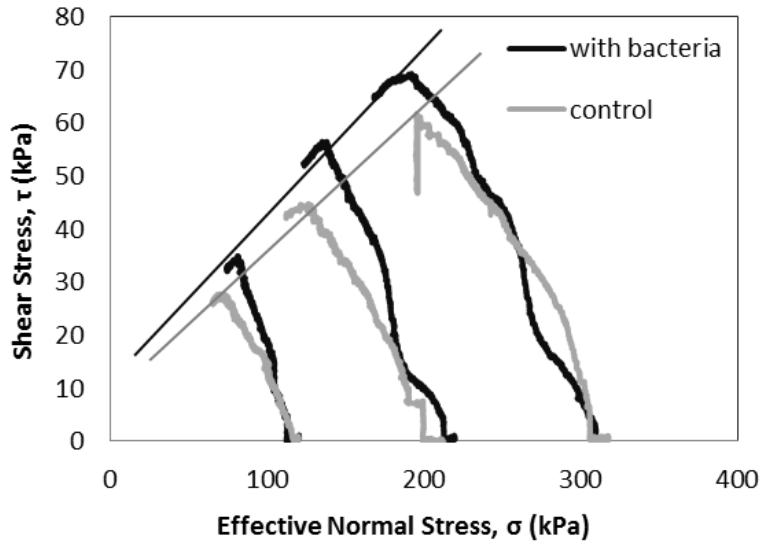

c)

Figure 8.6 The results of DSS tests on biocemented kaolin/control; a) Shear stress (τ) vs. strain, b) normal stress (σ) vs. strain, c) σ vs. τ

The stress-strain curves of the bacteria treated samples reached a higher peak with some strain softening after the peak, as shown in Fig. 8.6a. The changes in σ_n' during shearing are shown in Fig. 8.6b. As this is an undrained test and the total σ_n is maintained constant, the change in the effective vertical stress is also the change in pore water pressure (Chu et al., 1999; Chu et al., 2003; Meng, 2010). A decrease in σ_n' implies an increase in pore water pressure, which in turn indicates normally consolidated (NC) behavior (Meng, 2010). This is also consistent with the effective stress paths showing in Fig. 8.6c which bent to the left.

8.2.6 Oedometer tests

Two oedometer tests were conducted and the e vs. log σ_v' curves are plotted in Fig. 8.7. The method for oedometer test has been described in Section 3.5.6. The specimens for the oedometer tests were prepared using a method similar to that for the DSS tests, as described in Section 8.2.5. A summary of the test conditions for the oedometer tests is given in Table 8.5. The biotreated soil seems to have a lower compressibility, as shown in Fig. 8.7; the compression indexes C_c are calculated to be roughly 0.17 and 0.15 for control and bacteria mixed specimen respectively. The preconsolidation stresses σ_p' determined form the two tests are 86 and 100 kPa for the control and bacteria treated specimens respectively. The σ_p' value for both groups might be partially caused by the mixing process.

Table 8.5 Summary of clay specimens' properties conducting oedometer tests

Test	$CaCl_2$ (M)	Urea (M)	UPB suspension (ml/100g soil)	Intial void ratio	Final void ratio	w/c pre-test (%)
1	0.75	1.5	-	0.56	0.29	48.50
2	0.75	1.5	20	0.56	0.32	49.30

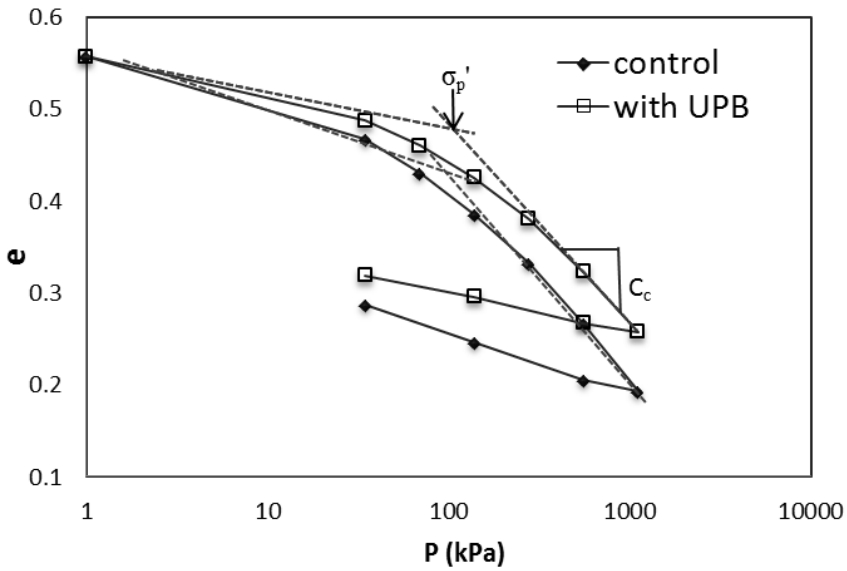

Figure 8.7 Result of oedometer tests on biocemented clay and control

8.2.7 K_0 consolidated undrained (CK_0U) triaxial tests

Several sets of K_0-consolidated undrained (CK_0U) tests using a triaxial machine were conducted on kaolin. The sample preparation method used is the same as that described in Section 8.2.2. However, on contrary to the chemical added control specimens in previous experiments, pure kaolin was used for the control group, as shown in Table 8.6. For specimens in the control set, kaolin was mixed with distilled water to reach 50% of water content. The soil was then put into cylindrical moulds and placed into moisture room for one to two days for curing.

The samples were trimmed into cylindrical specimens of 38mm diameter and 76mm height for triaxial testing. The specimens were consolidated along a K_0 path to vertical stresses of 50 kPa, 100 kPa, and 200 kPa respectively. The procedure for conducting CK_0U tests was described in Section 3.5.2.

Table 8.6 Summary of clay specimens' properties conducting CU tests

Test	Condolidation pressure σ_3' (kPa)	Maximum q (kPa)	$CaCl_2$ (M)	Urea (M)	UPB suspension (ml/100g soil)	Intial void ratio	Water content upon test (%)
1a	50	72.5	-	-	-	1.31	49.36
1b	100	106.6	-	-	-	1.36	49.98
1c	200	171.2	-	-	-	1.42	52.69
2a	50	53.2	0.75	1.5	20	1.31	47.93
2b	100	135.5	0.75	1.5	20	1.35	49.32
2c	200	163.2	0.75	1.5	20	1.48	51.20

The q versus ε_a, excess pore water pressure Δu versus ε_a curves, and q vs. p' curves are shown in Fig. 8.8a, 8.8b and 8.8c respectively. The effective stress paths during K_0 consolidation are also plotted in Fig. 8.8c. As shown in Fig. 8.8b, the PWP decreased after the initial increasing, demonstrating a dilating behaviour as typically observed in over-consolidated clayey soil. Both sets of tests appear to approach similar failure envelope with bacteria treated set only slightly higher, as shown in Fig. 8.8c. This observation is different from the test results of UC and CID tests, where the bacteria treated soil shows a higher strength peak and higher effective failure envelope respectively.

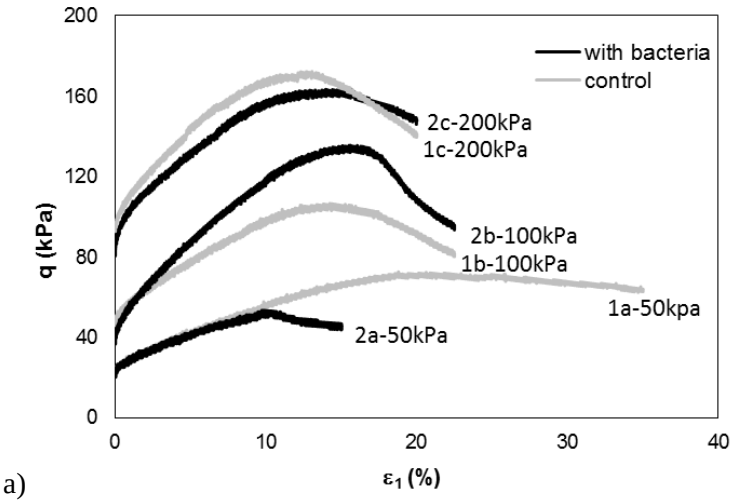

a)

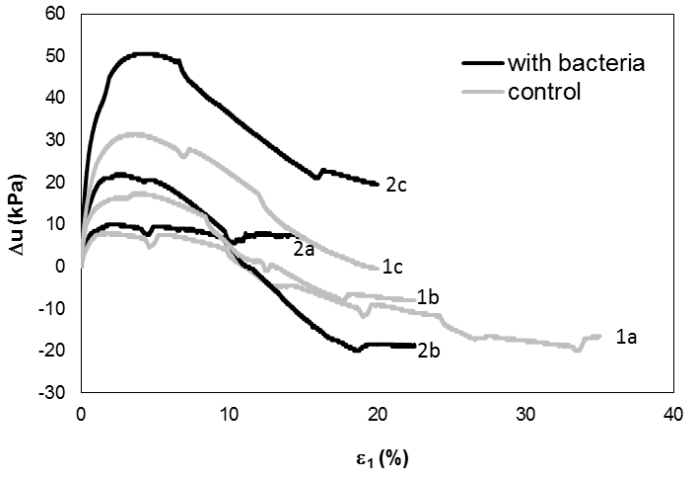

b)

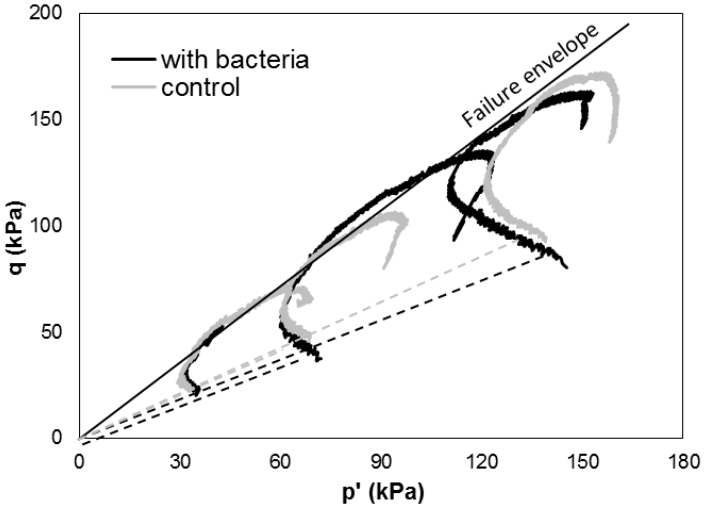

c)

Figure 8.8 Curves of a) q vs. ε_1, b) excess pore water pressure Δu changes q vs. ε_1, and c) stress paths during shearing in k_0-CU test conducted by bacteria added kaolin and control

Note that the samples used in the control groups are different. The samples in the UC and CID tests were mixed with chemicals $CaCl_2$ and urea, whereas the samples

in CK_0U tests were pure kaolin. The effective failure envelopes obtained from these two sets of tests are plotted together in Fig. 8.9. Failure envelopes for the UPB mixed samples getting from the two tests (presented in red) are consistent with each other, which is similar yet slightly higher than it of the pure kaolin (presented in blue). A lower failure envelope was obtained for kaolin mixed with $CaCl_2$ and urea set, which is shown as yellow line in Fig. 8.9. The difference in the effective failure envelope may be due to the chemical effects. For this reason, some studies on the influence of chemicals on the behaviour of kaolin were also carried out.

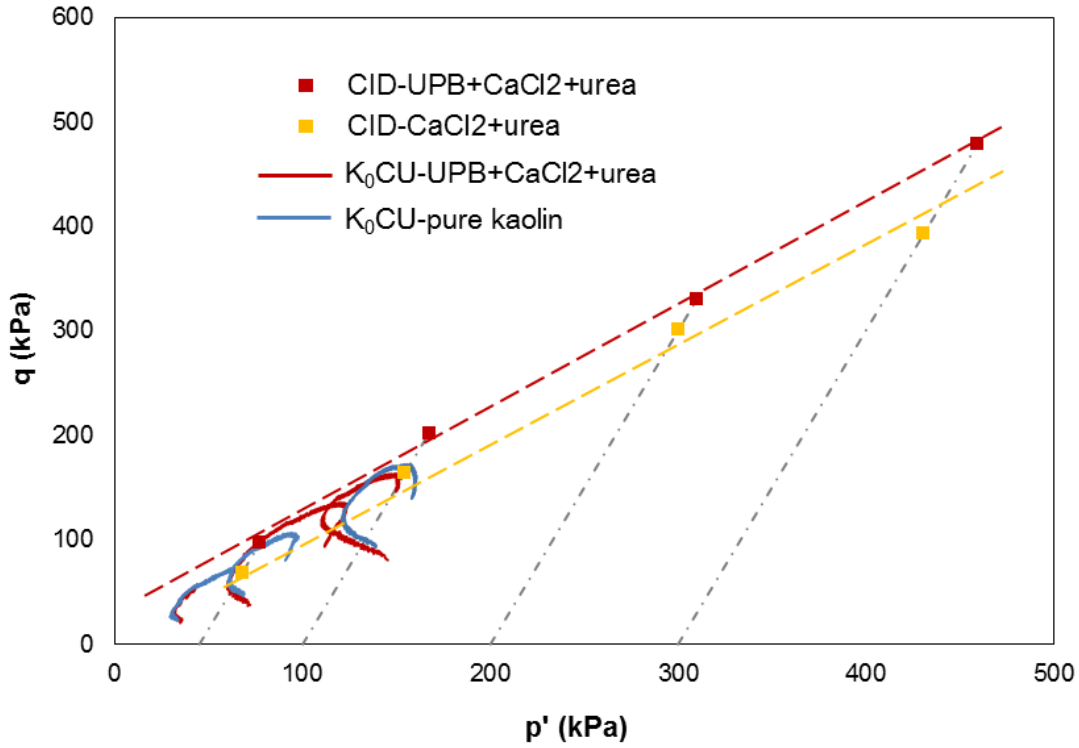

Figure 8.9 Effective failure envelopes of kaolin mixed with UPB plus chemicals, chemicals only, and pure kaolin obtained in CID and K_0CU tests

8.2.8 Atterberg limits variation of kaolin mixed with chemicals and UPB

It is well known that Atterberg limits, in particular liquid limit (LL) indicates the water holding capacity of clay minerals. With the use of chemicals or microbial treatment, the soil strength may have changed. This may lead to a change in the Atterberg limits of soil.

Atterberg limits of kaolin mixed with different amount of chemicals, including LL,

plastic limit (PL) and plasticity index (PI), were measured following BS 1377-2 (British Standards Institution, 1990), which employed the cone penetration and kneading method respectively. A summary of the tests is given in Table 8.7 and the results are shown in Fig. 8.10a, 8.10b and 8.10c respectively. Specimens mixed with 0.5, 1, and 2 times of applied chemical dosage in biocementation by MICP in sand were tested, which are 0.375, 0.75 and 1.5M for $CaCl_2$ and 0.75, 1.5 and 3M for urea. Samples just use pure kaolin and with 0.75M $CaCl_2$ plus 1.5M urea are also shown in the figure.

Table 8.7 Atterberg limits, including liquid limit (LL), plastic limit (PL), and plasticity index of chemicals $CaCl_2$/urea mixed kaolin

Test	$CaCl_2$ (mol/L)	Urea (mol/L)	UPB (ml/100g soil)	LL (%)	PL (%)	Plasicity Index (%)	Remarks
1	0	0	-	91.0	48.2	42.8	pure kaolin
2	0.75	1.5	-	69.7	39.9	29.8	with both chemicals
3	0.75	1.5	15	73.3	47.8	25.6	with chemicals+UPB
4	0.375	0	-	70.9	44.1	26.8	with $CaCl_2$ only
5	0.75	0	-	69.5	43.6	26.0	
6	1.5	0	-	66.0	40.1	25.9	
7	0	0.75	-	84.3	48.7	35.6	with urea only
8	0	1.5	-	82.8	46.0	36.8	
9	0	3	-	79.3	46.1	33.2	

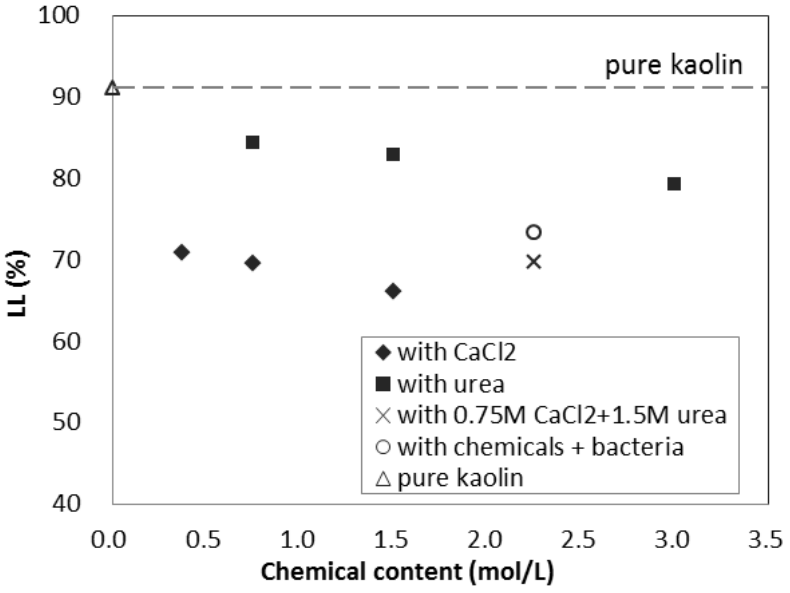

a)

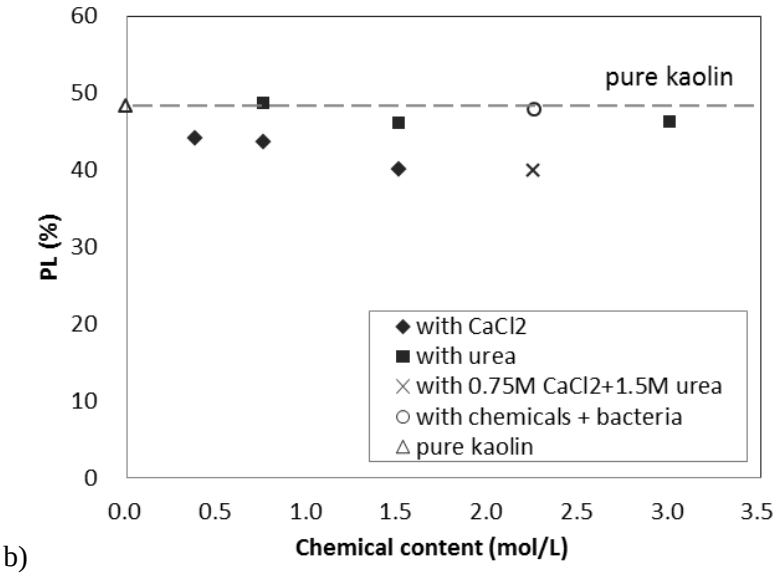

b)

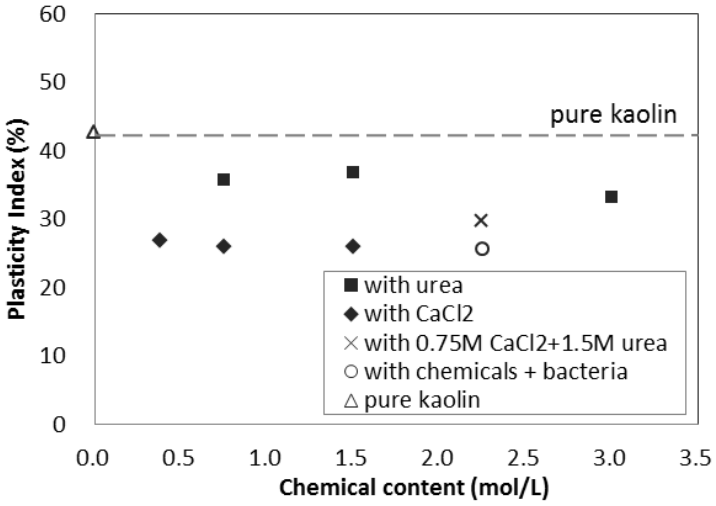

c)

Figure 8.10 Atterberg limits of kaolin mixed with different amount of chemicals; a) liquid limits, b) plastic limits, and c) plasticity indices

As observed in Fig. 8.10, the plasticity properties of kaolin, especially the values of LL were altered by the addition of $CaCl_2$ or urea. Both liquid and plastic limits were decreased with increasing degree of chemicals. As shown in Fig. 8.10a, LL of kaolin reduced from 91% to 79% and 66% when 3M urea and 1.5M $CaCl_2$ was added respectively. Similarly, the PI value reduced from 43% to 33% and 26% with the addition of 3M urea and 1.5M $CaCl_2$ respectively (Fig. 8.10b).

The drop of LL and PL in kaolin with the increasing usage of $CaCl_2$ might be attributed to the fact that adding Ca^{2+} cation increased the pore fluid electrolyte concentration and thus reduced the thickness of double layer around clay particles; i.e. clay particles became more flocculated rather than dispersed, which allows

higher proportion of water to exist in the form of pore water rather than absorbed water. Such observation was also made in Heeralal at al. (2012). For soil mixed with urea, a similar trend of LL decreasing with urea content is observed, although the effect was not as big as $CaCl_2$. Values of PL did not change much by the urea added.

As $CaCl_2$ contributed the major part in such Atterberg limits lowering effect, soil mixed with 0.75M $CaCl_2$ and 1.5M urea (Test 2) resulted in similar LL and PL values (69.7% and 39.9% respectively) with it mixed with 0.75M $CaCl_2$ (Test 5) (69.5% and 43.6% respectively), as expected. Noted the added UPB increased both LL and PL values in Test 3 to 73.3% and 47.8% respectively, comparing to the values in chemical only sample in Test 2.

8.3 Potential MICP application on dredged clayey material

Increasing land supply through land reclamation has been an important aspect in sustaining the economic development in lowland area like Singapore. A major problem in land reclamation at the present is the shortage of granular fill material. One way to overcome this problem is to use other non-granular materials such as industrial wastes, excavated soil, or clayey soil dredged from sea for reclamation. However, the dredged clay is always soft and has to be treated before it can be used for reclamation. Experiments to verify the possibility of applying MICP in treating the dredged clayey material were also conducted.

8.3.1 UC Strength of MICP treated kaolin

To simulate the process for dredged material treatment, a different sample preparation method was adopted. Kaolin powder was mixed with distilled water pre-dissolving different amount of chemicals and/or UPB. The initial water content in each sample during mixing was all set to be 100%, to simulate the freshly dredged marine clay. The mixed slurry was then poured into cylindrical moulds of 38*76mm and put into 40°C oven for curing, and also for accelerating the drying process. UC strength of each specimen was measured at various levels of water content, achieved by different period of curing.

Kaolin samples mixed with 0.375/0.75/1.5M of $CaCl_2$, 0.75/1.5/3M of urea, 0.75M $CaCl_2$ plus 1.5M urea, 0.75M $CaCl_2$ plus 1.5M urea with original/centrifuged UPB suspension, and also pure distilled and deionized (DI) water were prepared and tested. The results of UC strengths versus water contents of all sets are summarized in Fig. 8.11. Detailed information of each specimen is presented in Appendix F.

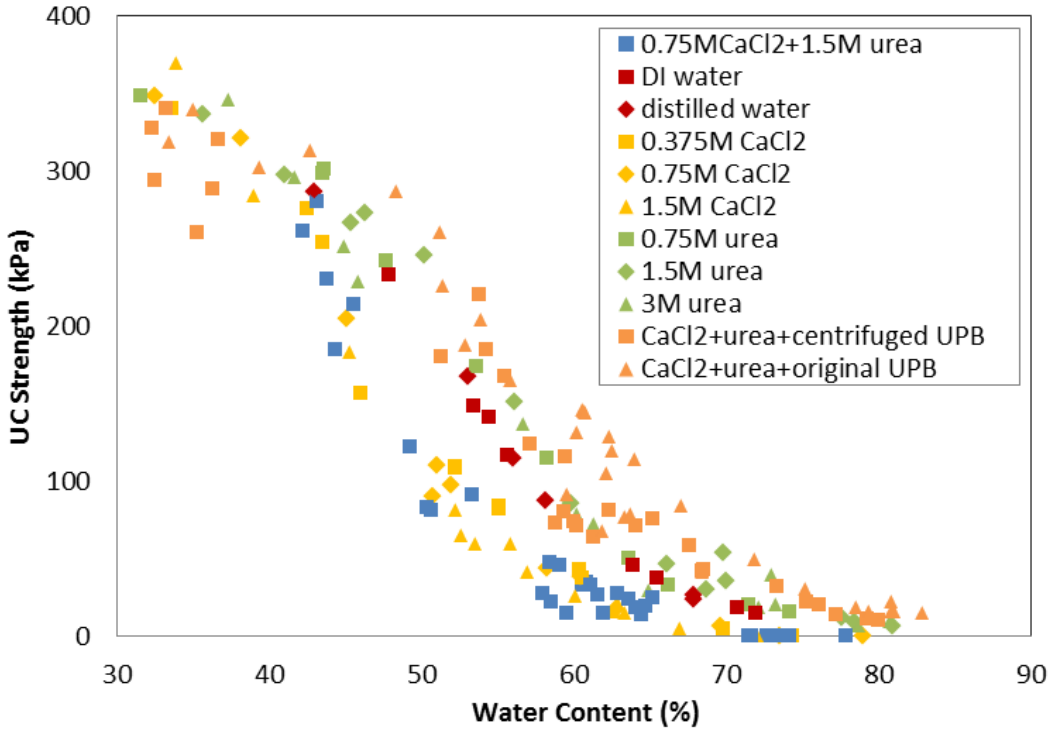

Figure 8.11 UC Strength vs. water content curves of UPB treated kaolin group and different control group

The three sets of pure kaolin mixed with DI/distilled water, kaolin mixed with $CaCl_2$ and urea, and kaolin with both chemicals and UPB are selected and plotted in Fig. 8.12, to present the effect of UPB and chemicals in clayey soil more clear. It can be observed that lowest UC strengths were measured for specimens mixed with 0.75M $CaCl_2$ and 1.5M urea with the same water content. The bacteria set gained the highest UC strength under the same water content level, which is slightly higher than the results of pure kaolin. The greatest improvement on UC strength after biotreatment was observed from a range of water content 60% to 70%, amounting to around 250% of the value obtained in pure kaolin.

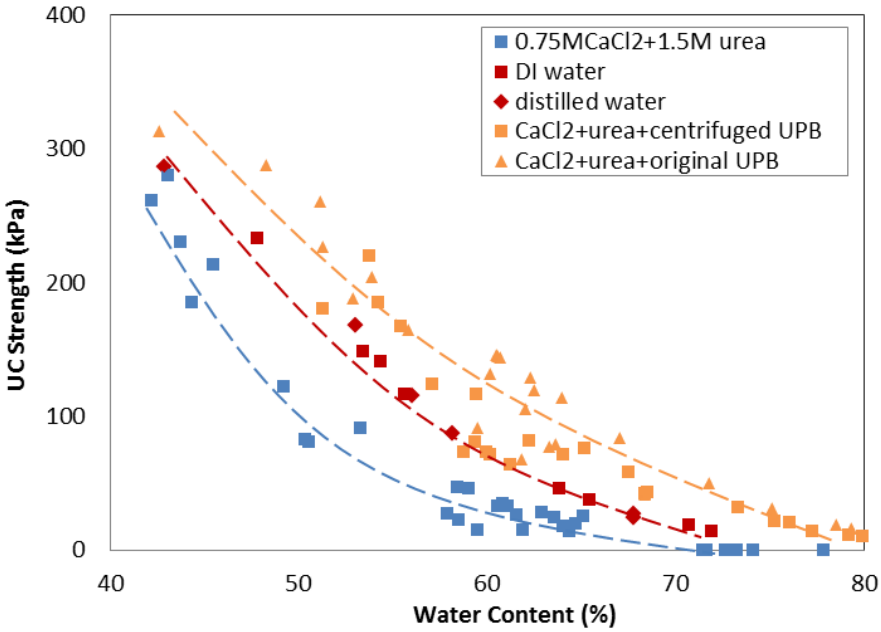

Figure 8.12 UC Strength vs. water content curves of pure kaolin with DI/distilled water, kaolin mixed with $CaCl_2$ and urea, and kaolin with both chemicals and UPB

Such observation is consistent with which made from the tests presented in Section 8.2. In the UC tests, CID tests, DSS tests and oedometer tests using specimens prepared by kneading method (which presented in Section 8.2.3, 8.2.4, 8.2.5 and 8.2.6 respectively), the UPB mixed sets showed higher failure envelopes and less compressibility compared to the sets mixed with $CaCl_2$ and urea only. On the other hand, in the K_0-consolidated CU test described in Section 8.2.7, the differences between failure envelopes getting from the pure kaolin set and UPB mixed set were not much. It might be concluded that introducing MICP in clayey soil does show improvement regarding to the strength of clayey soil. However, as addition of the cementation chemicals $CaCl_2$ and urea reduces the strengths in the meantime, the improvement made by MICP is not prominent while comparing to pure kaolin.

Results getting from kaolin samples mixed with 0.375/0.75/1.5M of $CaCl_2$, 0.75/1.5/3M of urea, 0.75M $CaCl_2$ plus 1.5M urea, and pure distilled and deionized (DI) water are plotted together in Fig. 8.13, to evaluate the source of strength reduction effect by the chemicals. As shown in Fig. 8.13, kaolin mixed with different amount of urea resulted in similar UC strength with pure kaolin under the same water content level, which indicates that the addition of urea does not vary the strength much. On the other hand, UC strengths of specimens mixed with

$CaCl_2$ are similar with those mixed with both $CaCl_2$ and urea. Both of them are lower than the values of pure kaolin sets and urea-mixed sets.

It may then be conclude that such strength reduction effect caused by the addition of cementation chemicals all came from $CaCl_2$, not urea. One explanation of this strength reduction effect caused by $CaCl_2$ could be similar to what caused the decrease of liquid limit. As explained in Section 8.2.8, adding Ca^{2+} cation increased the pore fluid electrolyte concentration and thus reduced the thickness of double layer around clay particles. Clay particles became more flocculated rather than dispersed, which allows higher proportion of water to exist in the form of pore water rather than absorbed water. Under the same water content level, the higher portion of pore water could lead to lower strength of clay.

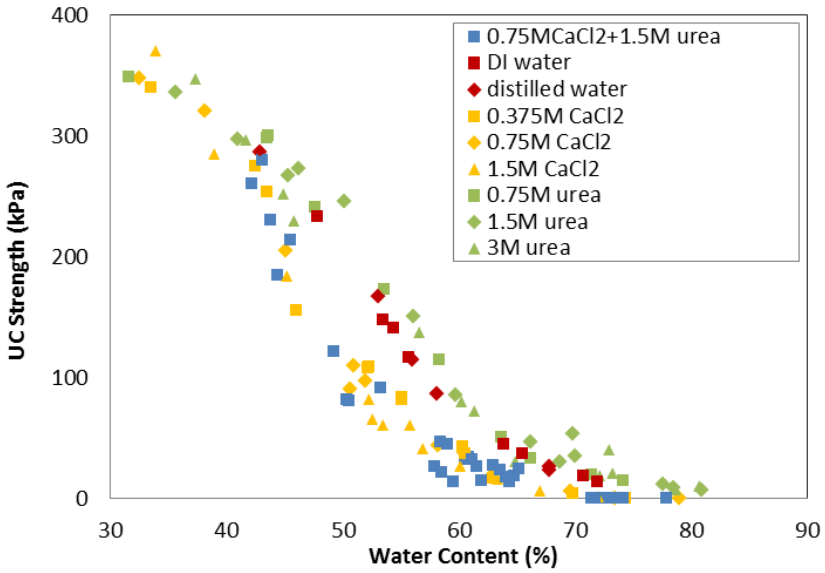

Figure 8.13 Strength vs. water content of kaolin specimens mixed with different amount of chemicals

Part of the specimens containing similar water content (56%±4%) is selected to evaluate the relationship between the dry unit weight and UC strength. The detailed information of these specimens are summarize in Table 8.8. Water content vs. UC strength and dry unit weight are plotted in Fig. 8.14a and 8.14b respectively. The water content vs. UC strength relationship as shown in Fig. 8.14a is similar to what present in Fig. 8.12. As shown in Fig. 8.14b, UC strengths increase with increase of the dry unit weight of specimens in all sets. With same dry unit weight, specimens mixed with UPB have higher UC strengths, followed

by pure kaolin. Soil mixed with $CaCl_2$ and urea gained the lowest UC strength with the same dry unit weight.

Table 8.8 Summary of chemical/UPB mixed kaolin specimens properties with water content of 56%±4%

Test	$CaCl_2$ (mol/L)	urea (mol/L)	UPB (ml)	Curing Time (hr)	Average water content (%)	UC Strength (kPa)	ρ_d (Mg/m^3)	Initial void ratio	DOS (%)	Remarks
A1	-	-	-	92.0	56.0	115.0	1.05	1.48	98.5	pure kaolin with distilled water
A2	-	-	-	100.0	53.0	167.6	1.08	1.41	97.7	
B1	-	-	-	91.5	54.4	140.8	1.07	1.42	99.3	pure kaolin with DI water
B2	-	-	-	115.5	53.4	148.2	1.06	1.45	96.1	
B3	-	-	-	115.5	55.7	116.7	1.04	1.50	96.2	
C1	0.75	1.5	-	87.5	58.4	47.0	1.01	1.36	95.0	with $CaCl_2$+urea
C2	0.75	1.5	-	111.5	53.3	91.2	1.06	1.29	91.2	
C3	0.75	1.5	-	98.0	57.9	27.1	0.99	1.40	91.6	
D1	0.75	1.5	15	114.5	53.8	220.0	1.07	1.31	90.6	with $CaCl_2$ + urea + centrifuged UPB
D2	0.75	1.5	15	111.5	54.2	184.5	1.04	1.29	93.5	
D3	0.75	1.5	15	111.5	55.5	167.2	1.02	1.30	94.9	
E1	0.75	1.5	15	114.5	53.9	203.9	0.99	1.31	91.0	with $CaCl_2$ + urea + oringinal UPB
E2	0.75	1.5	15	114.5	52.9	187.6	0.97	1.31	89.7	
E3	0.75	1.5	15	100.0	60.2	131.2	0.98	1.44	92.7	

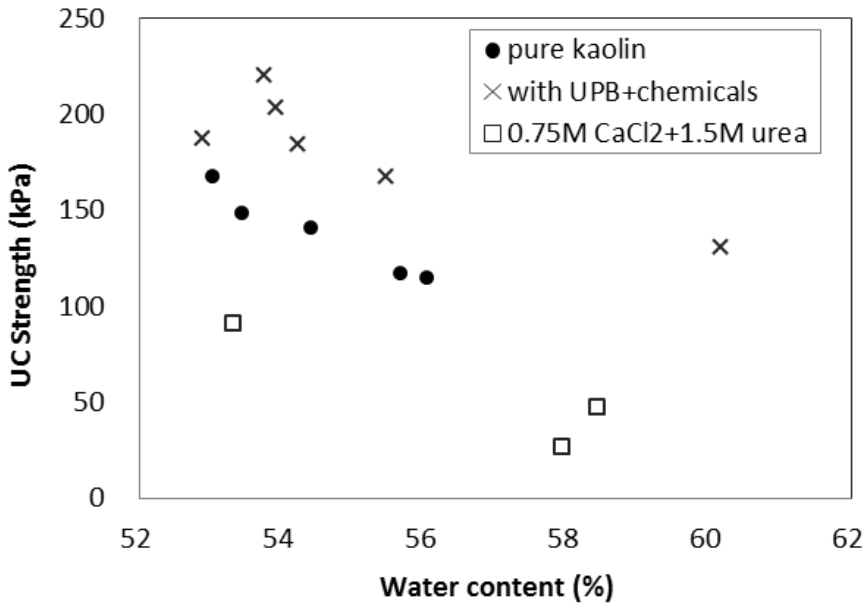

a)

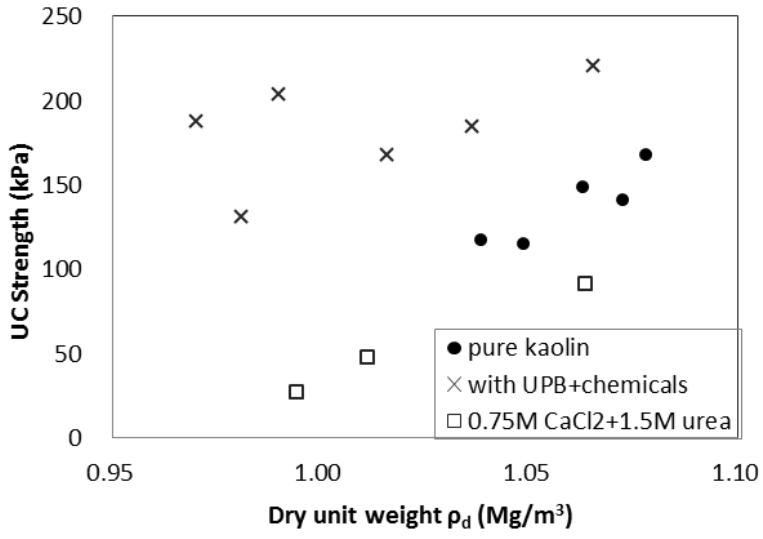

b)

Figure 8.14 Water content vs. a) UC strength and b) dry unit weight of chemical/UPB mixed kaolin specimens with water content of 56%±4%

8.3.2 Strength of specimens after drying

To simulate the resulted strength of the dredged material after drying under the sun, a set of specimens were prepared under totally dry condition. Kaolin mixed with water and/or chemicals and UPB to reach the water content of 100%, poured into PVC moulds and then dried in 105°C oven for 48 hrs. The designed chemical content and resulted UC strength are summarized in Table 8.9. For each group, several identical specimens were prepared and their UC strengths are presented as Strength 1, 2, 3 and 4.

Table 8.9 Summary of chemical/UPB mixed dry kaolin specimens properties

No.	$CaCl_2$ (mol/L)	Urea (mol/L)	UPB type	UC Strength 1 (kPa)	UC Strength 2 (kPa)	UC Strength 3 (kPa)	UC Strength 4 (kPa)	Note
1	-	-	-	231.0	324.0	-	-	Distilled water
2	-	0.75	-	108.9	123.6	-	-	Urea only
3	-	1.5	-	60.4	56.0	-	-	
4	-	3.0	-	0.0	0.0	-	-	
5	0.375	-	-	569.8	357.6	298.1	-	$CaCl_2$ Only
6	0.75	-	-	448.0	443.7	442.6	-	
7	1.5	-	-	551.1	496.5	496.5	897.2	
8	0.75	1.5	-	1665.1	1470.7	1807.4	1765.7	$CaCl_2$+urea
9	0.75	1.5	centrifuged	982.1	617.1	648.1	601.5	UPB+ $CaCl_2$+urea
10	0.75	1.5	original	899.8	812.5	-	-	

The UC strengths of totally dry samples prepared by mixing with different amount of $CaCl_2$ and urea are plotted in Fig. 8.15a and 8.15b respectively. It can be seen from Fig. 8.15a that the UC strength of dry kaolin samples increased with increasing $CaCl_2$. It could be caused by crystal binding effect of $CaCl_2$ at dry state. Another possibility is the calcium ion added reduced the thickness of double layer by increasing the cation exchange electrolyte concentration, making the microstructure of clay sheets flocculating rather than dispersing after drying. The reason behind such phenomenon will be discussed in Section 8.5.

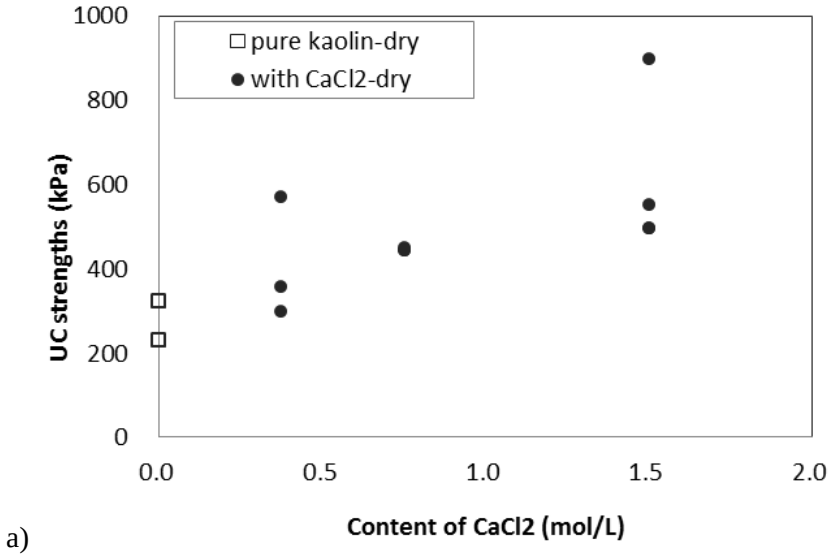

a)

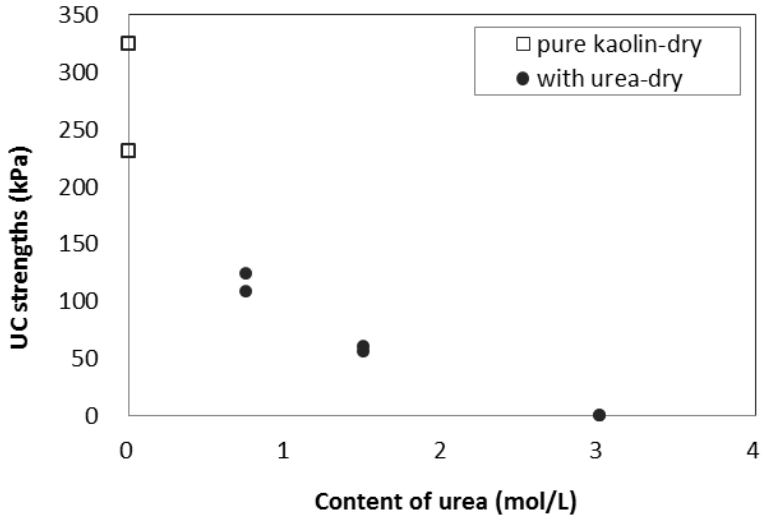

b)

Figure 8.15 Summary of UC strength of kaolin at 0% water content mixed with different amount of a) $CaCl_2$, and b) urea

On the other hand, the use of urea decreases the UC strength of dry specimens. By adding 3M urea, the UC strength of kaolin can be reduced to zero (Fig. 8.15b).

Figures of one specimen mixed with 3M urea is shown in Fig. 8.16a. It had powdering quality and was easy to be crushed by hand. Feather-like urea crystal leaching from the surface of the specimen was observed (Fig. 8.16b). Its composition is confirmed by the SEM picture shown in Fig. 8.16c.

a)  b) 

c) 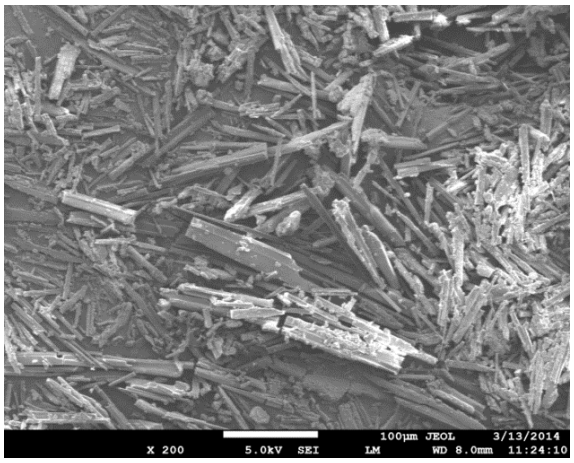

Figure 8.16 Figure of kaolin specimens at zero water content: a) mixing with 3M urea; b) urea crystal leaching from specimen's surface; c) SEM picture of the urea crystal in b)

UC strengths of dry specimens in all sets are plotted in Fig. 8.17. The 0.75M $CaCl_2$ plus 1.5M urea mixed specimen gained the highest UC strength. The combined effect of $CaCl_2$ with urea is yet to be discovered. Bacteria group showed higher UC strength than distilled water mixed specimens after drying, yet lower than the set mixed with chemicals only. The reason behind such phenomenon will also be discussed in Section 8.5.

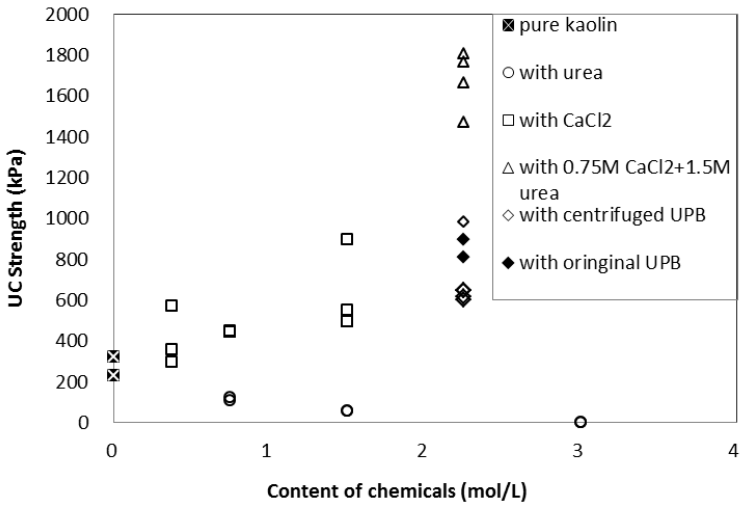

Figure 8.17 Summary of UC strength of chemical/UPB mixed kaolin at zero water content

8.3.3 MICP treated marine clay (MC)

The assessment on effect of MICP on clayey soil is extended to marine clay. Properties of marine clay used in this study can be found in Section 3.4.2. To be consistent with the previous study, a similar mixing method as employed for kaolin was engaged for marine clay. Initial water content of marine clay before mixing was about 70 to 80%. Distilled water was added in the samples to reach 100% of water content, added in chemicals and/or UPB during mixing, and then put into 40°C oven for curing and drying. Detailed properties of each specimen are listed in Table 8.10. A summary of the UC strengths in log scale vs. water contents of biocemented marine clay specimens by different types of bacteria along with control sets is presented in Fig. 8.18. The dry UPB powder in set D was produced by centrifuging and vacuum freeze drying as described in Section 3.6

The improvement made by MICP is clearer in marine clay. Marine clay mixed with UPB gained much higher UC strength compared to pure marine clay under the same water content. Under the water content of around 30%, the highest improvement in UC strength achieved was around 400%. This could be partially due to the sand presented in marine clay, which acted as bridges for the calcite binder to form in between. The types of UPB did not make much difference on the results. Note that fully saturated specimens (S=100%) were achieved with water content above roughly 30-35%.

Table 8.10 Detailed information of marine clay (MC) mixed with different amount of chemicals and/or UPB conducting UC tests

Test	$CaCl_2$ (mol/L)	urea (mol/L)	Wet Bacteria (ml/100g soil)	Dry Bacteria (g/100g soil)	Average Water Content upon UC test (%)	UC Strength (kPa)	Void Ratio	Remarks
A1	0.75	1.5	-	-	65.44	0.0	1.35	MC + $CaCl_2$+urea
A2	0.75	1.5	-	-	62.96	0.0	1.22	
A3	0.75	1.5	-	-	46.86	11.1	0.84	
A4	0.75	1.5	-	-	42.79	16.7	0.87	
A5	0.75	1.5	-	-	38.05	39.9	0.88	
A6	0.75	1.5	-	-	32.53	76.5	0.77	
A7	0.75	1.5	-	-	80.36	0.9	1.77	
A8	0.75	1.5	-	-	76.54	1.2	1.88	
A9	0.75	1.5	-	-	74.90	0.9	1.78	
A10	0.75	1.5	-	-	66.69	3.8	1.49	
A11	0.75	1.5	-	-	39.01	29.4	0.94	
A12	0.75	1.5	-	-	46.75	9.6	0.99	
A13	0.75	1.5	-	-	49.86	6.5	1.09	
A14	0.75	1.5	-	-	49.40	8.8	1.11	
A15	0.75	1.5	-	-	42.12	17.1	0.92	
A16	0.75	1.5	-	-	41.64	20.4	0.93	
A17	0.75	1.5	-	-	45.47	11.9	1.01	
B1	0.75	1.5	15	-	75.92	4.9	1.69	with centrifuged UPB
B2	0.75	1.5	15	-	67.35	9.8	1.47	
B3	0.75	1.5	15	-	43.73	85.3	0.98	
B4	0.75	1.5	15	-	42.11	101.9	0.93	
B5	0.75	1.5	15	-	31.58	350.0	0.76	
B6	0.75	1.5	15	-	31.70	341.3	0.70	
C1	0.75	1.5	15	-	64.18	8.7	1.40	with original UPB
C2	0.75	1.5	15	-	66.86	7.3	1.51	
C3	0.75	1.5	15	-	39.00	126.0	0.86	
C4	0.75	1.5	15	-	41.04	97.0	0.99	
C5	0.75	1.5	15	-	28.92	403.9	0.66	
C6	0.75	1.5	15	-	28.26	454.3	0.62	
D1	0.75	1.5	-	0.5	59.78	12.0	1.41	with dry UPB powder
D2	0.75	1.5	-	0.5	68.56	7.8	1.55	
D3	0.75	1.5	-	0.5	41.96	97.4	0.94	
D4	0.75	1.5	-	0.5	37.94	154.4	0.74	
D5	0.75	1.5	-	0.5	27.18	445.9	0.68	
D6	0.75	1.5	-	0.5	25.81	516.8	0.63	
E1	-	-	-	-	51.21	6.9	1.32	pure marine clay
E2	-	-	-	-	39.59	33.1	1.00	
E3	-	-	-	-	41.06	28.4	0.99	
E4	-	-	-	-	30.88	129.5	0.85	
E5	-	-	-	-	33.31	96.8	0.80	

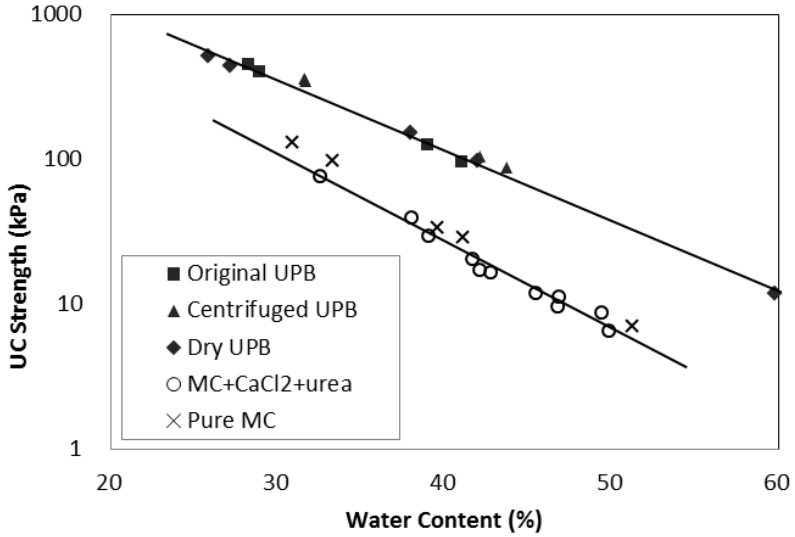

Figure 8.18 UC strength (in log scale) vs. water content of marine clay (MC) mixing with chemicals (0.75M $CaCl_2$ plus 1.5M urea), bacterial plus chemicals, and pure marine clay

8.3.4 MICP treated bentonite

A more extreme material having small clay particles, bentonite, was employed to understand the effect of MICP better in clayey soil. Properties of bentonite used in this study were described in Section 3.4.2.

Similar to the study on kaolin, the Atterberg limits of bentonite mixed with different amount of chemicals were measured using cone penetration method for LL and kneading method for PL (BS 1377 Part 2). The results are summarized in Table 8.11 and Fig. 8.19a, 8.19b and 8.19c respectively. Results on specimens mixed with 0.375/0.75/1.5M $CaCl_2$, 0.75/1.5/3M urea, along with the ones mixed with distilled water, and with 0.75M $CaCl_2$ plus 1.5M urea with/without bacteria are compared.

Comparing to the result on Atterberg limits of kaolin from Section 8.2.8, the plasticity properties of bentonite were altered by $CaCl_2$ more dramatically. The addition of 0.375M $CaCl_2$ resulted in a plummet of LL from 432% to 117.7%, which is one fourth of its original value (Fig. 8.19a). Higher $CaCl_2$ concentration resulted in further LL reduction, yet not proportional to its dosage. Addition of urea also reduced LL of bentonite, yet at much lower rate than $CaCl_2$, which might be attributed to the fact that adding Ca^{2+} cation increased the pore fluid electrolyte concentration and thus reduced the thickness of double layer around clay particles.

The effect of urea was limited compared to $CaCl_2$. Similar trend was observed for PL and the resulted PI, yet not as obvious.

Table 8.11 Atterberg limits, including liquid limit (LL), plastic limit (PL), and plasticity index of chemical/UPB mixed bentonite

Test	$CaCl_2$ (mol/L)	Urea (mol/L)	UPB (ml/100g soil)	LL (%)	PL (%)	Plasicity Index (%)	Remarks
1	0	0	-	432.0	60.1	371.9	pure kaolin
2	0.75	1.5	-	101.8	33.7	68.1	with both chemicals
3	0.75	1.5	15	118.9	76.4	42.5	with chemicals+UPB
4	0.375	0	-	117.7	38.5	79.2	with $CaCl_2$ only
5	0.75	0	-	109.2	43.1	66.1	
6	1.5	0	-	95.2	36.0	59.2	
7	0	0.75	-	386.7	47.4	339.2	with urea only
8	0	1.5	-	363.0	54.7	308.2	
9	0	3	-	318.6	29.4	289.2	

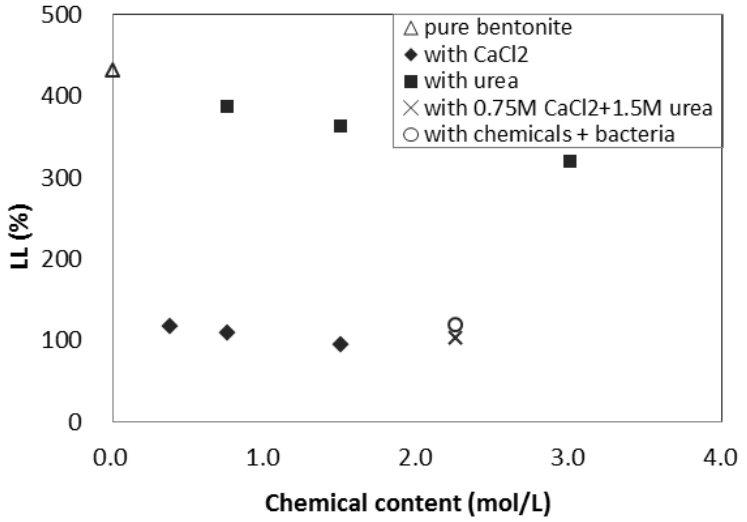

a)

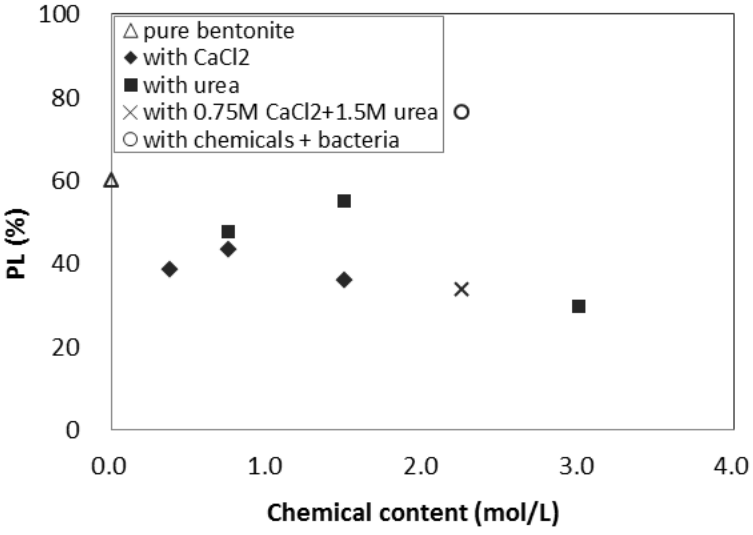

b)

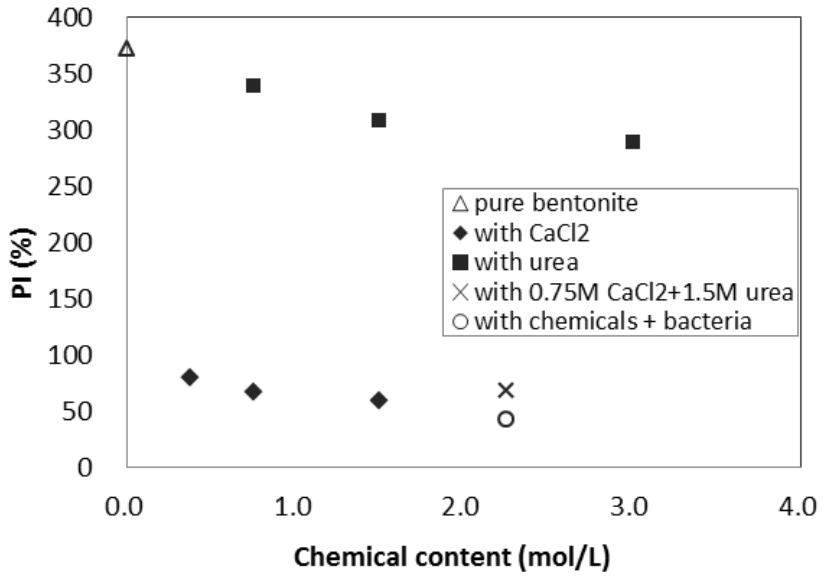

c)

Figure 8.19 a) Liquid limit; b) plastic limit; and c) plasticity index for bacterial/chemically treated bentonite

The added UPB (set 3) pushed LL from 101.8% in chemical added sample (set 2) to 118.9% (Fig. 8.19a), and increased PL nearly three times higher, from 33.7 to 76.4% (Fig. 8.19b). Combined effect of these two parameters resulted in a decreased plasticity index, from 68.1 to 42.5%. A lower plasticity index represents higher internal friction angle yet lower cohesion for clayey soil (Baumgartl, 2006; Kretschmer, 1997). Calcite might form in between the stack of flocculated clay particles rather than the clay sheets, which will be discussed in Section 8.6.

Pictures of bentonite specimen mixed with $CaCl_2$ plus urea, and pure bentonite are presented in Fig.8.20a and 8.20b respectively. It should be noted that the pure bentonite specimen shown in Fig. 8.20b had water content of 300%, while the one mixed with chemicals (Fig. 8.20a) had 100%, despite the fact that they could both stand on their own. Pure bentonite has the tactile impression and lustre feeling like plastic; such characteristic had been lost when chemicals were added.

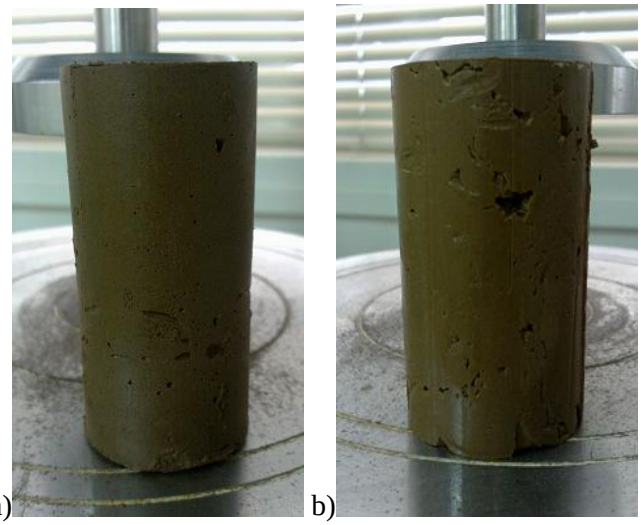

a) b)

Figure 8.20 Images of a) chemical mixed bentonite with 100% water content, and b) pure bentonite with 300% water content

A plot of UC strengths in log scale vs. water contents for all of the specimens tested is presented in Fig. 8.21. Detailed information of the specimens is summarised in Table 8.12. Similar to the results of kaolin and marine clay, improvement was observed in bacteria mixed specimens regarding to UC strength. Such effect might be partially attributed to the increased PL value resulted from addition of UPB. It should be noted that although pure bentonite could stand on its own under very high water content, no significant UC strength was detected until the water content was reduced to be around 150%. Note that fully saturated specimens (S=100%) were achieved with water content above roughly 40-45%.

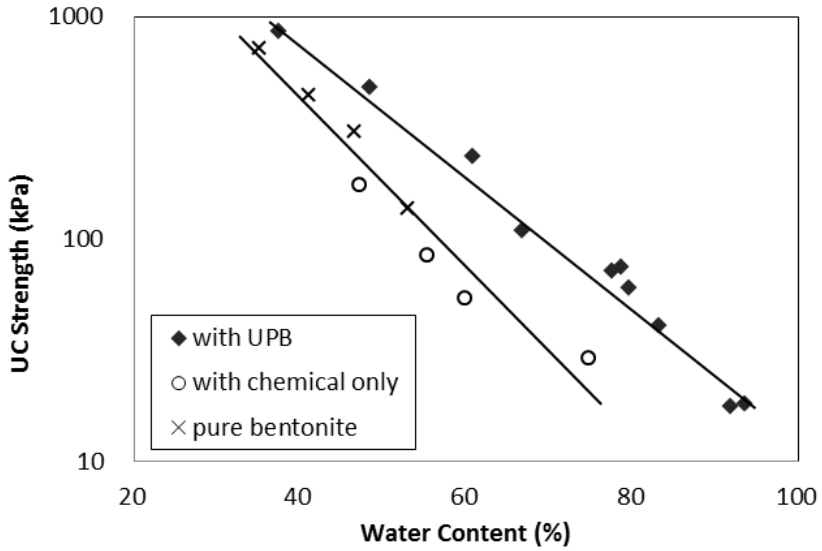

Figure 8.21 UC strength (in log scale) vs. water content of pure bentonite/mixed with bacteria/mixed with chemical

Table 8.12 Detailed information of bentonite mixed with different amount of chemicals and/or UPB conducting UC tests

Test	$CaCl_2$ (mol/L)	urea (mol/L)	UPB (ml/100g soil)	Average water content (%)	UC Strength (kPa)	Initial void ratio	DOS (%)	Remarks
A1	-	-	-	346.2	8.4	8.35	97.5	pure bentonite
A2	-	-	-	324.0	9.8	7.77	98.0	
A3	-	-	-	253.7	23.5	5.99	99.5	
A4	-	-	-	148.6	60.7	3.62	96.6	
A5	-	-	-	46.5	305.0	1.06	102.8	
A6	-	-	-	35.0	715.6	0.89	92.4	
A7	-	-	-	41.0	440.4	0.97	98.9	
A8	-	-	-	52.9	137.4	1.15	108.0	
B1	0.75	1.5	-	100.4	4.1	2.06	97.5	with $CaCl_2$+urea
B2	0.75	1.5	-	88.2	5.8	1.85	95.4	
B3	0.75	1.5	-	74.8	29.2	1.53	97.7	
B4	0.75	1.5	-	59.8	53.9	1.24	96.7	
B5	0.75	1.5	-	55.3	84.3	1.16	95.6	
B6	0.75	1.5	-	47.0	175.0	0.95	99.6	
C1	0.75	1.5	15	91.7	17.6	1.90	96.6	with $CaCl_2$ + urea + oringinal UPB
C2	0.75	1.5	15	93.5	18.1	1.86	100.8	
C3	0.75	1.5	15	83.2	40.5	1.70	98.1	
C4	0.75	1.5	15	77.5	71.7	1.59	97.4	
C5	0.75	1.5	15	79.6	60.1	1.55	103.0	
C6	0.75	1.5	15	78.6	74.7	1.54	102.2	
C7	0.75	1.5	15	66.6	108.9	1.65	81.0	
C8	0.75	1.5	15	60.8	233.9	1.21	100.8	
C9	0.75	1.5	15	37.4	862.1	0.68	110.8	
C10	0.75	1.5	15	48.3	481.2	0.88	110.0	

8.4 Clay encapsulation

Another way to use MICP to treat clay is the bioencapsulation. It involves in making small balls from clay, of which the properties might be improved by a MICP approach. The treated clay balls may be used as fill materials. This is similar to the premixing method using cement that has been adopted in practice (Tatsuoka, 2004; Chu et al., 2009). It may also be a way to convert clay waste into value-added construction materials. Therefore, the aim of the present research was to study the feasibility of bioencapsulation of soft clay aggregates for the production of solid construction material.

8.4.1 Sample preparation method

Small clay balls in a variance of diameter from 5 to 20mm were made from kaolin and marine clay (MC), attempting to increase the strength of biocemented clay balls. Two different preparation methods were used: one is to form a shell outside, namely "shell method"; another is to mix soil with bacteria and chemicals evenly, namely "ball method".

Detailed procedure for shell method is as follows:

1. Mixing clay with deionized water at 50% water content, then form small clay balls with 5 to 20mm in diameter by hand; wrap them with dry UPB powder on surface;

2. Dipping/Soaking the clay balls into 0.75M $CaCl_2$ and 1.5 M urea solution for two days, making sure all balls were submerged under the solution;

3. Dry the balls in a 40 degree oven overnight.

For the ball method, similar procedures as step 1 and 3 in wet method described before were involved. Clay was mixed with chemicals and different types of bacteria all together and left for drying for two days, either oven-dried at 40°C or air-dried. No dipping in chemical solution process (step 2) was involved.

Table 8.13 Summary of clay ball samples prepared

No.	Material Type			Treatment methods			Bacteria type			Remarks
	Pure MC	MC + 10% Cement	MC + chemical	Wet (dipping)	Dry		Dry UPB powder		Wet UPB (uniformly mixed)	
					Air-dry	Oven-dry	Wrap on surface	Mixed uniformly		
1	√									pure soil^
2		√								soil + cement^
3	√			√			√			shell forming method
4*		√		√			√			
5	√			√				√		
6	√			√					√	evenly mixed method
7			√			√		√		
8			√		√			√		

*Shell formed yet not separated clearly from core
^Control sets

As summarized in Table 8.13, eight sets of clay ball samples were made, employing different types of material (marine clay, bentonite, and marine clay plus cement), treatment methods and bacteria types (original wet UPB suspension and the dry UPB powder). Properties of the balls made in each group will be evaluated.

8.4.2 Split test for strength measurement

As the clay balls are not standard in size or shape to fit any existed soil strength test, compression tests of single clay balls was adopted to access roughly the strength properties of the clay balls. This test is similar to the split cylinder test used for concrete. As shown in Fig. 8.22a, a single clay ball was put under UC machine for compression until it failed. A typical clay ball specimen prepared by ball method after split test is displayed in Fig. 8.22b. Most of the clay ball split half right from the middle, as the balls are weaker in tensile strength.

Shell separated from its core was found to be formed outside the clay ball making by the shell method, as shown in Fig. 8.22c. The outer part of clay ball contacts directly to the chemical solution, at where the reaction was supposed to happen first. This pre-formed hard shell then tended to separate from its inner part, which shrink during the drying process. Yet such shell formed was moderately thin. Noted that for samples in set 4 (marine clay plus 10% of Portland), the shells were formed, yet was inseparable from its core.

a) 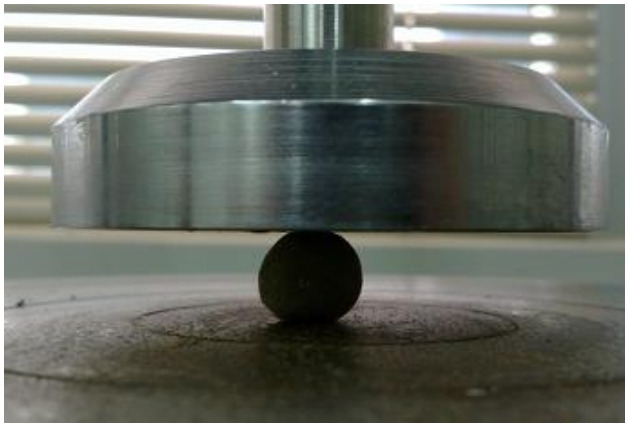

b)  c) 

Figure 8.22 Images of a) biocemented clay balls made by evenly mixing method during split test by UC apparatus, and specimens prepared by b) ball method, and c) shell method after testing

Typical force vs. displacement curves of clay balls making by the ball method and shell method are shown in Fig. 8.23a and 8.23b respectively. As shown in Fig. 8.23b, two force peaks were detected, of which the first one was from shell breakage and the second was supposed to be from the core splitting. As the ball is considered to be failed after the breakage of shell, only the first peak is concerned. On the other hand, only one peak was detected for the balls made by the ball method as expected (Fig. 8.23a).

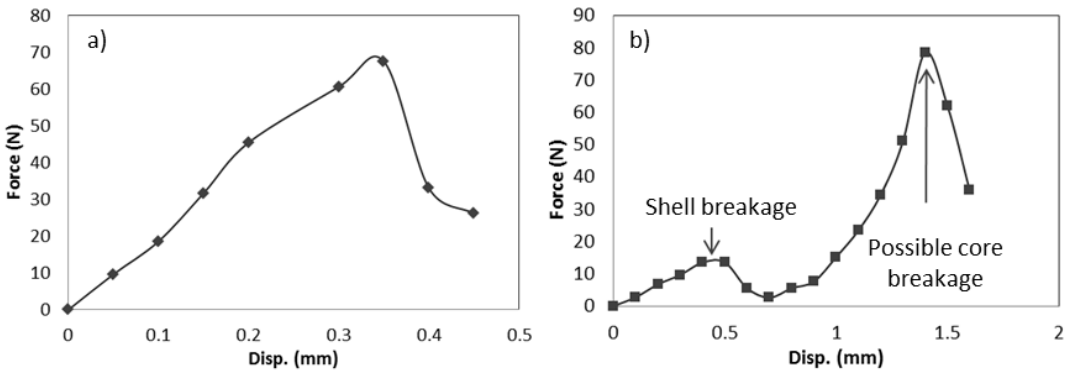

Figure 8.23 Typical force vs. displacement curve in split test of clay ball made by a) ball method, and b) shell method

Microstructures of this shell outside marine clay pictured by FESEM machine and its elementary composition by EDS are shown in Fig. 8.24, including elements calcium (Ca), oxygen (O), carbon (C), aluminium (Al), and magnesium (Mg). The common elements of marine clay, Al, Mg and O, along with the introduced elements Ca, C and more oxygen, are observed to distribute within the sample, mingling with each other.

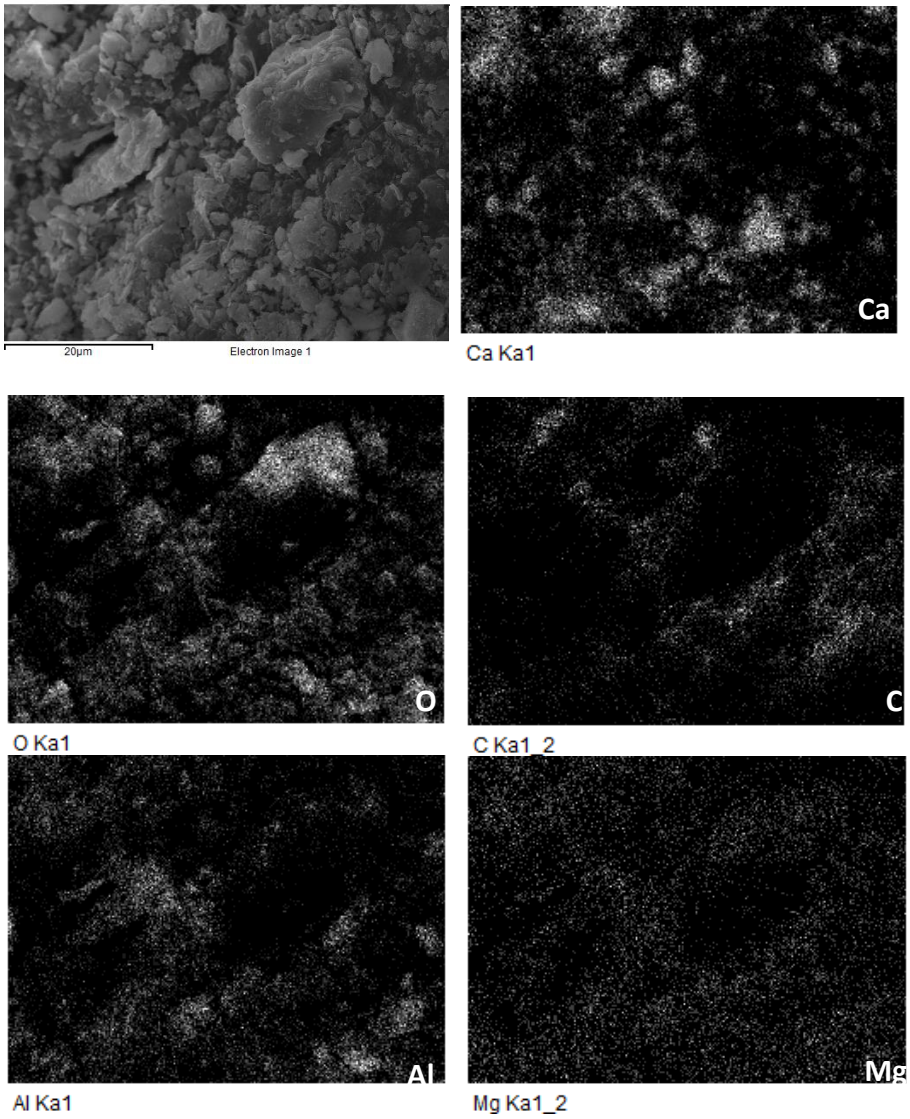

Figure 8.24 FESEM images of the shell formed outside clay balls made by wet method, and the EDS images showing elements calcium(Ca)/oxygen(O)/carbon(C)/aluminium(Al)/magnesium(Mg) at the same site

The maximum breakage forces endured by the crystal shell in sets 3 and 5, which was normalized by diameter square of the shell, were drawn against the ball diameter in Fig. 8.25. The normalized forces are found to be decreased with increasing diameter. It should be noted that the strength of shell formed outside clay ball are generally very weak (enduring force less than 15 N; could be breaking by hand); furthermore, the soaking treatment reduced the strength of clay in the core comparing to pure clay, thus making shell-forming an unfavourable method for clay ball. Yet it has advantage in terms of endurance when soaking into water by the shell formed, which will be presented in later section.

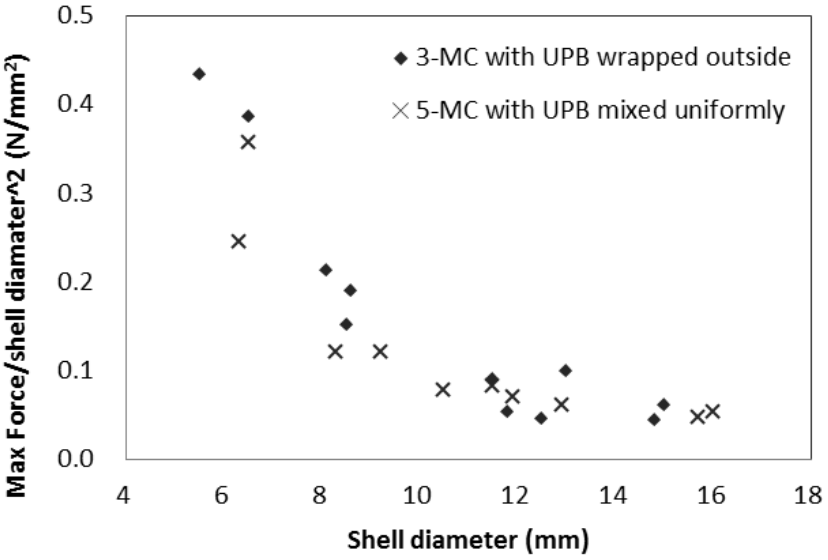

Figure 8.25 Maximum normalized force from shell breakage divided by diameter^2 vs. diameter for clay balls prepared by shell forming method

Effectiveness of evenly mixing method could be examined by the comparison of set 6, 7, 8 with control sets 1 and 2, as shown in Fig. 8.26. No obvious difference was observed in sets 1, 2, and 7, 8. However, improvement was observed for specimens in set 7, engaging wet UPB instead of dry UPB powder. This might indicates the advantage of wet UPB suspension in bioencapsulation over dry UPB.

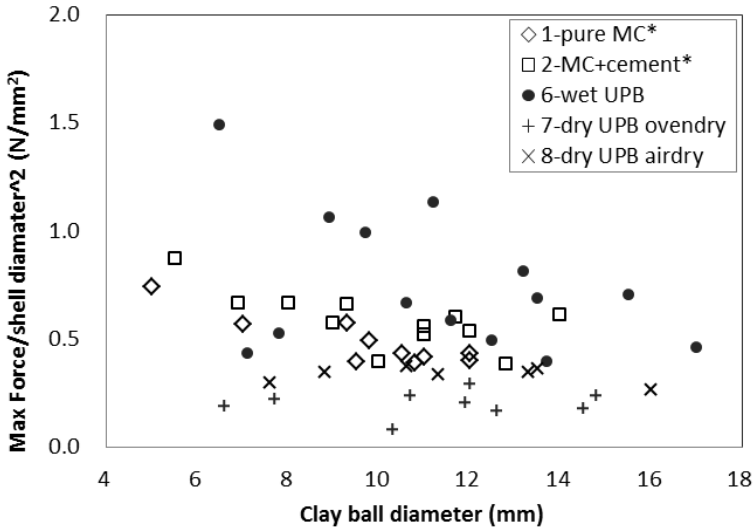

Figure 8.26 Normalized maximum force vs. diameter getting from clay ball made by ball method (set 6/7/8) with control* (set 1/2)

8.4.3 Slaking tests

Slaking tests were conducted for assessing the adhesion bacteria added to soil (Mitchell & Soga, 2005). Specimens for biocemented and control group were suspended into water simultaneously; photo were taken at interval of 1min, 3min, 10mins, 1 hour, 2hr, 4hr, 1day, 2day, 3day, 1 week, etc., until it is fully dissolved in water. Pictures will then be tabulated and organized to see the trend.

Slaking tests were conducted on clay balls (5mm to 20mm in diamter) prepared with UPB and with pure kaolin mixed with distilled water, as shown in Fig. 8.27, both employing the dry mixing method. Base on the trend of the disintegration of the kaolin balls sample, it is noted that the kaolin balls with UPB has much better resistance against being soaked in water while the kaolin balls without UPB disintegrate fastest as one can see the notable difference after 30 mins where the drastic disintegration of the kaolin balls sample starts. This endurance could be attributed to the lowering of permeability due to the re-construction of microstructure of clay particles by chemicals and bacteria added.

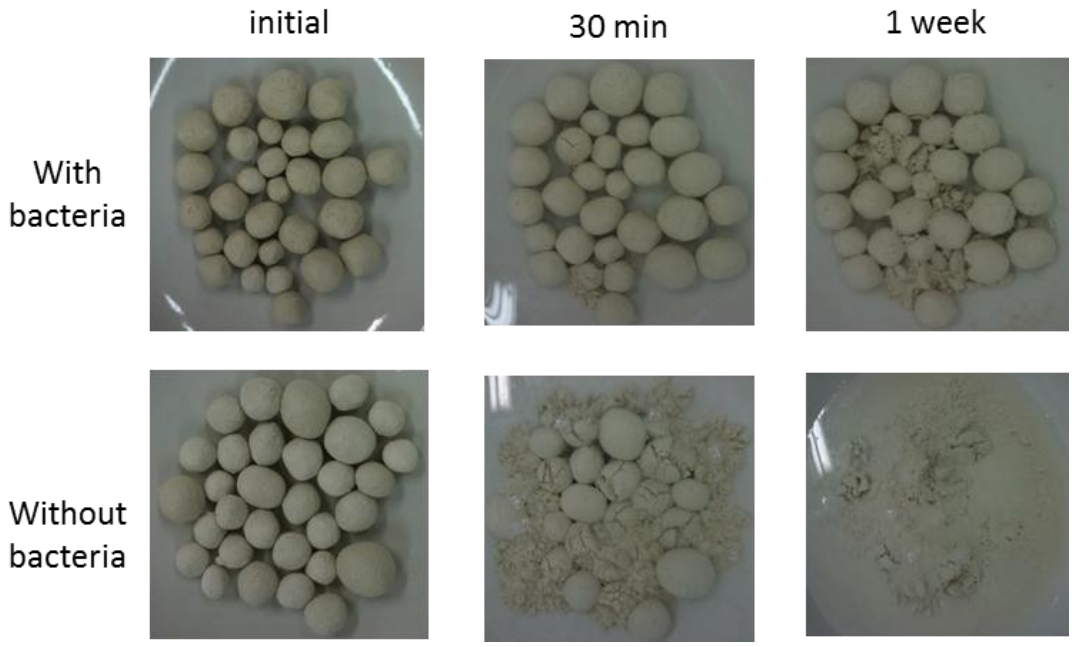

Figure 8.27 Slaking test on UPB treated kaolin and pure kaolin

Another set of marine clay balls as described in Section 8.4.1 were submerged under water and tested for their endurance. Group 1 on top was taken from the sets

making by evenly mixing method, including set 6, 7, 8. Group 2 on left of the bottom contains MC balls having calcite shells enwrapped on the outside, including set 3, and 5; other control groups containing MC only (set 1) only were put in Group 3 on the bottom of right for comparison.

As shown in Fig. 8.28, the shell formed outside seemed to protect the MC balls from water well, as no balls were observed to be cracked after soaking by 2 months. On contrast, balls in group 3 dissolved completely into water by then; yet it can be observed that the chemicals added did prevent the dispersive properties of MC comparing to Fig. 8.28, and kept the shape of the balls longer. Specimens in group 1 behaved in between of the other two groups, in which the balls cracked yet basically kept their shape after two months.

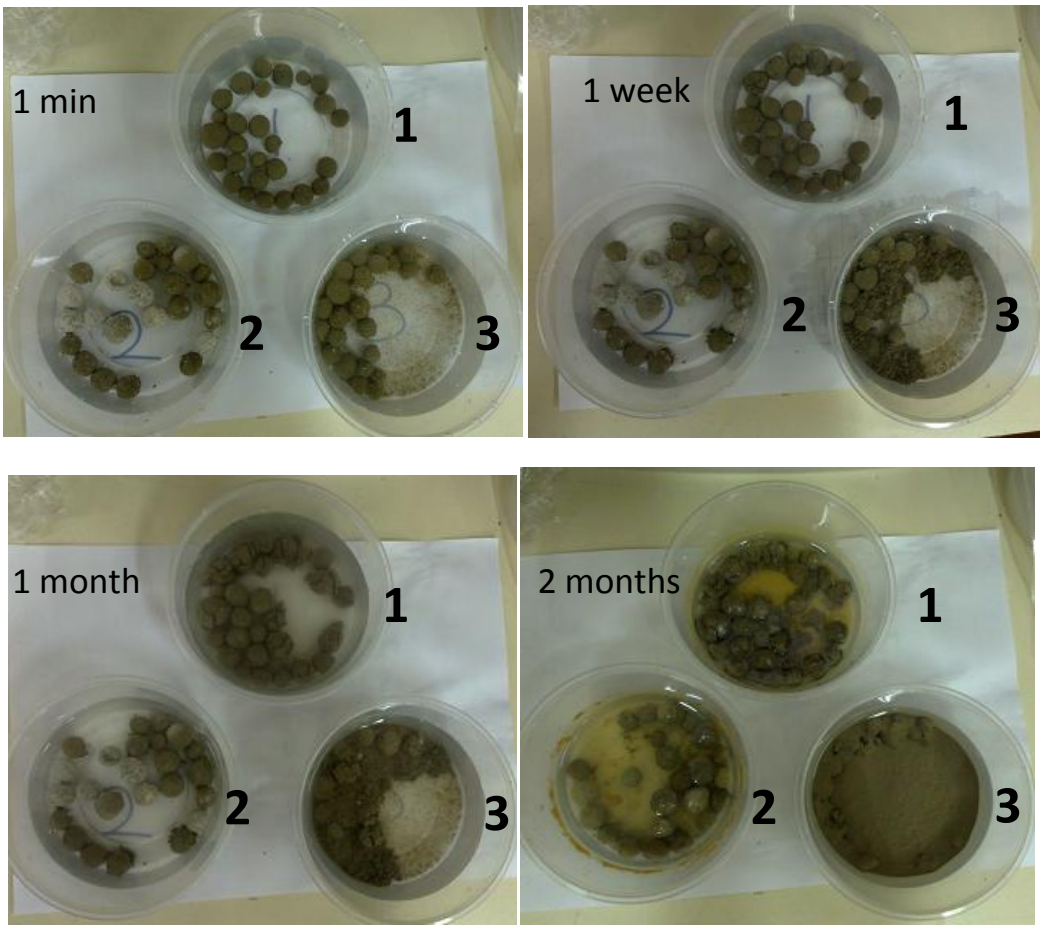

Figure 8.28 Slaking test of MC balls making by evenly mixed method (group 1), shell forming method (with shell outside, group 2) and control (pure MC, group 3) after submerged under water by 1 min, 1week, one month and two months

8.5 Hypothesis on mechanism of MICP in clay

As the mechanism of MICP formation in clay is yet to be discovered, one hypothesis intending to provide an explanation for the observation made in this chapter is established and discussed.

Microstructures of kaolin mixed with chemicals ($CaCl_2$ plus urea) and UPB pictured by FESEM machine, and its elementary composition by EDS are shown in Fig. 8.29, including elements oxygen (O), calcium (Ca), and aluminum (Al). The common elements of kaolin, Al and O, along with the introduced elements Ca and more oxygen, are observed to distribute within the sample, mingling with each other. Calcite seems to be formed in between the stack of flocculated clay particles.

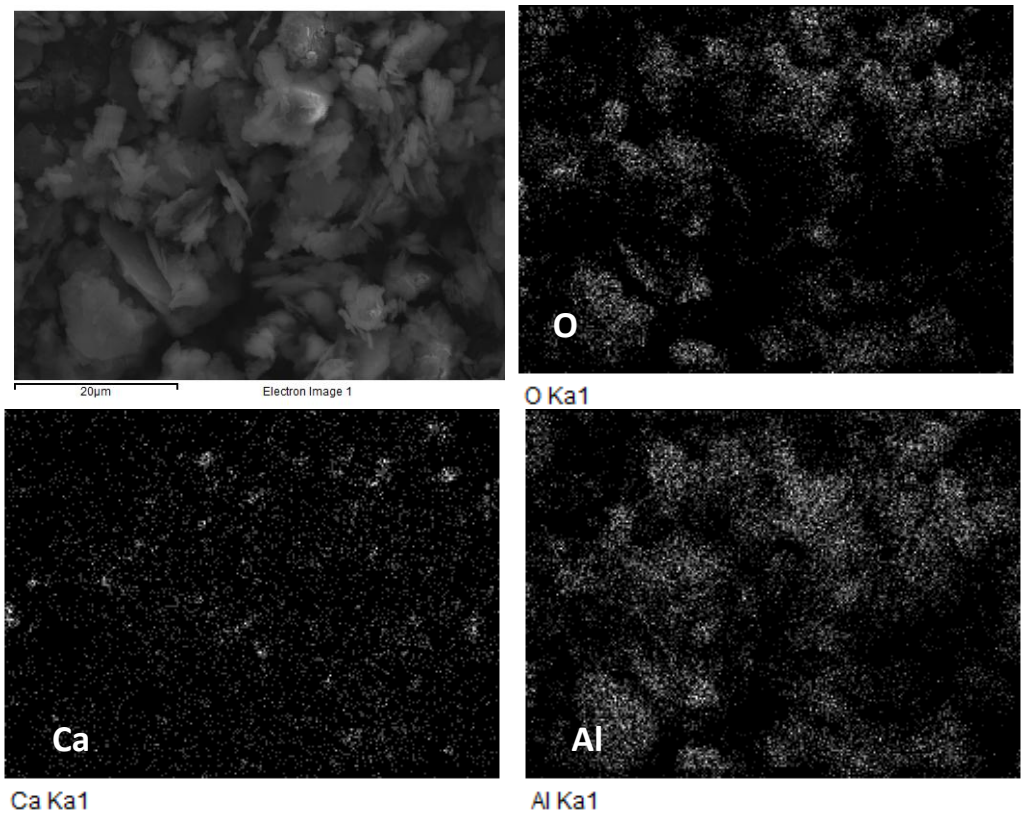

Figure 8.29 FESEM images of kaolin mixed with chemicals ($CaCl_2$ plus urea) and UPB, and the EDS images showing elements oxygen (O)/ calcium (Ca)/ aluminium (Al) at the same site

Microstructures representing by SEM images of pure clay mixing with distilled water and with 0.75M $CaCl_2$ and 3M urea are shown in Fig. 8.30a and 8.30b respectively. The arrangement of bentonite sheets changed from a disordered face

to edge particles structure as shown in Fig. 8.30a, to a more ordered face to face form of clay particle stacks as shown in Fig. 8.30b. Absorbed water layer around bentonite particles was reduced along with the diminished double layer as Ca^{2+} cation increased the pore fluid electrolyte concentration, released the interlayer water to become free pore water and made mixture flowing more easily at the same water content level.

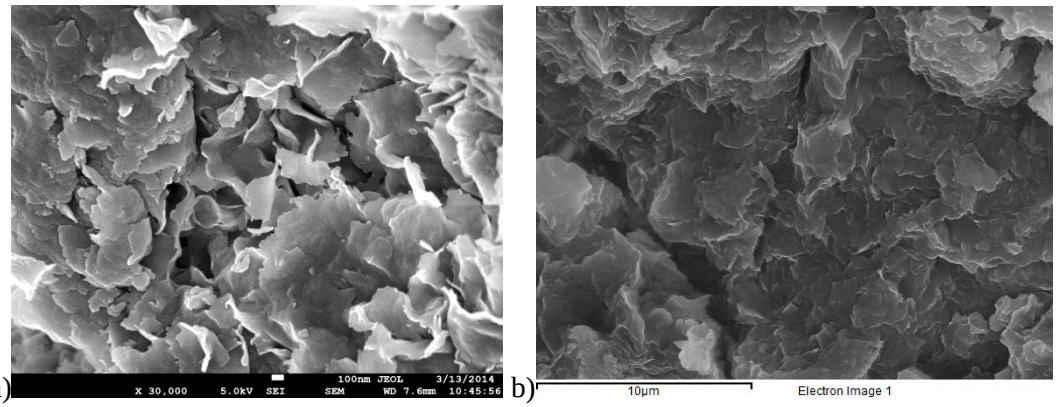

a) b)

Figure 8.30 SEM images of a) pure bentonite with distilled water, and b) bentonite mixed with 0.75M $CaCl_2$

Besides MICP precipitation, possible mechanisms behind the biocementation effect on clay may include ion-exchange between bacteria and clay particles, breaking of the diffused double layer of clay (water hull) and adsorption water in between, bacterial attachment to the surface of clay to prevent further water absorption, stranded bonding of clay platelets. SEM images of possible spots of calcite crystal precipitation and stranded bonding are shown in Fig. 8.31a and 8.31b respectively.

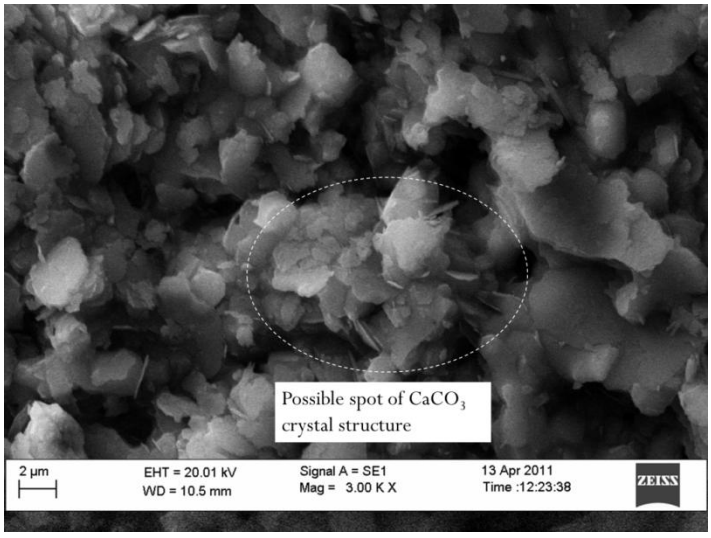

a)

b)

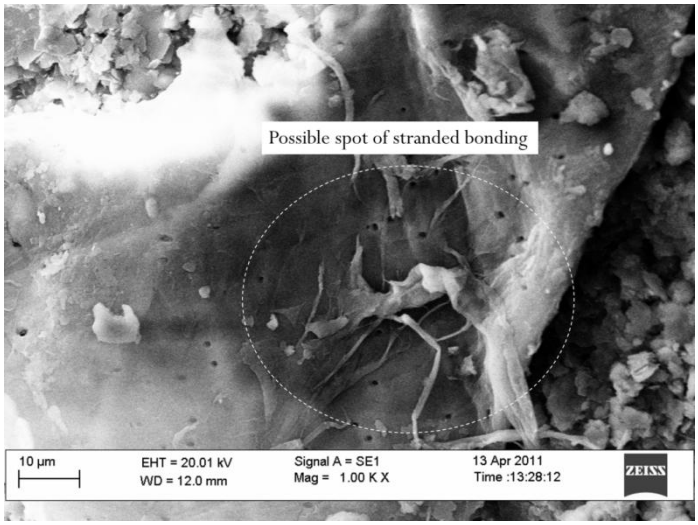

Figure 8.31 SEM images of possible spots of a) calcite crystal precipitation and b) stranded bonding provided by UPB

Mechanism of biotreatment in clay is sketched in Fig. 8.32. Fig. 8.32a sketches the circumstances when clay mixed with distilled water. Water trapped in between of the flocculated clay pellets and also between each clay layers, especially in the case of bentonite. Such ability of water absorption gives clay its property of high plasticity. Clay could maintain in plastic form in a large range of water content. Fig. 8.32b shows the microstructure of clay suspension after applying chemicals. Calcium cation added reduced the double layer repulsion. Flocculated/aggregated fabric was formed, thus releasing a lot of free water from trapping inter-pellets. This would also explain the great reduction of LL and PL as illustrated in Section 8.2.8 for kaolin and 8.3.4 for bentonite.

As shown in Fig. 8.32c, after adding UPB, larger clusters might be formed because of the calcite crystal and stranded bonding forming. Water would be trapped in between the aggregated platelet groups. This could explain the increase of LL and PL by UPB added, as percentage of free pore water had been reduced. Besides the calcite crystal and strand bonding produced by UPB, strength at the same water content level would also be increased partially because of this inter-platelet water trapped comparing to Fig. 8.32b.

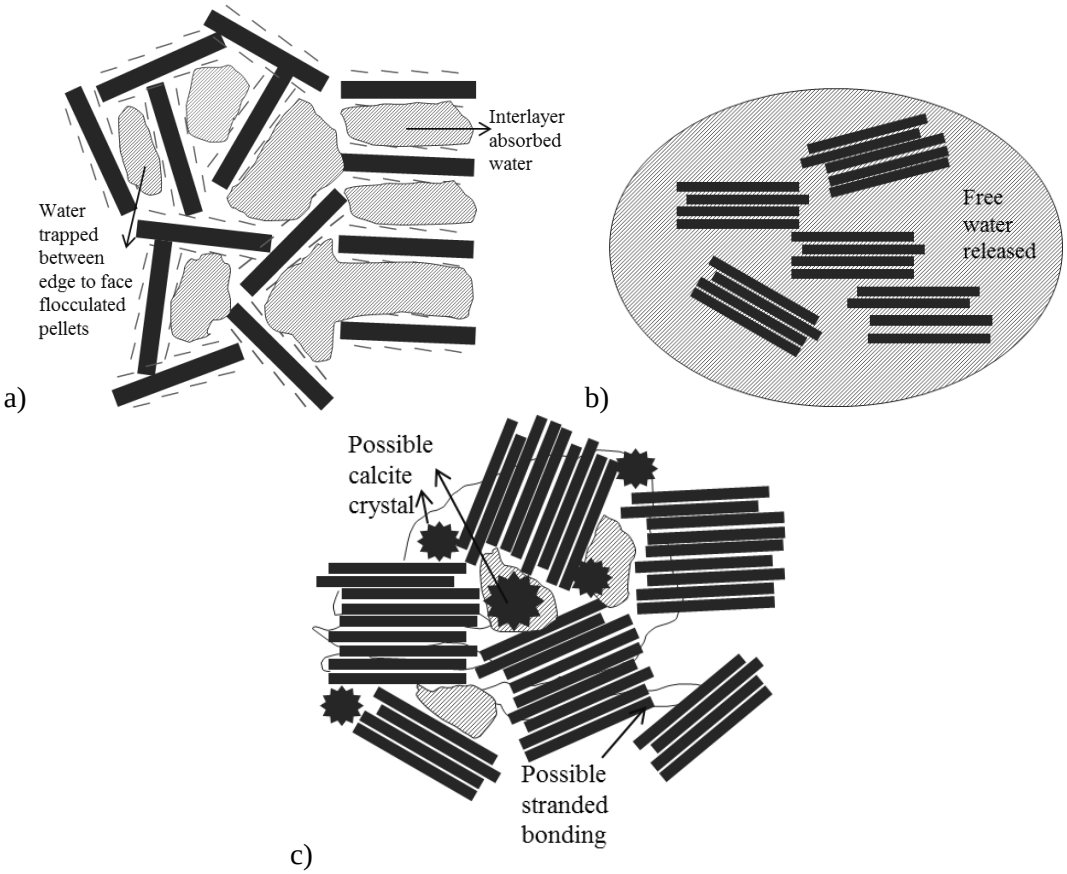

Figure 8.32 Sketched hypothesized microstructure of a) pure clay with distilled water, b) clay mixed with chemicals, and c) bio-treated clay

Structure of pure clay, chemical added clay and bio-treated clay after drying at 105˚C oven are shown in Fig. 8.33a, 8.33b and 8.33c respectively. The chemical mixed group might have the most condensed structure at zero water content (Fig. 8.33b). This could explain the result presented in Section 8.3.2, in which chemicals-only set gained the highest UC strength (four times higher than pure clay and two times higher than bacteria group). Results of slaking test in Section 8.4.3 might also be explicated by the microstructure. Bio-treated clay balls (Fig. 8.33c) should have more stable structures with true binding in between when soaking under water, while pure clay might behave as dispersed soil in pure water and dissolved layer by layer (Fig. 8.33a).

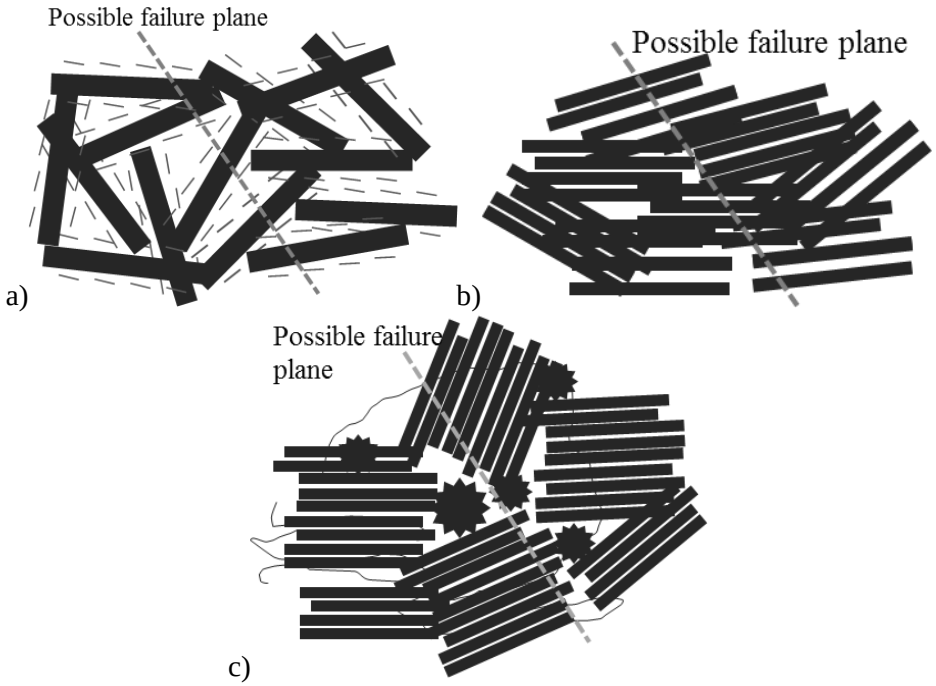

Figure 8.33 Sketched hypothesized microstructure of specimens with zero water content: a) pure clay with distilled water; b) clay mixed with chemicals: and c) bio-treated clay

8.6 Conclusions

The feasibility of using biocementation to improve the mechanical properties of fine-grained soils was explored in this chapter. The materials tested included kaolin, bentonite and marine clay. Effectiveness of biocementation on fine-grained soil through the MICP process and the possible related chemical effect were evaluated. A new methodology namely bio-encapsulation conducted by clay was also assessed. Main conclusions can be summarized as follows:

The UPB mixed kaolin samples in the UC, CID, DSS and oedometer tests showed higher strength, higher failure envelopes and lower compressibility respectively compared to the control samples mixed with chemicals $CaCl_2$ and urea. Nevertheless, the failure envelopes in CK_0U tests for UPB mixed samples and pure kaolin were similar. The difference in the effective failure envelope was due to the chemical effects.

A higher UC shear strength was observed for soil mixed with UPB and cementation chemicals compared to pure soil under the same water content. Such a phenomenon was observed in all types of clayey soil tested in this study, including

kaolin, marine clay and bentonite. The unconfined compression (UC) strength of biotreated sand has increased by 150% in kaolin and 400% in marine clay compared to pure soil under a given range of water content.

On the other hand, the calcium cation used for biocementation may result in lower UC strength of clayey soil. This should be attributed to the fact that addition of Ca^{2+} cation increases the pore fluid electrolyte concentration and thus reduced the thickness of double layer around clay particles; i.e. clay particles became more flocculated rather than dispersed, which allows higher proportion of water to exist in the form of pore water rather than absorbed water.

Chapter 9
Conclusions and Recommendations

9.1 Conclusions

In this research project, optimization of biocementation in sand and feasibility of using biocement to improve the mechanical properties of clayey soil were studied. Element tests using small cylindrical samples as well as model tests using soil of up to one cubic meter in volume were carried out. Different chemical compositions and types of bacteria were tested for both sand and clay. The following conclusions can be made from this study:

Optimization of MICP in Sand

The use of centrifuged UPB resulted in a more gentle permeability reduction after each round of treatment as compared with the use of original UPB. This is the intended purpose of using centrifuged UPB. Compared with tests using the original UPB suspension, the ureolysis/calcium precipitation rate in tests using centrifuged UPB suspension is lower and the pH rising was also delayed. Little difference was observed between tests using original UPB suspensions with relatively higher urease activity and that with lower urease activity.

A sample treated using centrifuged UPB result in a more uniform calcite distribution in the sample and a higher UC strength than that using original UPB suspension. However, such an effect could only be observed when a cementation

solution with calcium to urea ratio of 1:2 is used. The rising in pH is slower when a 1:1 cementation solution is used. The above differences can affect the calcium carbonate precipitation process in sand.

Geotechnical properties of sand treated using the crust and bulk cementation methods

Two biocementation methods were adopted in this study: crust and bulk cementation. Use the first method, a layer of 5 to 9 mm calcite crust was formed on the top surface and the surrounding surfaces of the sand in the box after 30 rounds of treatment. The outer fibre stress of the curst as measured using a 4-point bending test was as high as 20 MPa. The coefficient of permeability of the crust layer was reduced from 10^{-4} m/s before treatment to 10^{-9} m/s. Thus the crust method is capable of forming an imperious layer on the surface of sand for bioclogging purpose.

Using the bulk cementation method, the UC strength of the treated sand can be as high as 5977 kPa. The UC strength increases with increasing calcite content. The uniformity of biocementation within the sand block was increased with the increased rounds of treatment. The FESEM pictures and the corresponding EDS images for biocemented sample confirmed that it is the presence of the calcium carbonate which leads to the increase in strength and decrease in permeability of the sand.

Up-scaled model test of biocementation in sand

Cementation efficiency is a measure of the mean calcite content achieved in sand divided by the initial total calcium supply calculated using the chemical formulae. For the one cubic meter box model test, the cementation efficiency was calculated to be 93%. This value is considerably higher compared with that in the small cylindrical samples and the values reported in the literatures which range from 50

to 92% (Al Qabany et al., 2012; DeJong et al., 2006; Rebata-Landa, 2007; Whiffin et al., 2007). These test data confirmed that the effectiveness of the low activity UPB strain VS1 and the treatment method used in the study.

Within the one cubic meter sample, specimens at the top layer gained the highest calcite content and the highest UC strength. This is followed by the bottom layer. Specimens in the middle layer had the lowest calcite content as well as the lowest UC strength. In spite of its higher calcite content and greater UC strength, sand sample in the top layer resulted in a higher coefficient of permeability compared to that for the sample having the same calcite content in the middle and bottom layer. Preferential flow paths were developed due to a faster seepage velocity around the clogs.

Mechanisms of Biocementation on Sand

Triaxial CD tests were carried out on pure sand samples and sand treated using the dry MICP method. CD tests on biotreated samples show a higher effective stress failure envelope than that obtained from the CD tests on pure sand. Different failure envelopes are resulted on samples with different $CaCO_3$ contents. Within the tested stress range, these failure lines appear to be straight and parallel with each other. The higher the $CaCO_3$ content, the higher the friction angle. In other words, the failure envelopes moved upward with increased calcite content. These observations reveal that the effect of biocementation contributes mainly to the increase of cohesion. Similar observation has been reported for sand treated using cement grout.

The relationship between the maximum dilatancy versus void ratio obtained from CD tests on both cemented and pure sand specimens are more or less the same. However, the maximum stress ratio versus dilatancy relationship for cement sand is different from that for non-cemented sand. The maximum stress ratios of the cemented sand are higher than that for pure sand. As the amount of dilatancy for

both cemented and pure sand is about the same, the increase in the mobilized stress ratio is a result of biocementation.

Biocementation of Fine-Grained Soil

A higher UC shear strength was observed for soil mixed with UPB and cementation chemicals compared to pure soil under the same water content. Such a phenomenon was observed in all types of clayey soil tested in this study, including kaolin, marine clay and bentonite. The unconfined compression (UC) strength of biotreated sand has increased by 150% in kaolin and 400% in marine clay compared to pure soil under a given range of water content.

On the other hand, the calcium cation used for biocementation may result in lower UC strength of clayey soil. This should be attributed to the fact that addition of Ca^{2+} cation increases the pore fluid electrolyte concentration and thus reduced the thickness of double layer around clay particles; i.e. clay particles became more flocculated rather than dispersed, which allows higher proportion of water to exist in the form of pore water rather than absorbed water.

9.2 Recommendations

Some recommendations and suggestions for further studies are proposed as follows.

9.2.1 Cost estimation for biocementation by MICP

The current costs of industrial grade (di-hydrate) calcium chloride, urea, and bacterial suspension are around US$260, US$300, and US$500 per ton respectively based on my laboratory scale procedure. Using an average conversion efficiency of chemicals to calcite binder as 84% (Section 4.4), the treatment price per cubic meter versus calcite content/UC strength can be estimated the chart shown in Fig. 9.1. The calcite content vs. UC strength relationship can be modelled

as $y = 6.5455x^{2.3872}$, in which *x* is calcite content in percentage and *y* is the correspondent UC strength in kPa. However, it has to be pointed out this is a very conservative estimate based on my laboratory scale tests. For industrial scale operation, the material costs can be lower and the cost involved in the production of UPB can be much lower. Furthermore, bacteria might be used for more than one cycle and much higher conversion efficiency can be achieved as in the 1 m^3 model test. Theoretically the cost of chemicals could be as even lower than $100 per cubic meter for achieving UC strength of 1MPa.

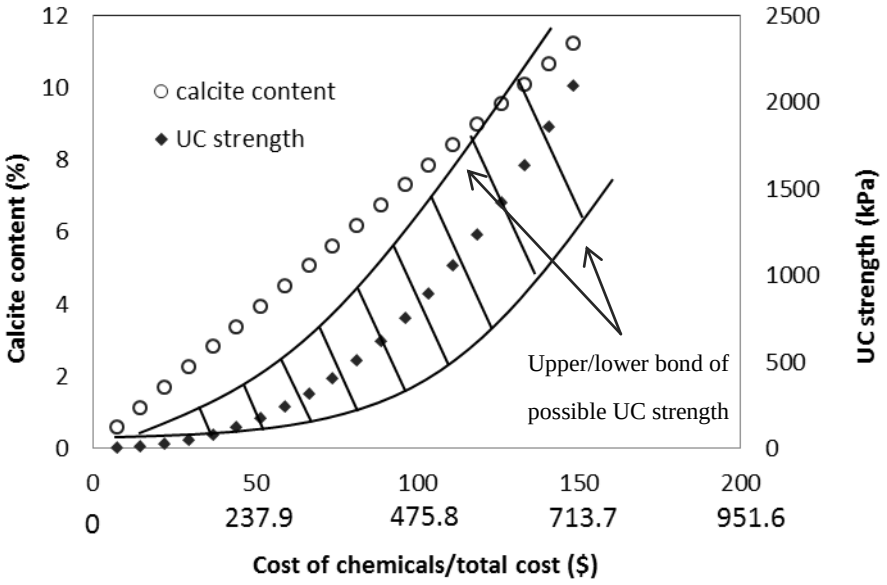

Figure 9.1 Cost/m^3 for bio-treatment of sand with different UC strength

Cost presented in Fig. 9.1 is pertinent to biocementation to increase strength. For bioclogging using the crust method, the estimated cost of the chemicals is US\$90.6/m^2 in order to reduce the coefficient of permeability to 10^{-8} m/s based on the laboratory scale operation in this study.

Further study should be carried out to develop methods that could extract Ca from waste material or to reduce the usage of urea. One method to use limestone mining waste and agriculture by-products to produce biogrout to remove the need for calcium chloride or other types of calcium has been developed at Iowa State University (personal communications).

9.2.2 Mechanism of MICP in clayey soil

The mechanism of MICP applications in clay has not been fully understood. More effort should be devoted to this study.

References

Acar, Y.B. & El-Tahir, A. (1986). Low strain dynamic properties of artificially cemented sand, *J. Geotech Engrg.*, 112(11), 1001–1013

Al Qabany, A., Mortensen, B., Martinez, B., Soga, K., and DeJong, J., (2011). Microbial carbonate precipitation: Correlation of S-wave velocity with calcite precipitation. *Proc. ASCE Geo-Frontiers 2011 Conf.*, ASCE, Reston, VA.

Al Qabany, A., Soga, K. & Santamarina, J. C., (2012). Factors affecting efficiency of microbially induced calcite precipitation. *J. Geotech. Geoenviron. Eng* 138(8), 992–1001

Al Thawadi S, Cord Ruwisch R (2012). Calcium carbonate crystals formation by ureolytic bacteria isolated from Australian soil and sludge. *J Adv Sci Eng Res* 2, 12–26

Alonso E.E., Josa A., & Gens A. (1993). Modelling the Behaviour of Compacted Soils. *Unsaturated Soils.* pp. 103-114.

Anson, R. W. W. & Hawkins, A. B. (1998). The effect of calcium ions in pore water on the residual shear strength of kaolinite and sodium montmorillonite. *Geotechnique* 48(6): 787–800.

Asghari, E., Toll, D. G. & Haeri, S. M., (2003). Triaxial behaviour of a cemented gravely sand, Tehran alluvium. *Geotechnical and Geological Engineering*, 21(1): 1-28

ASTM D422-03(1998). Standard Test Method for Measurement for Particle Size Analysis of Soils, *Annual book of ASTM Standards, 04.08, Soil and Rock (II)*, West Consohocken, PA: American Society for Testing and Materials.

ASTM D4318 (1998). Standard Test Method for Liquid Limit, Plastic Limit and Plasticity Index of Soils, *Annual book of ASTM Standards, 04.08, Soil and Rock (II)*, West Consohocken, PA: American Society for Testing and Materials.

ASTM D854 (1998). Standard Test Method for Specific Gravity of Soils, *Annual book of ASTM Standards, 04.08, Soil and Rock (II)*, West Consohocken, PA: American Society for Testing and Materials.

ASTM D698 (1998). Standard Test Methods for Laboratory Compaction Characteristics of Soil Using Standard Effort, *Annual book of ASTM Standards, 04.08, Soil and Rock (II)*, West Consohocken, PA: American Society for Testing and Materials.

ASTM D2487 (1998). Standard Classification of Soils for Engineering Purpose (Unified Soil Classification System), *Annual book of ASTM Standards, 04.08, Soil and Rock (II)*, West Consohocken, PA: American Society for Testing and Materials.

ASTM D2435-90 (2003). Standard Test Method for One Dimensional Consolidation Properties of Soils, *Annual book of ASTM Standards, 04.09, Soil and Rock (II)*, pp203-213, West Consohocken, PA: American Society for Testing and Materials.

Atkinson, J. H. & Bransby, P. L. (1982). Foundations and slopes: an introduction to applications of critical state soil mechanic. Mcgraw-Hill Book Company Limited, UK.

Bachmeier K.L., Williams A.E., Warmington J.R., Bang S.S., (2002). Urease activity in microbiologically-induced calcite precipitation. *J Biotechnol* 93:171–181

Baker, R. (2004). Nonlinear Mohr envelopes based on triaxial data. *Journal of Geotechnical and Geoenvironmental Engineering*, 130 (5): 498-506

Bang S.S., Galinat, J.K., & Ramakrishnan, V., (2001). Calcite precipitation induced by polyurethane-immobilized *Bacillus pasteurii*. *Enzyme Microb Technol* 28: 404–409

Baumgartl, T., (2006). Atterberg Limits. *Encyclopedia of soil science* Vol.1: 135-138. Edited by Lal, R.; published by Taylor & Francis Group, NW, 2006.

Baveye, P., Vandevinerge, P., Hoyle, B.L., deleo, P. C., & Sanchez de Lozada, D. (1998). Environmental impact and mechanism of the biological clogging of sturated soils ans aquifer materials. *Critical review in environmental science and technology* 28(2): 123-191.

Bejerrum, L. (1967). Engineering geology of normally consolidated marine clays as related to settlement of buildings. *Geotechnique* 17(2): 82-118.

Bennett, H.R., O'Brian, N.R. & Hulbert, M.H. (1992). Determinants of clay and shale microfabric signature: Processes and mechanisms in microstructure of fine-grained sediments: From mud to shale, volume IV. Bouma (ed). Springer-Verlag, New York.

Bjerrum, L. & Landva, A. (1966). Direct simple-shear tests on Norwegian quick clay, Oslo, Norway, *Norges Geotekniske Institutt*, 1-20

Bowles, J.E. (1984). Physical and Geotechnical of Properties of Soil. McGraw-Hill Book Company, Kolkata.

Brinkgreve, R.B.J. (2005). Selection of soil models and parameters for geotechnical engineering application. *Geotechnical Special Publication* No.128, ACSE, 69-98.

BS 1377-2 (1990). Methods of test for soils for civil engineering purposes. Classification tests. *British Standards Institution* 2014

Burke, V. & Gibson, F.O. (1933). The gram reaction and the electric charge of bacteria. *J Bacteriol.* 26(2): 211–214.

Burland, J. B., Rampello, S., Georgiannou, V. N. & Calabresi, G. (1996). A laboratory study of the strength of four stiff clays. *Geotechnique* 46(3): 491-514

Cabeen, M. & Jacobs-Wagner, C. (2005). Bacterial cell shape. *Nat Rev Microbiol* 3(8): 601–10.

Chattopadhyay, P. K. (1972). Residual shear strength of some pure clay minerals. PhD thesis. University of Alberta, Edmonton, Canada.

Cheng, L. & Cord-Ruwisch, R., (2014). Upscaling Effects of Soil Improvement by Microbially Induced Calcite Precipitation by Surface Percolation, *Geomicrobiology Journal*, 31(5): 396-406.

Cheng, L. (2012). Innovative ground enhancement by improved microbially induced CaCO3 precipitation technology. Doctoral dissertation, Murdoch Univ., Perth, Western Australia.

Chin, K.G. (2006). Constitutive behaviour of cement treated marine clay. PhD thesis. National University of Singapore, Singapore.

Chu, J. (1991). Strain softening behavior of granular soils under strain path testing. PhD Thesis, Department of Civil and Marine Engineering, The University of New South Wales, Australian Defence Force Academy, Australia

Chu, J., Choa, V. And Bo, M. W. (1999). Determination of undrained shear strength of clay by direct simple shear tests. *Proceedings of 11th Asian Regional Conference on Soil Mechanics and Geotechnical Engineering*, Hong et al. (Eds), 49-52

Chu, J., Ivanov, V., Lee, M. F., Oh, X. M., & He, J. (2009). Soil and waste treatment using biocement. *Proc. International Symposium on Ground Improvement Technologies and Case Histories (ISGI09),* 9-11 Dec, Singapore, 165-170.

Chu, J., Stabnikov, V., & Ivanov, V. (2012). Microbially induced calcium carbonate precipitation on surface or in the bulk of soil. *Geomicrobiol J* 29: 544–549

Chu, J., Ivanov, V., Stabnikov, V., & Li, B. (2013). Microbial method for construction of an aquaculture pond in sand. *Géotechnique*, 63(10): 871–875

Collins, K. & Mcgown, A. (1974). The form and function of microfabric features in a variety of natural soils. *Geotechnique* 24(2): 223–254.

Consoli, N.C., Prietto, P.D.M. and Ulbrich, L.A. (1998). Influence of fiber and cement addition on behaviour of sandy soil, *Journal of Geotechnical and Geoenvironmental Engineering*, 124(12): 1211 – 1214.

Coop, M. R. & Atkinson, J. H. (1993). The mechanics of cemented carbonate sands, *Geotechnique*, 43(1): 53-67.

Cripps, J. C., Hawkins, A. B., & Reld, J. M. (1993). Engineering problems with pyrite mudrocks. *Geoscientist*. G. Society. London 3: 16-19.

Cuccovillo, T. & Coop, M. (1999). On the mechanics of structured sands. *Geotechnique*, 49(6): 741-760.

Dade, W.B., Self, R.L., Pellerin, N.B., Moffet, A, Jumars P.A. & Nowel, A.R.M. (1996). The effects of bacteria on the flow behaviour of clay-seawater suspensions. *Journal of Sedimentary Research*, 66(1): 39-42.

Deflaun, M.F. & Mayer, L.M. (1983). Relationships between bacteria and grain surfaces in intertidal sediments. Limnology and Oceanography, 28(5): 873-881.

Dejong, J.T., Fritzges, M.B., & Nusslein, K. (2006). Microbially induced cementation to control sand response to undrained shear. *Journal of the Geotechnical and Geoenvironmental Engineering Division*, ASCE 132(11): 1381-1392.

DeJong, J., et al. (2009). Upscaling of bio-mediated soil improvement. *Proc., 17th Int. Conf. on Soil Mechanics and Geotechnical Engineering*, Millpress Science, Rotterdam, Netherlands, 2300–2303.

DeJong, J. T., et al. (2010). Soil engineering in vivo: Harnessing natural biogeochemical systems for sustainable, multi-functioning engineering solutions. *J. Roy. Soc. Interface*, 8(1): 1–15.

Dejong, J.T., Mortensenb, B.M., Martinezb, B.C., & Nelson, D.C. (2010b). Bio-mediated soil improvement. *Ecological Engineering* 36: 197–210.

Desrues, J. & Viggiani, G. (2004). Strain localization in sand: an overview of the experimental results obtained in Grenoble using stereophotogrammetry. *International Journal for Numerical and Analytical Methods in Geomechanics*, 28(4): 279-321.

Di Maio, C. & Fenelli, G.B. (1994). Residual strength of kaolin and bentonite: the influence of their constituent pore fluid. *Geotechnique* 44(2): 217–226.

Di Maio, C., Santoli, L. & Schiamone, P. (2004). Volume change behaviour of clays: the influence of mineral composition, pore fluid composition and stress state. *Mech. Mater.* 36(5): 435–451.

Dniker, S., Rhoton, F., Torrent, J., Smeck, N., & Lal, R. (2003). Iron hydroxide crystallinity effects on soil aggregation. *Soil Sci Soc American Journal* Vol. 67: 606-611.

Ehlers, C.J., Chen, J., Roberts, H.H. & Lee, Y.C. (2005). The origin of near-seafloor "crust zones" in deepwater. *Frontiers in Offshore Geotechnics: ISFOG 2005* – Gourvenec & Cassidy (eds) Taylor & Francis Group, London.

Ehrlich, H.L. (1998). Geomicrobiology: its significance for geology. Earth-Science Reviews 45: 45-60.

Fan, H.H., (2006). Study on soil-stabilizing mechanism and molding technique of MBER soil stabilizer. PhD thesis, Chinese Academy of Science, P.R.China.

Favor, L.J. (2003). Bacteria. The Rosen Publishing Group, New York.

Ferris, F.G., Stehmeier, .LG., Kantzas, A., & Mourits, F.M., (1996). Bacteriogenic mineral plugging. *J Can Pet Technol* 35: 56–61

Ferris, F.G., Phoenix, V., Fujita, Y., & Smith, R., (2000). Kinetics of Calcite Precipitation Induced by Ureolytic Bacteria. Geochimica et Cosmochimica Acta, 68(8): 305-318

Fidaleo, M., & Lavecchia, R. (2003). Kinetic study of enzymatic urea hydrolysis in the pH range 4-9. Chem. Biochem. Eng., 17(4): 311–318.

Foppen, J.W.A., & Schijven, J.F. (2005). Transport of E.-coli in columns of geochemically heterogeneous sediment.*Water Research* 39: 3082 – 3088.

Fujita, Y., Ferris, F.G., Larson, R.D., Colwell, F.S., & Smith, R.W., (2000). Calcium carbonate precipitation by ureolytic subsurface bacteria. *Geomicrobiology Journal* 17: 305-318.

Gajo, A. & Loret, B. (2007). The mechanics of active clays circulated by salts, acids and bases. *J. Mech. Phys. Solids* 55(8): 1762–1801.

Gajo, A. & Maines, M. (2007). Mechanical effects of aqueous solutions of inorganic acids and bases on a natural active clay. *Geotechnique* 57(8): 687–699.

Ghatak, S.,Manna,S.,Roy,D.,& Saha, P. (2013). Sand strengthening by bacteriogenic exocellular polymeric substances. *Geotechnique*, received manuscript

Gilbert, P., Evans, D.J., Evans, E., Duguid, I.G., & Brown, M.R.W. (1991). Surface characteristics and adhesion of Escherichia coli and Staphylococcus epidermidis. *Journal of Applied Bacteriology* 71: 72 – 77.

Goldstein, J. (2003). Scanning Electron Microscopy and X-Ray Microanalysis. Characterization & Evaluation of Materials, Springer, ISBN 978-0-306-47292-3. Retrieved May 2012.

Goldstein, G. I., Newbury, D. E., Echlin, P., Joy, D. C., Fiori, C., & Lifshin, E. (1981). *Scanning electron microscopy and x-ray microanalysis*. New York: Plenum Press.

Griffiths, F. J. & Joshi, R. C. (1990). Clay fabric response to consolidation. *Applied Clay Science* 5: 37–66.

Grim, R.E. (1962). Applied clay mineralogy. Mcgraw-Hill, New York.

Grunwald, P. (1984). Imparting some biochemical fundamentals in the course of basic education of chemistry students with the system urease/urea as an example. *Biochemical Education* 12: 170-173.

Guo, H.X., Cheng, X.H., & Li, M. (2013). Experimental analysis of bio-stimulated sealing process in environmental geotechnical engineering. *Science China Technological Sciences* 56 (3): 732–738

Hammes, F. & Verstraete, W. (2002). Key roles of pH and calcium carbonate metabolism in microbial carbonate precipitation. *Reviews in the Environmental Science & Biotechnology* 1: 3-7.

Hammes, F., Boon, N., de Villiers, J., Verstraete, W., & Siciliano, S.D., (2003). Strain-specific ureolytic microbial calcium carbonate precipitation. *Appl Environ Microbiol* 69: 4901–4909

Hanss, M. & Rey, A. (1971). Application de la conductimetrie a letude des reactions enzymatiques – systeme uree – urease. *Biochmica et Biophysica Acta* 225: 630-638.

Harkes, M.P., van Paassen, L.A., Booster, J.L., Whiffin, V.S., & van Loosdrecht, M.C.M., (2010). Fixation and distribution of bacterial activity in sand to induce carbonate precipitation for ground reinforcement. *Ecological Engineering* 36: 112 ‐ 117

Heeralal M., Murty V. R., Praveen, G.V., & Shankar S., (2012). Influence of Calcium Chloride and Sodium Silicate on Index and Engineering Properties of Bentonite. *Proceeding of International Conference on Chemical, Environmental Science and Engineering* (ICEEBS'2012) July 2012, Thailand

Henkel, D.J., 1960. The shear strength of saturated remolded clays. Res. Conf. On shear strength of cohesive soils. ASCE, boulder, Colorado: 533-554.

Horpibulsuk, S., Bergado, D.T., & Lorenzo, G.A. (2004).[(1)] Compressibility of cement admixed clays at high water content. *Geotechnique*, 54(2): 151-154.

Horpibulsuk, S., Miura, N., & Bergado, D.T., (2004). Undrained shear behavior of cement admixed clay at high water content. *Journal of Geotechnical and Geoenvironmental Engineering*, ASCE, 130(10): 1096-1105.

Horpibulsuk, S., Miura, N., & Nagaraj, T.S. (2005). Clay-water/cement ratio identity of cement admixed soft clay. *Journal of Geotechnical and Geoenvironmental Engineering*, ASCE, 131(2): 187-192.

Huertas, F. J., Chou, L., & Wollast, R. (1998). Mechanism of kaolinite dissolution at room temperature and pressure: Part 1. Surface speciation. *Geochim. Cosmochim. Acta* 62(3): 417– 431.

Hugh, C.P., (1985). Drilling Technology. Ox anion Press Pvt Ltd, New Delhi,.

Ivanov, V., & Chu, J. (2008). Applications of microorganisms to geotechnical engineering for bioclogging and biocementation of soil in situ. *Reviews in Environmental Science and Biotechnology* 7: 139-153.

Jiang, M.J., Yan, H.B., Zhu, H.H. & Utili, S. (2011). Modelling shear behaviour and strain localization in cemented sands by two-dimensional distinct element method analyses. *Computers and Geotechnics* 38(1): 14 – 29.

Kandianis,M.T.; Fouke, B. W.; Johnson, R. W.; Veysey, J.; & Inskeep, W. P. (2008). Microbial biomass: A catalyst for $CaCO_3$ precipitation in advection-dominated transport regimes. *Geol. Soc. Am. Bull.*, *120* (3-4), 442–450.

Kanji, M.A., (1974). The relationship between drained friction angles and Atterberg limits of natural soils. *Geotechnique* 24 (4): 671-674.

Karol, R. H. (2003). Chemical grouting and soil stabilization. New York, M. Dekker.

Kavvadas, M. J., Anagnostopoulos, A. G. and Kalteziotis, N. (1993). A framework for the mechanical behaviour of cemented Corinthmarl. *Proc. 1st Int. Symp. on Geotech. Engng of Hard Soils–Soft Rocks*, 1, Athens, 577–583.

Khan, H.A., (2009). Shear induced relative permeability change in uncemented sands. Thesis for Master of Science in Engineering, UT Austin.

Kirihara, M., Asai, Y., Ogawa, S., & Noguchi, T. (2007). Synthesis of Disulfides. *Synthesis,* 3286-3289.

Klein, C., & Hurlbut, C.S.J. (1999). Manual of mineralogy (21st edn). John Wiley & Sons Inc., New York.

Knorst M.T., Neubert R., & Wohlrab, W., (1997). Analytical methods for measuring urea in pharmaceutical formulations. *Journal of Pharmaceutical and Biomedical Analysis* 15: 1627–1632

Konhauser, K. (2007). Introduction to geomicrobiology. Wiley-Blackwell.

Kretschmer, H. & Koernung und konsistenz, (1997). In Handbuch der Bodenkunde; Blume, H.P., Felix-Henningsen, P., Fischer, W.R., Frede, H.G., Horn, R., Stahr, K., Eds.; Landsberg/Lech: Ecomed, 1-45

Kulhawy, F.H. & Mayne, P.W. (1990). Manual on estimating soil properties for foundation design. Report EL-6800, Electric Power Research institute, Palo Alto, 360

Kuo, M.Y-H. & Bolton, M.D. (2008). Preliminary investigation into the bio-geomechanics of marine sediments. 1st Bio-Geo-Civil Engineering Conference, Delft, The Netherlands, 76-81.

Ladd, C.C. (1986). Stability evaluation during staged construction. *Journal of Geotechnical engineering,* ASCE , 117(4): 540-615.

Ladd, C. C., & Foott, R. (1974). New design procedure for stability of soft clays. *Journal of the Geotechnical Engineering Division*, ASCE, 100(7): 763-786.

Lade, P.V., & Overton, D.D. (1989). Cementation effects in frictional materials. *Journal of Geotechnical Engineering,* 115 (10): 1373 – 1387.

Lambe, T.W. & Whitman, R.V. (1991). Soil Mechanics. Wiley.

Liu, J., Shi, B., Jiang, H.T., Huang, H., Wang, G.H. & Kamai, T. (2011). Research on the stabilization treatment of clay slope topsoil by organic polymer soil stabilizer. *Engineering Geology* 117(2): 114-120.

Lo, K. Y. & Morin, J. P. (1972). Strength Anisotropy and Time Effects of Two Sensitive Clays. *Canadian Geotechnical Journal*, 9(3): 261-277

Lo, K. Y. and Hinchberger, S. D., (2007). Stability analysis accounting for macroscopic and microscopic structures in clays. 4th International Conference on Soft Soil Engineering - Soft Soil Engineering, Oct 2006, Vancouver, Canada, Taylor and Francis/Balkema: 3-34

Lo, S. C. R. & Chu, J. (1991). Discussion of "Instability of Granular Materials with Nonassociated Flow". *Journal of Engineering Mechanics, ASCE* , 117(4)930-933.

Ma, C. & Eggleton, R,A. (1999). Cation exchange capacity of kaolinite. *Clays and Clay Minerals,* 47(2): 174-180.

Madigan, M.T. & Martinko, J.M. (2003). Brock biology of microorganisms (11th edn). Prentice Hall, Upper Saddle River, NJ, 992.

Maio, C.D & Fenelli (1994). Residual strength of Kaolin and Bentonite: the influence of their constituent pore fluid. *Geotechnique*, 44(2): 217-226.

Marri, A., (2010). The Mechanical Behaviour of Cemented Granular Materials at High Pressures. *PhD thesis*, the University Of Nottingham.

Martinez et al. (2013). Experimental Optimization of Microbial-Induced Carbonate Precipitation for Soil Improvement. *J. Geotech. Geoenviron. Eng.* 139: 587-598.

Meng, G.H. (2010). The strength and deformation behavior of a residual soil in Singapore. PhD thesis, Nanyang Technological University, Singapore.

McConnaughey, T.A., & Whelan, J.F. (1997). Calcification generates protons for nutrient and bicarbonate uptake. *Earth-Science Reviews* 42: 95-117.

Mitchell, A.C., & Ferris, F.G., (2005) The coprecipitation of Sr into calcite precipitates induced by bacterial ureolysis in artificial groundwater: temperature and kinetic dependence. *Geochim Cosmochim Acta* 69: 4199–4210

Mitchell, J.K. & Soga, K. (2005). Fundamentals of soil behavior. John Wiley & Sons, 3rd edition, New York.

Mitchell, J.K. & Santamarina, J.C., (2005). Biological considerations in geotechnical engineering. *Journal of the Geotechnical and Geoenvironmental Engineering Division,* ASCE 131(10): 1222-1233.

Miura, N., Horpibulsuk, S., & Nagaraj, T.S. (2001). Engineering behavior of cement stabilized clay at high water content. *Soils and Foundations*, 41(5): 33-45.

Mobley, H.L.T. & Hausinger, R.P. (1989). Microbial ureases: significance, regulation, and molecular characterization. *Microbiological Reviews* 53: 85-108.

Mohamed, A.M.O. & Antia, H.E. (1998). Geoenvironmental Engineering. Amsterdam, Elsevier.

Mohapatra, M. & Anand, S. (2010). Synthesis and applications of nano-structured iron oxides/hydroxides – a review. *International Journal of Engineering, Science and Technology* 2(8): 127-146.

Molendijk W.O., van der Zon W.H., van Meurs G.A.M. (2009). SmartSoils, Adaptation of soil properties on demand. *Proceedings of the 17th International Conference on Soil Mechanics and Geotechnical Engineering*, M. Hamza et al. (Eds.), 2443-2446.

Moore, R. (1991). The chemical and mineralogical controls upon the residual strength of pure and natural clays. *Geotechnique* 41(1): 35–47.

Mortensen, B.M., & DeJong, J.T., (2011). Strength and stiffness of MICP treated sand subjected to various stress paths. *GeoFrontiers: Adv Geotech Eng*:4012–4020

Murthy, V. N. S. (2003). Geotechnical Engineering: Principles and Practices of Soil Mechanics and Foundation Engineering (6^{th} edn). Hoboken: Marcel Dekker Inc.

Nagaraj, T. S., & Miura, N. (2001). Soft clay behaviour analysis and assessment. Netherlands, A.A.Balkema.

Ng, W.S., Lee, M.L., Tan, C.K., & Hii, S.L. (2014). Factors affecting improvement in engineering properties of residual soil through microbial-induced calcite precipitation. *J. Geotech. Geoenviron. Eng.*, 140(5), 04014006.

Orband, J. L. R. & Geldart, D. (1997). Direct measurement of powder cohesion using a torsional device. *Powder Technology* 92(1): 25-33.

Parks, S. L., (2009). Kinetics of calcite precipitation by ureolytic bacteria under aerobic and anaerobic conditions. M. Sc thesis, Montana state university.

Parkes, R.J., Cragg, B.A. & Wellsbury, P. (2000). Recent studies on bacterial populations and processes in subseafloor sediments: a review. *Hydrogeology Journal* 8: 11-28.

Phillips, A.J., (2013). Biofilm-Induced Calcium Carbonate Precipitation: Application in the Subsurface. PhD thesis of Montana State University, United States

Powrie, W. (2004). Soil Mechanics (2nd edn). Spon Press.

Proctor R.R. (1933). Fundamental Principles of Soil Compaction. *Engineering News Record 111:* 245-248; 286-289; 348-351.

Pusch, R. (1970). Clay microstructure: a study of the microstructure of soft clays with special reference to their physical properties. *Statens geotekniska institut, proceedings vol. 24.* Byggforskningen, Stockholm.

Qian, C.X., Pan, Q.F., & Wang R.X. (2010a). Cementation of sand grains based on carbonate precipitation induced by microorganism. *Science China Technological Sciences* 53(8): 2198-2206.

Qian, C.X., Wang J.Y., Wang R.X., & Cheng, L. (2009).Corrosion protection of cement-based building materials by surface deposition of CaCO3 by *Bacillus pasteurii*. *Materials Science and Engineering: C* 29(4): 1273 – 1280.

Qian, C.X., Wang R.X., Cheng, L. & Wang J.Y. (2010b). Theory of Microbial Carbonate Precipitation and Its Application in Restoration of Cement-based Materials Defects. *Chinese Journal of Chemistry* 28(5): 847–857

Rabbi A. T. M. Z. & Kuwano J. (2012). Effect of Curing Time and Confining Pressure on the Mechanical Properties of Cement-treated Sand. *Proceeding of GeoCongress:* 996 – 1004

Rabus, R., Hansen, T.A., & Widdel, F. (2006). Dissimilatory sulfate- and sulfur-reducing prokaryotes. In D. Martin, *The Prokaryotes* (659-768). New York: Springer.

Rand, B. & Melton, I. E. (1977). Particle interactions in aqueous kaolinite suspensions I. Effect of ph and electrolyte upon the mode of particle interaction in homoionic sodium kaolinite suspensions. J. Colloid. Interface Sci. 60(2): 308–320.

Rebata-Landa, V. (2007). Microbial activity in sediments: Effects on soil behaviour. Doctoral dissertation, Georgia Institute of Technology, Atlanta, GA.

Reeves, G.M.; Sims, I., & Cripps, J. C., (2006). Clay Materials Used in Construction. Bath, UK: The geological society publishing house.

Roeselers, G., & van Loosdrecht, M.C.M. (2010). Microbial Phytase-Induced Calcium-phosphate Precipitation– a Potential Soil Stabilization Method. *Folia Microbiol* 55 (6): 621–624

Roden, E.E., & Zachara, J.M. (1996). Microbial reduction of crystalline iron(III) oxides: influence of surface area and potential for cell growth. *Environmental Science and Technology*, 30(5): 1618-1628.

Rong, H., Qian, C.X., & Wang R.X. (2011). A cementation method of loose particles based on microbe-based cement. *Science China Technological Sciences* 54(7): 1722-1729.

Roscoe, K.H., Schofield, A.N., & Wroth, C.P. (1958), On the Yielding of Soils. *Geotechnique* 8: 22–53.

Ross, C.W., Mew, G., & Childs, C.W. (1989). Deep cementation in late quaternary sands near Westport, New Zealand. *Australian Journal of Soil Research*, 27(2): 275-288.

Rowe, P. W. (1962). The stress-dilatancy relation for the static equilibrium of an assembly of particles in contact. *Proc. R. Soc*. 269: 500-527.

Saitoh, S., Suzuki, Y., & Shirai, K. (1985). Hardening of soil improved by deep mixing method. *Proc. 11th ICSMFE,* Vol. 5: 1745-1748.

Schnaid, F., Prietto, P. D. M. & Consoli, N. C., (2001). Characterization of cemented sand in triaxial compression. *Journal of Geotechnical and Geoenvironmental Engineering*, 127(10): 857-868.

Schofield, A.N. (2006). Disturbed soil properties and geotechnical design. Thomas Telford, London.

Scholen, D. E. (1992). Non-Standard Stabilizers. Federal Highway Administration, Office of Direct Federal Programs, U.S.

Singh, A., Kuhad, R.C., & Ward, O.P. (2009). Advances in applied bioremediation, Springer Berlin Heidelberg.

Siva Pullaiah, P.V & Savitha, S (1997). Performance of Bentonite clay liner with electrolytic leachets. *Proc. Of IGC, Vadodara*, 363-366.

Sivapullaiah, P.V. & Manju (2005). Kaolinite – alkali interaction and effects on basic properties. *Geotechn. Geol. Engng* 23(5): 601–614.

Sivapullaiah, P.V. & Manju (2007). Induced swelling of kaolinitic soil in alkali solution. *Soil Found.* 47(1): 59–66.

Sridharan, A. & Ventakappa Rao, G. (1973). Mechanism controlling the volume change of saturated clays and the role of the effective stress concept. *Geotechnique* 23(3): 359–382.

Sridharan, A. & Ventakappa Rao, G. (1979). Shear strength behavior of saturated clays and the role of the effective stress concept. *Geotechnique* 29(2): 177–193.

Sridharan, A., Rao, S. M. & Murthy, N. S. (1988). Liquid limit of kaolinitic soils. *Geotechnique* 38(2): 191–198.

Stocks-Fischer, S., Galinat, J.K., & Bang, S.S. (1999). Microbiological precipitation of $CaCO_3$. *Soil Biology and Biochemistry* 31: 1563-1571.

Schroth, B.K. & Sposito, G. (1997). Surface charge properties of kaolinite. *Clay Miner.* 45(1): 85–91.

Stabnikov, V., Chu, J., Ivanov, V., & Li, V., (2013). Halotolerant, alkaliphilic urease-producing bacteria from different climate zones and their application for biocementation of sand. *World J Microbiol Biotechnol*,29(8): 1453-1460

Stackebrandt, E. & Goebel, B.M. (1994). A place for DNADNA reassociation and 16S rRNA sequence analysis in the present species definition in bacteriology. *Int. J. Syst. Bacteriol.* 44: 846-849.

Stuttgart, G.T. (2008). Recent developments in disulfide bond formation. Department of Organic Chemistry, Chemical Faculty, Gdansk University of Technology, 2491-2509.

Sumner, M.E., & Naidu, R. (1998). Sodic Soils: Distribution, Properties, Management, and Environmental Consequences. Oxford University Press, USA

Suzuki, K. and Yamada, T., (2006). Double strain softening and diagonally crossing Shear bands of sand in drained triaxial tests. *International Journal of Geome-chanics,* 6(6): 440-446.

Tagliaferri, F., Waller, J., Andò, E., Hall, S.A., Viggiani, G., Bésuelle,P., & DeJong J.T. (2011). Observing strain localisation processes in bio-cemented sand using x-ray imaging. *Granular Matter* 13: 247–250.

Tan, X ., Zhang, G.*, Reed, A.H., & Furukawa, Y. (2014). Flocculation and particle size analysis of expansive clay sediments affected by biological, chemical, and hydrodynamic factors. *Ocean Dynamics* 64(1): 143-157.

Terzaghi, K. (1942). Theoretical Soil Mechanics. Wiley, New York.

Terzaghi, K. & Peck, R.B. (1976). Soil mechanics in engineering practices (2nd edn). John Wiley & Sons, New York.

Terzaghi, K., Peck, R.B., & Mesri, G. (1996). Soil mechanics in engineering practice (3rd edn). John Wiley & Sons, New York.

Thian, S. Y., & Lee. C.Y., (2013). The effect of low confining pressures on cemented sand. *J. of Research in Architecture and Civil Engineering (ISTP-JRAC)* 1(3): 1-4

Tiwari, M. (2007). Time-effect and Instability Behavior of Cohesive Soils. PhD Thesis, School of Civil and Environmental Engineering, Nanyang Technological University, Singapore

Tombácz, E. & Szekeres, M. (2006). Surface charge heterogeneity of kaolinite in aqueous suspension in comparison with montmorillonite. *Applied Clay Science* 34(1-4): 105-124.

Torkzaban, S., Tazehkand, S.S., Walker, S.L., & Bradford, S.A., (2008). Transport and fate of bacteria in porous media: coupled effects of chemical conditions and pore space geometry. *Water Resources Research* 44: 1 – 12.

Turley, C.M., Lochte, K. & Lampitt, R.S. (1995). Transformations of biogenic particles during sedimentation in the Northeastern Atlantic. Philosophical Transactions of the Royal Society of London Series Biological Sciences, 348(1324): 179-189.

U.S. Silica Company, (2010). Material Safety Data Sheet for OTTAWA white® sand series.

van Paassen, L. A. (2009). Biogrout (ground improvement by microbially induced carbonate precipitation). Doctoral dissertation, Delft Univ. of Technology, Delft, The Nethelands.

van Paassen, L.A., Ghose, R., van der Linden, T.J.M., van der Star, W.R.L., & van Loosdrecht, M.C.M.. (2010). Quantifying biomediated ground improvement by ureolysis: large-scale biogrout experiment. *J. Geotech Geoenviron Eng* 136:1721–1728.

van Paassen, L.A., Harkes, M.P., van Zwieten, G.A., van der Zon, W.H., van der Star, W.R.L., & van Loosdrecht, M.C.M., (2009). Scale up of biogrout: a biological ground reinforcement method. *Proceedings of the 17th International Conference on Soil Mechanics and Geotechnical Engineering*, The Academia and Practice of Geotechnical Engineering, Egypt, 2328–2333.

Vandevivere, P. & Baveye, P. (1992). Relationship between transport of bacteria and their clogging efficiency in sand columns. *Applied Environ. Microb.* 58(8): 2523-2530.

Voight, B., 1973.Correlation between Atterberg plasticity limits and residue shear strength of natural soils. *Geotechnique* 23 (2): 265-267.

Walworth J. (2006). Soil structure: the roles of sodium and salts. Lecture notes, AZ1414, University of Arizona.

Wahid A.S., Gajo A., & Di Maggio R. (2010). Chemo-mechanical effects in kaolinite. Part 1: prepared sample. *Geotechnique*, 61(6): 439 –447.

Weiss, J.E. (2005). Rhizosphere iron (III) deposition and reduction in a Juncus effusus L-dominated wetland. *Soil Science Society of America Journal*, 69: 1861-1870.

Whiffin, V.S. (2004). Microbial $CaCo_3$ precipitation for the production of biocement. Phd thesis, Murdoch University, Western Australia.

Whiffin, V.S., van Paassen, L.A., & Harkes, M.P., (2007). Microbial carbonate precipitation as a soil improvement technique. *Geomicrobiology Journal* 24 (5): 417 ‑ 423.

Wieland, E. & Stumm, W. (1992). Dissolution kinetics of kaolinite in acidic aqueous solutions at 25°C. *Geochim. Cosmochim. Acta* 56: 3339–3355.

Yamanata, T., Miyasaka, H., Aso, I., Tanigawa, M., & Shoji, K. (2002). Involvement of sulfur- and iron-reducing bacteria in heaving of fouse foundations. *Geomicrobiol. J.* 19: 519-528.

Zhang, C., Dehoff, K., Hess, N., Oostrom, M., Wietsma, T. W., Valocchi, A. J., Fouke, B. W., & Werth, C. J., (2010). Pore-scale study of transverse mixing induced $CaCO_3$ precipitation and permeability reduction in a model subsurface sedimentary system. *Environmental Science & Technology*, 44 (20): 7833-7838.

Zhang, G., Yin, H., Lei, Z., Reed, A.H., & Furukawa, Y. (2013). Effects of exopolymers on particle size distributions of suspended cohesive sediments. *Journal of Geophysical Research: Oceans* 118: 1-17.

Zhou, Z. & Gunter, W.D. (1992). The nature of the surface charge of kaolinite. *Clays and Clay Minerals*, 40: 365-368.

Zwietering, M.H, Jongenburger, I., Rombouts, F.M., & Van, T.R.K. (1990). Modeling of the Bacterial Growth Curve. *Applied and Environmental Microbiology* 56(6): 1875–1881.

Appendices

Appendix A – Relationship between Conductivity and Activity of UPB

Conductivity of NH_4Cl (ms/cm) in 0.001-0.01 M concentration

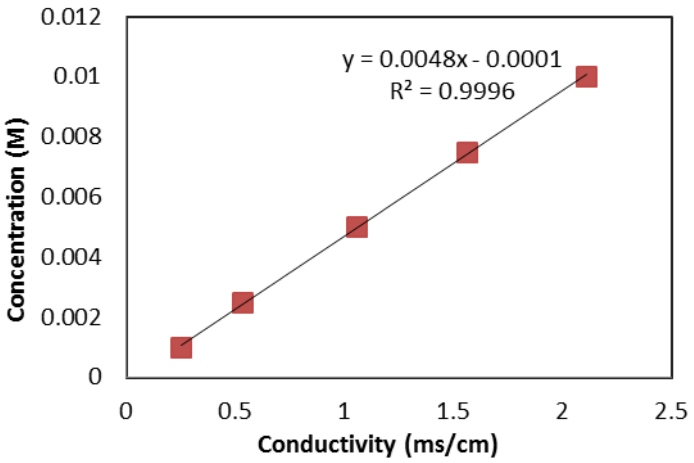

Conductivity of NH_4Cl (ms/cm) in 0.025-0.1 M concentration

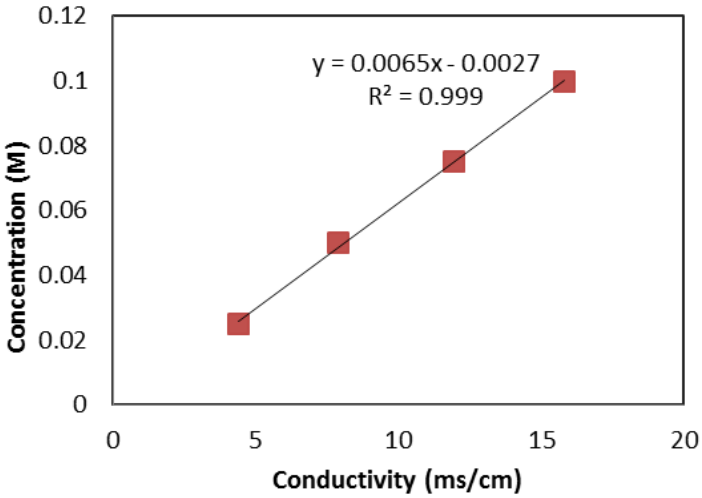

Conductivity of NH_4Cl (ms/cm) in 0.25-1 M concentration

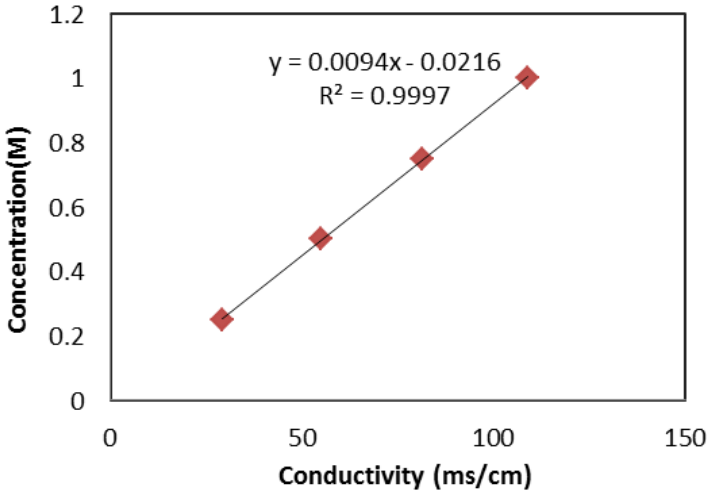

Appendix B – Calibration Curve between Optical Density at 422nm and Urea Content in Solution

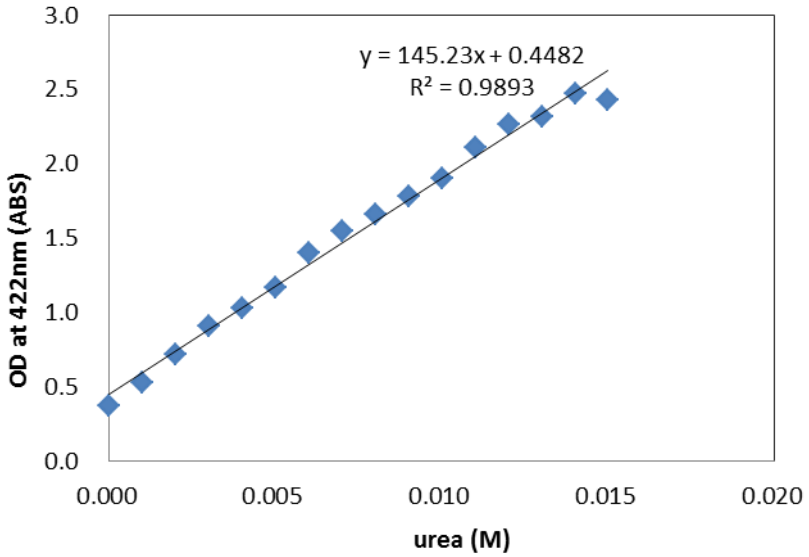

Appendix C –Optical density during in UPB cultivation and its relationship with biomass concentration

Dynamics of Optical Density (OD)

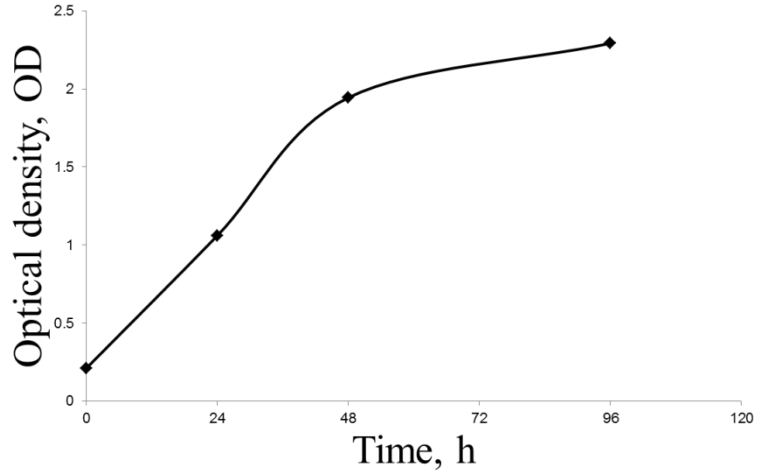

Calibration curve for determination of biomass concentration, g/L

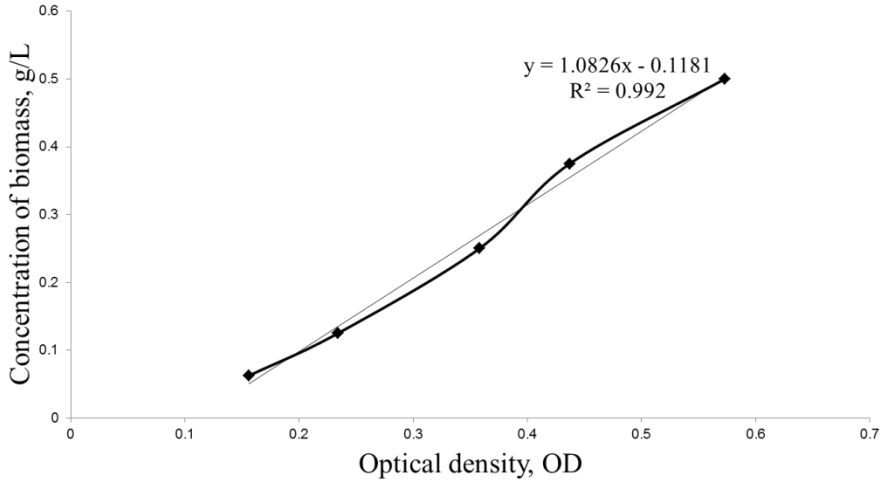

Appendix D –Parameters variation (pH value, conductivity, calcium cation, and urea remaining in solution) against time in Test 2 (1:2 low), Test 4 (1:1 high), and Test 5 (1:1 low) (Section 4.3.2)

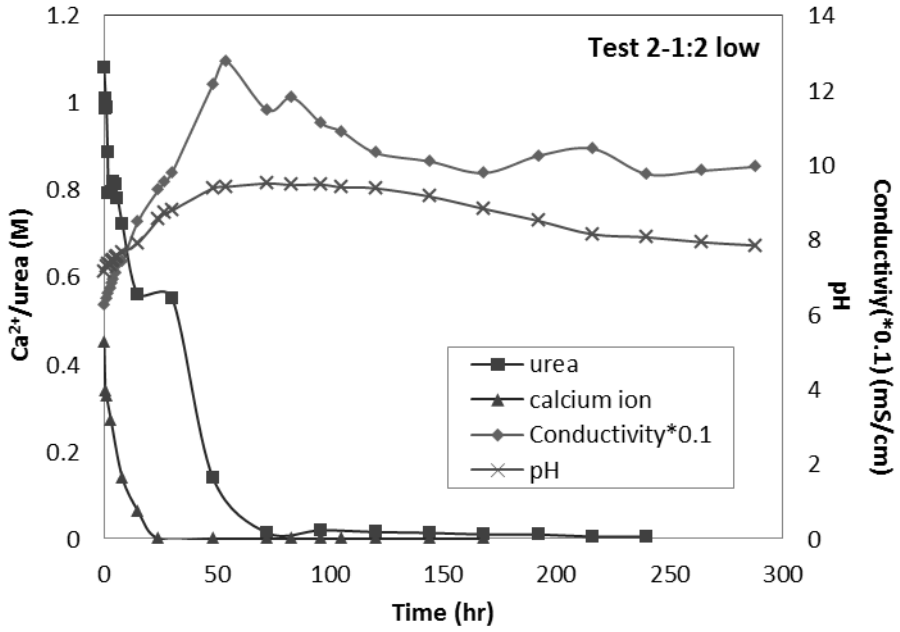

Test 2

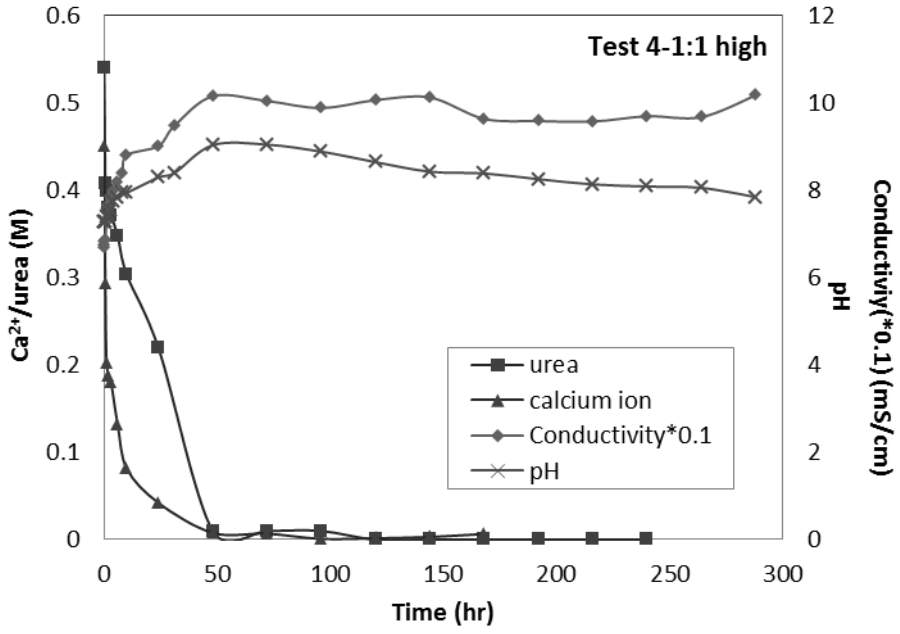

Test 4

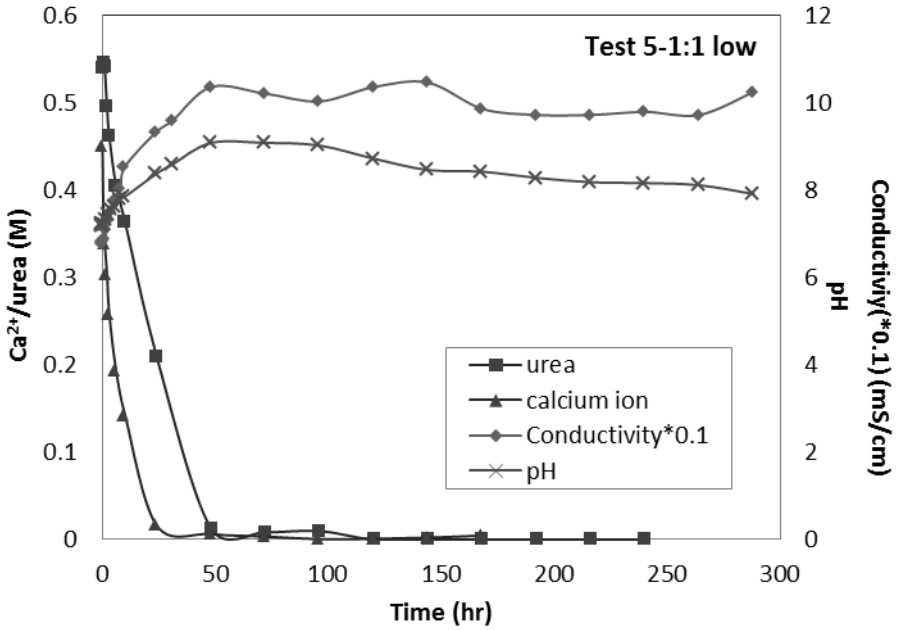
Test 5-1:1 low
Ca2+/urea (M)
pH
Conductivity(*0.1) (mS/cm)
Time (hr)
urea
calcium ion
Conductivity*0.1
pH
0
0.1
0.2
0.3
0.4
0.5
0.6
0
2
4
6
8
10
12
0
50
100
150
200
250
300

Test 5

Appendix E –Parameters variation (pH value, conductivity, calcium cation, and urea remaining in solution) against time in Test 2, Test 4, Test 5 and Test 2a in Section 4.3.2

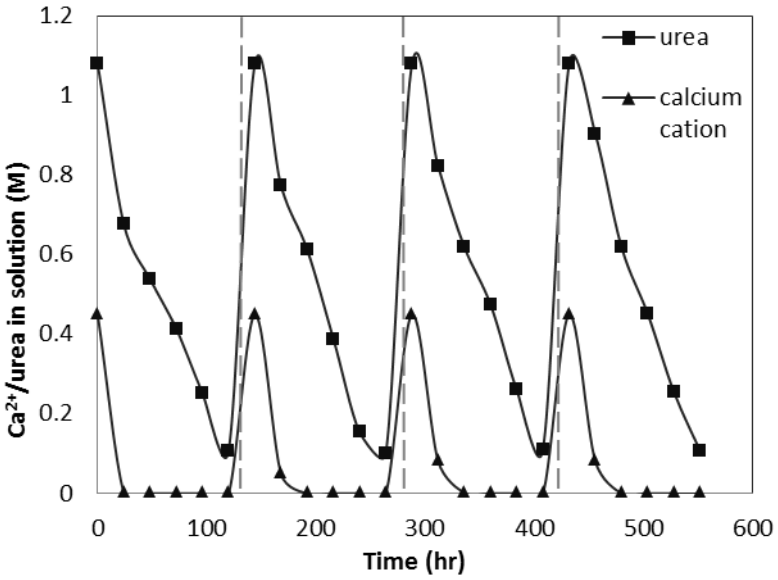

Test 2

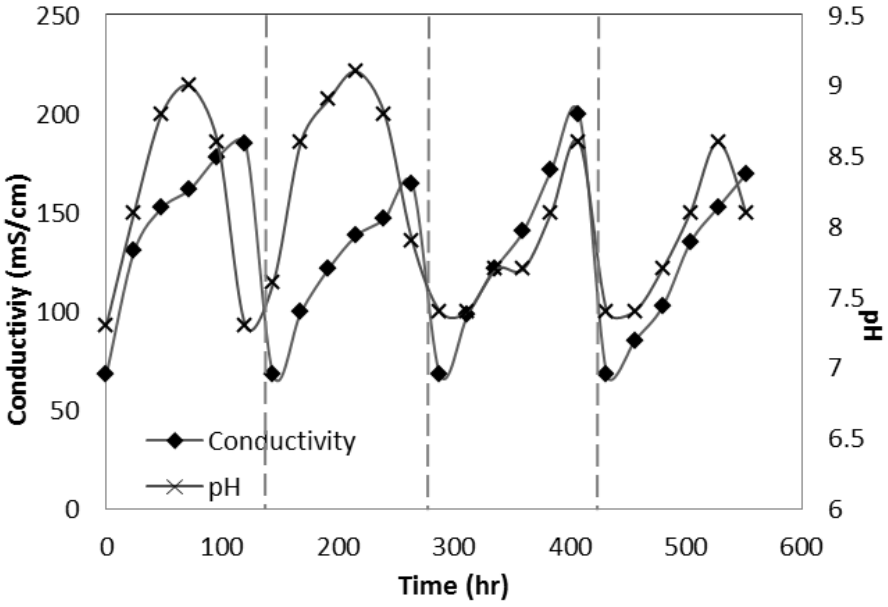

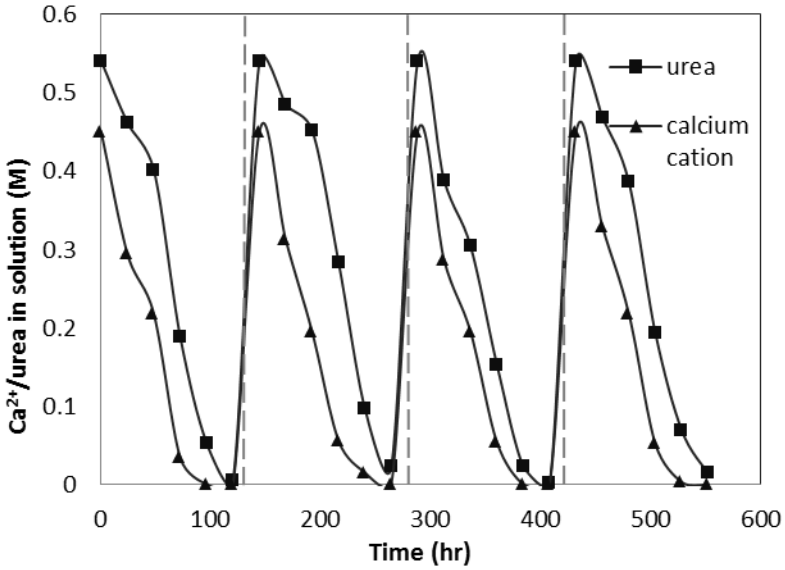
0.6
0.5
0.4
0.3
0.2
0.1
0
0
100
200
300
400
500
600
Ca2+/urea in solution (M)
Time (hr)
urea
calcium cation

Test 4

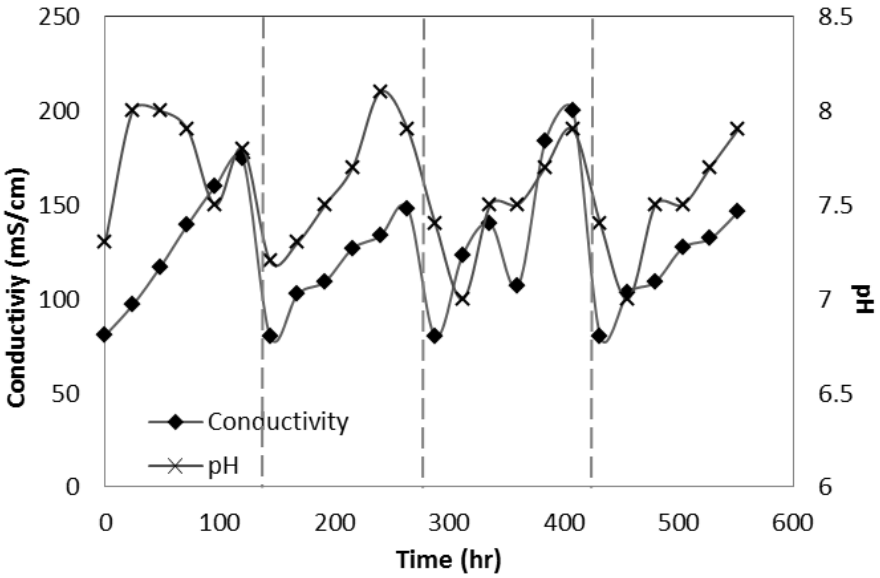
250
200
150
100
50
0
8.5
8
7.5
7
6.5
6
0
100
200
300
400
500
600
Conductiviy (mS/cm)
pH
Time (hr)
Conductivity
pH

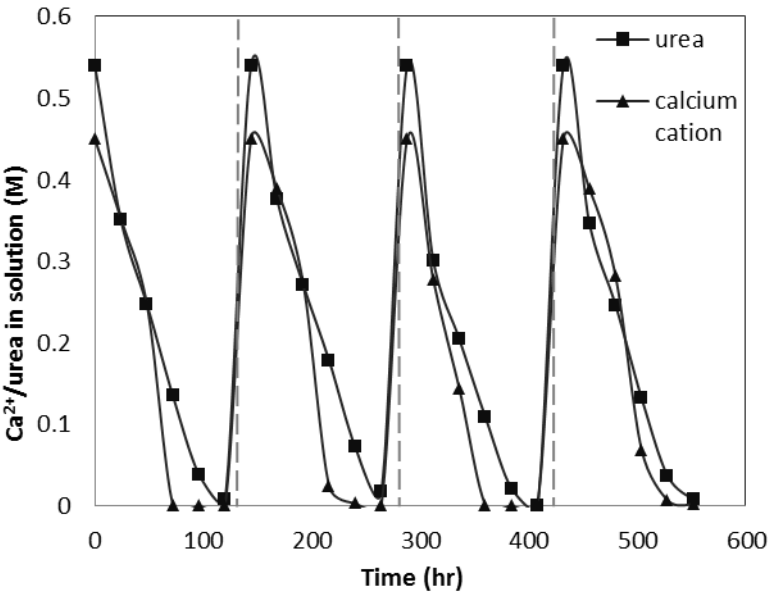
0.6
0.5
0.4
0.3
0.2
0.1
0
0
100
200
300
400
500
600
Ca2+/urea in solution (M)
Time (hr)
urea
calcium cation

Test 5

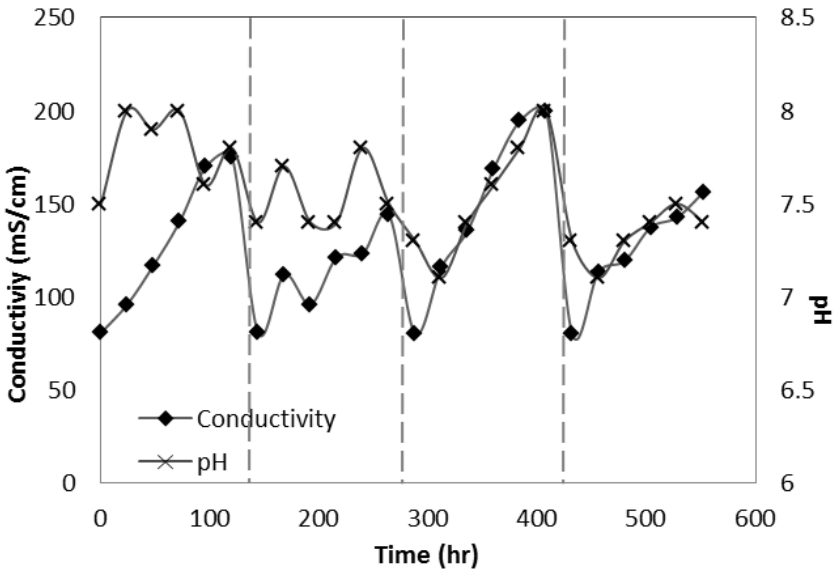
250
200
150
100
50
0
8.5
8
7.5
7
6.5
6
0
100
200
300
400
500
600
Conductiviy (mS/cm)
pH
Time (hr)
Conductivity
pH

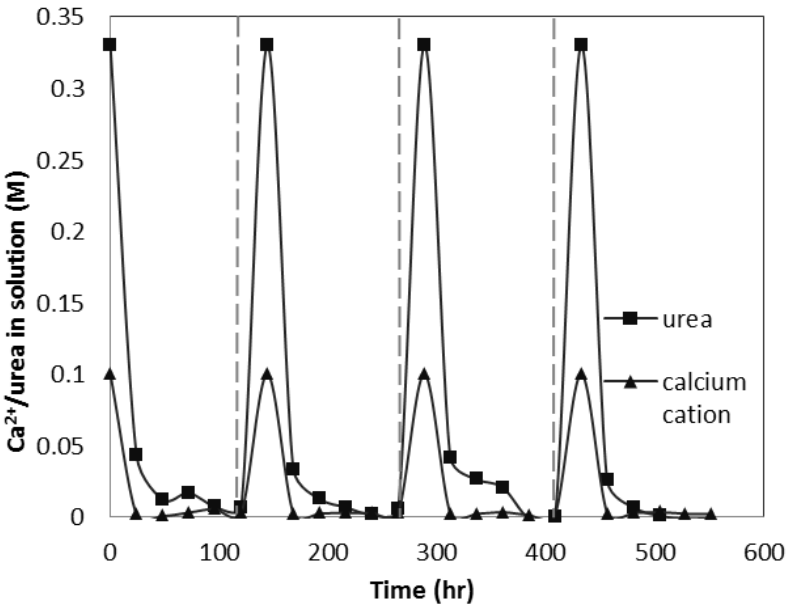
0.35
0.3
0.25
0.2
0.15
0.1
0.05
0
Ca2+/urea in solution (M)
0
100
200
300
400
500
600
Time (hr)
urea
calcium cation

Test 2a

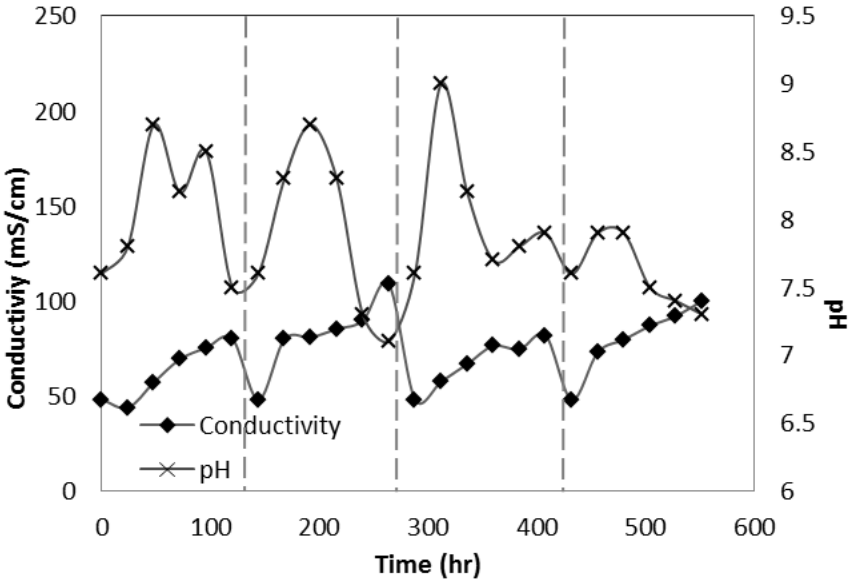
250
200
150
100
50
0
Conductiviy (mS/cm)
9.5
9
8.5
8
7.5
7
6.5
6
pH
0
100
200
300
400
500
600
Time (hr)
Conductivity
pH

Appendix F –Detailed information on kaolin specimens mixed with chemicals/UPB conducting UC tests

Test	$CaCl_2$ (mol/L)	urea (mol/L)	UPB (ml)	Water content (%)	UC Strength (kPa)	Void Ratio	DOS (%)	Remarks
A1	-	-	-	67.83	26.77	1.74	101.29	with distilled water
A2	-	-	-	67.83	24.03	1.74	101.29	
A3	-	-	-	56.04	115.02	1.48	98.47	
A4	-	-	-	58.16	87.28	1.60	94.28	
A5	-	-	-	53.04	167.59	1.41	97.68	
A6	-	-	-	42.91	286.60	1.32	84.28	
B1	-	-	-	70.73	18.47	1.91	96.09	with DI water
B2	-	-	-	71.93	14.25	1.91	98.02	
B3	-	-	-	63.85	45.38	1.70	97.68	
B4	-	-	-	65.48	37.15	1.79	94.94	
B5	-	-	-	54.41	140.83	1.42	99.32	
B6	-	-	-	47.82	232.94	1.35	92.16	
B7	-	-	-	53.45	148.22	1.45	96.11	
B8	-	-	-	55.67	116.70	1.50	96.24	
Ca1	0.375	-	-	74.35	0.00	1.31	141.16	with $CaCl_2$
Ca2	0.375	-	-	69.81	4.26	1.66	105.07	
Ca3	0.375	-	-	60.36	43.14	1.55	97.23	
Ca4	0.375	-	-	60.53	37.41	1.55	97.47	
Ca5	0.375	-	-	52.23	109.35	1.39	93.45	
Ca6	0.375	-	-	43.50	254.09	1.18	92.31	
Ca7	0.375	-	-	55.11	84.18	1.36	101.46	
Ca8	0.375	-	-	42.44	275.23	1.16	91.25	
Ca9	0.375	-	-	33.53	340.48	1.15	72.54	
Ca10	0.375	-	-	24.48	370.75	1.18	51.97	
Ca11	0.375	-	-	16.99	393.33	1.17	36.12	
Ca12	0.375	-	-	17.76	400.86	1.11	39.84	
Ca13	0.375	-	-	55.10	81.89	1.51	91.30	
Ca14	0.375	-	-	52.20	108.44	1.42	91.51	
Ca15	0.375	-	-	46.03	156.10	1.33	86.51	
Cb1	0.75	-	-	78.98	0.00	1.45	130.61	
Cb2	0.75	-	-	73.49	0.00	1.75	100.66	
Cb3	0.75	-	-	69.62	6.34	1.56	107.39	
Cb4	0.75	-	-	62.78	17.47	1.56	96.36	
Cb5	0.75	-	-	58.20	43.66	1.43	97.57	

Test	$CaCl_2$ (mol/L)	urea (mol/L)	UPB (ml)	Water content (%)	UC Strength (kPa)	Void Ratio	DOS (%)	Remarks
Cb6	0.75	-	-	50.68	90.33	1.34	90.82	
Cb7	0.75	-	-	51.92	97.67	1.29	96.35	
Cb8	0.75	-	-	45.11	204.84	1.18	91.80	
Cb9	0.75	-	-	38.12	320.69	1.14	80.04	
Cb10	0.75	-	-	32.49	348.18	1.11	70.24	
Cb11	0.75	-	-	26.30	383.71	1.14	55.53	
Cb12	0.75	-	-	24.68	425.08	1.12	53.09	
Cb13	0.75	-	-	60.42	37.94	1.52	95.45	
Cb14	0.75	-	-	50.98	110.56	1.34	91.54	
Cc1	1.5	-	-	72.03	0.00	1.22	131.37	
Cc2	1.5	-	-	66.96	4.97	1.39	107.35	
Cc3	1.5	-	-	62.68	15.71	1.54	90.87	with $CaCl_2$
Cc4	1.5	-	-	56.92	40.65	1.35	93.79	
Cc5	1.5	-	-	55.82	59.42	1.30	95.76	
Cc6	1.5	-	-	52.59	64.86	1.27	92.31	
Cc7	1.5	-	-	62.90	21.13	1.34	104.77	
Cc8	1.5	-	-	53.52	59.64	1.28	92.89	
Cc9	1.5	-	-	52.24	81.26	1.18	98.47	
Cc10	1.5	-	-	45.24	182.69	1.09	92.92	
Cc11	1.5	-	-	38.95	283.62	1.00	86.69	
Cc12	1.5	-	-	33.86	369.02	1.00	75.22	
Cc13	1.5	-	-	63.31	14.94	1.38	102.11	
Cc14	1.5	-	-	60.12	25.27	1.39	96.18	
Da1	-	0.75	-	90.32	8.58	2.12	106.02	
Da2	-	0.75	-	74.17	15.40	1.91	96.70	
Da3	-	0.75	-	71.47	19.72	1.85	96.10	
Da4	-	0.75	-	66.22	33.03	1.70	97.08	
Da5	-	0.75	-	58.26	114.84	1.53	94.75	
Da6	-	0.75	-	53.58	173.50	1.36	97.82	
Da7	-	0.75	-	43.53	298.41	1.30	83.52	with urea
Da8	-	0.75	-	43.63	300.65	1.32	82.04	
Da9	-	0.75	-	31.55	348.74	1.27	61.87	
Da10	-	0.75	-	28.44	367.71	1.34	52.86	
Da11	-	0.75	-	20.82	364.61	1.36	38.11	
Da12	-	0.75	-	12.37	230.08	1.39	22.17	
Da13	-	0.75	-	63.62	50.50	1.67	94.79	
Da14	-	0.75	-	47.65	241.55	1.31	90.21	

Test	$CaCl_2$ (mol/L)	urea (mol/L)	UPB (ml)	Water content (%)	UC Strength (kPa)	Void Ratio	DOS (%)	Remarks
Db1	-	1.5	-	80.94	6.77	1.81	106.51	
Db2	-	1.5	-	78.45	8.86	1.92	97.29	
Db3	-	1.5	-	77.55	11.64	1.84	100.80	
Db4	-	1.5	-	68.70	30.38	1.75	93.71	
Db5	-	1.5	-	66.14	46.80	1.71	92.11	
Db6	-	1.5	-	59.76	85.77	1.52	93.57	
Db7	-	1.5	-	45.32	266.85	1.28	84.68	
Db8	-	1.5	-	46.25	273.21	1.29	85.23	
Db9	-	1.5	-	41.00	297.30	1.31	74.70	
Db10	-	1.5	-	35.58	336.32	1.30	65.16	
Db11	-	1.5	-	22.17	364.54	1.37	38.73	
Db12	-	1.5	-	19.15	329.40	1.42	32.15	
Db13	-	1.5	-	69.77	54.12	1.67	99.85	
Db14	-	1.5	-	50.14	245.99	1.28	93.50	
Db15	-	1.5	-	70.01	35.50	1.49	98.43	
Db16	-	1.5	-	56.09	151.24	1.70	89.98	with urea
Dc1	-	3	-	78.73	6.41	1.86	93.36	
Dc2	-	3	-	80.74	9.16	1.85	96.14	
Dc3	-	3	-	72.12	17.86	1.69	93.90	
Dc4	-	3	-	64.86	29.21	1.61	88.61	
Dc5	-	3	-	61.30	71.66	1.46	92.73	
Dc6	-	3	-	60.20	78.68	1.43	92.46	
Dc7	-	3	-	44.91	251.26	1.09	91.08	
Dc8	-	3	-	45.84	228.08	1.12	90.12	
Dc9	-	3	-	41.67	295.29	1.17	78.58	
Dc10	-	3	-	37.31	345.81	1.25	65.70	
Dc11	-	3	-	27.16	344.28	1.32	45.20	
Dc12	-	3	-	24.05	311.58	1.36	39.11	
Dc13	-	3	-	73.27	19.79	1.66	97.32	
Dc14	-	3	-	72.97	38.90	1.65	97.54	
Dc15	-	3	-	56.63	136.39	1.42	87.77	
E1	0.75	1.5	-	59.49	14.29	1.60	82.22	
E2	0.75	1.5	-	61.94	14.66	1.59	86.38	
E3	0.75	1.5	-	57.94	27.06	1.40	91.64	$CaCl_2$ + urea
E4	0.75	1.5	-	58.50	21.88	1.48	87.68	
E5	0.75	1.5	-	50.60	80.71	1.28	87.74	
E6	0.75	1.5	-	50.38	82.43	1.24	90.35	

Test	$CaCl_2$ (mol/L)	urea (mol/L)	UPB (ml)	Water content (%)	UC Strength (kPa)	Void Ratio	DOS (%)	Remarks
E7	0.75	1.5	-	74.17	0.00	1.86	88.18	$CaCl_2$ + urea
E8	0.75	1.5	-	73.28	0.00	1.64	98.74	
E9	0.75	1.5	-	64.40	13.96	1.62	88.07	
E10	0.75	1.5	-	61.58	26.40	1.50	91.14	
E11	0.75	1.5	-	71.68	0.00	2.00	79.47	
E12	0.75	1.5	-	77.87	0.00	2.04	84.78	
E13	0.75	1.5	-	45.49	213.48	1.15	87.74	
E14	0.75	1.5	-	43.10	279.81	1.07	89.12	
E15	0.75	1.5	-	42.20	260.82	1.04	90.34	
E16	0.75	1.5	-	43.79	230.07	1.10	88.40	
E17	0.75	1.5	-	64.75	19.17	1.53	93.71	
E18	0.75	1.5	-	61.11	32.79	1.51	89.43	
E19	0.75	1.5	-	58.44	47.02	1.36	94.95	
E20	0.75	1.5	-	59.03	45.28	1.42	91.98	
E21	0.75	1.5	-	53.31	91.18	1.29	91.23	
E22	0.75	1.5	-	73.20	0.00	1.61	100.99	
E23	0.75	1.5	-	71.45	0.00	1.50	105.38	
E24	0.75	1.5	-	63.59	24.02	1.47	95.91	
E25	0.75	1.5	-	64.07	18.00	1.52	93.28	
E26	0.75	1.5	-	65.14	24.87	1.47	98.44	
E27	0.75	1.5	-	62.90	27.69	1.40	99.34	
F1	0.75	1.5	15	61.29	63.83	1.46	93.24	$CaCl_2$ + urea + centrifuged UPB
F2	0.75	1.5	15	59.96	73.39	1.55	85.96	
F3	0.75	1.5	15	58.76	72.74	1.42	91.79	
F4	0.75	1.5	15	60.17	70.84	1.40	95.21	
F5	0.75	1.5	15	51.28	180.15	1.23	92.36	
F6	0.75	1.5	15	53.76	220.01	1.31	90.61	
F7	0.75	1.5	15	79.96	9.96	1.59	111.65	
F8	0.75	1.5	15	79.22	11.40	1.56	112.87	
F9	0.75	1.5	15	67.55	58.36	1.61	93.10	
F10	0.75	1.5	15	65.18	75.56	1.54	93.91	
F11	0.75	1.5	15	73.38	31.75	1.70	95.84	
F12	0.75	1.5	15	75.27	21.55	1.67	99.90	
F13	0.75	1.5	15	36.25	288.62	1.22	65.92	
F14	0.75	1.5	15	33.23	339.90	1.26	58.26	
F15	0.75	1.5	15	32.50	293.93	1.21	59.75	
F16	0.75	1.5	15	32.24	327.05	1.19	60.10	

Test	$CaCl_2$ (mol/L)	urea (mol/L)	UPB (ml)	Water content (%)	UC Strength (kPa)	Void Ratio	DOS (%)	Remarks
F17	0.75	1.5	15	68.38	41.75	1.59	95.01	$CaCl_2$ + urea + centrifuged UPB
F18	0.75	1.5	15	68.51	43.29	1.55	98.17	
F19	0.75	1.5	15	59.44	116.00	1.38	95.52	
F20	0.75	1.5	15	64.05	70.95	1.42	99.65	
F21	0.75	1.5	15	54.24	184.54	1.29	93.51	
F22	0.75	1.5	15	55.46	167.20	1.30	94.86	
G1	0.75	1.5	15	63.33	76.76	1.58	88.89	$CaCl_2$ + urea + original UPB
G2	0.75	1.5	15	62.09	104.97	1.45	94.63	
G3	0.75	1.5	15	63.68	78.33	1.50	93.94	
G4	0.75	1.5	15	61.87	67.72	1.40	97.80	
G5	0.75	1.5	15	53.91	203.88	1.31	90.99	
G6	0.75	1.5	15	52.89	187.57	1.31	89.75	
G7	0.75	1.5	15	79.36	15.56	1.77	99.34	
G8	0.75	1.5	15	78.56	18.75	1.80	96.93	
G9	0.75	1.5	15	59.50	90.91	1.39	94.95	
G10	0.75	1.5	15	68.38	40.67	1.53	98.92	
G11	0.75	1.5	15	82.88	14.97	1.81	101.55	
G12	0.75	1.5	15	80.83	21.59	1.80	99.61	
G13	0.75	1.5	15	39.36	301.56	1.29	67.64	
G14	0.75	1.5	15	42.62	312.95	1.30	72.73	
G15	0.75	1.5	15	35.01	339.15	1.27	61.28	
G16	0.75	1.5	15	33.42	318.76	1.31	56.60	
G17	0.75	1.5	15	64.02	113.85	1.51	93.96	
G18	0.75	1.5	15	67.07	83.60	1.56	95.04	
G19	0.75	1.5	15	60.62	144.35	1.36	98.80	
G20	0.75	1.5	15	62.33	128.34	1.39	99.05	
G21	0.75	1.5	15	48.28	286.91	1.29	82.96	
G22	0.75	1.5	15	51.32	225.84	1.28	88.78	
G23	0.75	1.5	15	71.84	49.21	1.61	98.71	
G24	0.75	1.5	15	75.15	30.53	1.69	98.36	
G25	0.75	1.5	15	60.70	143.94	1.44	93.24	
G26	0.75	1.5	15	62.53	118.78	1.43	97.08	
G27	0.75	1.5	15	60.17	131.17	1.44	92.69	
G28	0.75	1.5	15	51.18	259.75	1.29	87.62	